SYNTHESIS AND CHARACTERIZATION OF PHOTOLABILE RUTHENIUM POLYPYRIDYL CROSSLINKERS WITH APPLICATIONS IN SOFT MATERIALS AND BIOLOGY

Teresa Rapp

A DISSERTATION

in

Chemistry

Presented to the Faculties of the University of Pennsylvania

in

Partial Fulfillment of the Requirements for the

Degree of Doctor of Philosophy

2018

Supervisor of Dissertation

_____

Ivan J. Dmochowski, Professor of Chemistry

Graduate Group Chairperson

_____

Gary A. Molander, Hirschmann-Makineni Professor of Chemistry

Dissertation Committee
Donald H. Berry, Professor of Chemistry
David Christianson, Roy and Diana Vagelos Professor in Chemistry and Chemical Biology
Sergei Vinogradov, Associate Professor of Biochemistry and Biophysics

SYNTHESIS AND CHARACTERIZATION OF PHOTOLABILE RUTHENIUM POLYPYRIDYL CROSSLINKERS WITH APPLICATIONS IN SOFT MATERIALS AND BIOLOGY

To Mr. Oliver and Dr. Gragson, the chemistry professors who inspired me to be just like them.

ACKNOWLEDGMENTS

This dissertation would not be possible without my family and friends who have supported me for the last 6 years. Firstly, to my advisor, Ivan. The only reason there are 6 chapters instead of 4 (or fewer) is because you allowed me to branch out and pursue my passion, even when it wasn't what I signed on to do. For that I am incredibly grateful, and because of that I have a clear idea of what I want to pursue in my career as an independent researcher.

Secondly, I'd like to acknowledge my committee, and all the hard work they did working with me throughout this process. From conversations about ruthenium chemistry, to manufacturing the LEDs that enabled much of this work, to discussions about the variety of possibilities in biological applications, your time has been invaluable to me in our annual meetings and all the other times I've stopped by for advice. Thank you for being available, for reading so many reports, and for taking the time to mentor me throughout my PhD.

Also, to the amazing people in my lab and the Chemistry Department who always kept my head on straight. My fellow cohorts Sean and Ben, those who come after us, Linlin, Serge, Yannan, Zhuangyu, Josh, and Kelsey our fabulous undergrad, you all are what make the Dmochowski lab the best lab in the department. Thank you for Waffles and Science, for eating up my less-than-perfect baked goods, and for listening to all my practice talks over the years.

I couldn't mention the people in the Chemistry Department who have supported me without thanking Katie Pulsipher, the first person I met in grad school outside my cohort. Katie, when I first saw you on one of the welcome panels at Open House, I thought you were quiet and meek, and a little … weird. Well, I was 100% wrong. You quickly became my best friend in the department, and one of the closest friends in my life. You saved my sanity while I worked through failure after failure, you rejoiced with me when an experiment actually worked out, and you regularly were the voice of reason when I was anxious about my future.

There were many others in the department who have supported me, taught me, and encouraged me over the years. Kristen, our grad coordinator, has been a huge blessing; her door is always open. Judith Currano, our librarian, has been more than helpful over the years with anything I've struggled with. The late George Furst helped me take my first 2D NMR, and figure out the initial problems I was having with my compounds, and Jun has followed in his footsteps. Dr. Ross has been beyond helpful as I struggle to figure out structures and identify products by mass spectrometry, he is a true asset to the department. Chris Jeffries is great as always, supportive and helpful with anything I need.

Outside the Chemistry Department I stumbled into the greatest church family I could have asked for at Freedom Church. To my pastor, Dr. Gabe Bouch, the fact that you have a PhD in mathematic physics yet you pastor this amazing church has inspired me to consider all aspects of life, educational, scientific, and spiritual. To Jen Bouch, you adopted me as your 7th kid, and let me teach science to your other 6. I'm not sure what I did to deserve that honor, but I am truly honored. To everyone else in my Freedom Family who has welcomed me with open arms, Micah and Tiffany, Jeremy Moore, Pannan, Andy, Jeremy Jester, Eugene, Katie Hess, Elisa, Brittanie, Tovah, Denise (my cheering squad!), Ryan, Laurel, Stephanie Lauren, and especially Shannon and Isaac Richardson, you all know I couldn't have done this without you. I am amazed at what God has done through you in my life. Thank you. For everything.

For my friends Emily, Heather, Vieen, and Rachel who have stood by me through the worst and celebrated the best, I am truly grateful.

And finally, my loving family. You've supported me as I made my way through this 6-year-long journey, and you've always been there for me when I needed to talk. Especially my Mom and Dad, who have listened, offered suggestions, and encouraged me when it seemed like nothing was going to work out. This is for you.

ABSTRACT

SYNTHESIS AND CHARACTERIZATION OF PHOTOLABILE RUTHENIUM POLYPYRIDYL CROSSLINKERS WITH APPLICATIONS IN SOFT MATERIALS AND BIOLOGY

Teresa L. Rapp

Ivan J. Dmochowski

Since its discovery in 1844, ruthenium has solidified its position as the most widely used transition metal in catalysis and excited state chemistry. Its lower toxicity and relatively low price (compared to other platinum group metals) have enabled many applications of ruthenium coordination compounds. In this dissertation I discuss ruthenium polypyridyl complexes that undergo photoinduced ligand exchange, and how this unique property can be harnessed to develop next-generation smart materials and responsive chemical biology tools.

$Ru(LL)_2X_2^{2+}$ complexes, where LL is a bidentate aromatic heterocycle such as 2,2'-bipyridine, 1,10-phenanthroline, or 2,2'-biquinoline, and X is a pyridine-, nitrile-, sulfur-, or imidazole-based monodentate ligand, have the unique capability to undergo ligand exchange under visible light irradiation. We have harnessed this property to develop a series of visible-light-sensitive photodegradable crosslinkers by choosing X ligands that contain reactive moieties such as alkynes (for copper-mediated azide-alkyne cycloaddition (CuAAC)) or aldehydes (for Schiff base reaction with hydrazines).

$Ru(bpy)_2$(3-ethynylpyridine)$_2$ (RuBEP) has been used in CuAAC reactions to circularize azide-terminated oligonucleotides important for gene regulation or transcriptome analysis. $Ru(bpy)_2$(3-pyridinaldehyde)$_2$ (RuAldehyde) alternately employed aldehydes to react with hydrazine-modified hyaluronic acid (HA-HYD). The resulting hydrogel was cytocompatible, efficiently degraded with visible light, and well adapted for the storage and delivery of active enzymes via lysine-mediated crosslinking into the hydrogel matrix. Finally, $Ru(biq)_2$(5-hexynenitrile)$_2$ and $Ru(bpy)_2$(5-hexynenitrile)$_2$ were developed as crosslinkers to form PEG-based hydrogel, which was subsequently degraded using two different colors of visible light, orange and blue.

TABLE OF CONTENTS

LIST OF TABLES

LIST OF ILLUSTRATIONS

CHAPTER 1 – Ruthenium and its Photochemistry

1.1 A Basic History of Ruthenium Chemistry

The element number 44 was first described as a new metal isolated from platinum ores by Jedrzej Sniadecki, a Polish chemist, in 1803. However, his work couldn't be reproduced by other chemists, and he withdrew his claim on the element, as well as the name he had given it, *ruthenium*. Eventually, in 1844, Karl Karlovich Klaus made and stood by his claim that the dross separated from platinum during the refining process was made up of several other metals with similar but distinct properties. He focused on isolating one, resuscitating the name ruthenium, named after the Latin term for the area traditionally covering Ukraine, Belarus, western Russia, and parts of Poland and Slovakia.

Work with ruthenium continued into the 20th century, though ruthenium is a rare metal (it's the 74th most abundant metal in the Earth's crust, at around 100 ppm). One of the first ruthenium coordination compounds published in the literature was $Ru(bpy)_3^{2+}$, where bpy is 2,2'-bipyridine, was published in a brief communication in 1936 by Francis Burstall.[1] Burstall investigated certain optical properties identifying stereoisomers of the compound, and laid the groundwork for future extensive work on these remarkably stable complexes. In 1959, Paris and Brandt demonstrated for the first time the luminescence of a $Ru(bpy)_3^{2+}$ complex due to a charge transfer mechanism.[2] Ruthenium was one of the first 2nd or 3rd row transition metals to demonstrate any kind of luminescence as a coordination compound with organic ligands, and its relative inertness compared to the other early examples (such as chromium(III) and molybdenum(III) compounds, both rather toxic) suggested the possibility of use in living systems. In fact, Ru(II) chelates were found early on to be unusually stable in the presence of cells, though at mid-to-high concentrations (10 mM) was toxic to bacteria.[3,4]

Extensive work with $Ru(bpy)_3^{2+}$ and $Ru(phen)_3^{2+}$ (phen = 1,10-phenanthroline) complexes led to offhand observations that some complexes were rather photosensitive, especially when dissolved

in solution.[5] It took chemists until 1978 to make quantitative study of this photosensitivity in $Ru(bpy)_3^{2+}$-type complexes. Gleria and coworkers published a brief, one-page communication on the photoinitiated exchange $Ru(bpy)_3 \rightarrow Ru(bpy)_2Cl_2$ in chlorinated solvents which was the first attempt to identify the photoproducts of the reaction.[6] Thomas Meyer picked up on this newly elucidated process in one of his first papers on the subject, published in 1980.[7]

His Inorganic Chemistry article published in 1980 was the first in-depth discussion on the photolability of certain coordinated ligands on a $Ru(bpy)_2^{2+}$ system.[7] In this exposition he and coworkers discussed the various photochemical reactions they observed when irradiating $Ru(bpy)_2(L)_2$ complexes in the low-energy absorbance band located around 450 nm. With a combination of pyridine-based ligands, halides, SCN, in various coordinating and non-coordinating solvents, they came to the conclusion that this process likely occurs in a dissociative mechanism resulting in a pentacoordinate intermediate $Ru(bpy)_2L^{2+}$, before subsequent coordination of a coordinating solvent or halide counterion (in non-coordinating solvents) (**Figure 1.1**).[7]

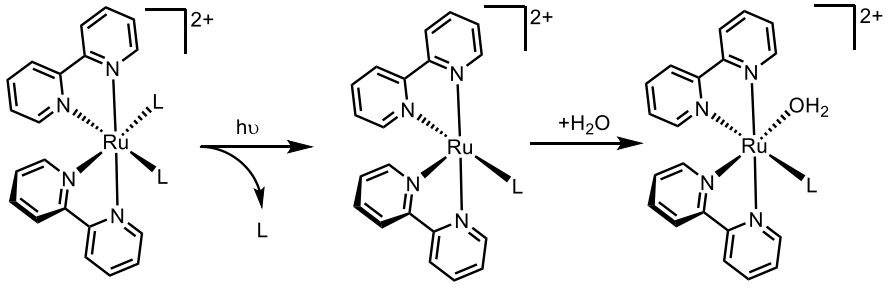

Figure 1.1. The first proposed mechanism for photoinduced ligand exchange, proposed by Meyer and coworkers in 1980.

In a follow-up paper published in 1982 Meyer and coworkers elucidated the first rough sketch of the energy diagram describing the process and the energy levels, this time for $Ru(bpy)_3^{2+}$ (**Figure 1.2**).[8] The electronic transition observed in an absorbance spectrum is a singlet metal-to-ligand charge transfer (^{1}MLCT in modern terms, ^{1}CT in **Figure 1.2**), which is coupled to two triplet states, one that is also MLCT in behavior, and one that is metal centered (^{3}d-d in **Figure 1.2**).

This energy diagram has been confirmed by DFT studies in recent years,[9] as well as a discussion on the relative levels of the ^{3}MLCT and ^{3}MC states, and the relationship for the quantum yield of photorelease.[10]

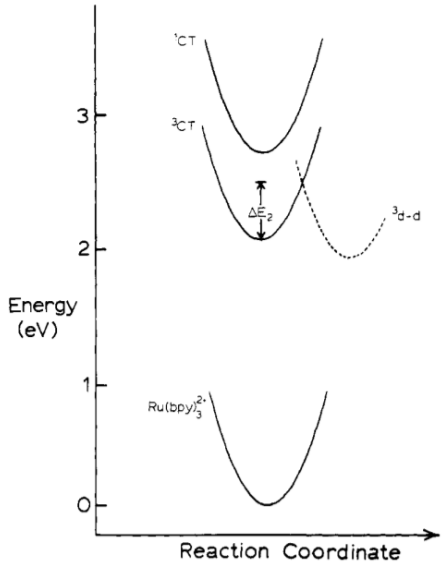

Figure 1.2. Sketch of the excited states of Ru(bpy)$_n$ complexes presented by Meyer in 1982. At this point the energy of the ^{3}d-d (later called ^{3}MC) state was unknown. Reproduced with permission (ACS Publications).

After this initial work in photosubstitution reactions with Ru(bpy)$_2^{2+}$-type complexes major avenues of research turned elsewhere, towards applications where excited electrons are the desired product, rather than a possible ligand exchange.[11,12] In some brief communications Walsh and coworkers investigated the photosubstitution reactions or Ru(tpy)(L)$_3^{2+}$, where tpy is terpyridine,[13] which occurred in a similar fashion to Ru(bpy)$_2^{2+}$ complexes. Ford and coworkers began work on Ru(η^6-arene)L$_3^{2+}$ complexes that were also photoreactive, exchanging one or more L ligands for a coordinating solvent.[14] Several mechanistic studies confirmed the dissociating mechanism for all ruthenium polypyridyl type complexes.[15,16] Yet this unique property of ruthenium polypyridyl complexes to undergo photoinitiated ligand exchange with a solvent molecule remained simply a parlor trick, a property that was inherent, annoying at times, and that had no positive application.

1.2 Photoinduced ligand exchange

It wasn't until 2003 that the first application of this photoresponsive property was presented in the literature. In his groundbreaking paper, cited over 110 times to date, Etchenique and coworkers described the coordination of neurotransmitter 4-aminopyridine (4AP) to $Ru(bpy)_2^{2+}$.[17] 4AP was then released with visible light irradiation into the ^{1}MLCT (<480 nm) on a timescale sufficient to observe the effects on neuronal firing in leeches. This positioned $Ru(bpy)_2^{2+}$ as a caging group for bioactive molecules, that is, a protecting group that blocks the activity of molecules until "uncaged" or removed by irradiation. While $Ru(bpy)_2(4AP)_2^{2+}$ is not the first example of a visible light-triggered uncaging event, it is the first visible light triggered caging group for complex bioactive molecules other than small molecules such as cations[18] or NO.[19] Then, in a subsequent paper just 2 years later, Etchenique showed that the same process was achievable using highly focused multiphoton activation with 750 nm light.[20] Multiphoton absorption pushed the wavelength of activation solidly into the wavelength region necessary for any clinical applications, known as the photodynamic therapy window, between 650 and 900 nm.

This groundbreaking work opened many new avenues of research in ruthenium photochemistry. Just a couple of years later Etchenique presented $Ru(bpy)_2^{2+}$ as a versatile caging group for amines as well. He presented the caging and release of several neurotransmitters such as tryptamine, butylamine, serotonin,[21] glutamate,[22] and GABA (gamma-aminobutyric acid).[23] Etchnenique also used $Ru(bpy)_2^{2+}$ to cage nicotine in the first ever example of a nicotine caging group, with the added benefit of the capability to use violet, blue, or even green single photon light for uncaging.[24]

In the midst of this work developing $Ru(bpy)_2^{2+}$ as a caging group for small molecules, the Turro lab also began work on ruthenium polypyridyl compounds, with a focus on developing their bifunctionality. In 2004 Turro and coworkers presented $Ru(bpy)_2(NH_3)_2^{2+}$ as a phototriggered second generation cisplatin.[25] Under irradiation with near-UV light both ammine ligands were exchanged with water, in a manner similar to the chemical changes cisplatin undergoes prior to

binding to DNA, except with light, instead of low chloride concentration, as the trigger. The subsequent photoproduct $Ru(bpy)_2(H_2O)_2$ was capable of binding to DNA like cisplatin.

Having a bioactive $Ru(bpy)_2(H_2O)_2^{2+}$ photoproduct is beneficial when designing cell-harming targets, like anti-cancer drugs that will bind to DNA or other protein targets. Turro's group used the $Ru(bpy)_2$ core to cage and deliver common anti-cancer drugs. Their first work described the caging, release, and cellular toxicity of 5-cyanouracil, a version of 5-fluorouracil, a chemotherapy drug that's been used for over 20 years in the treatment of multiple types of cancer, and as a co-drug to increase the efficacy of other chemotherapy agents.[26] A second generation of the dual-action prodrug used $Ru(tpy)(5\text{-cyanouracil})_3$ as the caging group/phototriggered prodrug, a construct that was successful in *in vitro* cell studies.[27]

This new dual-action drug delivery opened many new avenues of research, centered around the delivery of a bioactive molecule and a ruthenium-based DNA binding core. With their focus on cancer development and anti-cancer drugs, the Turro group has identified a specific need for the caging of nitrile groups.[28] With no other photocaging group available to use with nitriles and a whole class of cathepsin proteases implicated in cancer development that can be inactivated with nitrile-containing inhibitors (such as cathepsin B),[29,30] $Ru(bpy)_2$ and its derivatives become viable options. Turro and coworkers have caged several different cysteine protease inhibitors with $Ru(bpy)_2$ and Ru(TPA) (where TPA = tris(2-pyridylmethyl)amine), in each case successfully inhibiting cathepsin B after irradiation with visible light.[31,32]

1.3 Blue is great, red is even greater

One of the strengths of the ruthenium phototriggering system is the large amount of variations in ruthenium compounds, and the potential to shift the ^{1}MLCT further to the red. Meyer's first sketch of the electronic structure of these compounds has been confirmed by recent expositions of the electronic structure.[9] (**Figure 1.3**) In ruthenium polypyridyl complexes the lowest energy transition is a metal-to-ligand charge transfer (MLCT), with a λ_{max} in the visible region. This singlet MLCT is

electronically coupled to a triplet MLCT, where rapid intersystem crossing (ISC, QY = 1, <1 ps) occurs from the ^{1}MLCT to the ^{3}MLCT. From here there is a nearby triple metal centered state, ^{3}MC, with significant antibonding character between the ruthenium and its ligands, leading to the dissociation of a ligand. Recent work has confirmed a pentacoordinate intermediate for these types of reactions ($Ru(bpy)_2(L)$, **Figures 1.1, 1.3**) which may be relatively long-lived, on the order of ~70 ps, before backfilling with water to make the photolysis product $Ru(bpy)_2L(H_2O)$.[33,34]

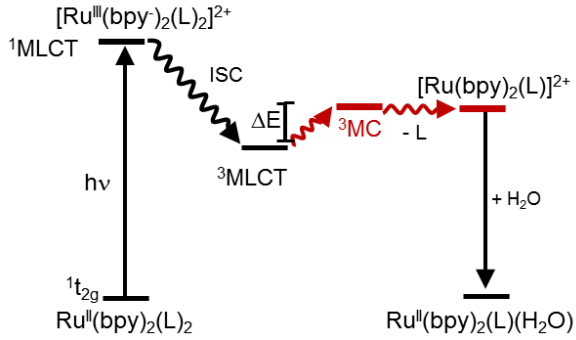

Figure 1.3. Modern Jablonski diagram showing the confirmed electronic states for the excitation of ruthenium polypyridyl compounds.

Shifting the ^{1}MLCT to the red is relatively simple: incorporating electron-poor ligands with extended pi structure will decrease the Δ_o and the energy gap for the MLCT, but concurrently it will widen the gap between the ^{3}MLCT and ^{3}MC, resulting in inefficient crossover and a poor QY. Therefore, it becomes necessary to not only reduce the ^{1}MLCT energy to red shift the absorbance, but also to reduce the ΔE between the ^{3}MLCT and the ^{3}MC states. Decreasing the energy of the ^{1}MLCT is accomplished by incorporating electron withdrawing ligands, decreasing ΔE is a little more complicated.

Adding steric strain and disrupting the octahedral field around the ruthenium effectively decreases ΔE and increases population into the ^{3}MC state. First described in a Ru(tpy)(LL)(py) system, the exchange of a bpy for a sterically crowded Me_2bpy (where Me_2bpy is 6,6'-methyl-2,2'-bipyridine) increased the quantum yield of pyridine exchange more than 1000-fold (from $<10^{-4}$ for bpy to 0.16 for Me_2bpy).[35] This technique for increasing the QY of photorelease has since been applied to

other systems as well.[36] The difficulty here lies in striking that fine balance between thermal stability and photolability. Too much strain and the monodentate ligands will exchange with solvent in the dark, and too little strain renders compounds with very low quantum yields.

1.4 The future of ruthenium photolabile complexes

Ruthenium now holds the prominent position as the most employed metal in catalysis and photochemistry. Its low toxicity and relatively low price point (compared to other platinum-group metals) have made ruthenium compounds the preferred choice for many applications.[37] In biology and biomaterials ruthenium polypyridyl complexes show unique promise as translational applications demand a red shift in absorbance. For nearly all applications in the clinic phototriggered events should respond to light in the photodynamic therapy window, 650 – 900 nm. Ruthenium-based prodrugs are already pushing into this window, albeit slowly and with minimal QYs.[38–40] Ruthenium polypyridyl complexes are also finding use in soft biomaterials, with several examples of ruthenium-based hydrogel materials or nanoparticles that can be degraded with light in the PDT window.[41]

For biological applications ruthenium is positioned well because of its extensive visible light absorbance, but in many cases where cell death is not desired, steps must be taken to mediate the cytotoxicity of the compounds. Thus, for these applications a ruthenium construct that remains attached to a larger framework or macromolecule is desirable. A $Ru(bpy)_2^{2+}$ construct as a photodegradable crosslinker had not been proposed at the beginning of my work in this thesis, and to date only one other application of ruthenium compounds as crosslinkers has been published.[42] Ruthenium photodegradable crosslinkers is a new field of research, one that warrants more innovation, and may be a vital part of the general push towards red and near-IR light activated prodrugs and materials.

CHAPTER 2 – Synthesis and Characterization of Alkyne-Modified Ruthenium Crosslinker, RuBEP

Material in this chapter was originally published in *Chemical Science*. It has been adapted here with permission from the publisher.

Reprinted with permission from Griepenburg, J.C.; Rapp,T.L.; Carroll, P.J.; Eberwine, J.; and Dmochowski, I.J. Ruthenium-Caged Antisense Morpholinos for Regulating Gene Expression in Zebrafish Embryos. *Chem. Sci.* **2015**, *6*, 2342-2346

2.1 Introduction

Though the photolability of some types of ligands on ruthenium compounds was first observed in the 1960s,[5] this property was not harnessed until 2003 when the first $Rubpy_2L_2$ compound (where L is a pyridine-type ligand) enabled photorelease of 4-aminopyridine, a neurotransmitter.[43] Etchenique et al. showed that the compound $Rubpy_2(4\text{-aminopyridine})_2^{2+}$ was photoactive exchanging one 4-aminopyridine ligand with water upon irradiation with visible light into the MLCT absorbing band. This ligand exchange was rapid, on the order of tens of picoseconds, which is much faster than almost all biological processes. This first description of photoinduced ligand exchange positioned the $Rubpy_2$ core as a caging group for small molecules, i.e., to block the activity of the small molecule until released with light.

Since the first breakthrough with 4-aminopyridine, the $Rubpy_2^{2+}$ core has been used to cage multiple different types of pyridine-based drug targets. Sadler and coworkers recently reported the viability of $Rubpy_2$ as a caging group for isoniazid, and anti-tuberculosis compound that contains a pyridine moiety.[44] The use of light in this case is a valuable targeting strategy, as isoniazid treats mycobacterial infections which occur primarily on the surface of skin or in the lungs. Their construct, $Rubpy_2(\text{isoniazid})_2^{2+}$ was found to be highly active against four strains of bacteria, with significant difference between samples kept in the light and in the dark.[44]

$Rubpy_2^{2+}$ has also been used to cage ligands via an imidazole, albeit with lower efficiency of ligand exchange. Mosquera et al. generated a histidine caging group $Ru(bpy)_2(PPh_3)$(His-fmoc), which could be subsequently incorporated into a peptide via standard solid-phase synthesis.[45] It knocked out the zinc-binding activity of zinc finger nuclease peptide RGH when the H was coordinated to the ruthenium, and restoring activity after irradiation. Zamora et al. also worked to generate an imidazole-based metyrapone prodrug to inhibit cytochrome P450, which can sensitize cells to anti-cancer drugs that modify DNA. They demonstrated that metyrapone can be caged in the compound $Ru(bpy)_2(\text{metyrapone})_2$, and released with a visible light trigger.[46] They found that extended irradiation with 463 nm light was sufficient to cleanly release both

metyrapone drugs, freeing up the $Ru(bpy)_2(H_2O)_2$ core to bind to DNA and trigger apoptosis, increasing the effectivity of the drug as an anti-cancer target.

In other cases, two free coordination sites (as in $Ru(bpy)_2$ complexes) are not necessary, and more multidentate polypyridyl ligands can be used to eliminate one of those positions. For this, the Ru(tpy)(LL)(X) complex is popular, where tpy is tripyridine, LL is one of several bidentate ligands, and X is the photolabile ligand. Lameijmer and coworkers recently caged a cytotoxic nicotinamide phosphoribosyltransferase (NAMPT) inhibitor with Ru(tpy)(biq), which exhibited phototriggered activity using red light (625 nm).[47]

The Turro group has also worked with the Ru(LLL)(LL) platform, incorporating a variety of bi- and tridentate ligands to shift the MLCT λ_{max} further red. An example of this is the recently published $Ru(py\text{-}dppn)(biq)(py)^{2+}$ complex that has dual actionality to intercalate with DNA via the py-dppn, absorb light into the photodynamic therapy window (600-850 nm) due to the extended pi structure of the biq, and exchange the pyridine upon irradiation with visible light.[48]

My first project built on this core principle: a pyridine-based ligand coordinated to $Ru(bpy)_2^{2+}$ will be exchanged rapidly upon irradiation with visible light, and likely only one of two coordinated pyridines will be exchanged in this process. Our initial goal for this project was to generate a visible-light responsive photodegrading crosslinker with alkyne groups for subsequent copper mediated azide-alkyne cycloaddition (CuAAC). The immediate application was to circularize and cage DNA oligonucleotides (ODNs) via azide modifications on both termini, wherein a series of ruthenium crosslinkers was proposed to complement the variety of constructs with *o*-nitrobenzyl caging groups. The first alkyne modified ruthenium crosslinker used for ODN cyclization was $Rubpy_2(3\text{-ethynylpyridine})_2^{2+}$, or RuBEP.

2.2 Results

Synthesis of RuBEP

RuBEP was synthesized via a triflate intermediate from commercially available *cis*-Ru(bipyridine)$_2$Cl$_2$ (Acros Organics) (**Scheme 2.1**) and 3-ethynylpyridine (3EP).[49] Reaction progress was monitored by UV-Vis spectroscopy until an MLCT band at 450 nm was observed. The PF_6^- salt (RuBEP[PF_6]$_2$), synthesized by metathesis with ammonium hexafluorophosphate in cold water, was purified in the dark by silica column chromatography using 1:9 acetonitrile: dichloromethane as the eluent. The water-soluble chloride salt (RuBEP) was then generated by metathesis with TBACl in cold acetone. Final yield was 60-70%.

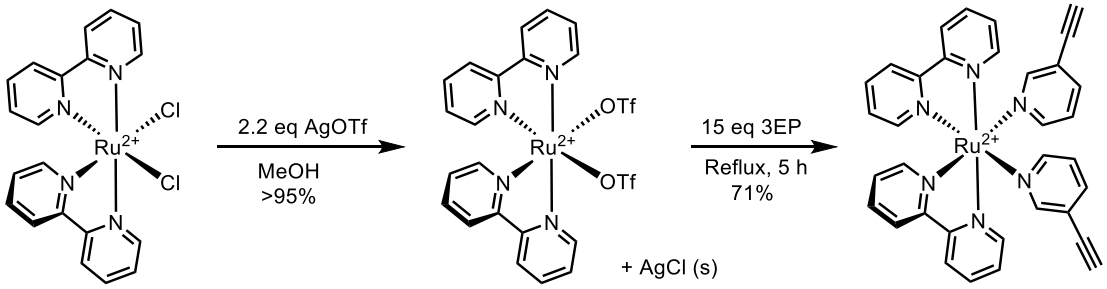

Scheme 2.1. Synthesis of RuBEP

Photochemistry

Various techniques are used to characterize the important electronic transitions for these compounds and discuss their viability for ligand photosubstitution. The ligand exchange is facilitated by the population of a metal-centered state with an excited electron. Irradiation into the low-lying singlet metal-to-ligand charge transfer (^{1}MLCT) band (~450 nm for RuBEP) excites an electron into the ^{1}MLCT, which is electronically coupled to two triplet states, the ^{3}MLCT and a metal centered state (^{3}MC). The ^{3}MC has antibonding character between the ruthenium and its ligands, and is thought to be responsible for ligand exchange. (**Figure 2.1**). Photoinduced ligand exchange occurs rapidly, on the order of tens of ps. Seminal work from the Turro lab described

the electronic process for $Rubpy_2MeCN_2$ → $Rubpy_2MeCN(H_2O)$, which involves the generation of a pentacoordinate intermediate $Rubpy_2MeCN$ formed within 18 ps of excitation, followed by water coordination over 77 ps.[33]

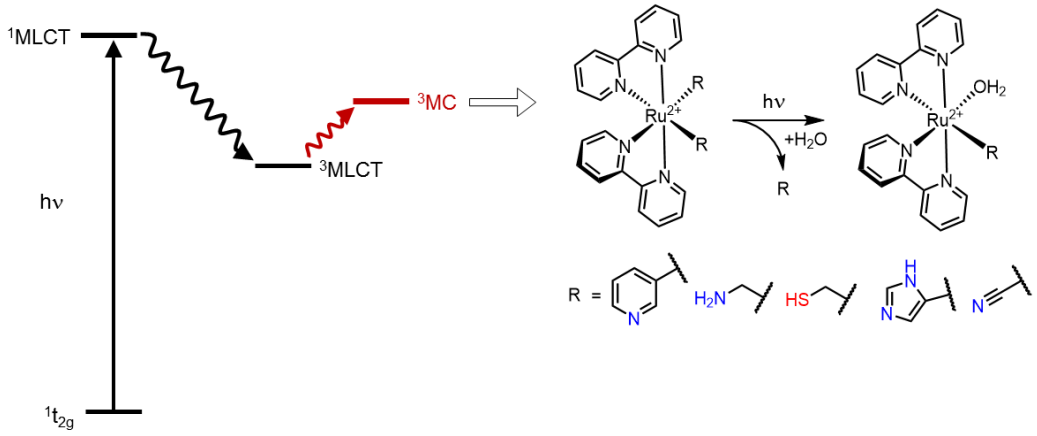

Figure 2.1. Jablonski diagram (left) showing the relevant electronic structure leading to ligand exchange.

The absorbance spectrum for a $Rubpy_2py_2^{2+}$ compound exhibits several maxima in the UV and in the blue region of the visible spectrum:[50] ~250 nm corresponds to a high energy MLCT, ~300 nm are the primary π → π* transitions in the bpy, the band at 350 nm corresponds to the t_{2g} → e_g metal centered state, and the important maximum at ~450 nm from the low-level MLCT. (**Figure 2.2**) Irradiation into any one of these maxima results in photoinduced ligand exchange, as the ^{3}MC state responsible for ligand exchange is accessible from any one of them.

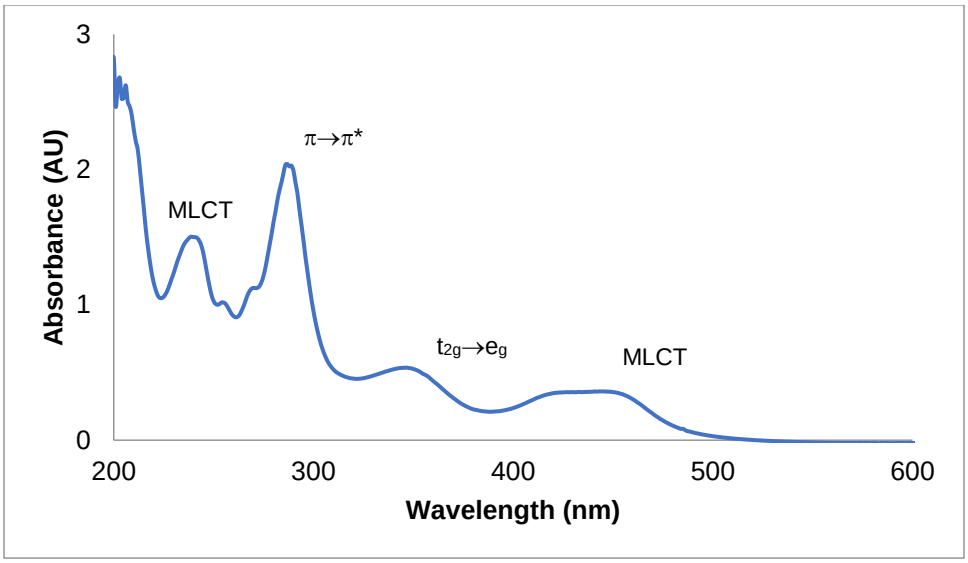

Figure 2.2. UV-Vis absorption spectrum of $Rubpy_2py_2$.

Because the direct result of irradiation is a change in the first coordination sphere on the ruthenium, we observe a shift in the 450 nm λ_{max} to the red, as in all cases a weak field ligand is exchanged for a strong field ligand. The photolysis can be tracked by UV-Vis absorption spectroscopy to determine a bulk timescale (min-hrs to completely degrade a large sample) and confirm photoproducts. Isosbestic points can be a handle on the mechanism of ligand exchange, as well as defining the cleanliness of the reaction. An isosbestic point is defined as a point in the absorption spectra at which the absorbance of the solution remains constant as the composition of the solution changes. For an isosbestic point to occur the starting material and the product must be linearly related by stoichiometry, that is, no other rate limiting intermediate species or third product occurs over the course of the reaction. The presence of one or more isosbestic points indicates that it is very highly likely that only two species stoichiometrically related to each other are present at any given time in the reaction, ruling out the occurrence of side products.

RuBEP has the same UV-Vis absorption as its cousin $Rubpy_2py_2$, with significant maxima in the UV corresponding to ligand-centered transitions and higher energy MLCT bands and a strong MLCT centered around 450 nm. (**Figure 2.3**) Photodissociation of 3EP from RuBEP was

monitored by UV-Vis, LCMS, and ^{1}H NMR (**Figure 2.4**) spectroscopies. The primary shift occurs in the visible region, for the λ_{max} of the compound due to the MLCT. Some small changes are also observed in the LC states in the UV, but this is more prominent in Ru(II)biquinoline compounds. Upon continuous irradiation with 450-nm laser (53 mW/cm^2, focused to 0.5 cm^2), the λ_{max} red-shifted from 450 nm to 473 nm. Complete photolysis of the bulk RuBEP solution (80 µM, 1.5 mL, stirred) occurred in 5 min. The red-orange photo-product with a λ_{max} at ~475 nm matches the spectrum of the with previously characterized $[Ru(bpy)_2(pyr)(OH_2)]^{2+}$ complex,[51] indicating that $[Ru(bpy)_2(3EP)(H_2O)]^{2+}$ was our final photoproduct. Two small isosbestic points were observed with one major point, as expected for the exchange of one pyridine ligand without formation of rate-limiting intermediates.[38]

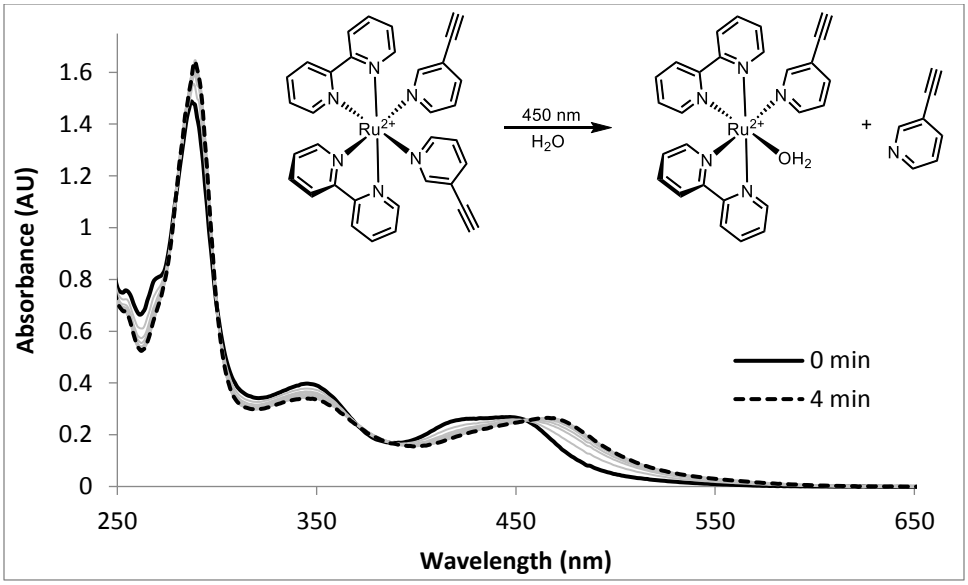

Figure 2.3. Photolysis of RuBEP observed by UV-Vis.

^{1}H NMR shifts during irradiation

^{1}H NMR also showed the exchange of only one 3EP ligand with a solvent water molecule, based on a shifted alkyne peak and change in integration (**Figure 2.4**). Over the course of irradiation, the primary alkyne peak at 3.707 ppm decreases and a new alkyne peak at 3.75 ppm appears, corresponding to free 3EP. The two alkyne peaks integrate to a ratio of 1.4:1 free:coordinated

3EP, indicating complete exchange of one 3EP, with some full conversion to $Rubpy_2(H_2O)_2$ under constant high-power irradiation. The loss of symmetry in the remaining complex gives a more complex peak pattern in the aromatic region as well. HR-MS also confirmed the major photoproduct assignment (**Figure 2.4**).

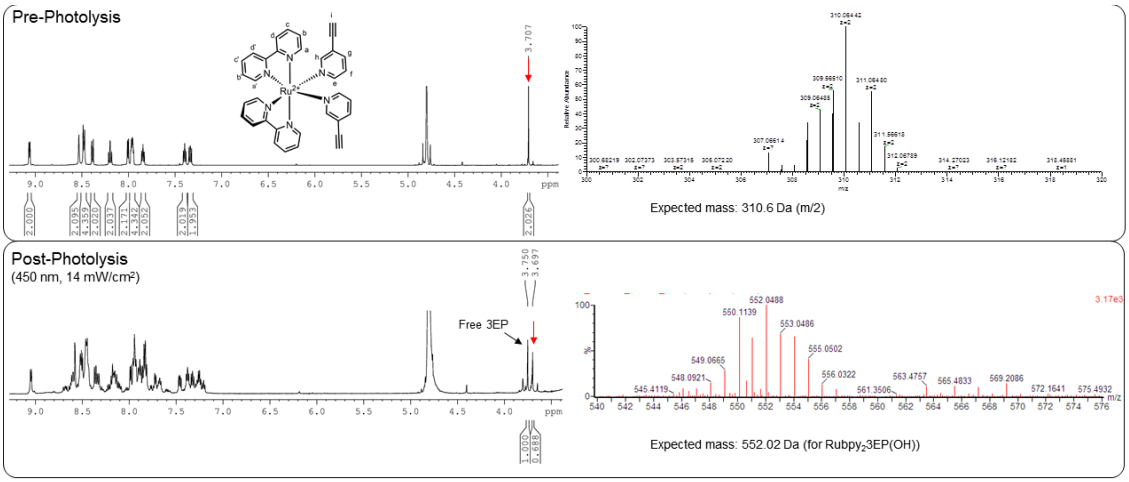

Figure 2.4. ^{1}H NMR and Hi-Res ESI pre- and post-photolysis.

Quantum Yield Determination

Each ruthenium compound is assigned a quantum yield of ligand exchange, a number similar to the quantum yields of fluorophores, but fundamentally different. The quantum yield of ligand exchange is defined as

$$\varphi = \frac{\Delta moles\ of\ product}{\Delta moles\ of\ photons}$$

The quantum yield of ligand exchange in water in ambient conditions (Φ_{pr} = 0.33 $\pm$ 0.06) was determined by fitting the initial kinetics of the photoreaction (**Figure 2.5**). This was comparable to the quantum yield of ligand exchange reported for $Ru(bpy)_2(pyr)_2Cl_2$ (Φ_{pr} = 0.4).[43] The uncaging efficiency for RuBEP (ε_{450} times Φ_{pr}) was determined to be 2.0 x 10^3 $M^{-1}cm^{-1}$ at 450 nm, which is much higher than measured for typical organic chromophores activated at near-UV wavelengths.

Commonly used nitrobenzyl derivatives, for example, have uncaging efficiencies less than 100 $M^{-1}cm^{-1}$ at 365 nm.[52,53]

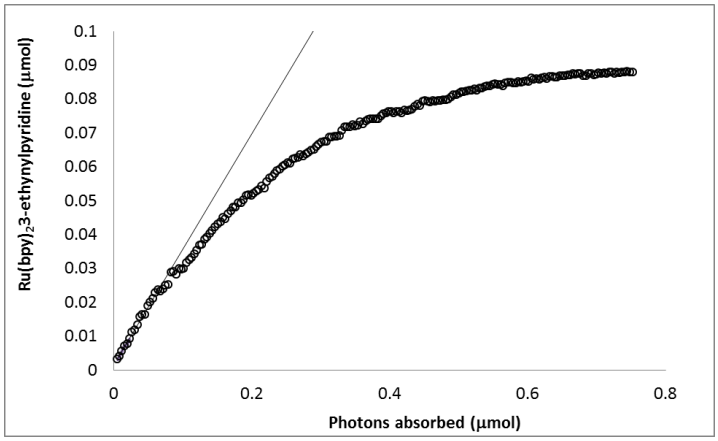

Figure 2.5. Determining the quantum yield of the photoreaction. The slope of the initial time points is the quantum yield.

Electrochemistry

Electrochemistry has long been used to discuss the relative ease of population of the excited states. The oxidation of Ru(II) to Ru(III) tends to correlate with the quantum yield, with some outliers.[54] In our own work, this trend is less evident than previously proposed. There does not appear to be a trend correlating $E_{1/2}$ and QY (**Figure 2.6**).

	Compound	QY	$E_{1/2}$ (eV)
1	$Rubiq_2PN_2^{2+}$	0.06	1.2
2	$Rubpy_23EP_2^{2+}$	0.33	0.965
3	$Rubpy_2py_2^{2+}$	0.4	1.17
4	$Rubpy_2$4-pentynenitrile$_2^{2+}$	0.43	1.095
5	$Rubpy_2(CH_3CN)_2$	0.4	1.00
6	$Rubpy_2$pyridinaldehyde$_2^{2+}$	0.6	1.00

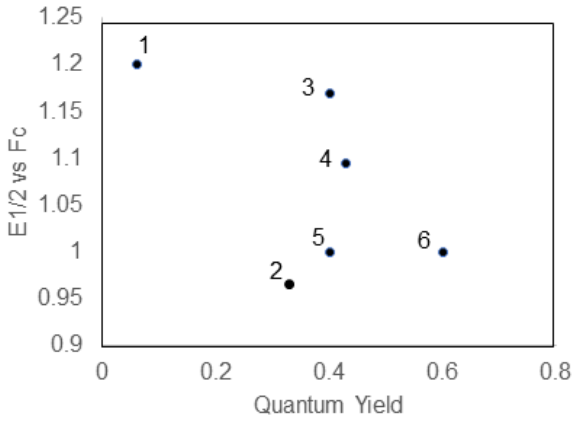

Figure 2.6. Graph of $E_{1/2}$ vs QY does not show any discernable trend between the two values.

The electrochemistry of RuBEP is exactly as we predict for a ruthenium polypyridyl complex with redox innocent ligands. (**Figure 2.7**) Two reduction peaks at -1.74 and -1.90 eV (vs Fc) are due to 1-electron reduction of each bpy (bpy → bpy^-). The oxidation peak at 0.965 eV corresponds to the oxidation of the metal center (Ru^{+2} → Ru^{+3}).

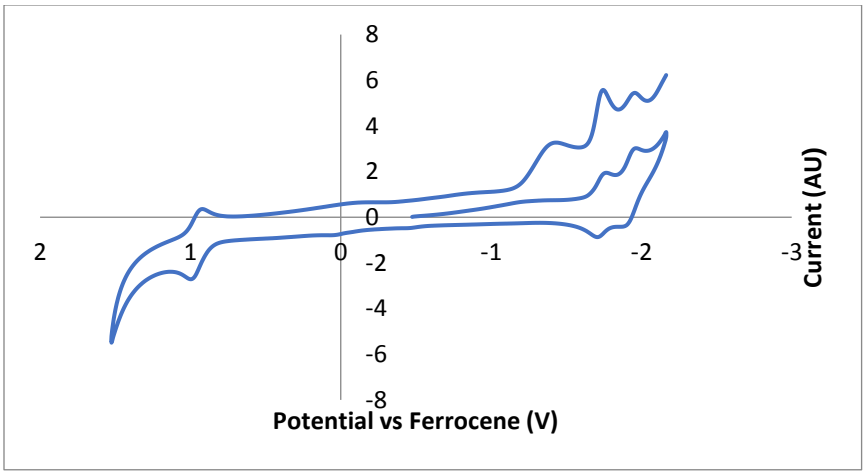

Figure 2.7. Cyclic voltammogram of RuBEP in acetonitrile.

Ultrafast Transient Absorption

The photoinduced ligand exchange of Ru(II) complexes is frequently described as being incredibly rapid, on the order of tens to hundreds of picoseconds. Liu and coworkers elucidated the timescale of ligand exchange for $Ru(bpy)_2(MeCN)_2$, identifying a pentacoordinate intermediate and the rate limiting step for the exchange as the coordination of a water.[33] In short, Liu determined that the population of the ^{3}MLCT state was ~5 ps, followed by a slower transition to the ^{3}MC state and generation of a pentacoordinate intermediate (~18 ps). Coordination of a water was the slowest step in the process, taking 77 ps to produce $Ru(bpy)_2(MeCN)(H_2O)$.

In recent work on $Ru(bpy)_2(nicotinamide)_2$, with a pyridine-based ligand similar to 3-ethynylpyridine, Greenough and coworkers determined a much slower timescale for ligand exchange compared to a nitrile-based ligand, as well as elucidating an intermediate signal occurring after the population of the ^{3}MC.[34] Greenough observed a signature with a time constant of 183 ps that corresponded to population of the ^{3}MC state from the ^{3}MLCT, followed by another

signature corresponding to the loss of the nicotinamide ligand and generation of the pentacoordinate intermediate, with a time constant of 168 ps. Coordination of water in their system took much longer, on the order of 151 ps to form the final product, $Ru(bpy)_2(nicotinamide)(H_2O)$.

We performed ultrafast transient absorption spectroscopy on RuBEP in collaboration with Prof. Jason Baxter at Drexel University. RuBEP (0.9 mM in DI water) was deoxygenated by bubbling with N_2 and the spectral changes were observed using a 350 nm pump laser. Our findings for RuBEP correspond more closely with the time constants Turro and coworkers, summarized in **Figure 2.8**.

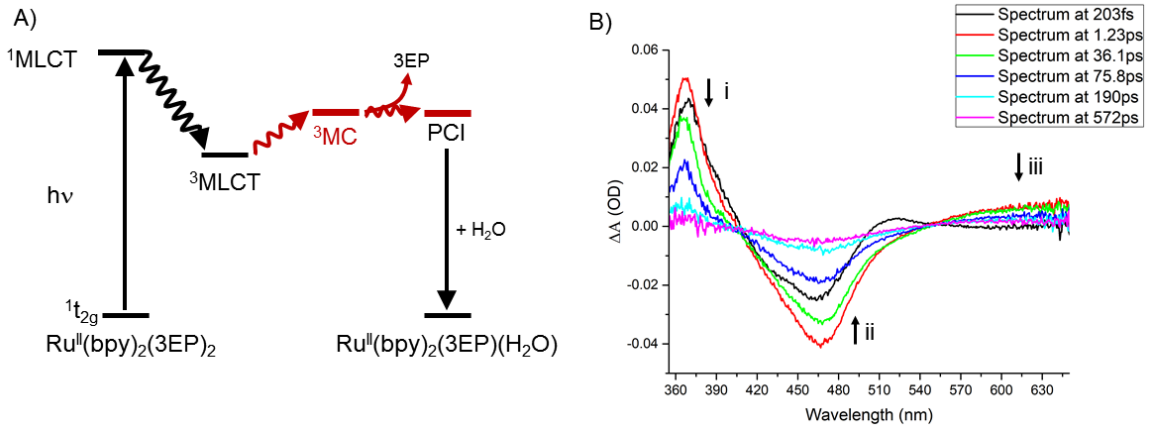

Figure 2.8. Ultrafast kinetics for RuBEP. A) Jablonski diagram for RuBEP with the times associated with each transition. B) Transient absorption spectra for RuBEP in water at select time delays.

Transient absorption spectra for RuBEP show three significant features appearing between 1 and 500 ps. The positive feature at 366 nm corresponds to an MLCT signal, specifically, a bpy^- anion generated by electron transfer from the Ru to a bpy; based on previous work with $Ru(bpy)_3^{2+}$ excited states.[55] A significant bleach at 460 nm was assigned to the ground state bleach,[34] and the plateu observed at >550 nm corresponds to a pentacoordinate intermediate (PCI), confirmed by gas-phase absorption studies.[56] Time constants for the features observed (i – iii) were determined by fitting the kinetics traces at each wavelength (366, 460, and 600 nm respectively).

They indicate that each of the three processes observed occur on similar timescales, 99 ± 7 ps for (i), 85 ± 5 ps for (ii), and 87 ± 9 ps for (iii).

Crystal Structure

Crystals of RuBEP[PF_6] for X-Ray diffraction were grown by evaporation of methanol and acetonitrile into water. Bond lengths and angles were compared to a crystal structure of $Ru(bpy)_2(pyridine)_2$ (Rupy), grown via the same method.

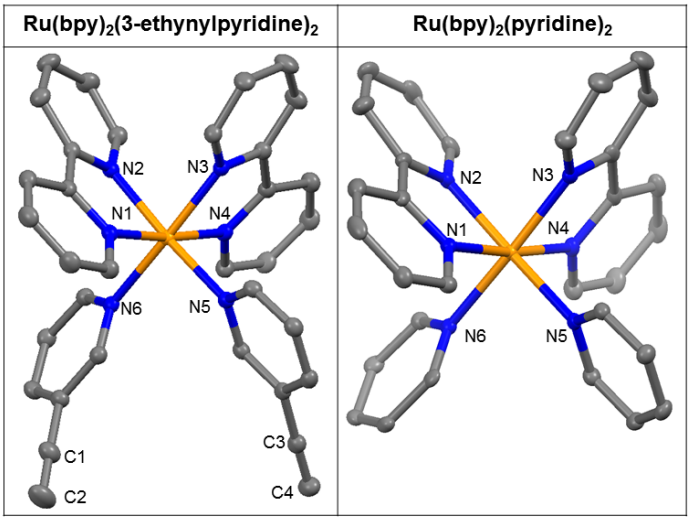

Figure 2.8. Crystal structures of RuBEP and Rupy.

Bond		**RuBEP**	**Rupy**
Ru-bpy (left)	Ru-N1	2.066	2.066
	Ru-N2	2.059	2.062
Ru-bpy (right)	Ru-N3	2.062	2.063
	Ru-N4	2.075	2.067
Ru-pyridine	Ru-N5	2.098	2.090
	Ru-N6	2.108	2.099
	C2-C4	6.188	N/A
	Py-Ru-Py	92.52°	91.26°

Table 2.1. Select bond distances for RuBEP and Rupy.

RuBEP does not differ from Rupy significantly, suggesting that the addition of the alkynes on the pyridine ligands does not affect the structure of the compound. Bond lengths to the pyridine ligands are within the expected range, with minor differences between the two (Ru-N5 vs Ru-N6 shows only a 0.1 Å difference). Notably, the distance between the two alkynes in RuBEP is around 6.2 Å, with twisting of the two 3-ethynylpyridine ligands pointing the alkynes away from each other and positioning them for subsequent click reaction. The inflexibility of the pyridine ring and appended alkyne suggest that this distance is likely the same in solution, with minimal rotation or repositioning. The angles between the two pyridines are close to 90° for both. Overall, the crystal structure suggests that RuBEP should be a thermally stable compound, with standard bond lengths and angles contributing to an overall stable structure in the absence of light.

Circularizing Oligonucleotides

Molecular caging groups have been in use in research and the clinic for over 50 years.[57,58] Many of these phototriggers are used to cage small biomolecules like the examples discussed previously, but a growing field of study is the development of caging groups for biomacromolecules. The Dmochowski lab has focused on the caging of oligonucleotides with photocleavable linkers, enforcing a secondary structure or attaching blocking strands of DNA or RNA to constructucts.[59,60] This enables us and others to determine when and where the oligonucleotide is biologically active in a sample of cells or in a growing embryo. RuBEP is the first photocleavable linker described that is capable of rapid degradation using minimal photon flux of visible light.

RuBEP was designed to circularize antisense single-stranded oligonucleotides (ASOs) through CuAAC. DNA ASOs (25-mer) were purchased from IDT with azides on both the 5’ and 3’ termini, and circularized with RuBEP in the presence of CuBr, sodium ascorbate, and TPTA in a solution of 5% DMSO(**Figure 2.9A**).

The circular ASOs were shown to be well-caged using a molecular beacon experiment. In brief, 3x excess of a molecular beacon with a complementary sequence was incubated with the linear, circular, and irradiated circular ASO at room temperature and the resulting fluorescence was measured. A high fluorescent intensity indicated opening of the beacon and high activity of the sequence (observed in the linear and irradiated samples), while a low fluorescence indicates the ASO is incapable of binding its complement and therefore inactive (observed for random sequences and the circular ASO). (**Figure 2.9B**) For *in vivo* experiments the same circularization method was used in the more robust morpholine-based oligonucleotide (same sequence, with a morpholine backbone instead of a charged phosphate linkage). The morpholino took longer to circularize fully, potentially due to copper coordination and sequestration by the morpholine backbone.

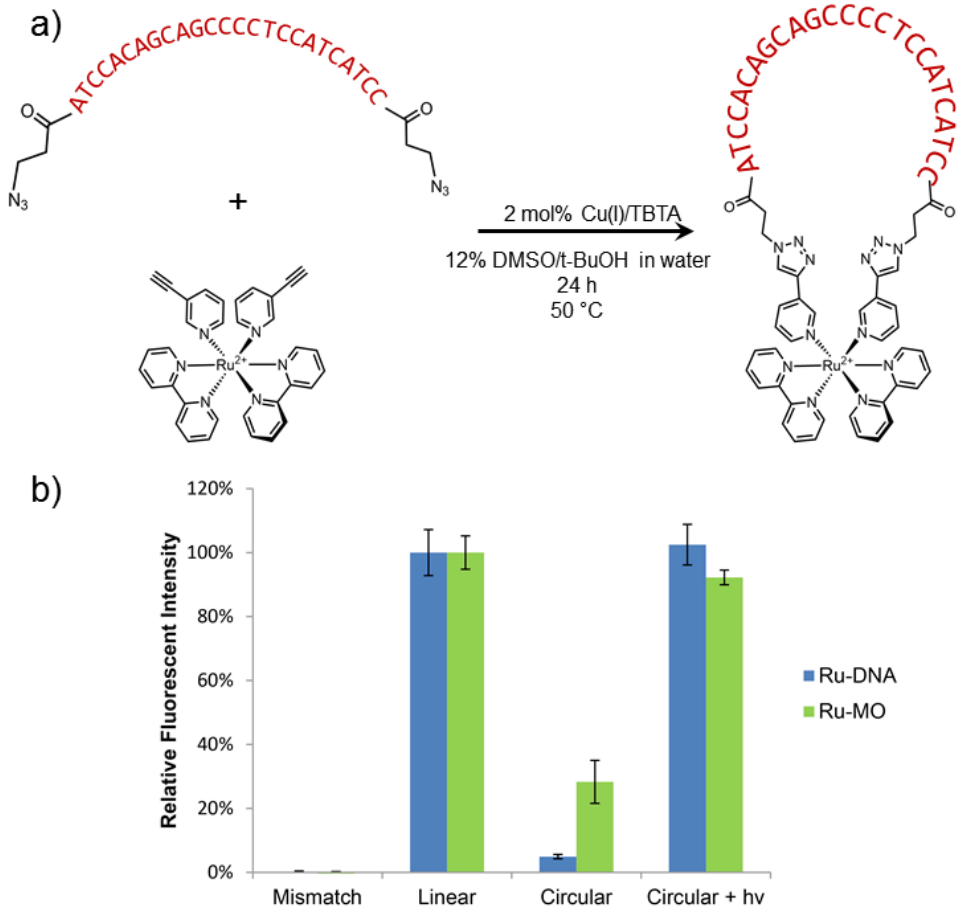

Figure 2.9. Circularized ASOs using RuBEP. A) Circularization scheme. DNA-based oligonucleotides took significantly less time to react than morpholine-based oligonucleotides, and were more caged overall. B) Molecular Beacon data demonstrating the effective caged-ness of the oligonucleotides, both for DNA-based oligos and morpholino-based (MO).

2.3 Conclusions

In conclusion, RuBEP is the first example in literature to date of a ruthenium-based photodegradable crosslinker for complex biomolecules. It has been used to cyclize ASOs and morpholinos, which are sufficiently caged to modulate gene knockdown in zebrafish embryos. It undergoes rapid photoinduced ligand exchange with ≤530 nm light with an unusually high quantum yield and efficiency. Based on this early success, subsequent compounds like RuBEP were synthesized and modified with different reactive moieties for other crosslinking applications.

2.4 Methods

Synthesis of Ru(bpy$_2$(3-ethynylpyridine)$_2$

$Ru(bpy)_2Cl_2$ (101.8 mg, 0.20 mmol) and $AgSO_3CF_3$ (105 mg, 0.41 mmol) were suspended in distilled methanol (10 mL). 3-ethynylpyridine (3EP, 201.7 mg, 0.40 mmol) was added and the reaction was heated to 75 ^oC for 5 h until no further changes were observed by UV-Vis spectroscopy. The methanol was removed under reduced pressure and product was redissolved in boiling water. Solid ammonium hexafluorophosphate was added to the chilled solution until a light orange precipitate was formed. This was vacuum filtered, washed twice with cold water and dried. Compound was further purified by 1.5 x 15 cm silica column (230-400 mesh) with 9:1 dichloromethane:acetonitrile as eluent and isolated in 71% yield (106.6 mg, 0.12 mmol). The water-soluble chloride salt was synthesized by addition of tetrabutylammonium chloride to a solution of $[Ru(bpy)_2(3EP)_2](PF_6)_2$ dissolved in acetone.

^{1}H NMR (500 MHz, CD_3CN) 3.74 (s, 1H, 3EP-H_5), 7.33 (dd, 1H, J = 7.9, 3EP-H_3), 7.39 (ddd, 1H, J = 6.7, bpy-H_3), 7.82 (ddd, 1H, J = 6.4, bpy-H_6), 7.90 (d, 1H, J = 5.4, bpy-H_1), 7.95 (dd, 1H, J = 5.8, 3EP-H_2), 7.97 (dd, 1H, J = 7.6, bpy-H_2), 8.19 (td, 1H, J = 7.9, bpy-H_7), 8.31 (d, 1H, J = 8.2, bpy-H_4), 8.32 (d, 1H, J = 5.2, 3EP-H_1), 8.38 (s, 1H, 3EP-H_4), 8.40 (d, 1H, J = 7.9, bpy-H_5), 8.95 (d, 1H, J = 5.2, bpy-H_8).

^{13}C NMR (500 MHz, CD_3CN) 78.8, 84.5, 122.8, 124.9, 125.2, 126.9, 128.7, 129.0, 138.9, 139.2, 142.1, 153.5, 153.7, 154.5, 156.5, 158.6, 158.7.

Anal. Calc. for $C_{34}H_{12}N_6RuP_2F_{12}$: C, 65.90; H, 4.23; N, 13.56. Found: C, 66.2; H, 4.30; N, 13.7. MS(ES): *m/2z* 310.06, expected: *m/2z* 310.06

Cyclization of DNA

Ru-oligo cyclization reactions were performed on a 10-12 nmol scale. Mono-azido DNA and bis-azido DNA were purchased from Integrated DNA Technologies, Coralville, Iowa. Bis-azido

oligonucleotides were premixed with RuBEP at the indicated stoichiometric ratios in water. CuBr was dissolved in 3:1 DMSO/t-butanol to make a 0.1 M solution. TBTA ([(1-benzyl-1*H*-1,2,3-triazol-4-yl)methyl]amine) (Anaspec, Freemont, CA) was dissolved in 3:1 DMSO/t-butanol to make a 0.1 M solution. CuBr and TBTA were mixed in a 1:2 ratio and preincubated. The azide/alkyne solution volume was adjusted 50 µL (0.2 mM). 12 vol% of the premixed CuBr/TBTA solution was added to the oligonucleotide solution. Solutions were blanketed with N_2 and sealed tightly with parafilm. Reactions proceeded for 3 h. Temperatures varying from RT to 55 °C were tested, and no significant correlation was found between temperature and product formation. Additionally, vortexing or not mixing did not seem to change product formation. After reaction completion, a NAP-5 desalting column (GE Healthcare) was used to remove unreacted RuBEP, CuBr, and TBTA. Circular product was stored in molecular biology grade water at -20 °C.

Reagent	**nmol**
Bis-azido-oligo	10 - 12
RuBEP	10.
CuBr	100.
TBTA	200.

CHAPTER 3 - Ruthenium-Crosslinked Hydrogels with Rapid, Visible-Light Degradation

Material in this chapter was originally published in *Chemistry – A European Journal*. It has been adapted here with permission from the publisher:

Reprinted with permission from Rapp, T.L.; Highley, C.B.; Manor, B.C.; Burdick, J.A.; Dmochowski, I.J. Ruthenium-Crosslinked Hydrogels with Rapid, Visible-Light Degradation. *Chem. A Euro. J.* **2018**, *24*, 2328-2333

3.1 Introduction

Dynamic, stimuli-responsive materials can be designed to provide spatiotemporal control over useful physicochemical properties. Responsive polymeric materials have biomedical applications including therapeutic delivery of payloads,[61–64] control of cell fate,[65] and dynamic materials that facilitate tissue regeneration.[66] Hydrogels are particularly useful biomaterials due to their tunable properties[67] and programmable response to various cues,[68] including pH,[69] local enzymatic activity,[70] ultrasound,[71] magnetic fields,[72] heat,[73] and light.[74] Hydrogels are attractive vehicles in which to encapsulate and release proteins, which are typically denatured if exposed to non-aqueous environments or interfaces.[67] Hydrogel formulations avoid harsh emulsion steps and incorporate high water content compared to polymeric[75] and lipid-based[76] materials, preserving proteins in their native state.

Photoresponsive hydrogels offer unique capabilities for spatial and temporal control over material properties in biomedical applications, in particular, protein delivery. A variety of illumination sources are now available in clinical settings for light delivery into complex tissues, expanding the role for photoresponsive materials as implantable depots in buried tissue.[77,78] In notable examples from the Anseth group, photoresponsive hydrogels have been used to modulate cell behaviour[79] and for therapeutic drug delivery.[77] Similarly, the Garcia group employed photocaged peptides to modulate cellular adhesion to a hydrogel scaffold *in vivo*, and showed that delayed presentation of adhesion peptides reduces inflammation and fibrosis in living tissue.[80]

In general, photoresponsive hydrogels make use of *o*-nitrophenyl or coumarin-based photocleavable moieties, either as a caging group to block peptide activity, or as a degradable crosslinker to modulate mechanical properties. These organic moieties can be synthetically difficult to incorporate and respond most sensitively to near-UV (350 – 400 nm) light, which has minimal tissue penetration due to scattering and absorption.[81] Recent advances have demonstrated the delivery of proteins cued by longer wavelengths (600 – 900 nm) using a red-shifted azobenzene guest-β-cyclodextran host interaction or upconverting nanoparticles,[82,83] and

the development of a hydrogel that responds rapidly to near-UV light.[84] However, there remain significant challenges to combine longer-wavelength-absorbing phototriggers with rapid hydrogel responses, as well as improving chemical syntheses in such materials systems.

To generate an efficient, visible-light-responsive hydrogel system, we synthesized a photodegradable crosslinker, $[Ru(bpy)_2(3\text{-pyridinaldehyde})_2]Cl_2$ (RuAldehyde, **Figure 3.1a**), designed to react in a simple 1-step procedure with hydrazide-modified hyaluronic acid (HA-HYD) to form a Ru-hydrogel. This system takes advantage of the rich photochemistry and ready synthesis of Ru(II) polypyridyl complexes,[85–88] as well as the well-known biocompatibility of HA, which has been FDA-approved for use in many biomedical applications.[89,90] Previous systems have successfully used ruthenium compounds, often coupled with upconverting nanoparticles, to achieve near-IR activation of the ruthenium and release of active protein.[91,92]

3.2 Results

Photochemistry

$Ru(bpy)_2L_2$ complexes such as RuAldehyde, where bpy is 2,2'-bipyridine, and L is a pyridine-based ligand, have been shown in the literature to undergo substitution of a single pyridine in water to yield $Ru(bpy)_2L(H_2O)$ and free ligand L,[24,86] a process which occurs in less than 20 ns (**Figure 3.1a**).[24] RuAldehyde visible absorbance (λ_{max} = 450 nm, ε450 = 6400 $\pm$ 300 $M^{-1}cm^{-1}$) is indicative of a MLCT band, commonly seen in ruthenium polypyridyl coordination complexes. RuAldehyde exhibits strong absorbance out to 500 nm with a tail extending past 530 nm (**Figure 3.1b**).

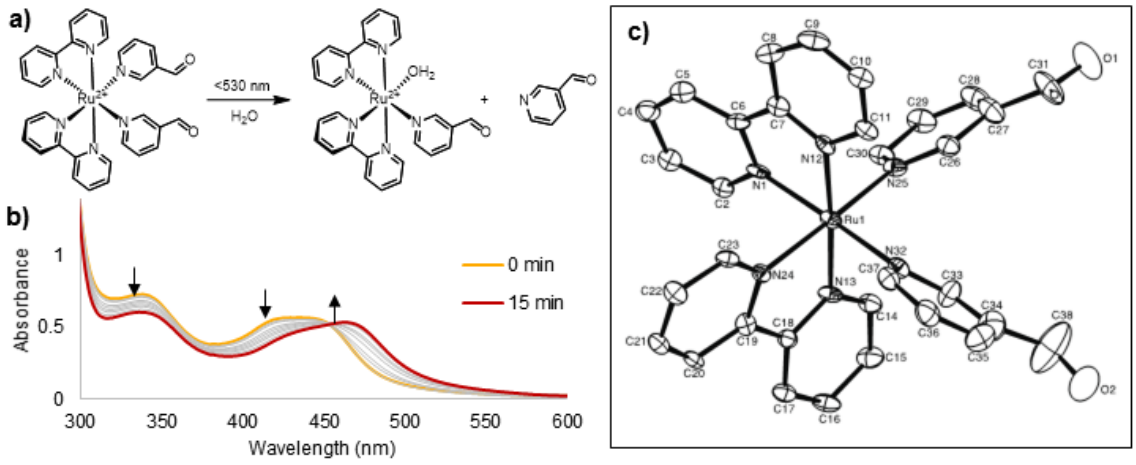

Figure 3.1. RuAldehyde structure and photochemistry. a) Visible light (<530 nm)-induced ligand exchange with water. b) UV-Vis spectra of the photolysis of RuAldehyde (λex = 450 nm, 14 mW/cm2). c) Crystal structure of RuAldehyde. The measured distance between aldehyde carbons is 5.6 Å.

Monitoring the photolysis reaction by UV-Vis spectroscopy, we observed red-shifted absorbance consistent with pyridine-to-water ligand exchange.[21] A single product peak with one isosbestic point (455 nm) was observed, suggesting complete photolysis of only one Ru – pyridine bond.[43] This model and the ^{1}H NMR and ESI data (**Figures 3.2, 3.3**) identify the primary photolysis product as Ru(bpy)$_2$(3-pyridinaldehyde)(H_2O) (**Figure 3.1b**). Thus, the Ru photoproduct remains attached to HA post irradiation, which is advantageous for biological applications of Ru-HA hydrogel. The crystal structure for RuAldehyde shows the two pyridinaldehyde ligands cis to each other, with approximately 5 Å between the aldehydes. (**Figure 3.1c**)

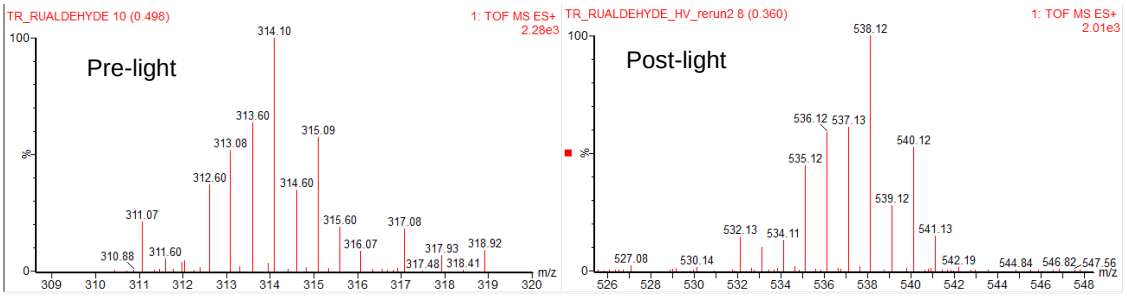

Figure 3.2. ESI mass spectrometry of RuAldehyde before and after irradiation. Expected masses: Rubpy$_2$(3-pyridinaldehyde)$_2^{2+}$: 627.67 (314.06 m/2) Da, Rubpy$_2$(3-pyridinaldehyde)(OH)$^+$: 538.57 Da.

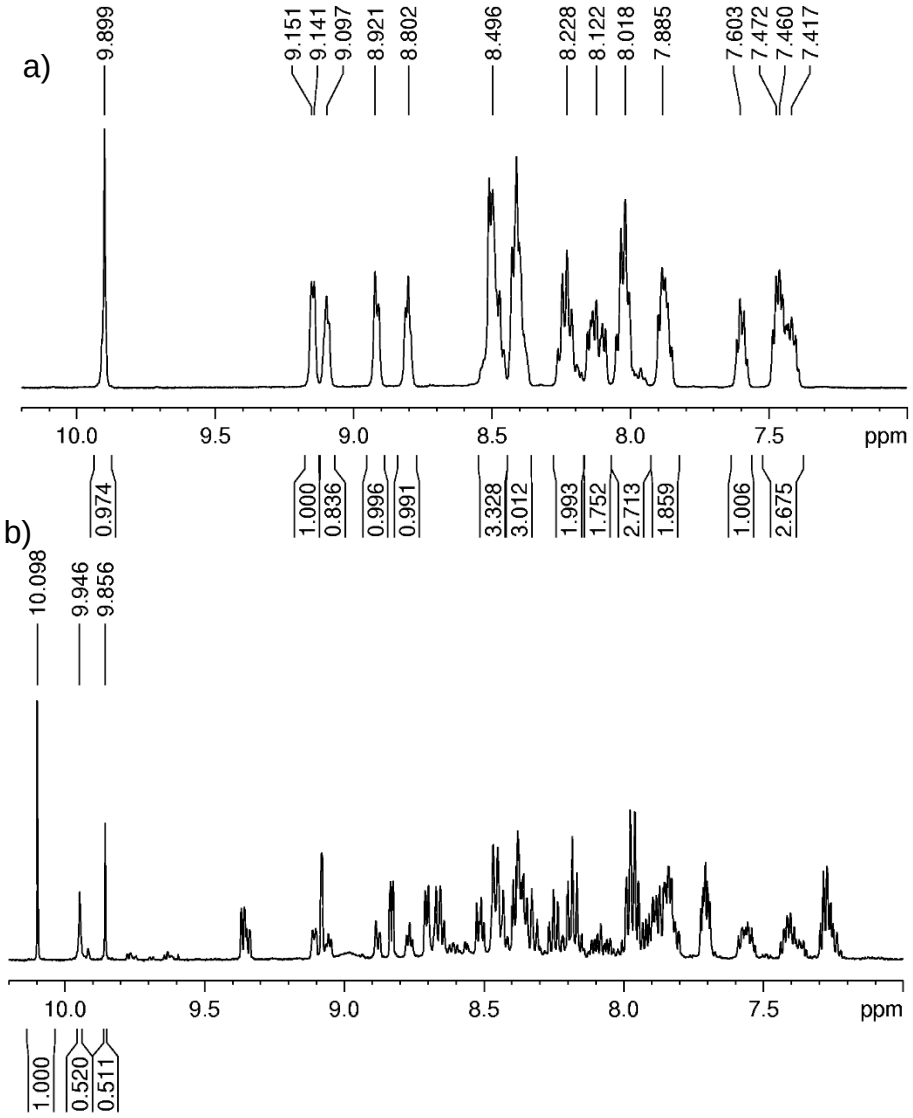

Figure 3.3. ^{1}H NMR spectra in D_2O pre- and post-photolysis show the formation of photoproduct $Ru(bpy)_2$(3-pyridinaldehyde)(OH). a) Prior to irradiation only one aldehyde signal is present at 9.856 ppm. c) After photolysis (45 min, 450 nm, 14 mW/cm^2), the appearance of a separate aldehyde signal at 10.098 ppm corresponds to free 3-pyridinaldehyde. The remaining aldehyde signal at 9.946 ppm corresponds to $Ru(bpy)_2$(3-pyridinaldehyde)(H_2O).

Quantum Yield Determination

Absorbance changes for RuAldehyde irradiation at 450 nm were fit to a single ligand substitution, pseudo-first-order kinetic model (**Figure 3.4**). Experimental data were fit to an equation of the form

$$Abs@470 = \varepsilon_A[A]_0 e^{-kt} - \varepsilon_B[A]_0 e^{-kt} + \varepsilon_B[A]_0$$

Where A is starting material $Ru(bpy)_2(3\text{-pyridinaldehyde})_2$, B is photoproduct $Ru(bpy)_2(3\text{-pyridinealdehyde})(H_2O)$, $[A]_0$ is the initial concentration of starting material in water, and ε_A and ε_B are the molar absorptivities of A and B, respectively. This model was derived from the following kinetic expressions:

$$Abs@470\ nm = Abs(A) + Abs(B)$$

where

$$\frac{d[A]}{dt} = -k[A]$$

$$\therefore\ [A]_t = [A]_0 e^{-kt}$$

and

$$[B]_t = [A]_0 - [A]_t$$

This model deconvolves the overlapping absorbances of starting material and photoproduct by determining the amount of product formed as well as starting material degraded based on pseudo-first order kinetics with respect to photons and water.

Based on pseudo-first order conditions for the photolysis reaction. Quantum yield Φ_{pr} was determined using the power of the light source (450 nm laser pointer, 52 mW/cm^2):

$$\Phi_{pr} = \frac{k_1[\mathrm{A}]_\mathrm{i}\mathrm{V}_\mathrm{sample}}{\frac{\mathrm{P}}{\mathrm{E}_\mathrm{ph}\mathrm{N}_\mathrm{A}}}$$

where k_1 is the observed rate constant derived from fitted data (s^{-1}), $[A]_I$ is the initial concentration of RuAldehyde in the cuvette (M), V_{sample} is the volume in the cuvette (L), P is the power of the light source (W), E_{ph} is the energy of light determined by $E = hc/\lambda$ (J), and N_A is Avogadro's number, 6.022×10^{23} per mole.

From this model, we determined the quantum yield of 3-pyridinaldehyde (3-pa) photorelease: Φ_{pr} = 0.63 ± 0.01. High quantum yield, coupled with large absorptivity in the visible region, give RuAldehyde unique photophysical properties. Efficiency ($\Phi_{pr} \bullet \varepsilon$) of 4.0 x 10^3 $M^{-1}cm^{-1}$ at 450 nm is a large improvement over commonly employed nitrobenzyl- or coumarin-based photodegradable linkers with efficiencies of 700-1100 $M^{-1}cm^{-1}$ at near-UV wavelengths.[77]

Hydrogel Formation and Characterization

To generate hydrogels, RuAldehyde was mixed with HA-HYD at a 1:2 molar ratio of RuAldehyde to hydrazide, to promote complete crosslinking (**Scheme 3.1**), with a final concentration of 3 wt% HA-HYD and a corresponding final concentration of 13.6 mM RuAldehyde. This formulation allowed the formation of robust hydrogels from low-viscosity solutions.

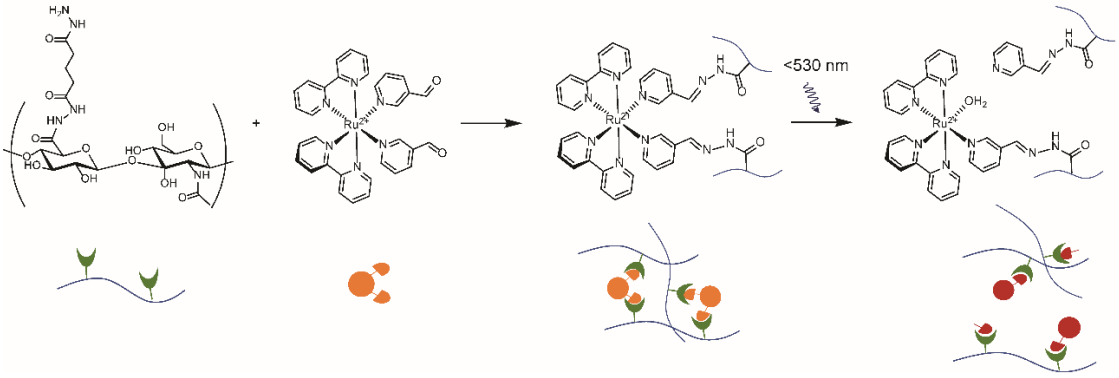

Scheme 3.1. Crosslinking hydrazide-modified HA (HA-HYD) with RuAldehyde, followed by visible-light degradation. Ruthenium photoproducts (red) remain attached to HA polymers (blue) after irradiation.

Rheometric data provided insight into the crosslinking kinetics and photodegradation of the hydrogel (**Figure 3.5a**). Gelation occurred rapidly, with full crosslinking occurring over approximately 10 min. Upon irradiation with Hg lamp (400-500 nm bandpass filter, 14 mW/cm^2), the storage modulus of the sample decreased, dropping from approximately 4000 Pa to < 200 Pa in less than 60 s, with an even faster response observed at higher light intensities. A continued decrease in storage modulus to less than 20 Pa was observed under continuous irradiation,

where the samples were observed to degrade into a viscous liquid with no significant elastic properties.

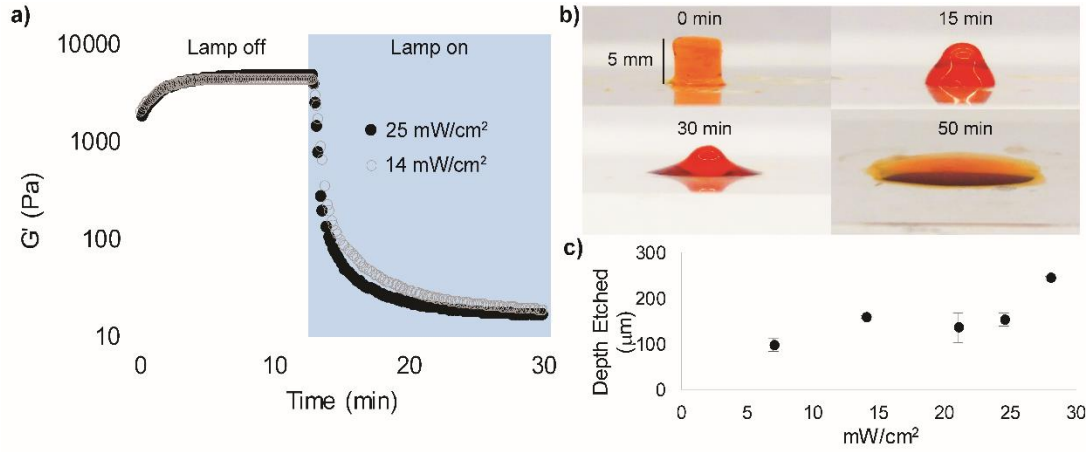

Figure 3.5. Hydrogel photodegradation. Hydrogels of hyaluronic acid crosslinked with RuAldehyde show rapid degradation upon irradiation with visible (400-500 nm) light, as illustrated in a) rheological profiles showing a rapid loss of storage modulus (G′) upon irradiation. b) Complete degradation of a macroscopic 4 x 5 mm hydrogel was observed within 50 min using 28 mW/cm^2 light intensity. c) Thin, 0.5 mm, hydrogels loaded with Texas Red © dextran (45 kDa, 1 mg/mL) were irradiated for 2 min through a photomask with varying intensities of visible light. Higher intensities penetrated deeper into the hydrogel.

The high molar absorptivity of RuAldehyde limits light penetration and slows degradation of larger Ru-hydrogels. A large 5 mm tall by 4 mm wide hydrogel formed on the benchtop took nearly 50 min of illumination to fully degrade using Hg lamp (400-500 nm bandpass filter, 28 mW/cm^2 light, **Figure 3.5b**), whereas somewhat smaller hydrogels (0.5 mm x 4 mm) required 8 min to degrade (see **Figure 3.8**). The selective masked irradiation of macroscale (0.5 x 4 mm) hydrogels using various intensities of visible light showed deeper etching with higher intensity light after the same time of light exposure (**Figure 3.5c**). A similar but diminished effect was observed when 523 nm light was used in the same experiment, due to the lower quantum yield at longer wavelengths (0.15 ± 0.05 @ 532 nm) and the lower absorptivity (**Figure 3.6**). These same hydrogels were opaque to blue light (**Figure 3.7**).

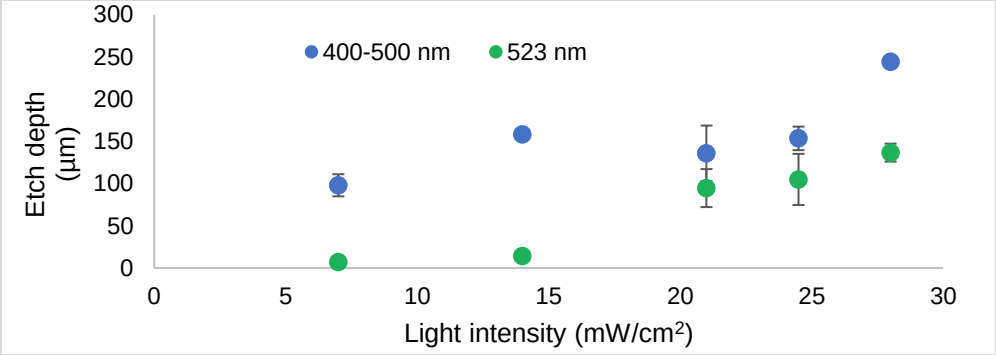

Figure 3.6. Figure 3.5c (blue circles) was repeated with 523 nm light, from an LED source. The longer wavelength light showed less degradation activity, as the quantum yield is lower (0.15 ± 0.05), and the absorptivity is minimal.

Therefore, hydrogels used for *in vitro* tests were kept to a thickness of ~500 μm, which enabled handling while minimizing the time needed for complete degradation. The light intensity and time of irradiation needed to degrade RuAldehyde-crosslinked hydrogels compares favourably to established photodegradable systems, which vary from 60 mW/cm^2 for 30 min for an ~5 mm gel using the red-shifted azobenzene derivative,[82] to 40 mW/cm^2 for 5 min for a coumarin derivatized gel formed on the rheometer (~30 μm in thickness).[93]

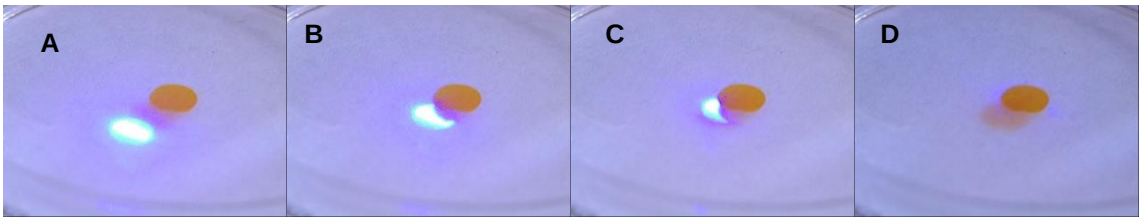

Figure 3.7. Images of a 4 x 0.5 mm gel suspended in PBS passing under a 450 nm, 52 mW/cm^2 laser pointer. In panel D the gel completely eclipses the light beam.

Cellular Toxicity Studies

The exchange of only one 3-pyridinaldehyde ligand minimizes the potential toxicity of the hydrogel Ru photoproducts. In this hydrogel system, the doubly ligand-substituted product $Ru(bpy)_2(H_2O)_2$ is never formed, and the ruthenium photoproduct remains attached to the HA backbone (**Scheme 3.1**). No decrease in viability was observed in cells exposed to non-degraded hydrogels or to acute (1 day) exposures to the hydrogel photoproducts from *in vitro* assays (**Figure 3.8**).

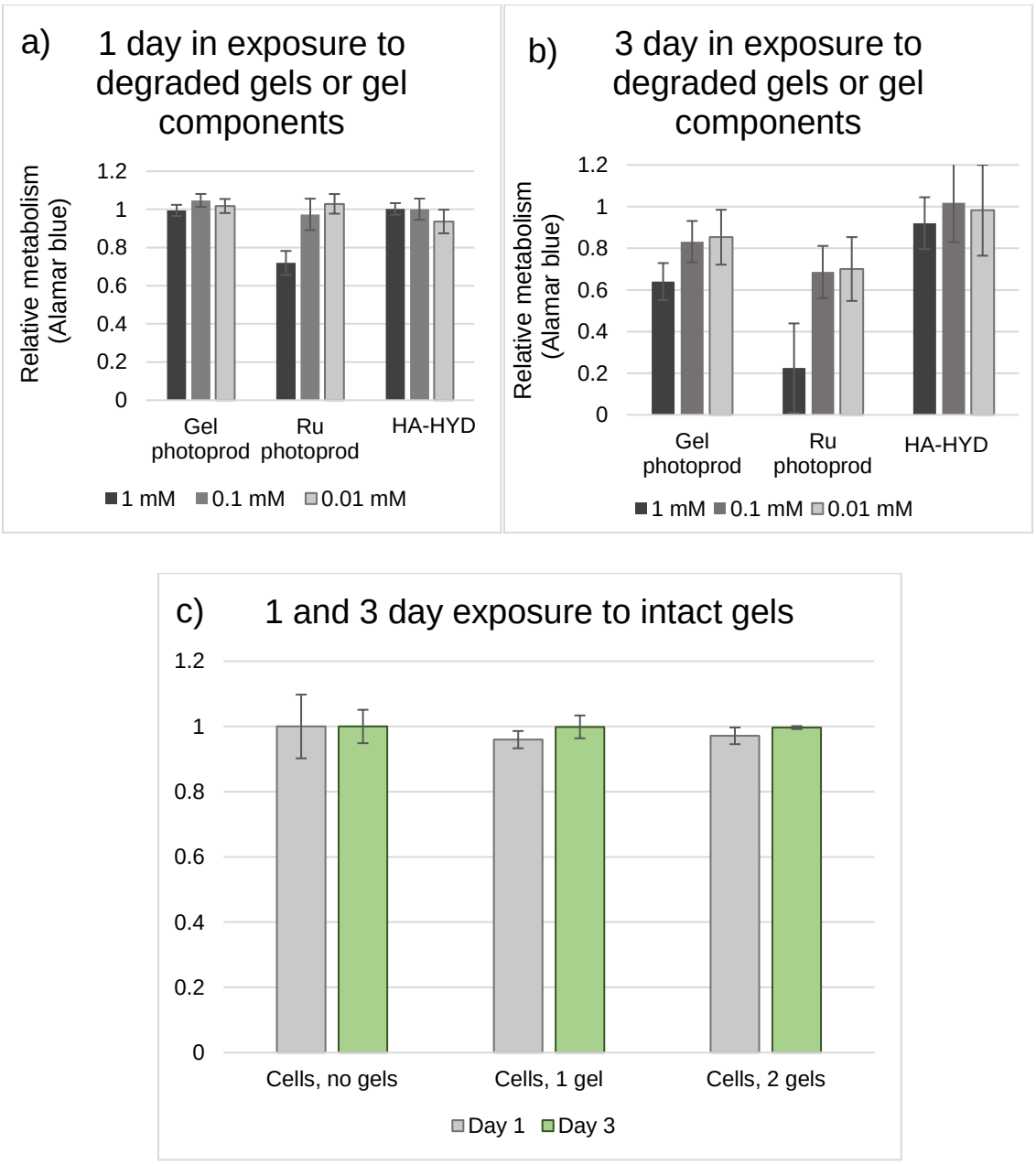

Figure 3.8: Cell viability as determined by colorimetric Alamar blue metabolism. A) RuAldehyde photoproducts are minimally cytotoxic at one day in lower concentrations, with toxicity increasing only at higher concentrations. Gel photoproducts show negligible cytotoxicity compared to free RuAldehyde photoproducts. B) Cells were incubated with photoproducts at high concentrations for 3 days, a scenario that loosely mimics the body. While toxicity increases over time in situ, in vivo concentrations of photoproducts would dissipate much faster, reducing the concentration (perhaps to nM levels) within the same time frame. C) Intact gels show no cytotoxicity after 3 days.

When ruthenium-based photoproducts are released from the polymeric backbone significant cell toxicity can be observed, as $RuL_5(H_2O)$ compounds are known ROS generators under irradiation. This was observed by Sun et al. in their block copolymer system designed to release Ru(biquinoline)(terpyridine)(H_2O) from the polymer and induce cell death.[94] With the lack of ruthenium release in our current system the potential toxicity is mitigated.

Active Enzyme Delivery

The Ru-HA system was explored for protein photo-delivery using macroscale hydrogel depots (discs: 4 mm diameter, 500 μm thick) encapsulating TEM1 β-lactamase (TEM1) as a model protein. TEM1 is a 29 kDa enzyme responsible for antibiotic resistance in bacteria by catalysing the ring-opening of beta-lactam groups present in many common antibiotics.[95] TEM1 is similar in size to other small bioactive proteins and peptides including human growth hormone (22 kDa) and light chain fragments of some antibody drug targets (24 kDa).[66,67,96,97] Importantly, TEM1 activity on nitrocefin can be measured using a colorimetric assay at wavelengths that are not affected by residual Ru-HA material in solution.

To retain active enzyme within the hydrogel until light-mediated release Ru-hydrogels loaded with TEM1 (0.5 mg/mL) were incubated briefly in a reducing buffer containing $NaCNBH_3$ to create stable crosslinks between lysine residues on TEM1 and RuAldehyde (**Figure 3.9a**). In the dark, the hydrogels showed < 1% release of TEM1 for up to 5 days (**Figure 3.10**).

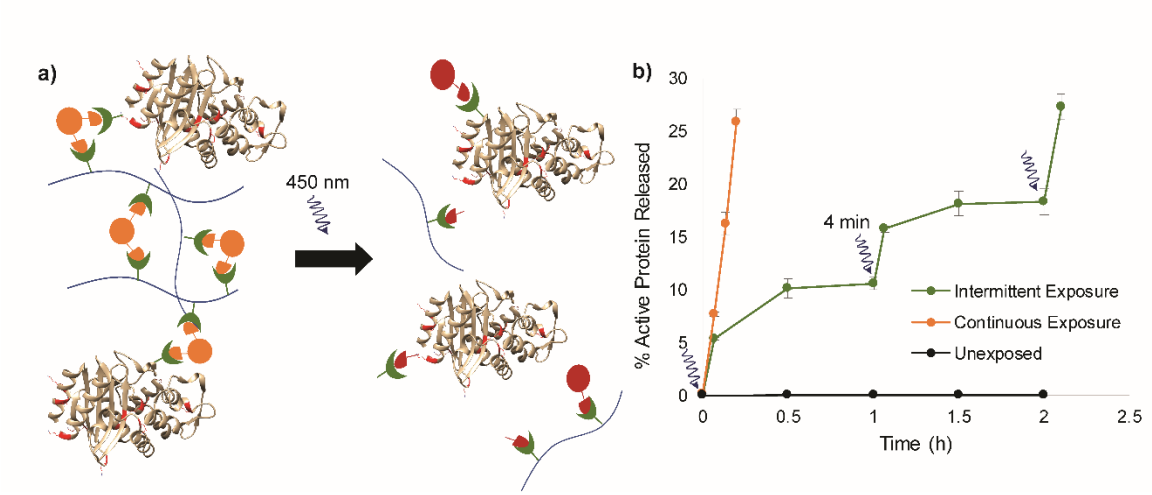

Figure 3.9 Protein photorelease from hydrogels. a) TEM1 protein was encapsulated within hydrogels that were then irradiated (450 nm, 14 mW/cm^2) to release active TEM1. b) Hydrogels were irradiated either continuously (orange), in 4-min intervals every hour (green), or left in the dark (black). % activity was determined by activity assay and compared to TEM1 activity prior to encapsulation.

The possibility for step-wise release of active enzyme in response to intermittent light was tested as well as more rapid, complete release under continuous irradiation (**Figure 3.9b**). These experiments confirmed that light exposure modulates release, enabling consistent step-wise dosing of an active protein from Ru-hydrogel via light-mediated surface erosion. Because one RuAldehyde ligand is exchanged, TEM1 protein released from the hydrogel was modified with residual ruthenium complex as $Ru(bpy)_2(H_2O)$(3pa-protein) or with 3pa ligand alone (**Figure 3.9a**).

It has been demonstrated for several proteins that physical crosslinking to gel matrices can minimally impact biological activity,[98,99] and may result in somewhat decreased activity for TEM1 released from Ru-hydrogels (**Figure 3.10**). Under mild gelation conditions (mixing and sitting at 4 °C for 1 h), 30% maximum enzyme release was observed from the hydrogels. All gels were completely degraded until no pieces were observed by eye. The low margin of error between gel samples and the low likelihood that any protein remained trapped within the gel matrix and inaccessible to nitrocefin during the assay suggests complete release from the gel.

Despite appropriate use of standards and controls, we observed a widespread loss of activity in protein samples extracted from a hydrogel. There are two likely reasons for this decrease in activity: either there is a lower concentration of TEM1 in the supernatant, or the activity was affected by encapsulation and/or crosslinking of the protein. As gels were irradiated to visible degradation in each experiment, we hypothesize that all protein was freed from the gel matrix and suspended in the solution, and subsequently tested. Therefore, the most significant factors in decreased activity observed in these experiments are the encapsulation and crosslinking of protein.

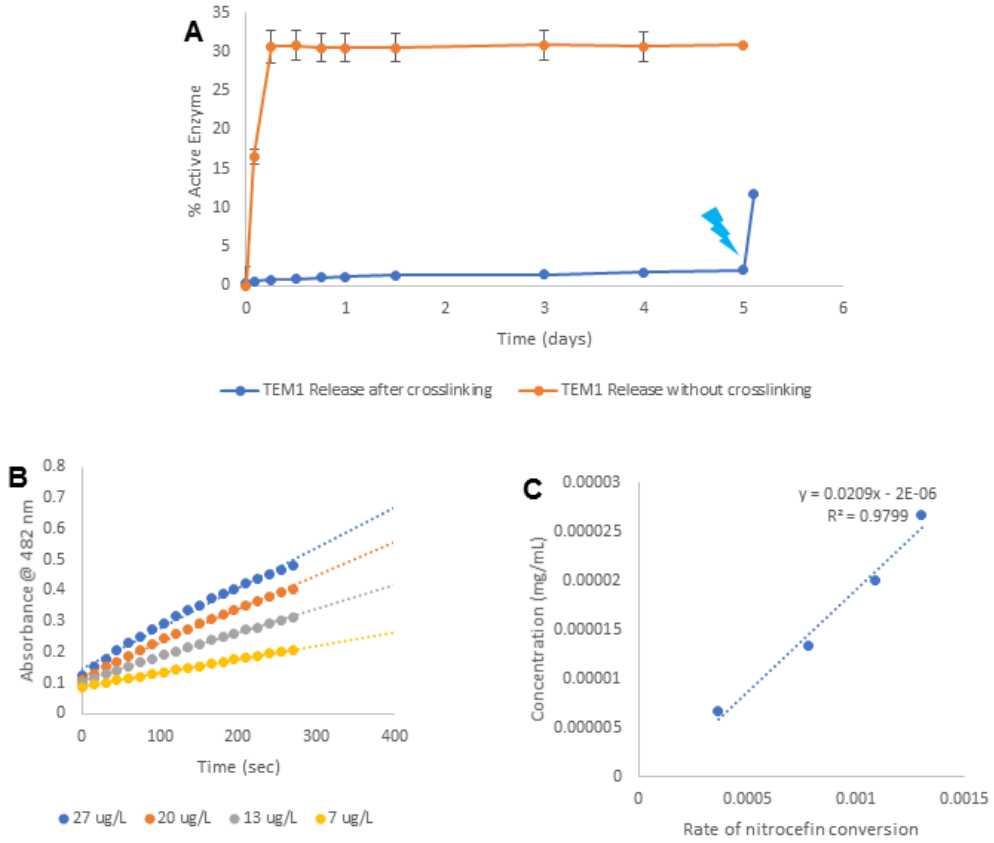

Figure 3.10. Protein release from gels. (A) TEM1 was released immediately from intact gels formed without $NaCNBH_3$ reduction (orange trace), but remained in the gel for up to 5 days with minimal burst release after $NACNBH_3$ reduction (blue trace). (B) Protein activity was determined using a standard curve generated from the same stock solution used to load hydrogels. The activity of these solutions (as determined by the rate of nitrocefin conversion, measured at A_{482}) is plotted. (C) Standard curve for variations in activity based solely on concentration of TEM1.

Microgel Generation

Microfluidic processing of Ru-hydrogels into microgels offered the possibility to combine the versatility of this photoresponsive material system with the strengths of delivery vehicles generated using microfluidics.[100] These include, for example, greater uniformity in size and mechanical characteristics and ease of injectability and implantability. An additional goal was to produce microgels capable of complete degradation upon very short exposures to light. in the collected microparticle emulsion.

Because of the rapid, but not instantaneous, gelation kinetics resulting from the use of the pyridine-aldehyde group as opposed to an aliphatic aldehyde,[101] gelation times allowed mixing of the hydrogel components in a microfluidic mixing device (**Figure 3.11a**),[102,103] with gelation and curing occurring

Microgels had an average diameter of 74 ± 6 µm (n = 100 particles) as determined by optical microscopy. Microgels suspended in phosphate buffered saline that were exposed to 10 mW/cm^2 for 5 s on the microscope stage were observed to experience rapid dilation and degradation (**Figure 3.11b**). Complete particle degradation and Ru-HA release occurred within 60 s of irradiation at 10 mW/cm^2 (**Figure 3.11c**). The microgel-Ru-crosslinker format thus offers the potential for rapid release of payloads with low doses of visible light.

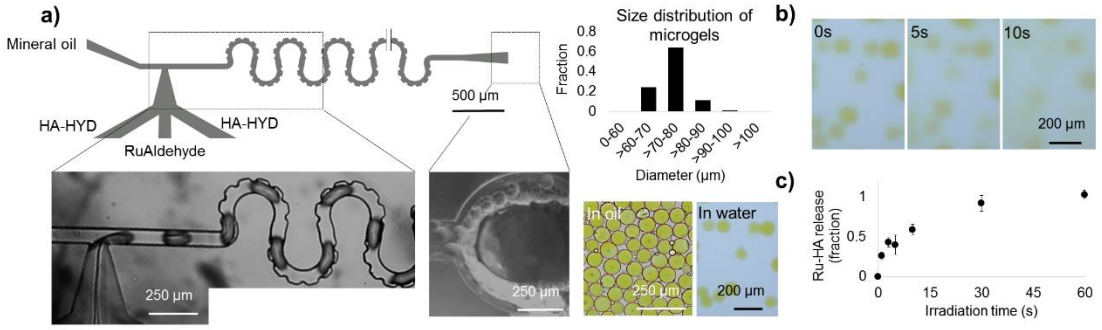

Figure 3.11. Generation of microgels with rapid degradation properties. a) Microfluidics were used to combine materials in aqueous droplets that were dispersed in mineral oil and mixed in curved channels to form uniform microgels, which were subsequently washed into an aqueous medium. b) Microgels in PBS were exposed to 10 mW/cm^2 light for 5 s, resulting in microgel degradation, which is shown with time post-

irradiation indicated. c) Complete degradation, determined from Ru-bound HA released, occurred within 60 s irradiation.

3.3 Conclusions

In summary, a photoactive ruthenium crosslinker enabled the creation of hydrogels that respond with unique speed and efficiency to visible light exposure. Ru-hydrogels were demonstrated as vehicles for the encapsulation and controlled delivery of viable protein with low doses of visible light, and produced in both macro- and microgel formats. The strong potential exists for tuning the polypyridyl coordination sphere on the ruthenium to develop new RuAldehyde crosslinkers that are responsive to additional visible wavelengths.[38,39] In this way, we envision ruthenium-crosslinked polymer systems that provide even greater spatiotemporal control over materials properties such as storage modulus and porosity, as well as regulation of drug delivery profiles and cellular function in biomedical applications.

3.4 Materials and Methods

$Rubpy_2Cl_2 \bullet 2H_2O$ was purchased from Strem Chemicals, $AgSO_3CF_3$, NH_4PF_6, and 3-pyridinecarboxaldehyde were purchased from Acros Organics. All solvents were purchased from Fisher Scientific and used without further purification unless otherwise specified. Sodium hyaluronate was purchased from Lifecore Biomedical. Adipic acid dihydrazide, hydroxybenzotriazole, 1-ethyl-3-(3-dimethylaminopropyl)carbodiimide, and Amberlite ® IRA-410 resin were purchased from Sigma Aldrich.

Synthesis of RuAldehyde: Ru(bipyridine)$_2$(3-pyridinealdehyde)$_2$

$Ru(bpy)_2Cl_2 \bullet 2H_2O$ (160 mg, 0.3 mmol, 1 eq) and $AgSO_3CF_3$ (173 mg, 0.68 mmol, 2.2 eq) were added to 50 mL of freshly distilled methanol. The solution was stirred under N_2 for 15 min until the formation of a white solid (AgCl) was observed. 3-pyridinecarboxaldehyde (0.439 mL, 4.7 mmol, 15 eq) was added and the reaction was heated to 65 °C for 4 h under N_2. DI water (15 mL) was added and the methanol was removed under reduced pressure. Approximately 2 g solid ammonium hexafluorophosphate (NH_4PF_6) was added and the resultant orange solid was

extracted into dichloromethane until the aqueous phase was mostly colorless. Ru(bipyridine)$_2$(3-pyridinecarboxaldehyde)$_2$[PF_6]$_2$ was then purified by silica column (1.5 x 36 cm) using 1:6:13 methanol:acetonitrile:dichloromethane as the solvent system. The chloride salt was prepared by Amberlite IRA-410 chloride form anion exchange column using methanol as eluent. ^{1}H NMR (500 MHz, CD_3CN) 7.40 (t, 1H), 7.49 (t, 1H), 7.80 (t, 1H), 7.95 (m, 2H), 8.16 (t, 1H), 8.28 (t, 2H), 8.37 (d, 1H), 8.52 (d, 1H), 8.68 (s, 1H), 8.94 (d, 1H), 9.87 (s, 1H). ^{13}C NMR (500 MHz, CD_3CN) 124.9, 125.22, 127.89, 128.82, 129.21, 135.01, 138.14, 138.14, 139.02, 139.30, 153.34, 153.73, 156.27, 158.55, 158.64, 159.02. ESI: expected mass: 628.11, observed mass, 313.9 (m/2)

Synthesis of HA-HYD

Sodium hyaluronate was dissolved in water at 1 wt% in a reaction vessel. Relative to the disaccharide repeat unit of the HA backbone, a large molar excess (~30x) of adipic acid dihydrazide (ADH) was added to the solution and allowed to dissolve. The pH was adjusted to 6.8 using HCl/NaOH, and first hydroxybenzotriazole (HOBt) then 1-ethyl-3-(3-dimethylaminopropyl)carbodiimide (EDC) were added to initiate the coupling of ADH to the HA backbone. The pH was adjusted to 6.8 every 30 min for 4 h, then the reaction was allowed to proceed overnight. The following day, the contents of the reaction vessel were moved to dialysis tubing for purification against H_2O. After dialysis, the product was lyophilized and further purified by precipitation against ethanol, repeated dialysis, and finally lyophilized to yield product. Degree of modification was determined by ^{1}H NMR spectroscopy (360 MHz, D_2O).

Rheometry

Rheological measurements were made using an AR2000 stress-controlled rheometer (TA Instruments) with a cone-plate geometry (20 mm diameter cone with 59 min 42 sec cone angle and a 27 μm gap). A quartz stage coupled to a visible light source by fiber optic cable enabled measurement of rheological properties during gelation and light-irradiation of the hydrogels. Oscillatory time sweeps were performed at 1 Hz and 5% strain.

Partial irradiation of hydrogels and confocal measurement of defect

Hydrogels were formed as described, but with the inclusion of 0.25 wt% Texas Red-dextran (40 kDa) dissolved with the HA-HYD to ultimately allow confocal imaging of the hydrogel. Hydrogels could be selectively irradiated by exposing them to visible light through a photomask designed to allow 1.5 mm wide lines of light to irradiate each gel to create channels in the gel surfaces. Masks were applied directly to the gel surfaces with the printed sides down. After irradiation, gels were incubated for 30 minutes at room temperature in 1x PBS to remove degraded photoproducts. Hydrogels were then imaged using confocal microscopy (TCS SP5 with HCX IRAPO L 25x/0.95 water immersion objective, Leica). Regions of irradiation were identified visually, and the depth of the irradiated channel was determined from z-stacks, by measuring the z-distance from the top of the gel to the channel floor. The z-plane at which fluorescence, indicating the presence of the Texas Red-dextran containing gel, was continuous 500 μm into the channel from the wall of the channel was determined to be the channel floor.

Quantification of TEM1 Release

Protein concentration upon release could not be measured by standard concentration assay (Bradford, Lowry, size exclusion FPLC) due to reactions with HA amines and the large size distribution of photolysis products. Fluorescence measurements with labeled cargo protein also yielded compromised results due to photobleaching caused by Ru-photolysis reaction. As the typical gel used for cargo delivery took 7-10min of constant irradiation with 14 mW/cm^2 light, extensive photobleaching was observed with multiple fluorophores. An activity assay was used instead to approximate protein release. Active TEM1 (0.5 mg/mL) was loaded into 4 x 0.5 mm hydrogels during gel formation, and lysine-aldehyde crosslinks were formed by the incubation of TEM1-loaded hydrogels in 50 mM $NaCNBH_3$ in a crosslinking buffer composed of 0.5 M Na_2SO_4, 0.2 M borate buffered at pH 8.0 for 30 min at 37 °C. Hydrogels were then transferred to PBS for the remainder of the experiment. 0.5 mL samples of the supernatant (in PBS) above a gel were taken at various time points and the hydrolase activity of 5 nM TEM1 was measured using 450

μM nitrocefin (EMD Millipore) as a substrate. The hydrolysis of nitrocefin was monitored at A_{482} for the appearance of the enzymatic product of nitrocefin using an Infinite M1000 Pro plate reader (Tecan) for 15 min. Three gels were used for each release experiment to account for variations in gel formulation and protein encapsulation.

% active enzyme was determined using a standard curve of activity generated using the same stock solution of TEM1 as was incorporated into the gel. This assumes the stock of TEM1 shows the maximum activity possible, and activity varies linearly with concentration of enzyme present (as confirmed by the standard curve fit). The rate of product generation (i.e., the initial slope of the curve) was plotted against concentration of TEM1 for the standard curve. Relative amounts of TEM1 released from hydrogels were determined using this method.

Fabrication of microfluidic devices

Microfluidic devices were built using standard soft lithography techniques. Briefly, photomasks were designed (AutoCAD), printed (CAD/Art Services), and used to pattern negatives of the channels on Si wafers coated with a negative photoresist (KMPR 1050). Polydimethylsiloxane (Sylgard 184, Dow Corning) was mixed at a 10:1 ratio with the curing agent and cast off this surface, punctured for fluidic connections, and bound to a PDMS slab.

Generation of microgels

Microgels were generated through the combination and mixing of hydrogel materials in microfluidic devices (Figure 4a). RuAldehyde and HA-HYD were introduced in separate inlet streams that converged at a t-junction with a channel carrying an oil stream. Aqueous droplets containing the hydrogel precursor materials were emulsified in mineral oil containing 3 wt% Span 80, and mixed within the device to allow for uniform gelation within droplets. Droplets were collected in oil off the device, and incubated at least an hour before use to allow for gelation to occur. Prior to use in degradation and release assays, microgels were washed to remove mineral

oil by pipetting a volume of the microgel emulsion into a tube containing PBS and centrifuging to separate the microgels into the PBS fraction.

Imaging microgels before and during degradation

After the microfluidic generation of microgel particles, particles were imaged both in suspension in mineral oil as well as after being washed into PBS. An Olympus BX51 equipped with an Olympus DP72 camera was used to image the gel particles, using the UPlanFL N 4x/0.13 and 10x/0.3 objectives. Single images and image sequences were obtained using the Olympus DP2-BSW software, which includes tools that allowed quantification of particle sizes directly from images. Phase contrast images were acquired using the equipped halogen light source. No particle degradation was observed as a result of the light exposures used for phase contrast imaging. Images were calibrated (μm/pixel) to the objective used, and circles were superimposed over particles ($n \geq 100$) to measure particle sizes. Microgel degradation was observed under the 4x objective as the working distance allowed for irradiation from an external lamp. While acquiring sequences of phase contrast images, a 5 sec irradiation by visible light at 10 mW/cm^2 (400-500 nm bandpass filter) from an external Hg lamp (OmniCure, Lumen Dynamics) was used to induce microgel degradation.

Quantifying degradation of microgels

Microgel degradation was quantified from the release of HA-bound RuAldehyde into the surrounding medium as a function of light exposure in a method analogous to that described previously for macrogels. 50 μL volumes of microgels, concentrated after centrifugation into PBS, were pipetted into larger 1 mL volumes of PBS. Samples were then lightly vortexed to suspend the microgels and subsequently exposed to doses of visible light in cuvettes. Samples were then gently agitated for 10 min, centrifuged to pellet any remaining microgels, and the supernatant was sampled. The absorbance of the supernatant at 460 nm was compared to a subsequent sample

taken from the same microgels after a 30-min irradiation to fully degrade any remaining particles to give a fraction Ru-HA released for each test condition as a proxy for hydrogel degradation.

CHAPTER 4 - Designing Ruthenium Polypyridyl Crosslinkers for Hydrogel Formation and Multiplexed, Visible-light Degradation

The content for this chapter has been prepared for publication. It has been adapted here:

Reprinted with permission from Rapp, T.L.; Wang, Y.; Dmochowski, I.J. Designing Ruthenium Polypyridyl Crosslinkers for Hydrogel Formation and Multiplexed, Visible-light Degradation

4.1 Introduction

Photoresponsive molecules and materials are transforming multiple areas of research, from drug delivery,[28,44,104–107] to materials engineering,[79,108–115] and biology.[60,86,116–124] Many natural biological processes are not photoresponsive, making light a versatile trigger for controlling complex biological systems.[125] The incorporation of photoactive moieties within biomolecules,[123] small-molecule drugs,[126] and materials[79] provides a method for modulating their activity. Likewise, photoactive moieties incorporated within soft materials, e.g., polymers, hydrogels, elastomers, enable spatiotemporally precise, light-guided modulation of structure-function properties. To expand methods for materials control, we developed two differentially photoresponsive ruthenium moieties suitable for hydrogel formation and multiplexed activation.

A drawback to most current photoresponsive molecules is the high-energy light required for bond dissociation. Common photoresponsive organic chromophores, e.g., *o*-nitrobenzyl,[127] azobenzene,[114] and coumarin,[77,93] respond to near-UV and blue light, which barely penetrates biomaterials or live tissue. Attempts to red-shift the activation wavelength have focused on multiphoton excitation,[41,110,128–130] coupling with upconverting nanoparticles[83,130] or chemically modified chromophores.[82] Some limiting factors include the small activation volume of multiphoton processes, the potential toxicity of embedded nanoparticles, and synthetic complexity.

To address these challenges, we have worked to develop inorganic photoactive molecules that absorb orange-red light, which has greater penetration depth and is less prone to photodamage in clinical applications.[41] Here we describe a series of ruthenium (Ru) complexes with absorption red-shifted via coordination with two polypyridyl ligands with extended pi-conjugation. Ruthenium was further coordinated with two photolabile nitrile ligands presenting terminal alkynes for subsequent crosslinking reactions. Copper-mediated azide-alkyne click chemistry (CuAAC) with a commercially available branched PEG polymer produced photoresponsive hydrogels. This

approach allowed facile incorporation of multiple Ru crosslinkers capable of sequential activation with orange and blue light.

The Dmochowski lab has expanded the use of photolabile ruthenium crosslinkers for biological applications, starting with (Ru(bipyridine)$_2$(3-ethynylpyridine)$_2$) (Ru-BEP). This alkyne-modified ruthenium bisbipyridine compound was used to circularize antisense oligonucleotides for gene knockdown in zebrafish embryos.[86] A related compound, Ru(bipyridine)$_2$(3-pyridinaldehyde)$_2$ (RuAldehyde), provided a light-responsive crosslinker for hydrogels.[131] These ruthenium polypyridyl complexes share the unique capability to exchange coordinated ligands with solvent upon irradiation with visible light (**Figure 4.1**). This property has been observed for pyridine-,[28,43,132,133] nitrile-,[31,134] and sulphur-containing ligands.[135] Excitation into the ^{1}MLCT band initiates intersystem crossing to a low-lying triplet state. In most Ru-polypyridyl complexes this triplet state is primarily ^{3}MLCT in character, with another triplet metal centred (^{3}MC) state close enough in energy to be thermally populated (**Figure 4.1B**).

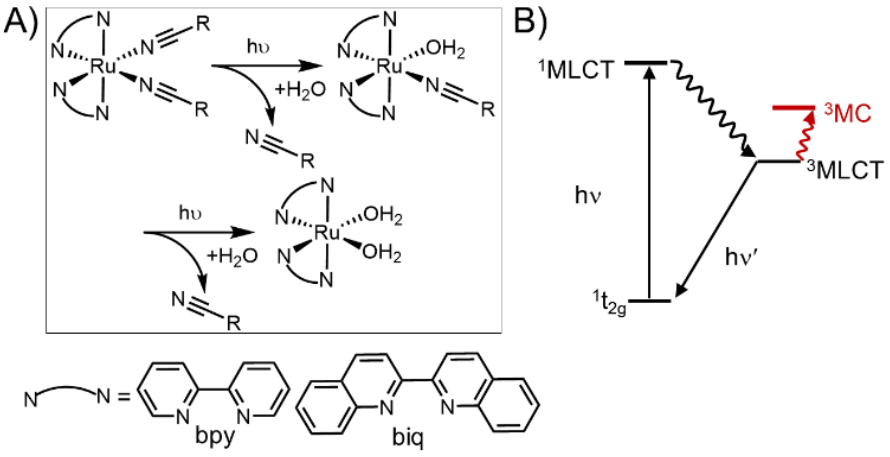

Figure 4.1. Photoinitiated ligand exchange in ruthenium polypyridyl complexes. A) Photolysis observed for Ru(II)-nitrile complexes is a two-step process in which both ligands are exchanged with coordinating solvent. B) Jablonski diagram showing excited states responsible for ligand exchange.

In this work we present a series of alkyne-bearing Ru(II) compounds with nitrile-based photolabile ligands (compounds **1-3**, **Figure 4.2**). Turro and coworkers demonstrated previously that incorporating bipyridyl ligands with extended pi-conjugation red-shifted the absorbance for

$Ru(biq)_2(acetonitrile)_2$,[39] and increasing the steric strain around the ruthenium center increased the Φ_{pr}.[35] Because of the steric bulk of the biquinoline ligands in compound **3** especially, nitrile-based ligands became a more viable option for coordination. Previous studies with RuBEP highlighted stable coordination by two pyridine ligands, where only 1 was photo-dissociable. In the current study, our goal was to red-shift the absorption, while incorporating two photolabile ligands for maximum photodegradation, a property of nitrile-based ligands.[39] Though pyridine-based ligands are often preferred for the stability of their coordination bonds, nitrile-based ligands are readily coordinated in mild conditions and around sterically crowded metal centres.

We initially synthesized a series of compounds utilizing 4-pentynenitrile as the alkyne-bearing ligand (**Figure 4.2**), starting from $Ru(bipyridine)_2(4\text{-pentynenitrile})_2$, with λ_{max} of each subsequent compound sequentially red-shifted by incorporating either 1 or 2 biquinoline ligands (**Figure 4.2**). Stability issues became apparent for these compounds when dissolved in water with a Cl^- counterion, an effect suggested to be due to a mild bidentate nature of the 4-pentynenitrile ligand. The effect of a longer alkyne-bearing ligand (5-hexynenitrile) was investigated not only to elucidate the mechanism of instability but also to facilitate efficient click reactions. Finally compounds **4** and **5** (identical to **1** and **3** save with a longer alkyne ligand) were reacted with an azide-modified branched polyethylene glycol (PEG) polymer (10 kDa). The resulting hydrogels with two Ru crosslinkers allowed spatially selective degradation via two different wavelengths of visible light (590 and 410 nm).

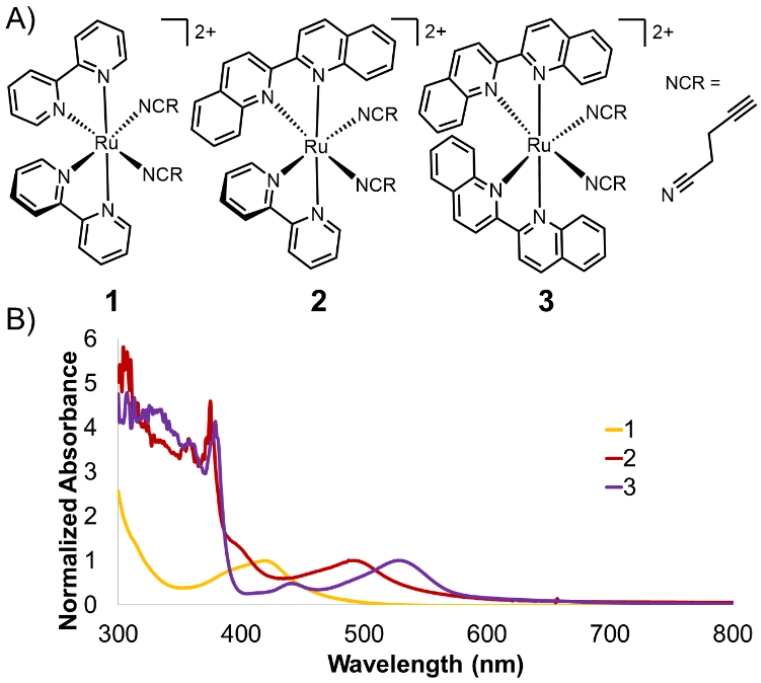

Figure 4.2. Red-shifted Ru crosslinkers with two photolabile nitrile ligands. a) Three compounds synthesized in this study. b) Normalized absorption spectra overlaid demonstrating the significant red shift observed upon inclusion of biquinoline ligands.

4.2 Results and Discussion

Synthetic Procedure

All compounds were synthesized with commercially available 4-pentynenitrile or 5-hexynentirile and purified with silica column chromatography (1:4 acetonitrile:dichloromethane mobile phase). The nitrile ligands were coordinated via a $Ru(LL)_2(H_2O)_2$ intermediate generated by the addition of $AgPF_6$ to form the AgCl precipitate, and purified as the PF_6^- salt. The PF_6^- was exchanged using an Amberlite© IRA-400 column, pre-soaked with either HCl or HNO_3 (see SI for synthetic details).

Compound **1** was synthesized from commercially available $Rubpy_2Cl_2$ and 4-pentynenitrile in reasonable yield (54%). To generate $Ru(bpy)(biq)Cl_2$ for **2** we found it necessary to use the benzene ruthenium dimer $[(benzene)RuCl_2]_2$ to ensure conversion to the mixed ligand product. Bipyridine was coordinated first to generate $Ru(bpy)Cl_4^{2-}$, which was purified by filtration, followed

by addition of biquinoline and heating to give the final product. $Ru(bpy)(biq)Cl_2$ was purified by precipitation into diethyl ether, final yield was 55%. Subsequent coordination of two 4-pentynenitrile ligands gave **2** in a final overall yield of 13.5%.

3 was synthesized starting with $RuCl_3$; 2.2 equivalents of biquinoline were added along with hydroquinone as the reducing agent and excess LiCl to generate the intermediate $Rubiq_2Cl_2$, which was isolable by precipitation into ether with a 33% yield. Coordination of 4-pentynenitrile proceeded according to the same procedure as for **1** and **2** giving **3** with overall 24% yield.

Absorbance Properties

Ruthenium polypyridyl complexes exhibit strong absorbance in the visible region due to a metal-to-ligand charge transfer (MLCT) band at low energies. In this state, electrons are excited from the ground state located primarily on the metal center to a low-lying excited state located on the polypyridyl ligand, at higher energy for bipyridine than biquinoline.[39] Ligands with more extended pi structures tend to lower the energy of the MLCT band, and red shift the absorbance.

The ^{1}MLCT absorption maxima for **1**, **2**, and **3** were 419, 491, and 529 nm, respectively (ε reported in **Table 4.1**). A shift of over 70 nm was observed with the first substitution of a bipyridine for biquinoline ligand, from **1** to **2** (**Figure 4.1a**), followed by a nearly 40 nm red-shift from **2** to **3**.[86] The spectra are nearly identical to previously published spectra for $Ru(phen)_2(MeCN)_2$ (λ_{max} = 420 nm), $Ru(phen)(biq)(MeCN)_2$ (λ_{max} = 497 nm), and $Ru(biq)_2(MeCN)_2$ (λ_{max} = 535 nm).[39]

Photolysis

The photolysis of ruthenium polypyridyl compounds can be observed using UV-Vis spectroscopy as the exchange of a coordinated ligand for a solvent molecule typically gives a significant red shift in the MLCT band. Under continuous 'irradiation, compounds **1**-**3** sequentially exchanged both nitrile ligands (**Figures 4.3A**). UV-Vis photolysis curve for **3** is shown in **Figure 4.3B**, where peaks at 560 and 590 nm indicate a stepwise process, with a monoaquated intermediate. The

expected isosbestic points at 550 and 570 nm also indicate the stepwise transition from **3** to monoaquated **3'** to bisaquated **3''**, though the first transition point at 550 nm is muddied by early formation of **3''** under continuous irradiation. The clear isosbestic points at 390 and 570 nm indicate clean conversion to the final bisaquated product.

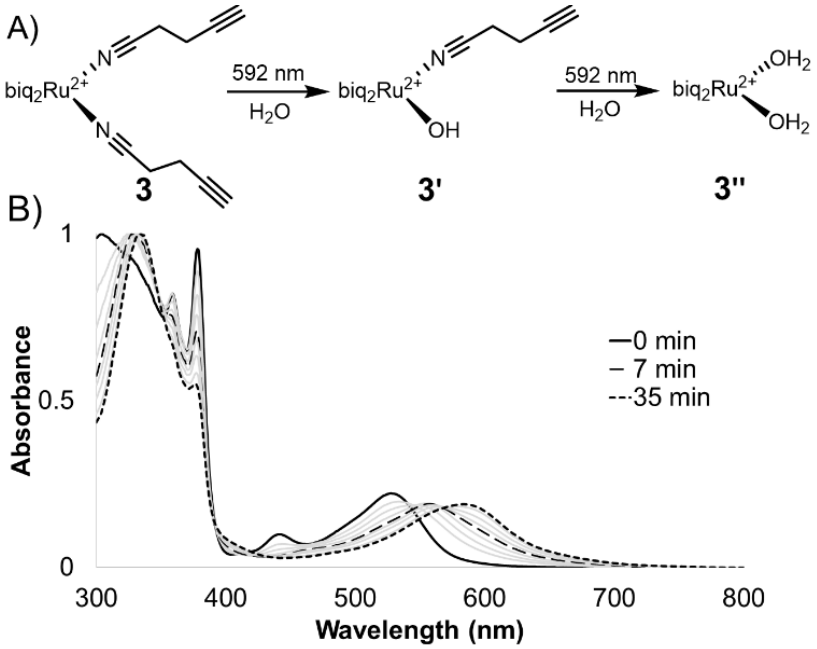

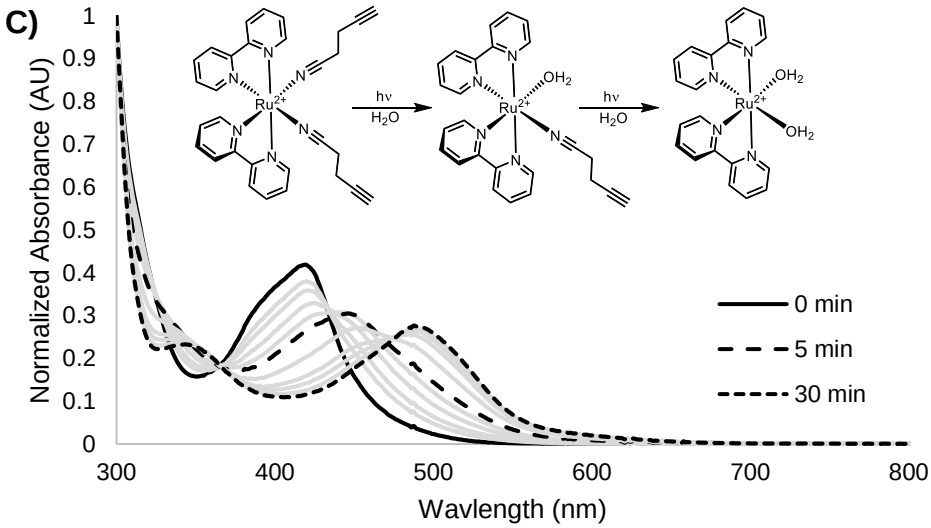

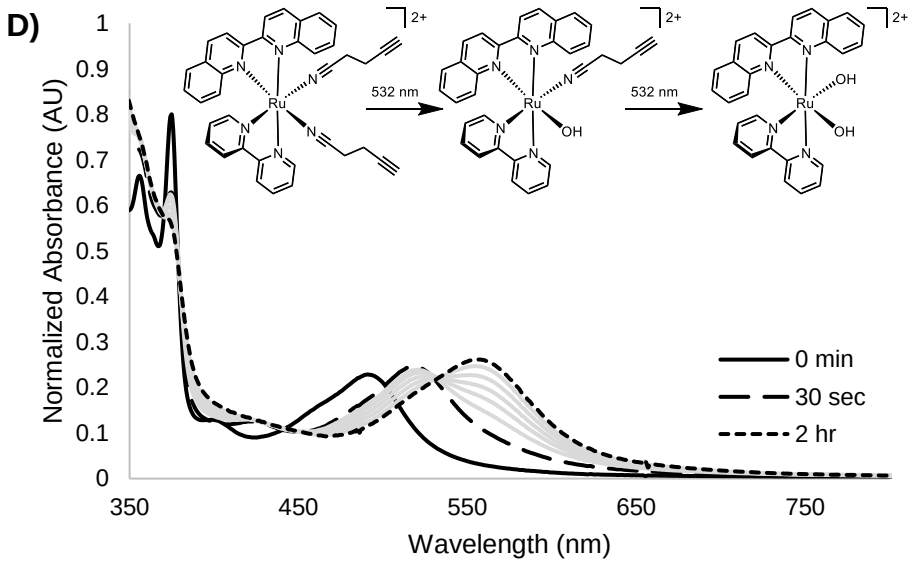

Figure 4.3. Photolysis of **1-3** in water. A) Compounds **1-3** undergo a stepwise ligand exchange of both nitrile ligands when irradiated in water. The second step takes much longer than the first. B) Photolysis trace of **3** in water under irradiation from 592 nm LED (25 mW/cm^2). C) Photolysis of **1** in water with 410 nm LED (25 mW/cm^2). D) Photolysis of **2** in water with 532 nm LED (25 mW/cm^2).

The loss of the second nitrile ligand is much slower, occurring on the order of 30-35 min, compared to the first ligand exchange event which is completed within minutes of constant irradiation. This trend is observed for **1** and **2** as well (**Figure 4.3C** and **D**), and is confirmed by ^{1}H NMR (**Figure 4.4**).

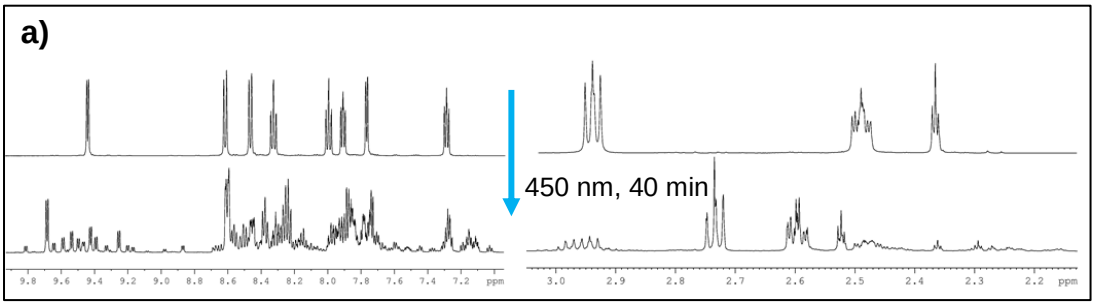

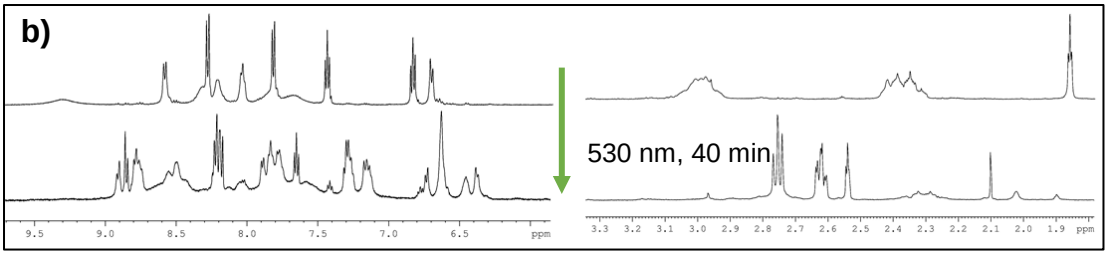

Figure 4.4. ^{1}H NMR observing the photolysis of **1** (a) and **3** (b) in D_2O. Upon irradiation of **3** in D_2O complete loss of the coordinated ligand signal (at 2.90, 2.35, and 1.83 ppm) is observed, and new peaks corresponding to free 4-cyano-1-butyne appear (at 2.75, 2.62, and 2.53 ppm). In the aromatic region changes in peak shape and chemical shifts are hard to assign, but indicate a loss in symmetry and a mixture of isomers in the final solution.

The Ru MLCT band extends well beyond the λ_{max}, which can be used to induce ligand exchange at longer wavelengths of light; irradiation at 600 – 700 nm (red incandescent light bulb, 5 mW) also was capable of photolyzing **3**, albeit at a slower rate (**Figure 4.5**).

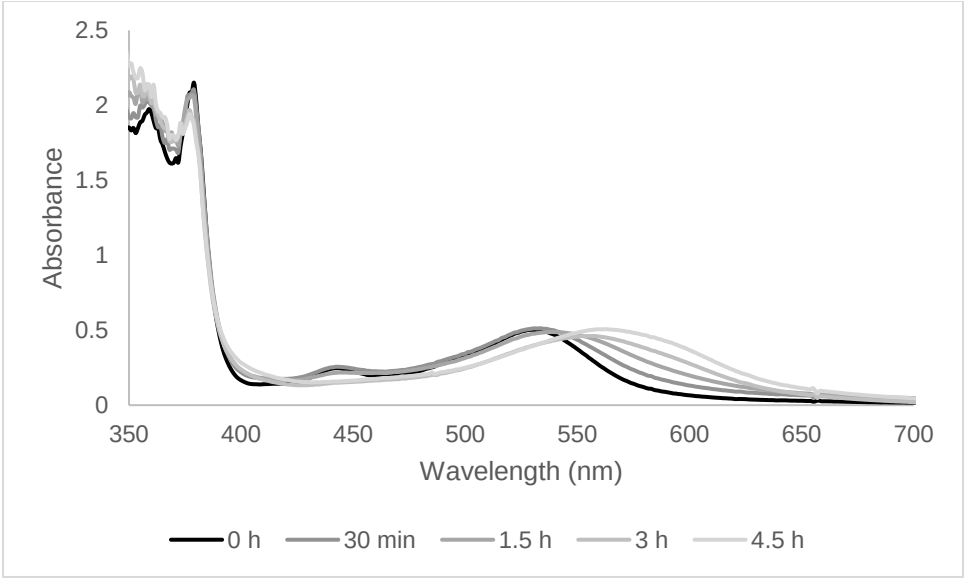

Figure 4.5. 80 μM solution of **3** ($Ru(biq)_2(4\text{-pentynenitrile})_2$) in water, irradiated with broadband 600 – 700 nm incandescent light (5 mW/cm^2).

Quantum Yield

Quantum yields were determined by measuring the kinetics of photolysis under constant irradiation by a single wavelength light source. For **1**, a 450-nm laser pointer was used (52 mW/cm^2), for **2** and **3** a 532-nm laser pointer (30 mW/cm^2) was used. The changes in absorbance

due to the generation and subsequent degradation of the intermediate Ru(polypyridyl)$_2$(4-pentynenitrile)(H_2O) were observed under constant irradiation. These data were fit to an equation derived from pseudo-first order kinetics equations, and the time constants were derived (**Figure 4.6, Table 4.1**).

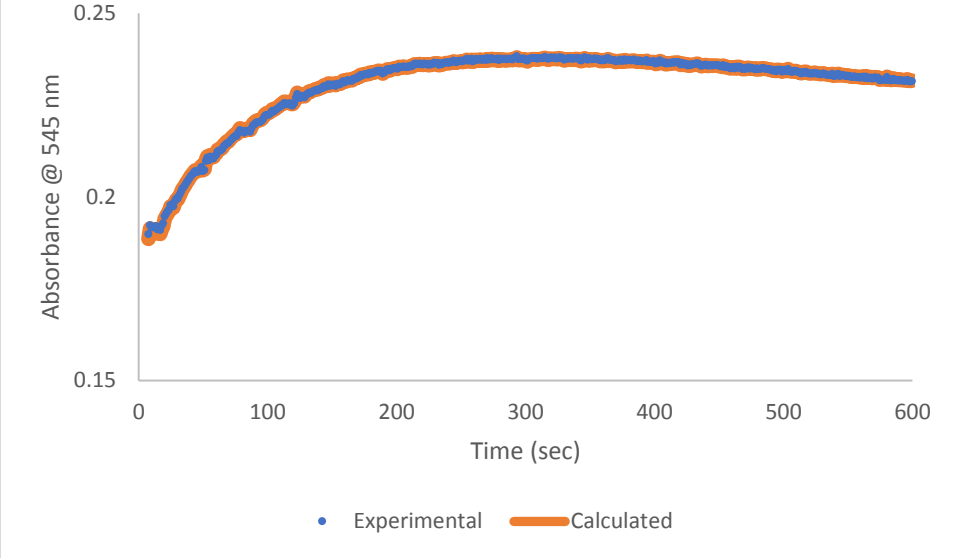

Figure 4.6. Kinetics trace for **3** under constant photolysis. The absorbance was measured at 545 nm throughout the experiment.

The data was fit to an equation of the form

$$y = A_1 e^{-x/\tau_1} + A_2 e^{-x/\tau_2} + y_0$$

With two time constants τ_1 and τ_2 that give rate constants k_1 and k_2 according to

$$Abs@470 = \varepsilon_A [A]_0 e^{-k_1 t} + \varepsilon_B [A]_0 e^{-k_2 t} + \varepsilon_B [A]_0$$

The rate constants for each step for **1**-**5**:

	τ_1 (s)	k_1 (s^{-1})	τ_2 (s)	k_2 (s^{-1})
1: $Ru(bpy)_2(pentynenitrile)_2$	103 ± 3	0.0097	488 ± 44	0.0021
2: $Ru(bpy)(biq)(pentynenitrile)_2$	127 ± 2	0.0078	600 ± 180	0.0017
3: $Ru(biq)_2(pentynenitrile)_2$	118 ± 4	0.00850	1340 ± 100	0.000785
4: $Ru(bpy)_2(hexynenitrile)_2$	100 ± 7	0.01	734 ± 28	0.0014
5: $Ru(biq)_2(hexynenitrile)_2$	131 ± 6	0.008	1034 ± 47	0.00097

Table 4.1. Time constants for **1-5**, determined by data fitting.

The quantum yield of photorelease, Φ_{pr}, was found for the first exchange event from the time constant as related to the rate constant and coupled with the laser power (**Figure 4.6**). As expected, the number decreased greatly in value as the MLCT band was shifted further to the red, decreasing from 0.43 (in **1**) to 0.06 (in **3**), **Table 4.2**.[10,47] **3** was significantly less efficiently photolyzed at 444 $M^{-1}cm^{-1}$ compared to **1** at 2640 $M^{-1}cm^{-1}$.

The Φ_{pr} for **1** and **4** are significantly different, with **4** being closer to literature values (Φ_{400} for $Ru(bpy)_2(MeCN)_2$ = 0.21).[33,39] Conversely, the Φ_{pr} for **3** and **5** are very similar, within standard error of each other. This suggests that the longer ligand may not have an effect on the photochemistry of the compounds, and that the solubility of each ligand has a negligible effect on the Φ_{pr} in this case.

	ε ($M^{-1}cm^{-1}$)	Φ_{pr}	Efficiency ($\varepsilon \bullet \Phi$, $M^{-1}cm^{-1}$)
1	6140 ± 98	0.43 ± 0.02	2640
2	4100 ± 500	0.16 ± 0.02	656
3	7400 ± 400	0.060 ± 0.005	444
4	6300 ± 980	0.16 ± 0.03	1008
5	4169 ± 490	0.07 ± 0.01	292

Table 4.2: Absorptivities and quantum yields for **1-5.**

Stability

Ruthenium (II) polypyridyl complexes can be solubilized in different solvents by exchanging counterions. In our initial experiments with **3** we observed significant thermal instability of the

compound when dissolved in water (**Figure 4.7**) as the chloride salt, e.g., the compound degraded within 24 h of dissolution and storage in the dark.

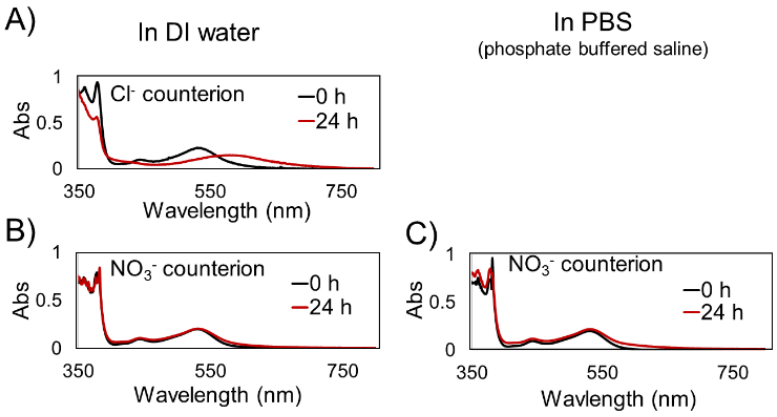

Figure 4.7. Stability of **3** in water and PBS. A) When solubilized with a chloride counterion **3** degraded within 24 h of dark storage. B) Switching to a nitrate counterion improved stability drastically, even in the presence of chloride in PBS (C).

This unusual stability issue was characterized by ESI and ^{1}H NMR for **3**$[Cl]_2$ (**Figure 4.8**). Samples stored in DI water for 24 hours showed the presence of a new mass at 692.5, which corresponds to the compound $Ru(biq)_2$(4-pentynenitrile). ^{1}H NMR shows the appearance of free 4-pentynenitrile, which coupled with the ESI results suggests that one nitrile ligand is exchanged, leaving the remaining ligand likely coordinated by both the nitrile and the alkyne. Due to the steric constraints of the molecule and the neutral-to-low pH of DI water especially in the presence of a Lewis acid, it is unlikely that the alkyne is deprotonated, indicating that the alkyne is η^2-bound to the ruthenium, a phenomenon seen previously for Ru(II) complexes.[136,137] The NMR shows incomplete ligand loss even after several days, indicating that the remaining alkyne ligand is stabilizing the $Ru(bpy)_2$(4-pentynenitrile) product and stalling further ligand exchange processes.

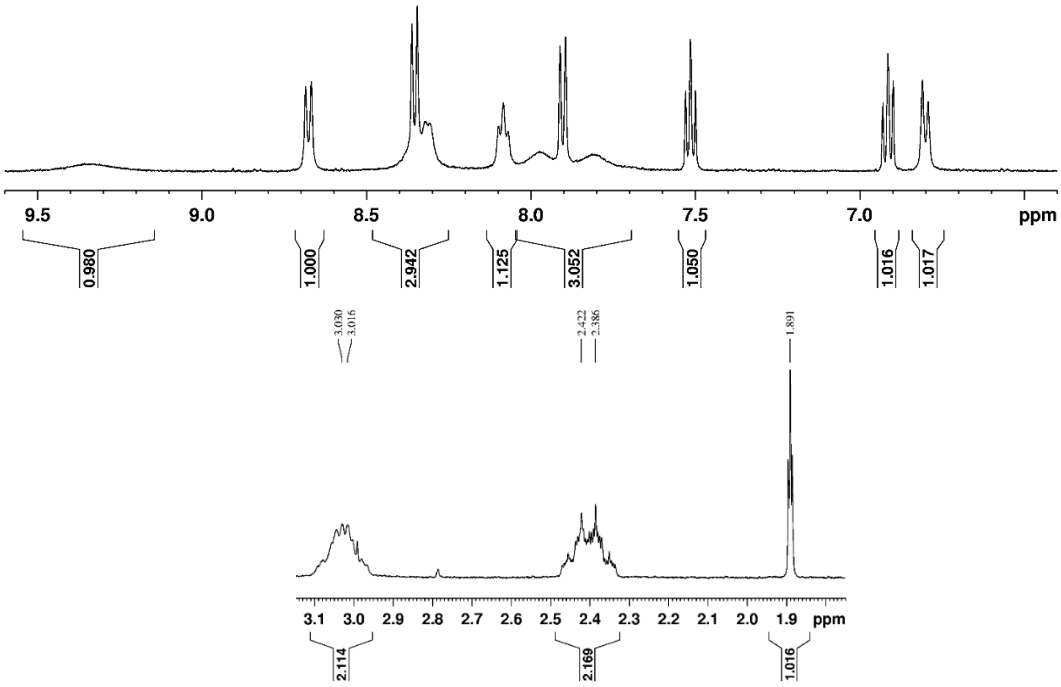

Figure 4.8A. Freshly dissolved Ru(biq)$_2$(4-pentynenitrile)$_2$[Cl]$_2$ in D_2O.

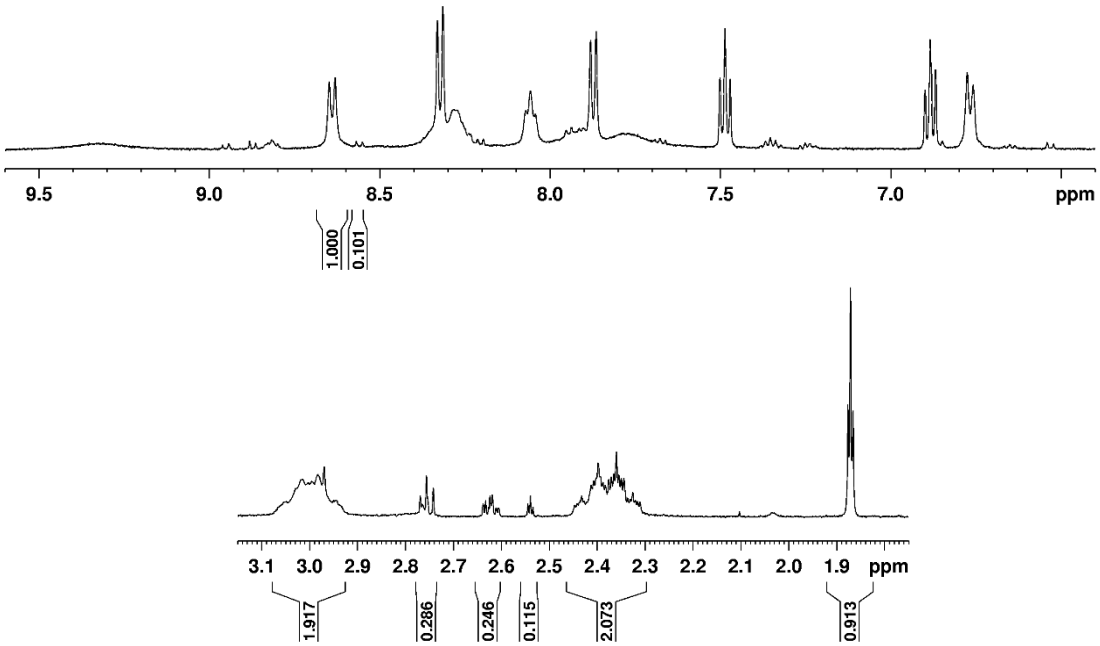

Figure 4.8B. Sample from A left in the dark on benchtop for 48 hours. Peaks at 2.75, 2.62, and 2.53 ppm correspond to free 4-pentynenitrile. Approximately 10% of **3** has converted into Ru(biq)$_2$(4-pentynenitrile), by relative integration values. The coordinated alkyne peak at 1.89 ppm has decreased by ~10% relative to the standard biquinoline integration, suggesting that apart from losing some coordinated 4-pentynentrile, ~10% has remained coordinated (note the lack of change in integration for multiplets at 3.00 and 2.39 ppm) but the alkyne has likely been deprotonated. Experiments are ongoing to confirm this hypothesis.

The shift of λ_{max} from 535 to a broad band around 570 nm is indicative of the coordination of an electron donating ligand such as an η^2-alkyne as a minor product. Raising the pH greatly decreases the stability, for samples stored in a pH 10 buffer we observe the appearance of a new $\lambda_{max} \cong$ 625 nm, indicative of a coordinated alkyne (**Figure 4.9**).

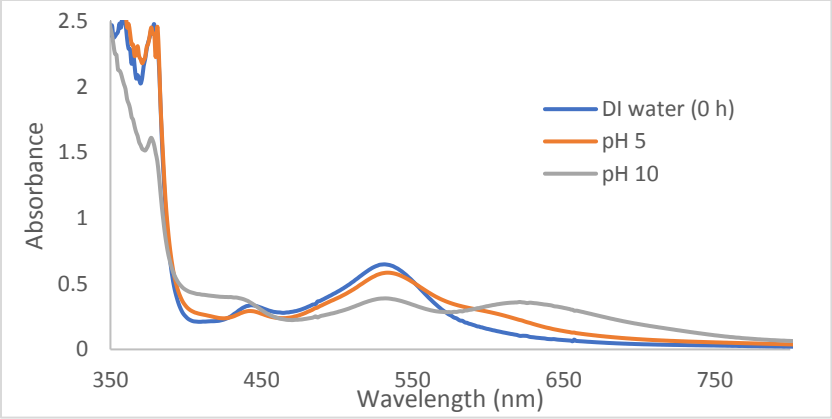

Figure 4.9. Samples of **3** were dissolved in buffers at pH 5 and 10 for 24 hours in the dark, and compared to a fresh sample of the same concentration (DI water). Higher pH renders **3** less stable, a significant shift to the red indicates coordination of the alkyne to the ruthenium as a carbanion. At lower pHs less degradation is observed, and a different product may form (e.g. coordinating the alkyne as η^2).

The alkyne coordination does not appear to have an effect on the photochemistry, with no significant trend is observed for the time constants for **1** and **4** (where **4** is $Ru(bpy)_2$(5-hexynenitrile)$_2$) and for **3** and **5** (where **5** is $Ru(biq)_2$(5-hexynenitrile)$_2$). There is no significant difference between the first time constants of **1** and **4**, with both values within the error of the other. The same is observed for τ_1 for **3** and **5**. τ_2 for **1** and **4** are significantly different, with τ_2 for **4** being significantly slower (734 s vs 488 s), suggesting that the longer ligand may stabilize the monoaquated intermediate. However, τ_2 for **3** and **5**, while significantly different, have the opposite trend, τ_2 for **5** is faster than **3** (1034 s vs 1340 s), possibly due to the steric bulk of the biquinoline reducing the amount of alkyne association. The difference between the time constants and subsequently Φ_{pr} for the compounds appears to be independent of solubility or alkyne stabilizing of the monoaquated intermediate.

This thermal instability was mitigated by a switch to nitrate as a counterion; after purification **2** and **3** were metathesized to the NO_3^- salt using an Amberlite IRA-410 resin pre-soaked in HNO_3 (confirmed by LC-MS). This salt was less soluble in water, as expected, but demonstrated dramatically improved stability in aqueous solution in the dark, even in the presence of biologically relevant concentrations of chloride (**Figure 4.7B** and **C**). This is likely due to a closer association of the nitrate counterion to the structure, as indicated by HR-MS characterization of the nitrate salt showing that NO_3^- flew with the compound on the HR-MS, an unusual property never observed previously for our Ru(II) complexes with Cl^- and PF_6^- counterions.

Crystal Structure

Crystals were grown of the PF_6^- salt of **3** and **5** via vapor diffusion of ether into a mixture of acetonitrile, methanol, and THF (**Figure 4.9**). Bond lengths between the Ru and the ligands were within expected ranges, with variations due to the steric strain in the system. The distance between Ru and the nitrogen of the biquinoline ligands was significantly longer than published previously for $Ru(biq)(phen)(MeCN)_2$,[39] attributed to the higher strain around the ruthenium center in **3**. The N≡C bond in these ruthenium-nitrile coordination compounds is consistently shorter than a free nitrile bond (1.13 Å vs 1.20 Å), in agreement with literature value (1.130 Å).[39] The most significant deviation from previous structures lies in the difference in Ru-nitrile bond lengths (Ru-N1 vs Ru-N2), indicating that the steric strain that is lengthening the bonds to the biquinoline ligand is also affecting the bond between the ruthenium and the nitrile, destabilizing it just enough to sensitize the compound to nearby coordinating ions such as Cl^-. Additionally, the angle between the nitrile ligands is stretched significantly to >95° perhaps due to the strain of a bulkier ligand coordinated to the Ru.

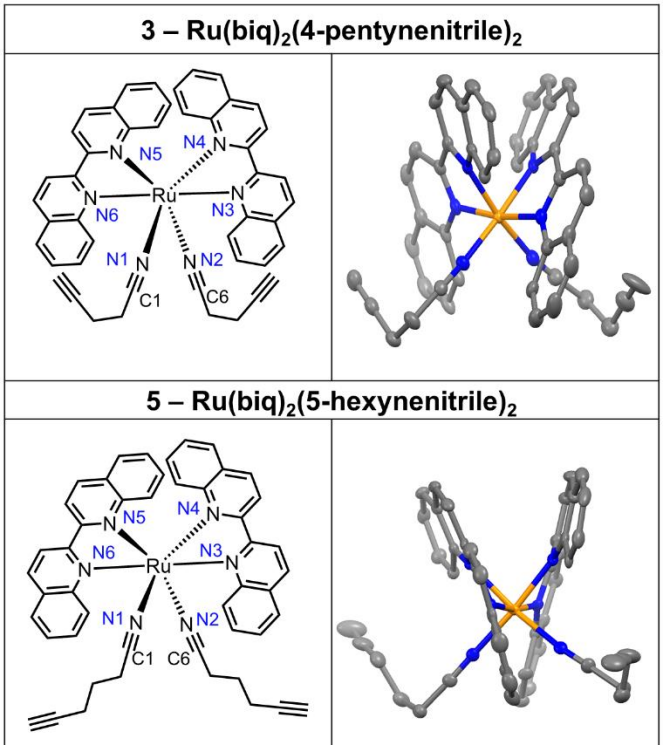

Figure 4.9. Crystal structures of **3** and **5.**

The crystal structure for **3** indicated that the two pendant alkyne groups may be less accessible to crosslinking than desired (**Figure 4.9**). The native *cis* conformation of the ligands places the alkynes very close to the biquinoline aromatic surface, only ~3.7 Å away. We found that **1 – 3** were incapable of reliably clicking to a terminal azide, likely due to this steric blocking (**Scheme 4.1**). To extend the alkyne beyond the crowded ligand field, compounds **4** $(Ru(bpy)_2(5\text{-hexynenitrile})_2$ and **5** $(Ru(biq)_2(5\text{-hexynenitrile})_2)$ were also synthesized. The crystal structure for **5** (**Figure 4.9**) confirms placement of the alkyne groups nearly 2 Å further from the biquinolines compared to **3**. Though most of the bond lengths for each compound are similar (**Table 4.3**) it is worth noting that both Ru-nitrile bonds are similar in length, as opposed to the inequality observed in **3**. This may contribute to higher stability of **5** in aqueous environments, especially when dissolved as the NO_3^- salt.

	Bond	3 (Å)	5 (Å)
Ru-biq	Ru-N4	2.093(4)	2.084(6)
	Ru-N3	2.095(4)	2.093(6)
Ru-N≡C	Ru-N1	2.050(4)	2.025(6)
	Ru-N2	2.039(4)	2.024(6)
C≡C to biq		3.717/3.765	5.128/5.27

Table 4.3. Select bond lengths.

Crosslinking Ability

CuAAC have been widely used for materials design, with several studies showing the generation of hydrogel materials. Hyaluronic acid,[138,139] polyethylene glycol (PEG),[140] dextran,[141] poly(vinyl) alcohol (PVA)[142] along with several others have been modified with azides and terminal alkynes to facilitate hydrogel formation. The need for a Cu(I) catalyst has limited some bio-applications as it can be toxic to cells,[143] but can also provide spatiotemporal control. In one example Bowman and co-workers used a photocatalyst to reduce Cu(II) for the formation of a hydrogel with precise control.[144] Copper is easily dialysed away from preformed hydrogels, which is acceptable for many drug delivery platforms.

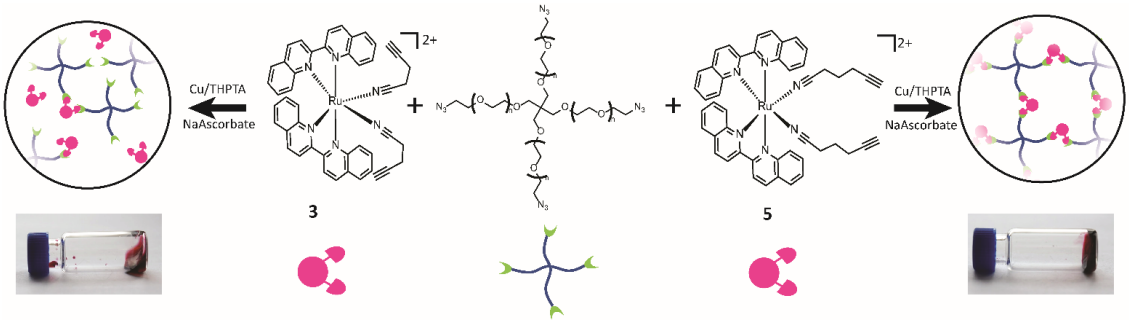

Scheme 4.1. Gelation using **3** vs **5**.

1 and **3** were designed as a multiplexed system of crosslinkers, as **3** is red-shifted enough to selectively absorb orange/red light, leaving **1** intact. To demonstrate their crosslinking ability as alkyne-based crosslinkers for CuAAC chemistry, and to determine if the stability issues we observed *in situ* persisted in more complex systems, we attempted to form a soft hydrogel from

branched azide-modified PEG (MW 10,000 Da) and **3**, in the presence of $CuSO_4$, THPTA, and Ascorbate (**Scheme 4.1**).

Despite multiple formulations including varying the wt% of the hydrogel, the amount of excess Cu^{2+} and THPTA, **1 – 3** failed to generate a hydrogel, likely due to the inaccessibility of the alkyne to the copper catalyst. **4** and **5**, however, rapidly clicked with the azido-PEG, forming a strong hydrogel within 30 s (**Figure 4.10**). Hydrogels formed at a final weight percent of 7.5 wt% with a stoichiometric amount of ruthenium crosslinker to encourage 100% crosslinking generated a hydrogel with an elasticity nearing 1 kPa (**Figure 4.10**). As expected, when exposed to visible light (400 – 500 nm) the hydrogel rapidly lost its elastic properties, becoming a viscous liquid within 5 min.

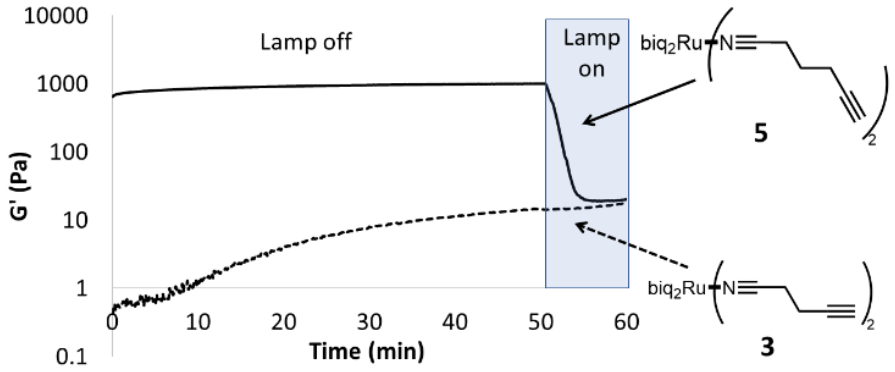

Figure 4.10. Rheometry demonstrating the significant gelation improvement upon coordinating a longer alkyl ligand (5-hexynenitrile). The hydrogel formed from 5 was effectively degraded under irradiation with 400 – 500 nm light (25 mW/cm^2).

4 and **5** (**Figure 4.11**) have sufficiently separated absorption maxima to be activated separately using orange (592 nm) and blue (410 nm) light. 592 nm light was sufficient to selectively degrade **5** while leaving **4** intact, as demonstrated quantitatively in **Figure 4.11B**. The absorbance of a solution of equal parts **4** and **5** was monitored at 423 and 590 nm under constant irradiation. The steady increase in absorbance at 590 nm shows the appearance of the bisaquated product $Ru(biq)_2(H_2O)_2$, the final photolysis product of **5**. The absorbance at 423 nm indicates the amount of intact **4** in solution. A slight variation in this absorbance within the first several seconds is due

to small changes in the spectra of **5** at 423 nm in the first step of photolysis (see **Figure 4.3B**). A significant drop in the absorbance due to **4** is observed only under irradiation with blue light (410 nm). An increase at 590 nm is expected from the $Ru(bpy)_2(H_2O)_2$ product (see **Figure 4.3C**). This significant separation of the λ_{max} for **4** and **5** enabled the generation of a hydrogel system wherein defined sections of a hydrogel can be degraded selectively, leaving other portions intact. This is shown in **Figure 4.11C**, where 592 nm light selectively degraded the red hydrogel sections, while leaving the orange sections intact.

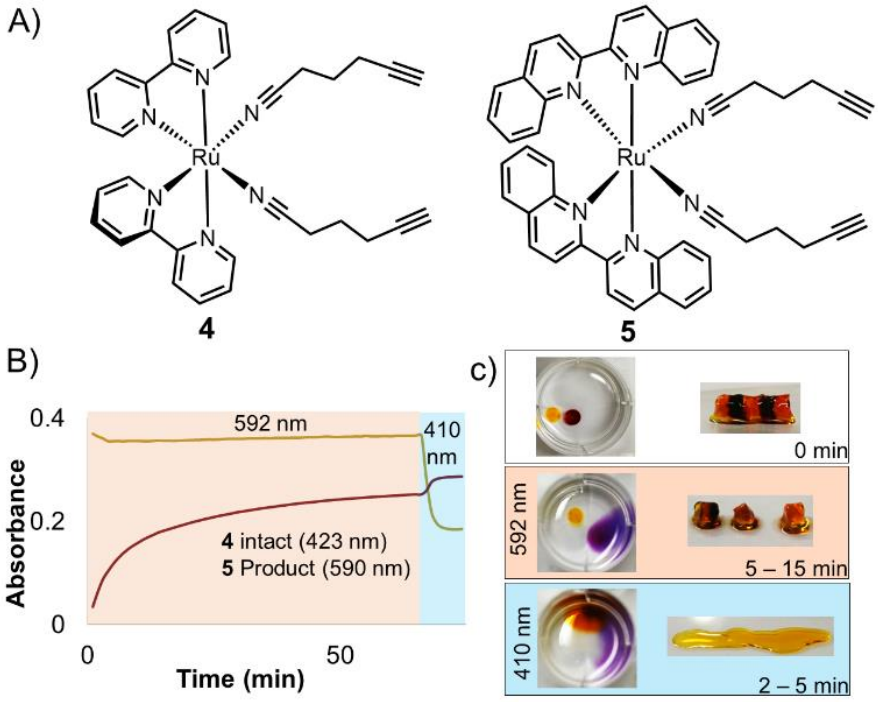

Figure 4.11. Selective degradation of **4** and **5**. A) Structures of **4** and **5** are identical to **1** and **3** save for the alkyne ligand, which is one methylene group longer. B) Selective degradation of **4** and **5** observed by absorbance spectroscopy. The absorbance of **4** remains steady under irradiation with 592 nm light, until irradiated with 410 nm light. C) Selective erosion of hydrogels under different wavelengths of light. Orange light leaves the orange/yellow hydrogels intact, while blue light degrades both.

4.3 Conclusions and Future Experiments

We developed photolytically-active, red-shifted ruthenium compounds with enhanced solution stability and crosslinking capability for gel formation. Replacing bipyridine with more pi-conjugated biquinoline ligands red-shifted the absorbance, but initially led to unstable compounds in water.

Stability problems were minimized by changing to a nitrate counterion, and alkyne accessibility was tuned using a longer alkyne-modified ligand. In this work we showed the development of a series of ruthenium-based crosslinkers that can be used together for selective incorporation and photoactivation in a hydrogel matrix. This represents the two-color wavelength-selective system to use 100% visible light published to our knowledge.

Future experiments are planned to address the thermal ligand exchange discovered in these alkyne-modified Ru(II) complexes, primarily to identify the primary product as a carbanion or an η^2-alkyne. Solution phase IR should be able to differentiate between the possible alkyne environments, and electrochemistry on the aqueous solutions may illuminate the charge and/or oxidation state of the ruthenium.

4.4 Methods and Materials

Materials

$Ru(bpy)_2Cl_2$ was purchased from Strem Chemicals; LiCl, CD_3CN, biquinoline, NH_4PF_6, $RuCl_3$, AgOTf, $AgPF_6$, and hydroquinone were purchased from Acros Organics, 4-pentynenitrile, 5-hexynenitrile, and the Amberlite resins were purchased from Sigma Aldrich, and all solvents were purchased from Fisher Scientific. All chemicals were used without further purification.

Azido-PEG was purchased from PegWorks, THPTA from Click Chemistry Tools, Sodium Ascorbate and copper sulfate from Aldrich. PBS was purchased from Hyclone.

Methods

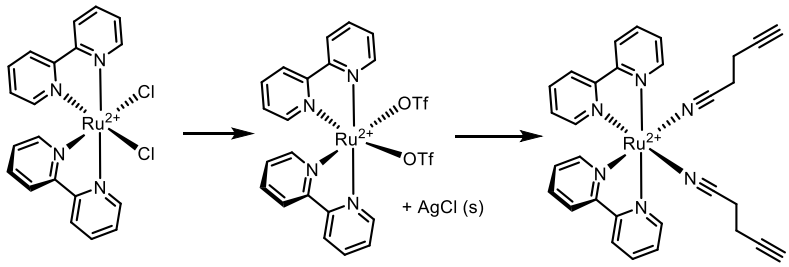

*Synthesis of Ru(bpy)$_2$(4-pentynenitrile)$_2$ (**1**)* Ru(bpy)$_2$Cl$_2$ (106.1mg, 0.20 mmol) and silver triflate (AgOTf, 112 mg, 0.43 mmol) were suspended in methanol (15 mL) and stirred for 10 min. 4-pentynenitrile (178 μL, 2 mmol) was added and the reaction was heated to 55 °C for 1.5 hours. The methanol was removed by rotary evaporation and NH_4PF_6 was added to precipitate the PF_6 salt of **1**, which was extracted using dichloromethane. The product was purified by flash chromatography on silica gel with a gradient of 1:4 acetonitrile:DCM The chloride salt was generated by passage through an Amberlite IRA-410 chloride form resin; 54 % yield (71.1 mg). ^{1}H NMR (D_2O): 9.4401 (d, 2H), 8.6175 (d, 2H), 8.467 (d, 2H), 8.3302 (t, 2H), 8.000 (t, 2H), 7.9125 (t, 2H), 7.7714 (d, 2H), 7.2394 (t, 2H), 2.9576 (t, 4H), 2.4976 (t of d, 4H), 2.3704 (t, 2H).

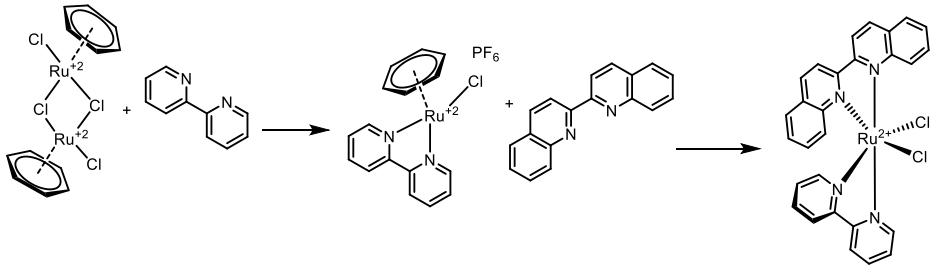

Synthesis of Ru(bpy)(biq)Cl$_2$ Bis[(benzene)dichlororuthenium] (530 mg, 1.06 mmol) and 2,2′-bipyridine (413 mg, 2.6 mmol) were added to methanol (50 mL). The solution was stirred at room temperature for 1 hour, then tetrabutylammonium hexafluorophosphate ($TBAPF_6$) was added until precipitation was complete (~200 mg). The light-yellow product Ru(bz)(bpy)Cl was isolated by vacuum filtration and used without further purification for the next step (crude yield: 908 mg, 83%).

Ru(bz)(bpy)Cl[PF_6] (908 mg, 1.76 mmol) and LiCl (612 mg, 14.4 mmol) were suspended in dimethylformamide (7 mL) and stirred under nitrogen for 10 min. Biquinoline (433 mg, 1.70 mmol) was added, and the solution heated to 130 °C for 1 hour. The reaction mixture was cooled to room temperature and added to 500 mL DI water and filtered to collect the dark green product. The precipitate was then redissolved in dichloromethane and washed 2x with water and

reprecipitated from diethyl ether for the final product, Ru(bpy)(biq)Cl_2 (614 mg, 67% yield, 55% overall yield).

*Synthesis of Ru(bpy)(biq)(4-pentynenitrile)$_2$[NO_3]$_2$ (**2**)* The same procedure for **1** was used: Ru(bpy)(biq)Cl_2 (23.4 mg, 0.04 mmol), AgOTf (23 mg, 0.09 mmol), and 4-pentynenitrile (47 μL, 0.54 mmol) dissolved in methanol (10 mL), purified by silica gel chromatography (1:4 acetonitrile:DCM). Final yield: 16.6 mg, 63% yield. The water-soluble nitrate salt was generated by passage through an Amberlite IRA 743 Free Base resin presoaked in HNO_3 with methanol as the eluent. ^{1}H NMR (CD_3CN): 9.5661 (d, 1H), 8.8821 (d, 1H), 8.8529 (d, 1H), 8.4770 (s, 2H), 8.2544 (t, 2H), 8.2384 (t, 2H), 8.1190 (d, 2H), 8.0490 (t, 2H), 7.9412 (m, 4H), 7.0770 (t, 2H), 7.5757 (t, 1H), 7.4435 (d, 1H), 7.3378 (m, 3H), 7.2118 (t, 2H), 3.691 (s, 1H), 3.7054 (s, 1H), 2.9442 (t, 2H), 2.7941 (t, 2H), 2.4730 (m, 2H), 2.3016 (m, 2H). Expected mass: 734.1464 ([**2**]$^{2+}$[NO_3^-]), observed mass: 734.1473 Da

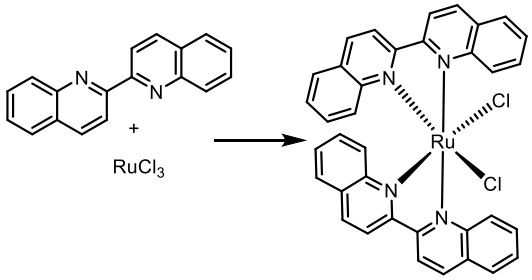

Synthesis of Ru(biq)$_2$Cl$_2$ $RuCl_3$ (207 mg, 1 mmol), hydroquinone (222 mg, 2 mmol), and LiCl (240 mg, 5 mmol) were suspended in DMF (5 mL) and stirred under nitrogen for 15 min. Biquinoline (498 mg, 1.9 mmol) was added and the reaction heated to 130 °C for 1 hour. The reaction mixture was added to 500 mL DI water and product isolated following the same procedure as Ru(bpy)(biq)Cl_2. Yield: 219 mg, 33%.

*Synthesis of Ru(biq)$_2$(4-pentynenitrile)$_2$[NO_3]$_2$ (**3**)* Ru(biq)$_2Cl_2$ from previous step (51 mg, 0.07 mmol) was dissolved in 10 mL of methanol. AgOTf (49 mg, 0.19 mmol) was added, reaction was stirred at room temperature for 10 min. 4-pentynenitrile (78 μL, 0.74 mmol) 4-pentynenitrile was

added and solution was heated to 50 °C for 1 hour. $Ru(biq)_2(4\text{-pentynenitrile})_2[PF_6]_2$ was extracted and purified as described for **1** (45.3 mg, 73%). The water-soluble salts (chloride or nitrate) were generated using an Amberlite resin, IRA-410 chloride resin for the chloride, IRA 743 Free Base resin for the nitrate. ^{1}H NMR (CD_3CN): 9.1485 (1H), 8.6791 (d, 2H), 8.3620 (d, 2H), 8.2986 (d, 2H), 8.2057 (s, 2H), 8.0071 (t, 2H), 8.050 (s, 2H), 7.9136 (d, 2H), 7.4970 (t, 1H), 6.8676 (t, 1H), 6.8165 (d, 2H), 2.8483 (m, 4H), 2.3369 (m, 4H), 1.8338 (t, 2H). Expected mass: 834.1779 ([**3**]$^{2+}$[NO_3^-]), observed mass: 834.1799 Da

*Synthesis of $Ru(bpy)_2(5\text{-hexynenitrile})_2[NO_3]_2$ (**4**)* was synthesized according to the protocol for **1**; with $Ru(bpy)_2Cl_2$ (106.7 mg 0.2 mol) and $AgPF_6$ (114 mg, 0.45 mmol) were added 20 mL methanol and stirred for 10 min. 5-hexynenitrile (320 μL, 3 mmol) was added and the reaction stirred at 50 °C for 1 hour. The methanol was removed by rotovap and the crude product purified by silica chromatography (1:4 acetonitrile:DCM). Yield: 100.6 mg, 68%. ^{1}H NMR (CD_3CN): 9.272 (d, 2H), 8.5144 (d, 2H), 8.3725 (d, 2H), 8.2741 (t, 2H), 7.9551 (t, 2H), 7.8510 (t, 2H), 7.6191 (d, 2H), 7.2636 (t, 2H), 2.7542 (m, 4H), 2.1804 (t, 2H), 2.0517 (m, 4H), 1.7048 (t, 4H). Expected Mass: 662.1462 ([**4**]$^{2+}$[NO_3^-]), observed mass: 662.1449 Da

*Synthesis of $Ru(biq)_2(5\text{-hexynenitrile})_2[NO_3]_2$ (**5**)* was synthesized according to the protocol for **4**; with 100 mg (0.15 mmol) $Ru(biq)_2(Cl)_2$, 105 mg (0.4 mmol) $AgPF_6$, and 230 μL (2.8 mmol) 5-hexynenitrile. Yield: 97.9 mg, 73%. ^{1}H NMR (D_2O): 9.3868 (s, 2H), 8.7955 (d, 2H), 8.4220 (m, 6H), 8.2398 (d, 2H), 8.1253 (t, 2H), 8.1097 (s, 2H), 7.9900 (d, 2H), 7.5695 (t, 2H), 6.9401 (t, 2H), 6.8261 (d, 2H), 6.8261 (d, 2H), 3.0657 (m, 4H), 2.1894 (t, 2H), 2.0125 (m, 4H), 1.7317 (m, 4H). Expected mass: 862.2093 ([**5**]$^{2+}$[NO_3^-]), observed mass: 862.2095 Da

Formation of a 10 wt% PEG hydrogel

Table 4.4 shows the amounts of reagents used to generate a 25 uL hydrogel

	[Stock]		Amt to add (μL)	Ratio (X:RuAlkyne)
PEG	600	mg/mL	4.17	0.5:1
RuAlkyne	50	mM	9.84	1
Ascorbate	2500	mM	2.6	10:1
THPTA	1000	mM	4.92	10:1
Cu	1.5	M	3.28	10:1
MeCN			0.25	
		Total	25.00	

PEG, Ascorbate, and RuAlkyne were mixed together, and the $CuSO_4$ and THPTA were mixed separately to allow the THPTA to fully coordinate the copper. The two were then combined and mixed thoroughly before being allowed to gel over the course of 5-10 min. Hydrogels were then soaked in PBS to remove any excess ruthenium and copper before any experiments were done.

CHAPTER 5 - Cyclizing Oligonucleotides with a Ruthenium Photodegradable Crosslinker

5.1 Introduction

Antisense single-stranded oligonucleotides (ASOs) are short, 16-25mer strands of nucleic acids linked together with a wide variety of backbone, from the standard sugar-phosphate backbone found in DNA and RNA to backbones that are more stable to nucleases such as amide or morpholine linkages. ASOs can act in a variety of mechanisms, each triggered with the binding of the ASO to target mRNA. They can be designed and redesigned as needed to modulate the expression of a particular gene with excellent selectivity, a feature which, as stability issues are resolved, could place ASOs at the frontier of drug research.[145,146]

ASOs were first proposed to modify gene expression by Zamecnik and Stephenson in 1978.[147,148] As a gene is transcribed into RNA it passes into the cytosol where it undergoes splicing into messenger RNA (mRNA) before binding to ribosomes and being translated into protein (**Scheme 5.1**). DNA- or RNA-based ASOs act by recruiting RNAse H to the double stranded section and initiating degradation of mRNA. Morpholino ASOs can act either by blocking splicing sites of pre-mRNA or blocking the start codon of mRNA after it has been spliced. For DNA- or RNA-based ASOs, if the sequence is complementary to the exon (coding region of the gene of interest) no matter where in the gene sequence that complementarity lies, it should knock down that gene, with some variations in activity often due to the accessibility of the region of mRNA.

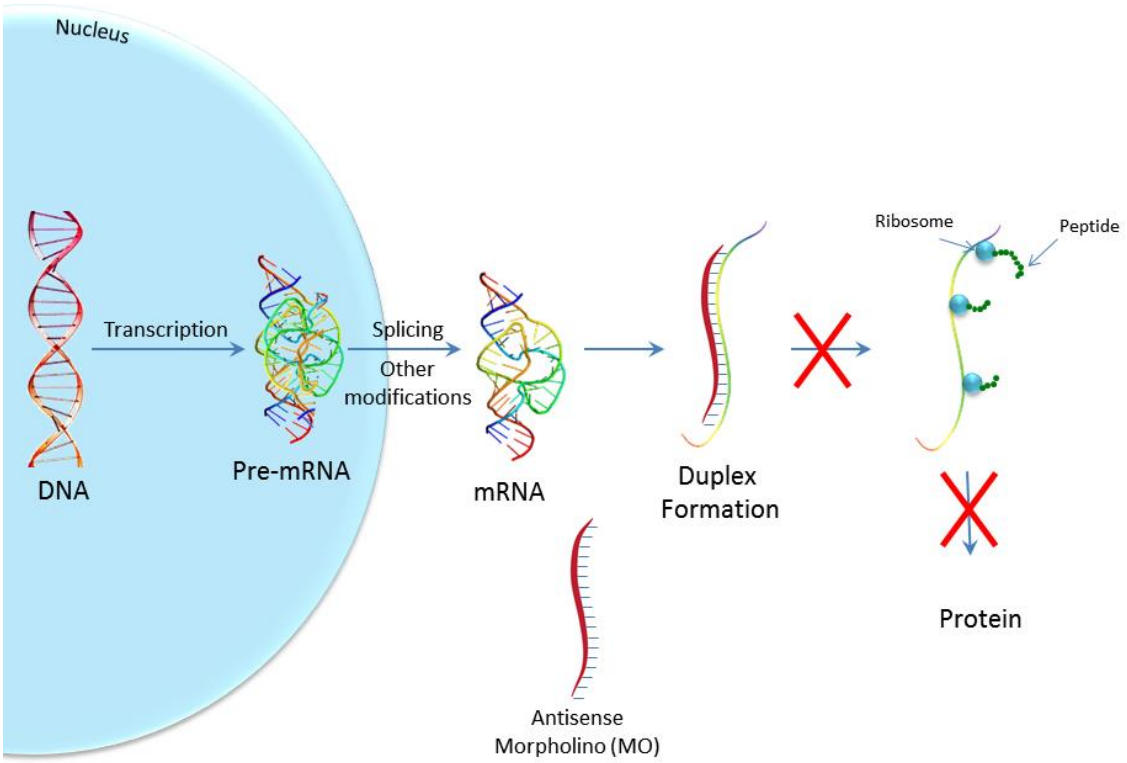

Scheme 5.1. The effect of an antisense oligonucleotide (ASO) on the Central Dogma of Biology.

DNA or RNA ASOs are more commonly used *in vitro*, as their stability *in vivo* (i.e., in a living organism, as opposed to in cell culture) is less than several hours, whereas their stability in cells can extend up to two days.[149] Other backbones such as locked nucleic acids (LNAs) or peptide nucleic acids (PNAs) have been used to generate ASOs that are more stable to serum nucleases to expand their use *in vivo* and in the clinic, where stability is a significant problem. Backbone modifications can also extend the half-life of ASOs, such as the chemical exchange of a sulfur for a non-bonding oxygen on the backbone (known as phosphorothioation).[146,150] Certain base modifications in the 2' position on RNA (such as the substitution of a fluorine or O-methyl) can also extend the stability to make ASOs more viable for *in vivo* applications; some RNA-based ASOs that were protected by phosphorothioation and 2' modifications have successfully completed clinical trials and entered the market as a treatment for diseases marked by unnatural enzyme levels.[151]

Complete alteration of the backbone from a charged phosphate to a neutral linker between bases as also been widely used to extend ASO stability to several days. One such modification is to use the amide backbone from protein structure to link bases together in nucleic acids.[152] These peptide nucleic acids (PNA) can be synthesized using standard FMOC solid phase synthesis commonly used for peptide synthesis, but as FMOC-protected nucleotides are more expensive to synthesize, longer PNA sequences are expensive and often have poor solubility.

Morpholine-based backbones are a more established method of generating serum stable oligonucleotides. Morpholinos, as morpholine-modified ASOs are called colloquially, have demonstrated stability for up to 4 days in zebrafish embryos[153] and excellent knockdown activity in multiple organisms. Their solubility is excellent, but purity can be an issue, as they are challenging to purify based on current HPLC methods for oligonucleotides, so any post-synthesis chemical modifications are challenging.

ASOs are important tools for controlling gene expression, and with improvements in cellular uptake and stability, are considered by some to be the next generation of drugs to target aberrant protein function. In some disease states and cellular systems, however, having spatial and temporal control over gene expression is desirable. In basic research to elucidate the activity of specific genes during embryogenesis, for example, it may be valuable to selectively knock down gene expression at a specific timepoint during development. Photoresponse is especially useful in ASO systems, providing researchers with highly focusable, orthogonal spatiotemporal control of biological processes. Photoresponsive oligonucleotides have been developed with a multitude of photoreactive moieties, each with their advantages and drawbacks.

o-Nitrobenzyl (*o*-NB) groups were among the first photoresponsive groups used in biology and in oligonucleotides. *o*-NB derivatives have a strong absorbance in the near UV, with a tail of absorbance extending out just into the visible region. They are commonly activated with 365 – 405 nm light, and have demonstrated some two-photon activity as well, albeit with relatively low crossections.[110,128] Photodegradable materials incorporating *o*-NB have been used to generate

drug delivery and tissue engineering platforms,[79,154] and since *o*-NB was introduced into oligonucleotide synthesis back in 1974[155] it's been used to conjugate fluorophores to oligos,[156] cage and block hybridization of individual bases,[157,158] and enforce a secondary structure that blocks the activity of an ASO or other oligonucleotide.[59,60,159,160]

Coumarin derivatives have also been used to incorporate photoresponse in oligonucleotide systems, as well as other materials with biological applications. It has the advantage of a λ_{max} closer to 400 nm, with an appreciable tail of absorbance out to 450 nm or beyond in some cases. Photocleavable coumarin derivatives are most commonly used as a caging group for small molecules. Coumarin derivatives have been incorporated into phosphate-containing molecules, including the backbone of DNA and ATP.[161,162] Small molecules can also be caged via attachment of the coumarin group to a carboxylic acid group. Hess and coworkers have successfully caged several neurotransmitters, including glutamate,[163] glycine,[164] and GABA.[165] In materials applications coumarin has been used to destabilize liposomes when incorporated between the hydrophobic head and hydrophilic tail.[166] Coumarin derivatized hydrogels permitted multiplexed degradation of a hydrogel system, when combined with o-nitrobenzyl.[77] The same multiplexing concept with *o*-nitrobenzyl groups was implemented in morpholino ASOs by Deiters and coworkers, who successfully triggered knockdown of two separate genes with two wavelengths of light.[167]

As researchers continue to develop photoresponsive ASOs as chemical biology tools, the wavelength required for activation with either *o*-NB or coumarin photoresponsive groups continues to be a challenge. Near-UV light, though generally accepted to be mostly harmless at low doses, has minimal penetration into complex tissues. Our recent work with RuBEP ($Ru(bpy)_2(3\text{-ethynylpyridine})_2$, where bpy = bipyridine) as a crosslinker to circularize DNA and morpholino ASOs represented a significant push into the visible region; RuBEP exhibited a much higher efficiency (measured as the quantum yield times the absorptivity) than the *o*-NB or coumarin compounds previously published.[86] Its red-shifted absorbance positioned it nicely to be

used in conjunction with *o*-NB caged ASOs for wavelength selective knockdown. In this work I will discuss various efforts to incorporate RuBEP into other DNA ASO constructs intended for multiplexed knockdown *in vitro*.

RuBEP is designed to circularize ASOs by copper-mediated azide-alkyne cycloaddition (CuAAC) with terminal azides, a commercially available option on both DNA and morpholino ASOs. A circular structure is proposed to sterically block the activity of the ASO until the crosslinker is broken and the ASO is linearized. The level of activity of the caged compound can be approximated by the ASO's ability to open a molecular beacon, or by its ability to bind to a longer reverse complementary strand, as observed by PAGE. Both techniques are described here as a method to determine if the product of the cycloaddition reaction is caged sufficiently.

5.2 Results

Challenges in cyclizing morpholinos – Post ntl and chd

CuAAC click reactions require the presence of copper as Cu(I), and a stabilizing ligand for the copper catalyst. TBTA (Tris[(1-benzyl-1H-1,2,3-triazol-4-yl)methyl]amine) can be used for less water-soluble reactions, as it requires at least 10% DMSO to be solubilized. THPTA (Tris(3-hydroxypropyltriazolylmethyl)amine) is more widely used as it is completely water soluble. Acetonitrile has also been used as the sole copper ligand in CuAAC reactions, but in CuAAC reactions with DNA more stable copper chelation was necessary to mitigate copper-mediated degradation of the DNA over the course of the reaction. As Cu(I) is less common and less stable in the presence of oxygen (which oxidizes the copper to Cu(II)), $CuSO_4$ is commonly used, and reduced *in situ* with an excess of TCEP or sodium ascorbate, with reactions maintained under inert atmosphere to exclude O_2, especially for longer reaction times. Because of this complexity in reaction conditions, there are multiple factors to troubleshoot and improve, including time and temperature for the reaction.

The biggest challenge in the cyclizing of morpholinos using RuBEP or any other method is the difficulty in purifying these constructs. Morpholinos, being uncharged, do not separate on reverse-phase HPLC like their DNA cousins, therefore any chemical modification must give pure product in the reaction. This was possible with the two sequences shown in Griepenburg et al, 2015 (*chd* and *ntl*), but in subsequent sequences was found to be impossible.

In collaboration with the Davidson lab at CalTech I worked to circularize 25-mer morpholinos antisense to *gcm* and *prox1* in the purple sea urchin *Strongylocentrotus purpuratus*. Both sequences (shown in **Table 5.2**) had moderate G content, which should be minimized to improve purity of the morpholino, and were modified with azides.

After significant time optimizing copper concentrations, chelating ligand identity and ratios, reaction times, temperatures, and secondary copper ligands, the click reactions for *gcm* and *prox1* never reached purity in final circularized product (**Figure 5.1A**). Click reactions were monitored using a modified gel shift, because unmodified morpholinos will not run on PAGE gels due to their neutral backbone. Morpholinos or crude click reactions were hybridized with complementary DNA in a 1:1 ratio, heated to 85 °C before shock cooling in an ice bath. The gel housing was submerged in ice and run in a chilled buffer at 10 °C to maintain hybridization.

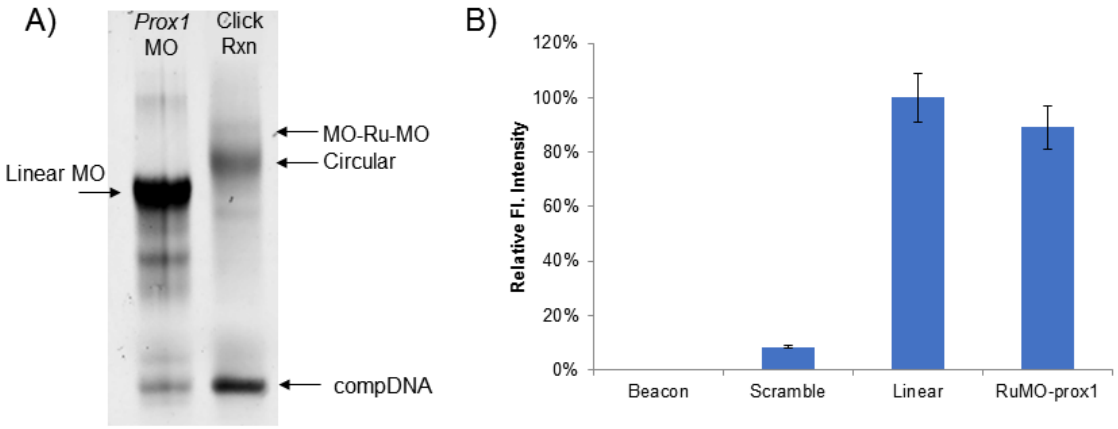

Figure 5.1. Click reactions with morpholinos (MOs). A) Gel shift of a crude click reaction (right lane) compared to linear MO received from GeneTools. B) Molecular beacon experiment using samples from the click reaction shown in A.

Circular morpholino runs slower than linear MO hybridized to the DNA, primarily because of the enforced secondary structure and weaker hybridization to the complementary DNA. In the click reaction lane of the gel we observe multiple products, even when all linear morpholino is reacted. The slowest running band likely corresponds to RuBEP crosslinked morpholino dimer, or morpholino-Ru-morpholino. The most prominent band is indicative of circular morpholino, the desired product. The faint fastest band is unassigned, and excess complementary DNA appears at the bottom of the gel. The presence of several less prominent bands in the morpholino lane in the gel demonstrate issues with purity of the purchased morpholino product. Purity varies from batch to batch of the morpholino, and has a significant effect on the success of the click reaction.

When tested against a molecular beacon it still showed significant activity (**Figure 5.1B**, sequence in Methods section). The molecular beacon is composed of a complementary strand to the morpholino, with an engineered stem. A fluorophore and a quencher are attached to the termini, such that if the beacon is closed the fluorescence will be minimal, but if it is capable of hybridizing to a complementary strand and opening, the fluorescence will increase. Thus, in **Figure 5.1B**, in the presence of a scramble sequence the beacon shows minimal fluorescence, while in the presence of linear morpholino the maximum fluorescence is observed. There is no statistical difference between the fluorescence of linear morpholino and that of “caged” morpholino, post click reaction, suggesting that either the click reaction did not give pure circular product despite its apparent near-purity, or that the circular design is not caged sufficiently.

Several attempts were made to purify the reaction, taking advantage of differences in hybridizing strength for the desired circular product and any linear morpholino. Crude click reactions were incubated with a small excess of longer strands of complementary DNA, 30-mer, with a weak stem (TM ~35 °C), according to Tang et al,[168] at 37 °C for 30 min. This mixture was then tested on a variety of purification columns, from a gravity-flow anion exchange column (Qiagen Plasmid Midi kit) to an anion exchange HPLC column, and a reverse-phase analytical C18 column. Any morpholino that remained unhybridized should elute first in the void/wash volume, while

hybridized morpholino should run slowly on the column. Representative HPLC traces for this process are shown in **Figure 5.2** for *gcm* and *prox1*.

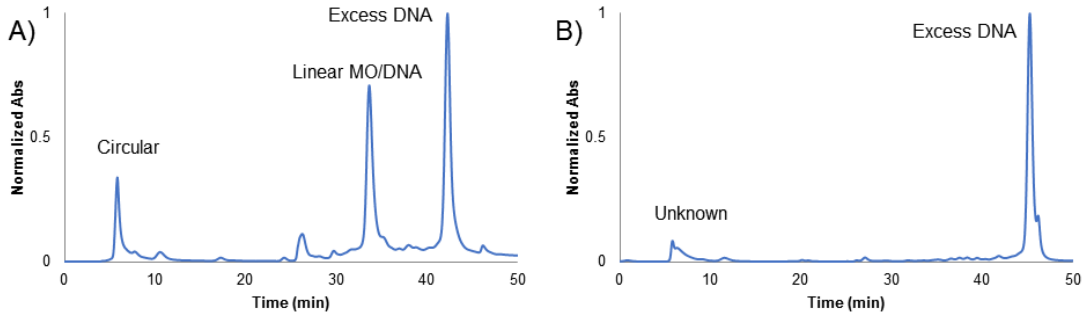

Figure 5.2. Attempted purification of morpholinos by reverse-phase HPLC. A) *gcm* morpholino click reaction. The <10 min peak should be circular morpholino. B) *prox1* HPLC under the same conditions.

This technique was minimally successful, more so for *gcm* than for *prox1*. A more pronounced peak is observed at <10min in the trace for *gcm* MO hybridized to DNA, but this result was limited to *gcm* (notice the lack of this peak in the *prox1* HPLC, as well as the lack of a hybridized morpholino/DNA peak) and was irreproducible in later attempts.

Through this and other attempts to circularize oligonucleotides with CuAAC and RuBEP we concluded that having completely pure linear oligonucleotide is vital to the success of the click reaction. In all vials of morpholino we received we observed suspicious bands running faster in the gel, indicative of shorter failed sequences in the original synthesis of the morpholino. While the presence of shorter sequences may be acceptable for biological applications, they hinder the success of any chemical modification attempted. Therefore, any further attempts to cage commercial antisense morpholinos should avoid chemical modifications, and focus on non-covalent caging methods.

Improvements in the click reaction – titrating in RuBEP

One of the most successful changes in the click reaction method, especially for DNA ASOs, was the innovation of titrating in RuBEP. The most dramatic change in click reaction yield was observed for a random test sequence used to improve click reaction yield for DNA-based ASOs.

This 25-mer sequence (shown in **Table 5.2**) was initially reacted with a bolus addition of RuBEP at the start of the reaction, following the protocol used for morpholinos and DNA in our previous paper.[86] Alternatively, when RuBEP was added slowly (1/3rd equivalents of RuBEP each hour), the yield improved dramatically, and the reaction proceeded to completion within 4 hours, rather than the 24 hours it took previously (**Figure 5.3**).

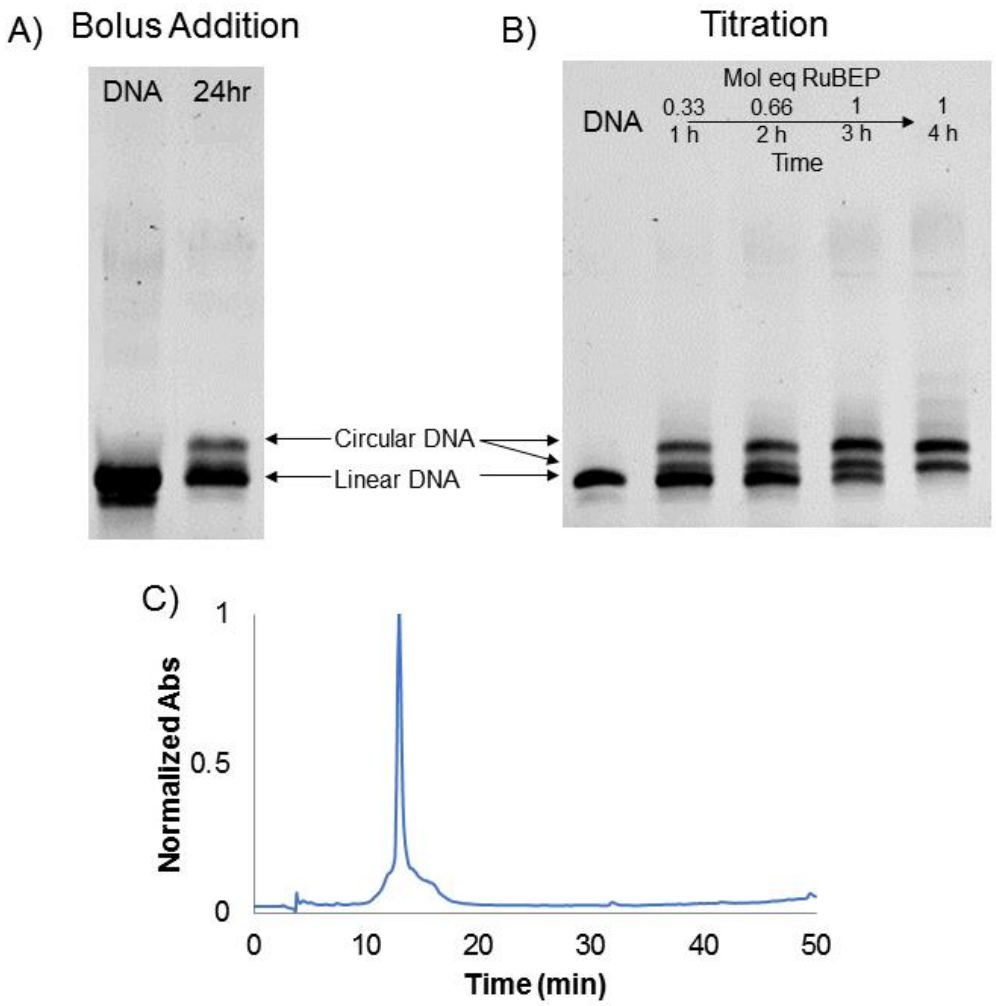

Figure 5.3. 20% Native PAGE shows improvement in click reaction yield due to titration of RuBEP crosslinker. A) Click reaction results after 24 hours with a bolus addition of RuBEP at 0 h. B) Click reaction progress over time with gradual addition of RuBEP. The reaction proceeds to completion within 4 hours, indicated by the loss of the linear DNA band. C) HPLC trace for the click reaction shown in (B). The single product at 13 min corresponds to circular DNA.

In these DNA click reaction gels we consistently observe two bands that correspond to product, as well as some polymerization and copper-mediated degradation (faint, slower bands). Circular DNA runs slower on these gels due to its secondary structure, preserved here by the native gel (**Figure 5.3C**). Two bands are frequently observed that resolve to one on the HPLC, primarily due to two different secondary structures that are dissociated on the HPLC column. The most dramatic improvement in the titration gel is the complete conversion of linear DNA to circular within 4 hours of reaction time. Titration of RuBEP is featured in nearly all RuBEP circularization protocols in my work.

Stem vs Nostem

One of the most important innovations in click reaction methods I developed was the incorporation of a stem into our ASO designs. With careful design and sequence selection a stem can be engineered in with the mutation of only one or two bases, and can lead to dramatic improvement in click reaction yield, with fewer side products and polymers forming over the course of a reaction.

A stem was mutated into new designs of *gcm* and *prox1* morpholinos in an attempt to improve the purity of the clicked product. With this design coupled with a gradual addition of RuBEP as described previously, improvements in the click reaction progress were observed. A noticeable difference between stemmed *gcm* and *gcm* with no designed secondary structure was observed by gel shift assay (**Figure 5.4**).

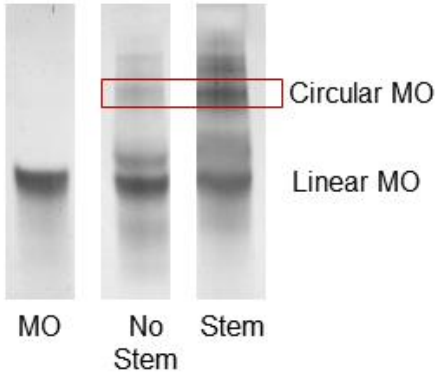

Figure 5.4. Gel shift showing improvement due to a stemmed design in a morpholino.

Though introducing a stem did not overcome the challenges in morpholino circularization, it showed more promise in DNA ASO circularization, with implications in other projects in the Dmochowski lab. A sequence adapted from Kim et al[169] was redesigned with a stem by mutating one base near the 5' end. The new stem had a T_M ~46-51 °C, which is optimal to allow for heating during the click reaction without disrupting the secondary structure. The stem was 4 base pairs long, with a weaker structure closing the loop even further (**Figure 5.5**). We propose that this design should give more complete caging *in vivo* as well as improve the click reaction yields and purity.

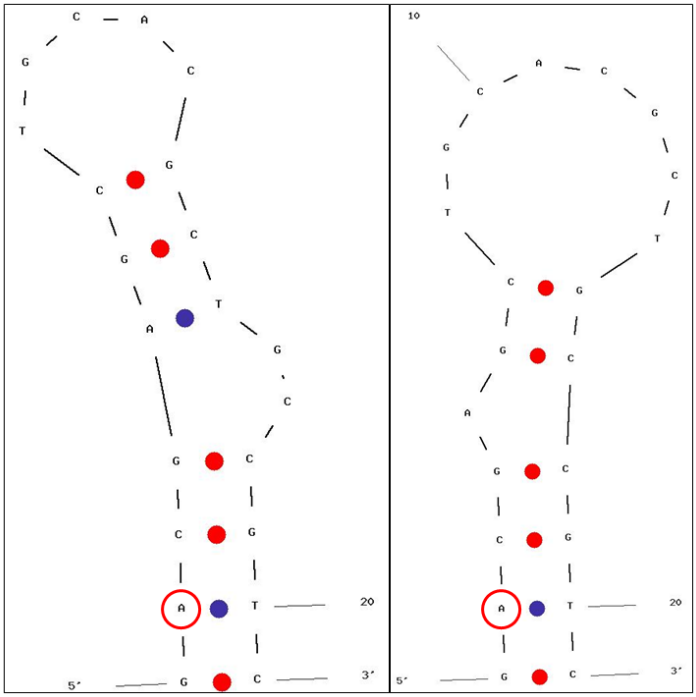

Figure 5.5. Stem designs for Stem-EGFP. The only mutation necessary was an exchange at the circled position (G → A)

Stem-EGFP demonstrated moderate improvement over nostem-EGFP in both click reaction purity and in effective cagedness as shown by a gel shift assay. Click reactions followed the trend predicted before (shown in **Figure 5.4**), that the stem helped drive the reaction to completion on a shorter timescale. Yield remained poor after purification, 20-30% depending on the reaction, with little difference in yield observed between stem- and nostem-EGFP, yet based on PAGE assays and HPLC traces stem-EGFP should have a higher yield, with less linear DNA left over (**Figure 5.6**). This can be explained by a higher amount of copper-mediated degradation observed for the stemmed structure.

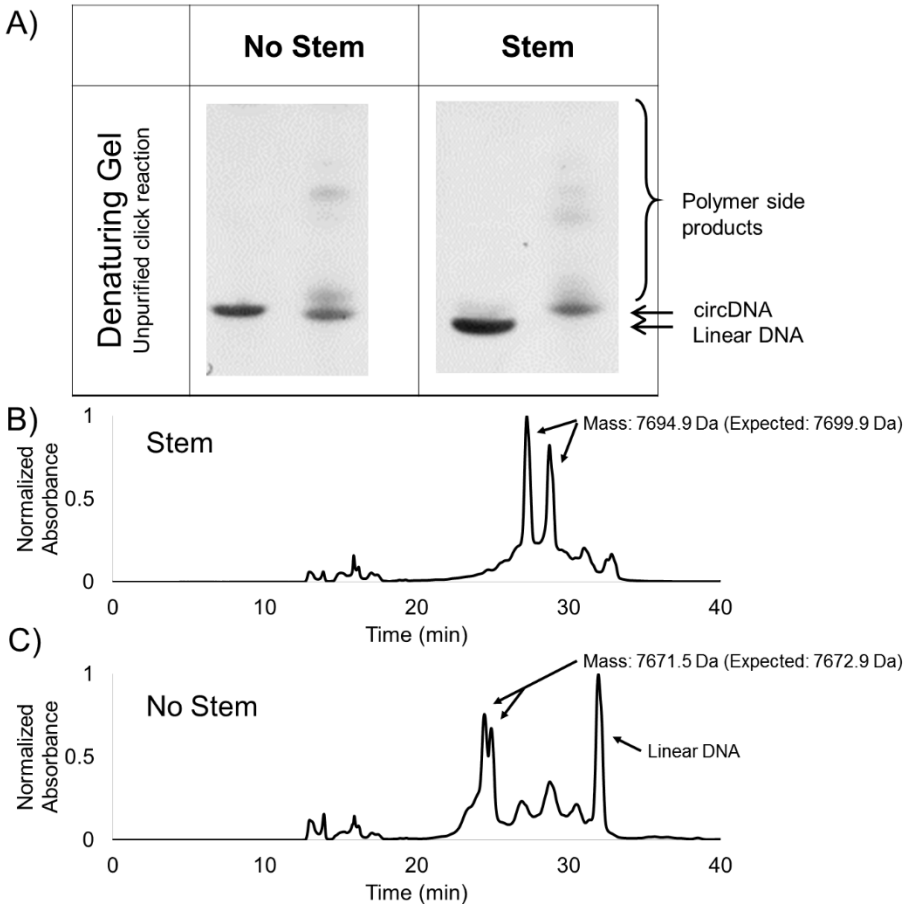

Figure 5.6. The effect of a stem on a click reaction. A) Denaturing gel showing reaction progression after 5 hours for both stem- and nostem-EGFP. While polymer side products appear in both reactions, stem-EGFP appears to generate more circular DNA. B) Reverse-phase HPLC for stem-EGFP. Note the loss of the linear DNA peak at 31 min. The two major peaks collected were confirmed by ESI-MS to be circular Ru-DNA. C) Reverse-phase HPLC for nostem-EGFP. A major peak at 31 min is observed corresponding to unclicked linear DNA.

The HPLC traces for stem- and nostem-EGFP click reactions show significant degradation of the DNA, thought to be copper mediated due to the relatively high amount of copper in the reaction (2-10 eq). This appears as the undefined peaks between 25 and 30 min. The peaks eluting at 27 and 29 min (stem-EGFP) and 25/26 min (nostem-EGFP) were confirmed by ESI-MS to match the desired product, circular RuBEP-crosslinked ASO. The two peaks are expected for stem-EGFP, as the secondary structure of the oligo may not be completely denatured on the column (run at nominally 60 °C, just at or below the T_M of the stem). The two peaks in the nostem-EGFP HPLC

trace were not predicted, but there may be some secondary structure present as well in the nostem-EGFP oligo.

A gel shift assay was devised to determine the amount of hybridization of the purified circular ASO would bind to its complementary strand. Molar equivalents of the circular ASO (stem- and nostem-EGFP) were incubated with a 40-mer complementary strand derived from the EGFP plasmid for 30 min at 37 °C. ASO:DNA hybrids are expected to run slower than the ASO or the DNA by itself (**Figure 5.7**).

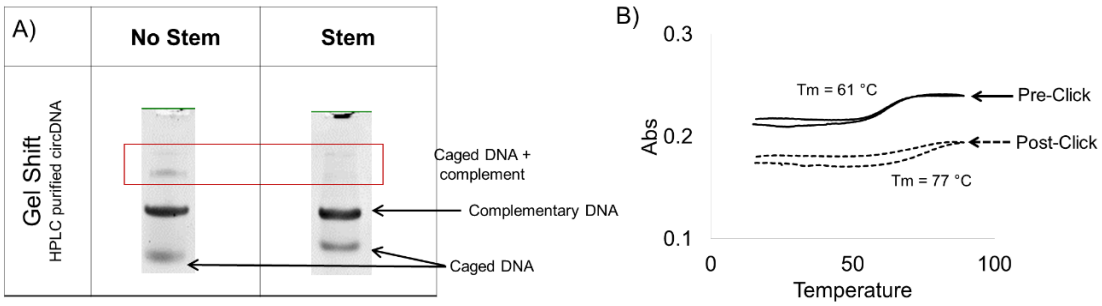

Figure 5.7. Comparison of native PAGE gels for stem- and nostem-EGFP. A) The gel shift assay with purified circular ASO shows a difference between stem-EGFP and nostem-EGFP in activity. Stem-EGFP binds negligibly to complementary DNA, while nostem-EGFP demonstrates higher binding affinity. B) Melting temperature data shows that the stem pre-click has a relatively high T_M of 61 °C, and circularization with RuBEP increases the T_M by over 15 °C.

In this experiment the stemmed caged construct showed slight but significant difference in binding the complementary DNA. A noticeable band corresponding to hybridized ASO:DNA is observed for circularized nostem-EGFP in the gel shift, due to being less optimally caged. The stem-EGFP ASO appears to be more caged in this assay, with very little-to-no undesired hybridization. Melting temperature data also suggest a significant increase in the stability of the stem post circularization with RuBEP. An increase of over 15 °C in melting temperature of the stem after circularization indicates that the presence of the stem *in vivo* will have a non-negligible effect on the cagedness of the ASO.

5. 3 Conclusion

While CuAAC showed promise in our early work as a method to circularize oligonucleotides with a small-molecule Ru crosslinker, it has failed to live up to initial expectations. Several attempts were made to improve the click reaction yields, though few had the desired effect (see **Table 5.1** below). Morpholinos have proved to be very difficult to circularize, primarily due to impurities in the samples purchased. Longer reaction times and higher amounts of copper were also necessary for morpholino click reactions, suggesting that some copper chelation may be occurring in the morpholine backbone hindering the reaction. Through the use of a molecular beacon we showed that even the best click reaction conditions yielded product that was not sufficiently caged. A more robust purification method must be developed to continue to use RuBEP to circularize morpholinos. Another possibility would be to develop a way to cage morpholinos without chemical modification, which would be preferable.

Of the two major modifications to the click reaction method, the gradual addition of RuBEP and the incorporation of a stem, both have increased the final purity of the reaction, and have been carried on to circularization applications elsewhere in the Dmochowski lab. Designing a stem into a different ASO design enabled coworker Linlin Yang to circularize and cage an ASO with near 100% yield before purification.[149] Stemmed structures are also showing promise as the next generation of Transcriptome *In Vivo* Analysis (TIVA) probes that will use RuBEP as the photodegradable linker (Sean Yeldell, unpublished). Here I laid the groundwork for generating circular ASO structures that are more caged and easier to synthesize, which will enable progress in other projects in the Dmochowski Lab.

Table 5.1. Click reaction troubleshooting

Variable		Range	Notes
Oligo Concentration	DNA	0.2 – 0.05 mM	0.1 mM was ideal, on a 5 nmol scale (5 nmol in total reaction volume of 50 μL)
	MO	– 0.05 mM	0.05 mM was optimal
Copper ligand	DNA	TBTA, THPTA	THPTA worked best, with a completely aqueous reaction environment. Optimized reaction conditions used a combination of THPTA and 1-5% v/v of MeCN.
	MO	TBTA, THPTA, $(CH_3CH_2)_3N$ (TEA), MeCN	THPTA did not work, MeCN alone didn't work, TEA was more successful but not as efficient as TBTA
Ratio of RuBEP to oligo	DNA	0.95 – 1.2	A small excess of RuBEP was beneficial to pushing the reaction to completion, optimized RuBEP ratio was 1.2:1 RuBEP:oligo (6 μL of 1 mM RuBEP added to 5 μL of 1 mM oligo gradually)
	MO	0.90 – 1.2	No difference was observed in reaction progress or purity, a small excess was often used (~1.05).
Excess of Cu(II)	DNA	2x – 10x	2x of Cu(II) was sufficient for stemmed oligos, but for others 10x was necessary for the reaction. No trend was observed to predict the need for higher levels of Cu(II).
	MO	2x – 10x	10x was necessary for the reaction to proceed, 2x did not give any products.
Temperature	DNA	RT – 40°	Elevated temperatures helped the reaction, final optimized conditions involved vortexing under tented foil to retain the heat of the vortexer; precise temperature was not measured, but approximated at 35-37°.
	MO	4° – 50°	Temperature did not appear to have an effect on reaction progress, or in decreasing reaction time.
TCEP vs Ascorbate	DNA/MO		TCEP proved incapable of reducing Cu(II) to produce any product. Subsequent experiments on a larger scale showed precipitation of

			Ru product and incomplete reduction of Cu(II).
Reaction Time	DNA	1.5-24 h	Longer reaction times were often unnecessary and led to degradation. Reactions often took 3 – 5 hours.
	MO	24 – 48 h	MOs consistently required longer reaction times, independent of temperature.
Solvent system	MO	Water/DMSO – water/MeOH	Changes in polarity of the solvent system did not affect the reaction progress or purity, DMSO consistently immediately gave a ppt which may have led to the purity of the final product (if ppt was polymerized MO).

5.4 Methods and Materials

Materials

Azido-modified DNA oligomers and short oligonucleotides for HPLC purification and gel shift assays were purchased from IDT. Azido-modified morpholinos were purchased from GeneTools. Copper(II) sulfate and sodium ascorbate were purchased from Acros Organics, THPTA was purchased from Aldrich, RuBEP was synthesized as discussed in Chapter 2. All HPLCs were performed on an Agilent HPLC with a XBridge peptide BEH C18 prep column. All gels were formed in-house at the specific % crosslinking given.

Table 5.2*: Sequences used in this report*

Name	Sequence (5'-3') (lowercase=mutated to form stem)	TM (°C)
gcm	GCTTTGGAGTAACCTTCTGCACCAT	N/A
gcm HPLC complement	gctttATG GTG CAG AAG GTT ACT CCA AAG C	32
Stem-*gcm*	gtGCTTTGGAGTAACCTTCTGCACC	46
prox1	ACACCAAAAAGGACTTACCGTGAAC	N/A
prox1 HPLC complement	acacaGTT CAC GGT AAG CCT TTT GTT GTG T	34.5
Random DNA	ACG CAG GCT ATG GTG AGC AAG GGC G	N/A

Stem-EGFP	GaC GAG CTG CAC GCT GCC GTC	61
Nostem-EGFP	GGC GAG CTG CAC GCT GCC GTC	N/A
EGFP gel shift complement	CAACATCGAGGACGGCAGCGTGCAGCTCGCCGACCACTAC	N/A

Circularization of gcm and prox1 morpholinos

Morpholino click reactions were performed at a 10 nmol scale.

	nMoles Added	Equivalents
Morpholino	10	1
RuBEP	10.5	1.05
Cu(II)	100	10
NaAscorbate	400	40
THPTA	1000	100
H_2O	Dilute to 100 μL	

Morpholino, RuBEP, and H_2O were mixed together, and Cu(II)sulfate, THPTA, and NaAscorbate were mixed separately. Appropriate amounts of the copper solution were added, and the reaction was sonicated briefly before sitting at room temperature for 24-48 hours. Reactions were quenched by dilution and salts were removed by Nap5 column.

Circularization of DNA ASOs including stem- and nostem-EGFP

Circularization was performed at the 5 nmol scale, diluted to 50 μL 0.5x PBS.

	Nmol added	Equivalents
DNA	5	1
RuBEP	6 (2 nmol/hour)	1.2
Cu(II) sulfate	10	2
NaAscorbate	100	20
THPTA	100	20
acetonitrile	1 v/v %	

Bisazido-DNA and RuBEP (2 nmol) were mixed together in 1x PBS. Cu(II) sulfate, NaAscorbate, THPTA, and acetonitrile were mixed separately and added to the DNA solution. 2 nmol of RuBEP were added each hour until 1.2 equivalents was reached, and the reaction was vortexed at ~37 °C for 5 hours total. Reaction was quenched by dilution into 250 μL of water and frozen until purification by HPLC.

HPLC gradient conditions

Analytical and prep column was run at 60 °C using a heat block.

Solvent A: 0.01 M TEAA

Solvent B: Acetonitrile

Time (min)	% B
0	10
10	15
30	50
45	85
55	85
60	10

Gel Shift Assay

20% native PAGE gels were formed on the benchtop by crosslinking with 10% APS and TEMED. Circular DNA and complementary samples were mixed in a solution of 1x STE and incubated at 37 °C for 30 min. Gels were run at 100 V for 2 hours at 10 °C suspended in an ice bath to maintain the temperature throughout the experiment.

Molecular Beacon Assay – prox1

Prox1 Molecular Beacon sequence design:

5’-IABkFQ-GGGTTCACGGTAAGCCTTTTGTTGTGTTGAACCC-6-FAM-3’

Beacon samples were as follows:

50 pmol beacon
150 pmol morpholino
75 μL total volume
33 mM NaCl
Samples were incubated at 37 °C for 30 min before fluorescence was measured. (λ_{ex} = 495 nm, λ_{em} = 520 nm)

CHAPTER 6 – Conclusions and Future Directions

6.1 Summary

The work in this thesis has shown the versatility of Ru(II) polypyridyl complexes in a new application as photodegradable crosslinkers. RuBEP ($Ru(bpy)_2(3\text{-ethynylpyridine})_2$) was the first Ru(II) polypyridyl-based crosslinker, modified with alkynes for a CuAAC click reaction, and it has been used in multiple projects in the Dmochowski lab since its initial success. It was used to circularize oligonucleotides, and was non-toxic when injected into zebrafish embryos. RuBEP has also been utilized in second- and third-generation TIVA designs to enable multiplexing in that work. RuAldehyde ($Ru(bpy)_2(3\text{-pyridinaldehyde})_2$) was very similar to RuBEP except for the use of an aldehyde rather than an alkyne as the reactive moiety, and was used to crosslink a hydrogel based on hydrazine-modified hyaluronic acid (HA-HYD). The resulting material had remarkable photodegradation properties, was cytocompatible intact and degraded, and was well adapted for the storage and delivery of active enzymes via lysine-mediated crosslinking into the hydrogel matrix. Red-shifting the absorbance of Ru(II) crosslinkers was a multi-year pursuit, as thermal stability became an issue with many previously published designs for red-shifted ruthenium complexes. Eventually $Ru(biq)_2(5\text{-hexynenitrile})_2$ and $Ru(bpy)_2(5\text{-hexynenitrile})_2$ were stabilized using a bulkier counterion, exchanging the typical chloride for a nitrate counterion greatly increased the thermal stability in water and in PBS. They were used to form a PEG-based hydrogel that was selectively degraded using two different colors of visible light, red and blue. There are many directions for Ru(II)-based crosslinkers that remain unexplored, some that have been suggested in the literature and others on which work has begun by myself and others.

6.2 The Future: Ruthenium-Coordinated Amino Acids

Ruthenium (II) polypyridyl complexes have been coordinated directly to amino acids for decades, dating back to Harry Gray's seminal work using the compounds for light-triggered electron transfer in proteins.[11,88,170,171] With Ru(II)'s versatility in possible biologically relevant ligands, from imidazoles[45] to thioethers,[87,172,173] to nitriles,[26,27,31,32] it seems that coordination should not be relegated to histidine residues, but methionine, cysteine, and potentially even lysine may also be

coordinated/caged, as well as unnatural amino acids modified with nitriles, such as cyano-phenylalanine or cyano-alanine.[174–178] Ruthenium is uniquely ubiquitous in coordinating to amino acid residues,[179] by changing the ligand sphere around a ruthenium center groups have coordinated amine and carboxylic acid residues of methionine,[180,181] proline,[182] phenylalanine,[182,183] cysteine,[184] and a range of others.[183]

Imidazoles are a natural ligand to coordinate to Ru(II), aromatic heterocycles have strong coordination affinity to Ru(II), and histidine residues were one of the first to be coordinated to a metal center. Vazquez and coworkers demonstrated the first example of a caged histidine residue in a biologically active peptide[185] (histidine has been caged before with *o*-nitrobenzyl, but to date the caging group hasn't been used in a biological setting to modulate activity[186,187]). In their protocol Boc-His-OH was coordinated to $Ru(bpy)_2PPh_3^{2+}$ in aqueous media with high yield (92%), followed by exchange of the protecting group to Fmoc-His for incorporation into a peptide via standard solid phases peptide synthesis. The quantum yield of the uncaging of the histidine was as expected (~0.06), with irradiation of purified peptides resulting in complete uncaging of the histidine residue and formation of $Ru(bpy)_2PPh_3$ photoproduct. The Ru(II)-caged histidine completely blocked the activity of RGH Ni(II) coordinating peptide, restoring activity after irradiation with 450 nm light.

Based on this initial success, several tetrapeptides were purchased to test the ability of $Ru(bpy)_2^{2+}$ to coordinate to and circularize short peptide sequences containing histidine and methionine. HGGH and MGGM were purchased from Pierce Custom Peptides and used without purification.

$Ru(bpy)_2(H_2O)_2$ was prepared from $Ru(bpy)_2Cl_2$ *in situ* with the addition of silver triflate before the addition of HGGH. Reactions with histidine were performed in acetate buffer at pH 5 and heated to 45 °C under inert atmosphere for 2-4 hours. All reactions were checked and purified by HPLC on a C18 peptide analytical column with a gradient of acetonitrile and 0.01 M TFA.

HGGH was successfully coordinated to make circular $Ru(bpy)_2$HGGH (**Figure 6.1,** shown at end of chapter). The reaction was far from clean, and occurred in low yield (<20%). Though product was formed, confirmed by comparison of absorbance traces to $Ru(bpy)_2(imidazole)_2$, it was not photolabile, as suggested by previous work with bis-imidazole coordination complexes (**Figure 6.1B**).[188]

Inspired by the success in generating a photolabile histidine residue presented by Vazquez and coworkers, I synthesized $Ru(bpy)_2(PPh_3)Cl$ in an attempt to generate a photocage in a similar manner. HGGH was successfully coordinated using a modified version of the synthesis described earlier: heating for 4 hours after *in situ* exchange of Cl for H_2O using silver triflate (**Figure 6.2**)**.** Methionine was also successfully coordinated to $Ru(bpy)_2PPh_3$, by vortexing for 48 hours at room temperature. $Ru(bpy)_2(PPh_3)$MGGM was also photolabile under visible irradiation (**Figure 6.3**).

This initial success in generating a photolabile caging group for select amino acids was not pursued any further, and may open the door to cage other coordinating residues, such as cysteine and potentially lysine.

6.3 The Future: Red Shifting Ru(II) Complexes

Several options have been pursued in the last three years for red-shifting the absorbance of Ru(II) complexes. A thermally stable, photolabile Ru(II) complex with decent quantum yield of ligand exchange when excited anywhere between 650 and 900 nm would see instant applications in small molecule delivery and materials engineering.

One thermally stable option was presented by Albani and coworkers in the Turro group, where he generated a dinuclear Ru(II) complex $\{[Ru(CH_3CN)_3]_2(tppz)\}^{4+}$ (tppz = tetra-2-pyridylpyrazine) that responded to ≥610 nm light, exchanging two CH_3CN ligands for coordinating solvent. Another dinuclear complex, *cis*-$\{[Ru(tpy)(L)]_2(bpm)\}^{4+}$ (tpy = 2,2′:6′,2″-terpyridine, bpm = 2,2′-bipyrimidine, L = CH_3CN, DMSO) was even further red-shifted, with significant absorbance >600 nm, but the acetonitrile was not photolabile, while the DMSO was.

Aside from dinuclear compounds, exchanging bipyridine for other polypyridine ligands has generated red-shifted ruthenium compounds with λ_{max}'s extending to 530 and beyond.[189] Phenylpyridine (phpy) was used with phenanthroline in one example to generate a low energy light absorbing Ru(II) complex Ru(phpy)(phen)(MeCN).[190] The covalent bonding of the σ-donating carbanion of phpy red shifts the MLCT by nearly 100 nm, from λ_{max} of 420 nm for $Ru(phen)_2(MeCN)_2$ to 505 nm. $Ru(phpy)(phen)(MeCN)_2$ was stable in aqueous solutions in the dark for at least 24 hours, suggesting that the C-Ru bond was stable enough to withstand *in vitro* conditions.

Bidentate polypyridyl ligands with extended π systems have also shown promise in extending the MLCT to the red end of the spectrum. In the first such example, Albani and coworkers synthesized $Ru(biq)_2(MeCN)_2$, where biq is 2,2'-biquinoline, a bidentate ligand with an extended π system and added steric bulk.[39] $Ru(biq)_2(MeCN)_2$ had a significantly red-shifted absorbance, with a λ_{max} of 535 nm, a shift of over 100 nm from $Ru(bpy)_2(MeCN)_2$. The quantum yield suffered with this red shift, dropping to just 0.15. However, with this red shift in the λ_{max} the compounds also had a significant tail of absorbance, allowing Albani and coworkers to achieve photoinduced ligand exchange with red light ≥ 610 nm. The furthest red-shifted compound published was a combination of phenylpyridine and biquinoline, $Ru(phpy)(biq)_2$, with the lowest energy λ_{max} at 640 nm. Unfortunately, with this significant red shift comes a complete loss in photoreactivity, $Ru(phpy)(biq)_2$ is not photolabile in water.

A red shifted aldehyde-modified compound RuAldehyde-Red has already been synthesized and characterized. RuAldehyde-Red, $Ru(bpy)(biq)(4\text{-pyridinepropanal})_2$, was synthesized from Ru-benzene dimer $[bzRuCl_2]_2$ and 4-pyridinepropanol (**Figure 6.4**).

RuAldehyde-Red can be photolyzed with orange light (592 nm, **Figure 6.5**) and multiplexed with RuAldehyde ($Ru(bpy)_2(3\text{-pyridinaldehyde})_2$) for selective degradation (**Figure 6.6**). With aldehyde-modified pyridine-based ligands, RuAldehyde-Red is stable in water and presents with

no stability issues observed for the nitrile-based compounds in Chapter 4. RuAldehyde-Red has been used to crosslink hydrazine-modified hyaluronic acid (**Figure 6.6C**) to form hydrogels that can be selectively degraded in the presence of RuAldehyde-crosslinked hydrogels.

RuAldehyde-Red is the most red-shifted compound generated during my tenure in the lab (**Figure 6.7**), and it is stable and capable of crosslinking in non-toxic conditions, i.e. in the absence of copper or other catalyst. RuAldehyde-Red represents the next major crosslinker for use in any of the applications discussed in this thesis. Future work with this compound and the $Ru(bpy)(biq)^{2+}$ platform could include the generation of non-toxic hydrogel materials for biological applications, using the 4-pyridinepropanal ligand to crosslink with hydrazine-modified polymers. Conversely, if $Ru(bpy)(biq)^{2+}$ was coordinated with an alkyne-modified pyridine, the resulting complex could be used to circularize DNA. The major restriction with the mixed bidentate ligand platform is that any modification on the pyridine must be in the *para* position, as steric crowding of the coordination sphere complicates the coordination of *meta* modified pyridine ligands.

6.4 Conclusion

The future of this project lies in the synthesis of red shifted ruthenium crosslinkers that are stable *in vivo*. As their primary application is in the circularization and caging of oligonucleotides, a future design should revolve around more facile incorporation into oligonucleotides, either via solid phase synthesis or by a copper-free, rapid click reaction. Because of the instability of the nitrile-based Ru(II) crosslinkers, a pyridine-based ligand should be pursued for future projects.

Ruthenium-based photodegradable crosslinkers are rapidly becoming the most viable option for simple, red-light responsive materials and molecules.[28,191] More work in Ru(II)-based crosslinkers is warranted by these examples, especially as the field moves further to the red end of the spectrum.

6.4 Figures

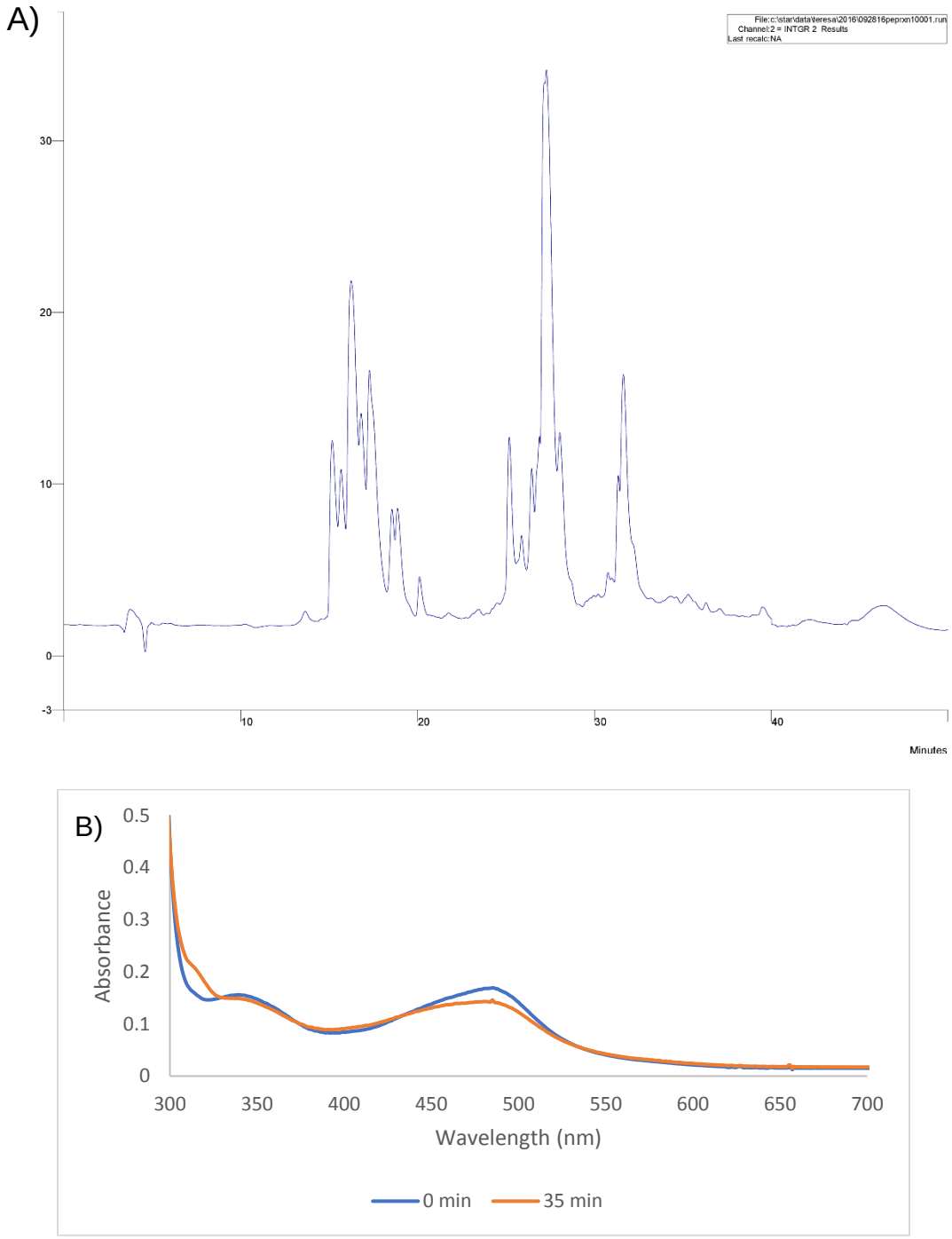

Figure 6.1. A) HPLC trace for the peptide circularization reaction with $Ru(bpy)_2(H_2O)_2$ and HGGH. The major peak at 27 min was collected and tested for photolability (B).

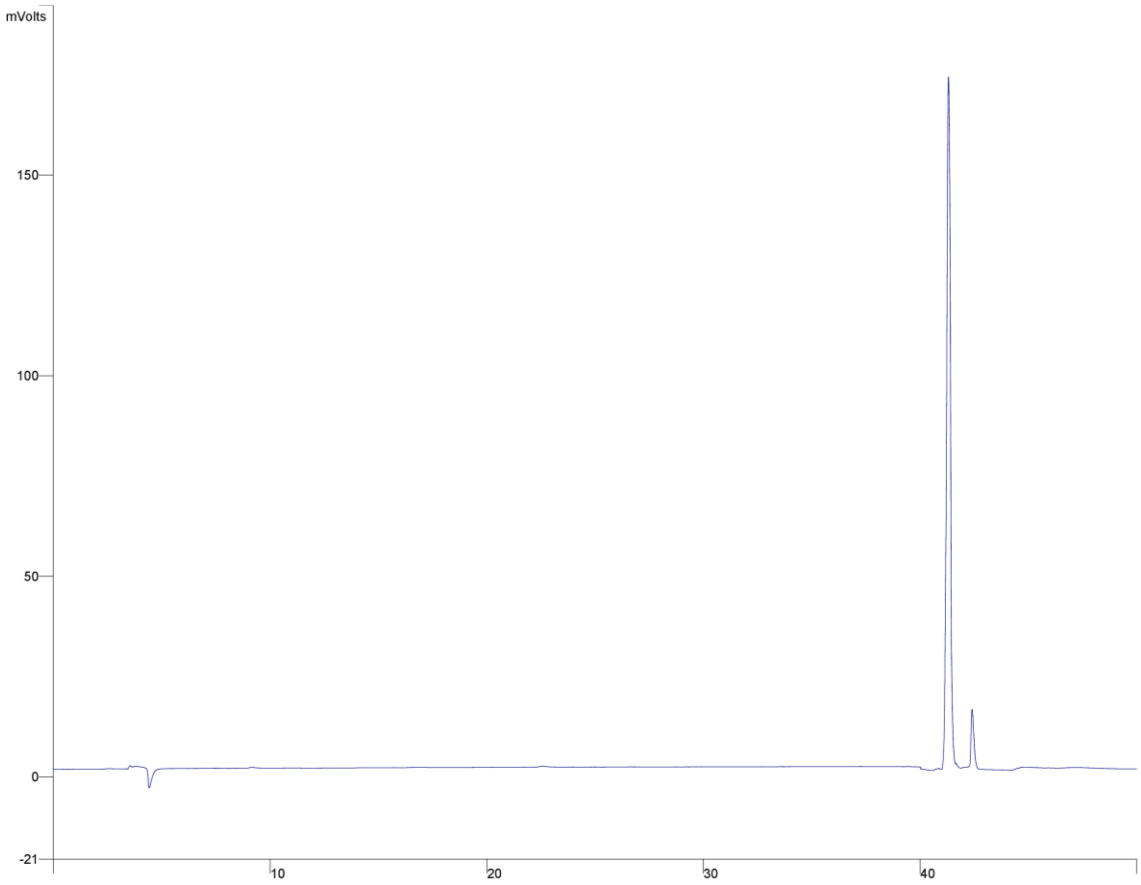

Figure 6.2. HPLC of $Ru(bpy)_2(PPh_3)$HGGH reaction. The major peak is excess $Ru(bpy)_2PPh_3$MecN (MeCN coordinated on HPLC), the small peak at 42 min was confirmed my ESI-MS to be $Ru(bpy)_2(PPh_3)$HGGH.

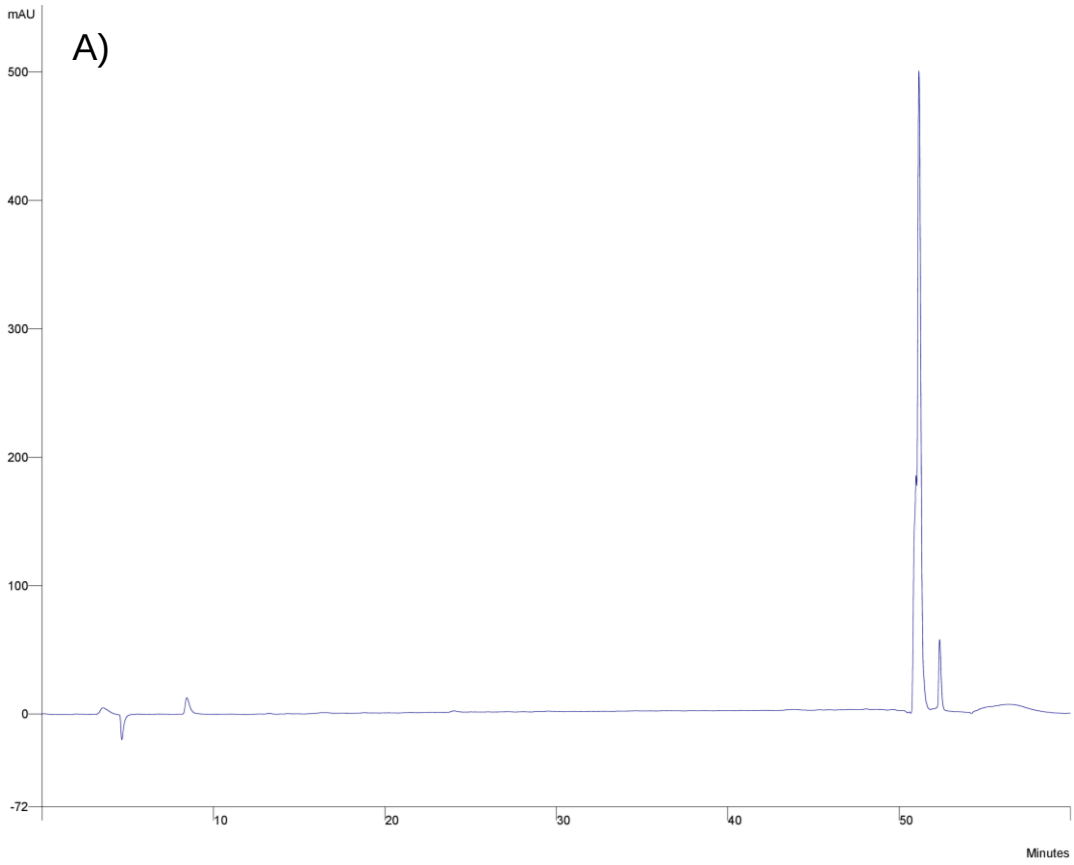

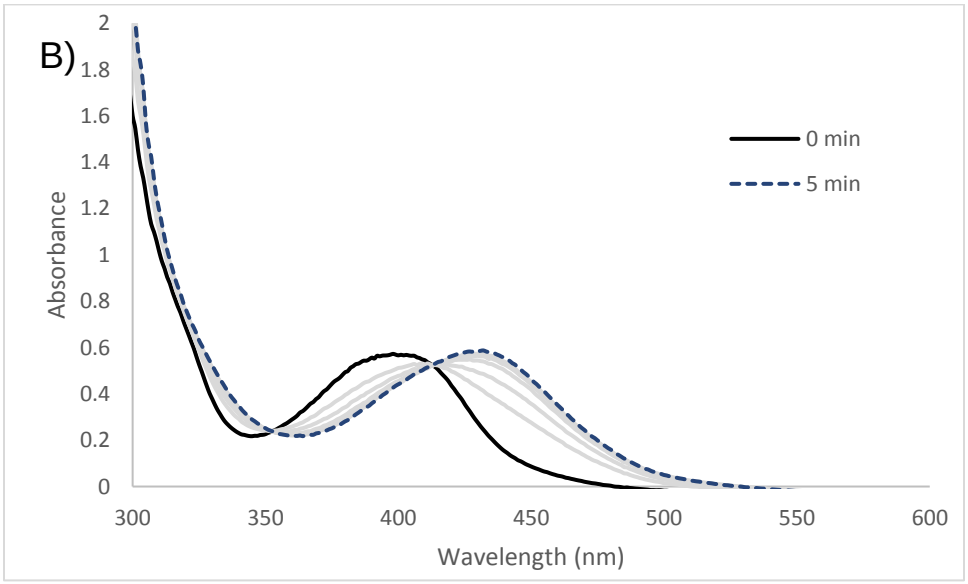

Figure 6.3. Synthesis of $Ru(bpy)_2(PPh_3)MGGM$. A) HPLC of synthesis, minor peak corresponds to product (confirmed by ESI-MS). B) Photolysis of minor peak in water shows photolytic activity.

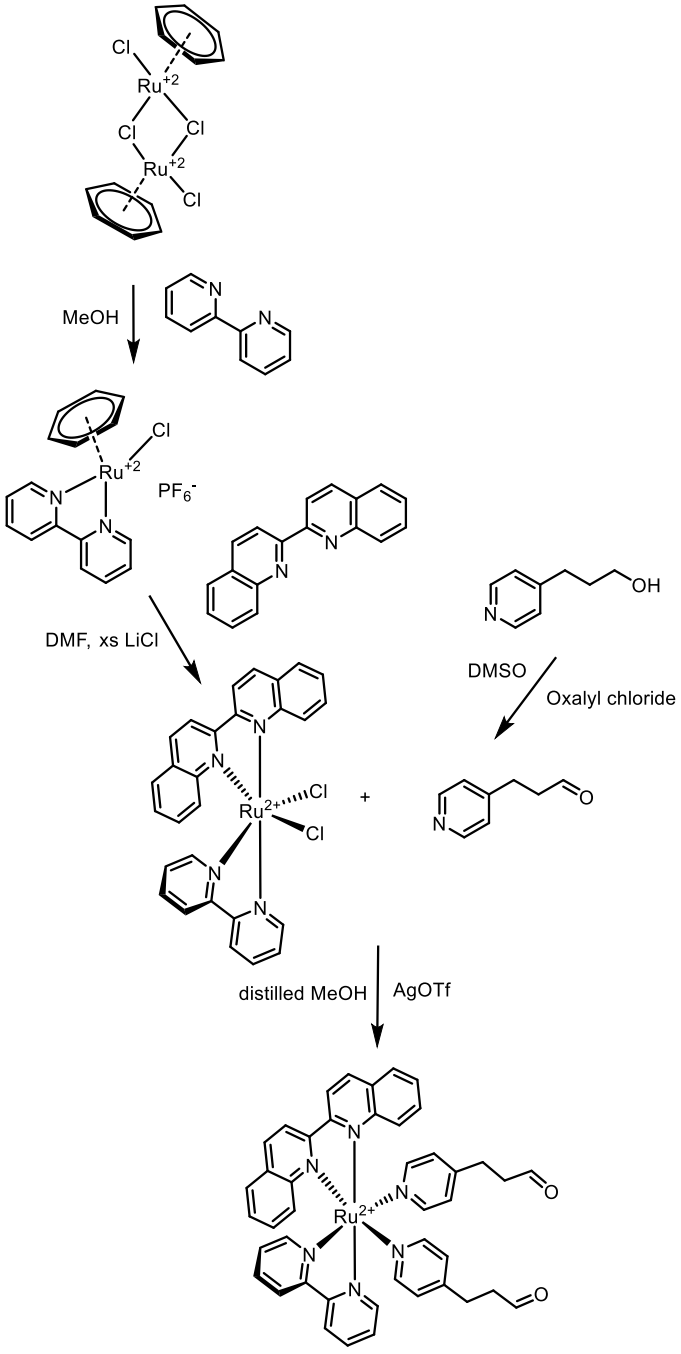

Figure 6.4. Synthesis of RuAldehyde-Red

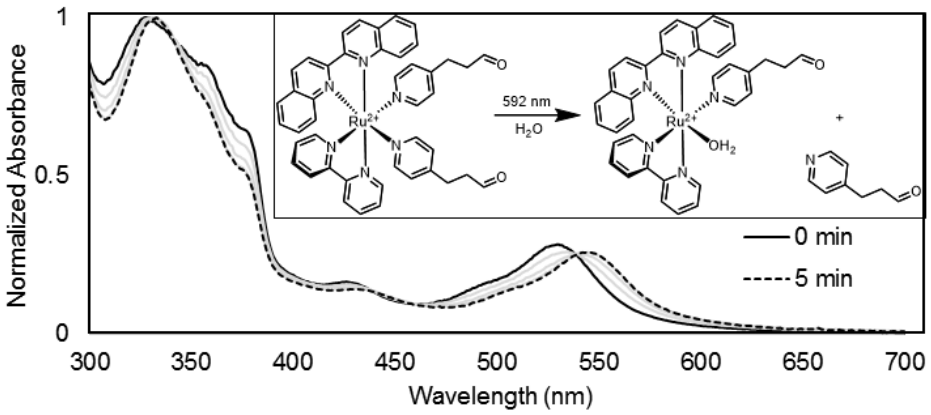

Figure 6.5. Photolysis of RuAldehyde-Red shows clean conversion to one photoproduct, monoaquated Ru(bpy)(biq)(4-pyridinepropanal)(H_2O).

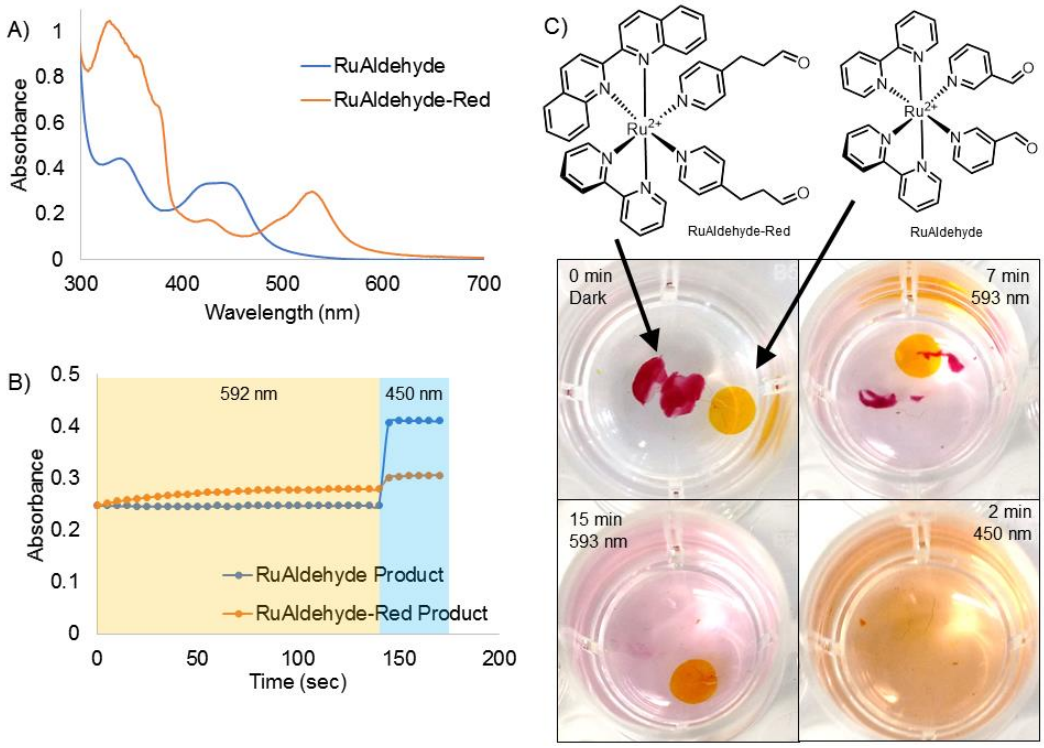

Figure 6.6. Multiplexing RuAldehyde and RuAldehyde-Red. A) Absorbance spectra of both showing the separation in absorbance. >590 nm light should be used to selectively degrade RuAldehyde-Red. B) Absorbance changes at 610 nm (RuAldehyde-Red product) and 455 nm (Rualdehyde product) under irradiation with 592 nm light (25 mW/cm^2) followed by 450 nm light (14 mW/cm$_2$). C) Selective hydrogel degradation of hyaluronic acid-based hydrogels crosslinked with RuAldehyde and RuAldehyde-Red.

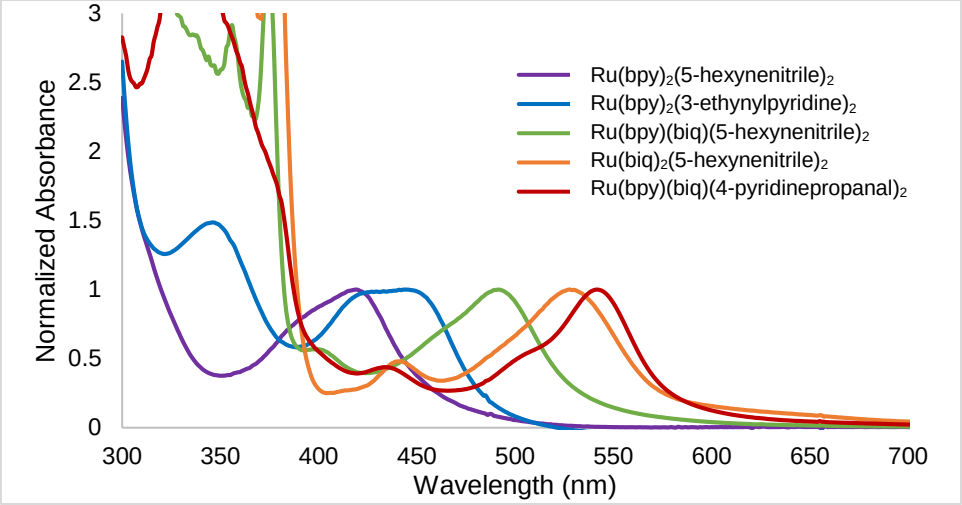

Figure 6.7. Overlapped spectra of all Ru(II) compounds synthesized over the course of this dissertation work.

6.5 Methods

$Ru(bpy)_2ClPPh_3$

$Ru(bpy)_2Cl_2$ (262 mg, 0.5 mmol) and PPh_3 (525 mg, 2 mmol) were added to 40 mL 80% ethanol in water. Solution was bubbled with N_2 for 10 min, then heated to reflux for 1 hour. The crude reaction was washed with ~100 mL ether, NH_4PF_6 was added to precipitate the PF_6 salt and filtered. Product was purified as the main orange band by neutral alumina column, 1:3 acetonitrile:toluene gradient. Yield: 159.4 mg, 45% yield.

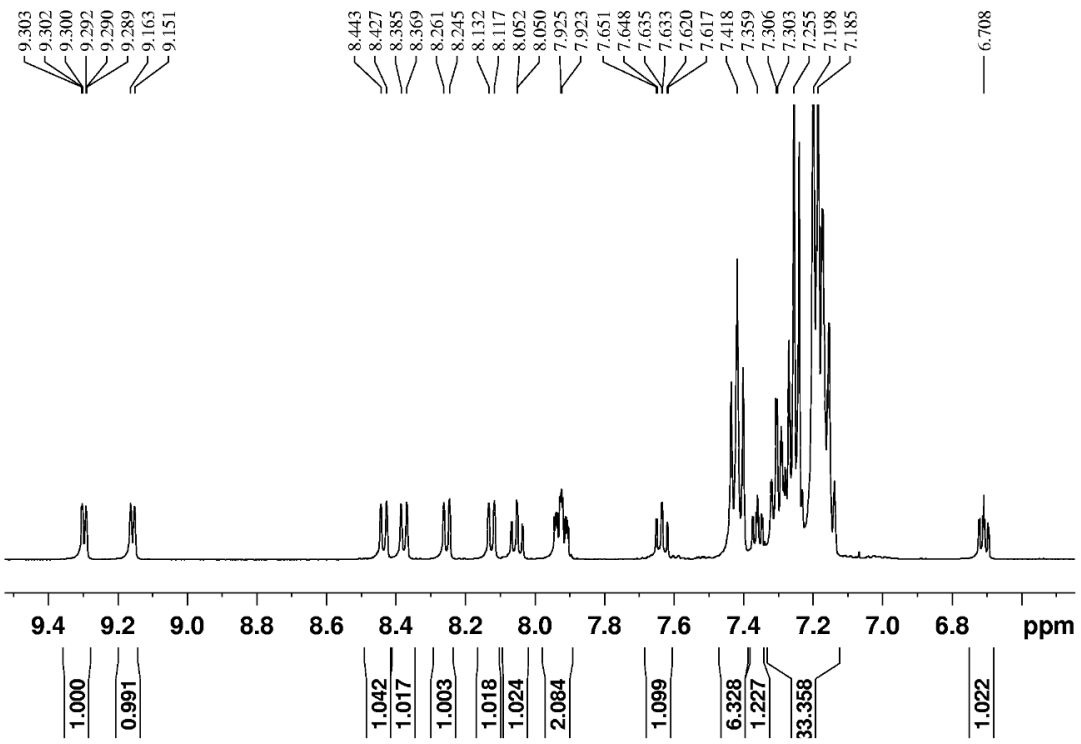

^{1}H NMR of $Ru(bpy)_2ClPPh_3$ in CD_3CN

4-pyridinepropanal

Synthesis was adapted from the literature:[192,193] A solution of oxalylchloride (0.7 mL, 0.05 mmol) dissolved in dry dichloromethane (DCM,10 mL) was chilled in an acetone/dry ice bath to -77°. DMSO (1.14 mL dissolved in DCM) was added slowly and the reaction was stirred for 15 min. 4-pyridinepropanol (1 g, 7.3 mmol) dissolved in dry DCM was added, and the reaction stirred for 45 min at -77°. The reaction was quenched with triethylamine (TEA, 2.56 mL, 18.4 mmol) and brought to room temperature. The solution was washed 3x with water and purified by flash silica gel chromatography with ethyl acetate as the eluent. The last major fraction was collected and dried down to a yellow oil, 334 mg, 34% yield. ^{1}H NMR (CD_3CN, 500 MHz): 9.783 (s, 1H), 7.494 (d, 1H), 7.187 (m, 1H), 2.919 (t, 2H), 2.781 (t, 2H).

Ru(bpy)(biq)Cl_2

Bis[(benzene)dichlororuthenium] (530 mg, 1.06 mmol) and 2,2′-bipyridine (413 mg, 2.6 mmol) were added to methanol (50 mL). The solution was stirred at room temperature for 1 hour, then tetrabutylammonium hexafluorophosphate ($TBAPF_6$) was added until precipitation was complete (~200 mg). The light-yellow product Ru(bz)(bpy)Cl was isolated by vacuum filtration and used without further purification for the next step (crude yield: 908 mg, 83%).

Ru(bz)(bpy)Cl[PF_6] (908 mg, 1.76 mmol) and LiCl (612 mg, 14.4 mmol) were suspended in dimethylformamide (7 mL) and stirred under nitrogen for 10 min. Biquinoline (433 mg, 1.70 mmol) was added, and the solution heated to 130 °C for 1 hour. The reaction mixture was cooled to room temperature and added to 500 mL DI water and filtered to collect the dark green product. The precipitate was then redissolved in dichloromethane and washed 2x with water and reprecipitated from diethyl ether for the final product, Ru(bpy)(biq)Cl_2 (614 mg, 67% yield, 55% overall yield).

Ru(bpy)(biq)(4-pyridinepropanal)$_2$

Ru(bpy)(biq)Cl_2 (51.3 mg, 88μmol) and silver triflate (44 mg, 0.17 mmol) were suspended in 15 mL freshly distilled methanol and stirred. 4-pyridinepropanal (167 mg, 1.23 mmol) was added and the reaction heated to 70 °C for 4 hours. 10 mL of DI water was added and the methanol removed by rotary evaporation. Excess NH_4PF_6 was added and the PF_6 salt was extracted by DCM. Product was purified by silica column with 1:9 methanol:DCM as the eluent, giving pure product as a red solid, 11.4 mg, 15% yield.

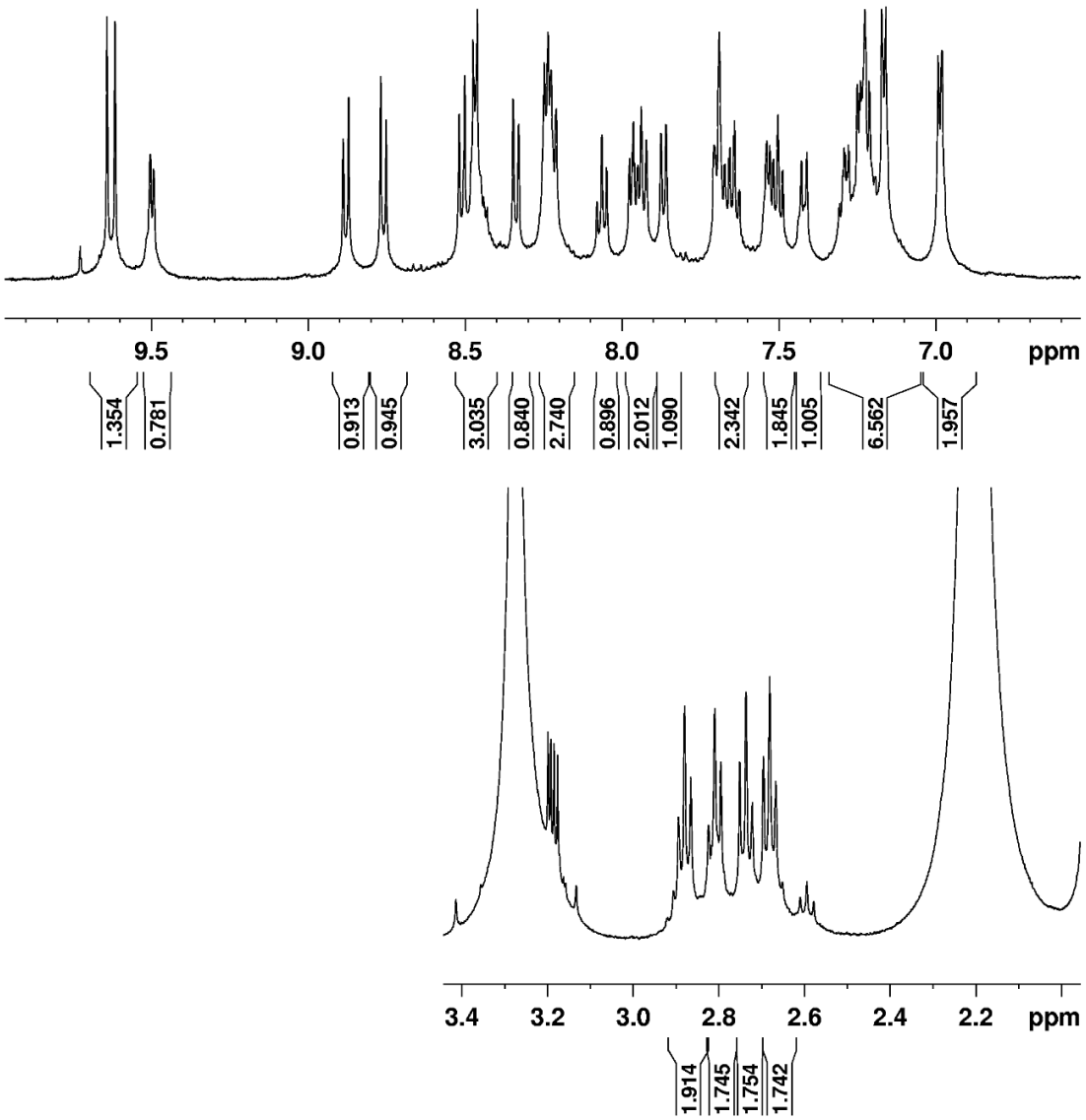

^{1}H NMR of Ru(bpy)(biq)(4-pyridinepropanal)$_2$ in CD_3CN

APPENDIX A – Determination of Quantum Yields by Kinetics

A1.1 – Single Ligand Exchange

In this process we assume that the following irreversible reaction is taking place:

$$RuLL_2(photolabile)_2 + photon \rightarrow RuLL_2(photolabile)(H_2O)$$

Where LL is a bidentate chelating ligand (either bpy or biq) and photolabile is the monodentate, photolabile ligand we expect to be exchanged. In one case, only one is exchanged, in the other, both are exchanged. The two different scenarios are addressed here.

For all QY experiments the light source (a laser pointer at either 450 nm or 523 nm, depending on the compound) is constantly on and the power is measured after the sample. No fluctuation (>0.1 mW) is observed throughout the course of the experiment, therefore it is assumed that a constant flux of photons is being added to the system, and the kinetics of reaction (1) can be described by a pseudo-first order rate law wherein

$$Rate = k'[RuLL_2photolabile_2]^1$$

Where k' is the pseudo-first order rate constant equal to k[photons].

For compounds in which the quantum yield (QY) of the first ligand exchange event is significantly higher than the second (>100x higher, ie, the second ligand effectively does not exchange), the kinetics of the photolysis process is relatively simple.

$$A \rightarrow B$$

$$Abs@470\ nm = Abs(A) + Abs(B)$$

$$\frac{d[A]}{dt} = -k[A]$$

$$\int_{A_o}^{A_t} \frac{1}{A} dA = \int_0^t -k dt$$

$$\ln\left(\frac{A_t}{A_0}\right) = -kt$$

$$A_t = A_0 e^{-kt}$$

$$[B]_t = [A]_0 - [A]_t$$

$$= [A]_0 - [A]_0 e^{-kt}$$

$$Abs@470 = \varepsilon_A [A]_0 e^{-kt} - \varepsilon_b [A]_0 e^{-kt} + \varepsilon_B [A]_0$$

A1.2 – Stepwise Two-Ligand Exchange

Given a reaction of the form:

$$A \rightarrow B \rightarrow C$$

$$k_1 \quad k_2$$

We can describe the change in concentration of each of the components by Equations 1-3:

$$\frac{d[A]}{dt} = -k_1[A] \tag{1}$$

$$\frac{d[B]}{dt} = k_1[A] - k_2[B] \tag{2}$$

$$\frac{d[C]}{dt} = -k_2[B] \tag{3}$$

Integrating these differential equations gives us equations 4-6:

$$[A] = [A]_i e^{-k_1 t} \tag{4}$$

$$[B] = \frac{k_1}{k_2 - k_1}(e^{-k_1 t} - e^{-k_2 t})[A]_i \tag{5}$$

$$[C] = \left(1 + \frac{k_1 e^{-k_1 t} - k_2 e^{-k_2 t}}{k_2 - k_1}\right)[A]_i \tag{6}$$

We know that at any given point in time during the reaction the absorbance at 450 nm must be due to the absorbance of all species (A + B + C) in solution:

$$\mathrm{Abs_t(450nm) = Abs_t(A) + Abs_t(B) + Abs_t(C)} \tag{7}$$

Where:

$$Abs(A) = \varepsilon_A[A] = \varepsilon_A[A]_i e^{-k_1 t} \tag{8}$$

$$Abs(B) = \varepsilon_B[B] = \varepsilon_B \frac{k_1}{k_2 - k_1}(e^{-k_1 t} - e^{-k_2 t})[A]_i \tag{9}$$

$$Abs(C) = \varepsilon_C[C] = \varepsilon_C\left(1 + \frac{k_1 e^{-k_1 t} - k_2 e^{-k_2 t}}{k_2 - k_1}\right)[A]_i \quad (10)$$

Combining all these equations we get

$$Abs_t(450nm) = [A]_i\left(\varepsilon_A + \varepsilon_B\frac{k_1}{k_2 - k_1} - \varepsilon_C\frac{k_2}{k_2 - k_1}\right)e^{-k_1 t} + [A]_i\left(-\varepsilon_B\frac{k_1}{k_2 - k_1} + \frac{k_1}{k_2 - k_1}\right)e^{-k_2 t} + \varepsilon_C[A]_i \quad (11)$$

Which has the basic form

$$y = A_1 e^{-t/\tau_1} + A_2 e^{-t/\tau_2} + y_o \quad (12)$$

A1.3 – Quantum Yield of Photorelease

The quantum yield of photorelease differs from a quantum yield of luminescence in that it describes a chemical change:

$$\varphi = \frac{\text{d reactant (moles)}}{\text{d photon (moles)}} \quad (13)$$

We can assume that all the products came from our starting material, therefore the rate of change of product will be equivalent to rate of change of reactant. Thus we can simplify equation 13 to

$$\varphi = \frac{\text{dA (moles)}}{\text{dphoton (moles)}} \quad (14)$$

To find this value, we need the power output of the light (in J/sec), the wavelength of light emitted, and some measure of the change in moles of reactant. Students should prove to themselves that the following is correct:

$$\varphi = \frac{k_1[A]_i V_{sample}}{\frac{P}{E_{ph} N_A}} \quad (15)$$

Where k_1 is the observed rate constant for the first reaction, $[A]_i$ is the initial concentration of solution in the cuvet, V_{sample} is the volume of sample in the cuvet, P is the power of the light source in watts, E_{ph} is the energy of the photons, and N_A is Avogadro's number.

APPENDIX 2 - Kinetics and Photochemistry of Ruthenium Bisbipyridine Diacetonitrile Complexes: An Interdisciplinary Inorganic and Physical Chemistry Laboratory Exercise

A2.1 Introduction

Chemical education has a need for interdisciplinary laboratory courses that expose students to exciting new applications of chemistry while preparing them to solve real-world problems that cross multiple scientific disciplines.[194–196] As a result, there has been an increase in the publication of new, strongly interdisciplinary laboratory experiments that span the classical divisions of chemistry; from organic/inorganic[197,198] to physical/inorganic[195] and biological/organic[199] examples, these experiments have begun to transform the undergraduate chemical laboratory curriculum.

Ruthenium compounds of the general form $Ru(polypyridyl)_2(L)_2$, where L is any monodentate ligand coordinated via N or S, experience photoactivated ligand (L) exchange with coordinating solvents (such as water) due to a thermally accessible triplet metal-centered state (**Figure A2.1**).[135,200] If the ligands (L) are biologically active this property is useful for photo-releasing a drug with high spatial and temporal control.[26] Even if the ligands are chemically inert, the ruthenium product $[Ru(polypyridyl)_2(H_2O)_2]^{2+}$ itself is biologically active: by binding irreversibly to DNA bases in a manner similar to cisplatin, it can induce cell apoptosis, which provides another opportunity to spatially target drug delivery.[201]

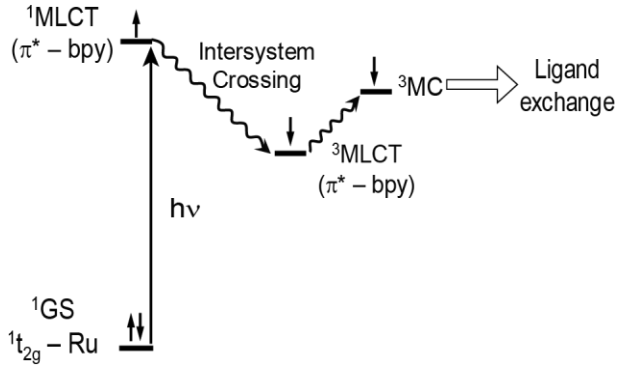

Figure A2.1. A typical Jablonski diagram depicting the electronic transitions responsible for light-mediated ligand loss observed in many $Ru(2,2'\text{-bipyridine})_2(L)_2$ compounds. An electron is excited from the ground state (^{1}GS) on the metal center into a metal-to-ligand charge transfer state (^{1}MLCT). It undergoes rapid intersystem crossing into a triplet MLCT state, from which it can populate the thermally accessible triplet metal-centered state, ^{3}MC, responsible for ligand exchange.

Photoactive ruthenium complexes recently described in the literature have used chelating polypyridyl ligands with extended pi systems in order to red-shift the absorbance of the complex and allow for photolysis within living tissue.[189,201] However, to facilitate synthesis and characterization for an undergraduate laboratory we worked with a model compound RuMeCN, which is readily synthesized from commercially available $Ru(bpy)_2Cl_2$[33,202] (where bpy is 2,2'-bipyridine) and acetonitrile, and is stable in red light, making it practical for student handling in a large laboratory setting. Upon continuous irradiation of RuMeCN under blue light, both CH_3CN ligands are exchanged sequentially, providing a "textbook example" of A→B→C kinetics. Multi-step kinetic processes are common in nature, but can be difficult to monitor spectroscopically. The RuMeCN photolysis reaction provides a valuable opportunity to collect and analyze data for a model 2-step kinetic process.

In addition to its symmetrical octahedral structure and beautiful yellow color, RuMeCN is distinctive for the pedagogical opportunities it provides. Synthesis of this molecule teaches students basic Schlenk line techniques on a system that is less sensitive to oxygen and water than many other inorganic syntheses. RuMeCN is also reversibly and cleanly oxidized and reduced, and cyclic voltammetry is useful for characterizing the electronic transition that gives rise to ligand exchange.[54] Students observe the characteristic MLCT band of RuMeCN and photolysis products by UV-Vis spectroscopy, giving an opportunity to discuss electronic transitions and ligand-field theory in detail. And lastly, quantitative analysis of the 2-step ligand exchange process, coupled with equation derivation and data fitting, complements the physical chemistry lab course. In completing these laboratory exercises with RuMeCN, students gain the requisite skills to design, synthesize, and characterize a wide variety of inorganic compounds, especially novel Ru-caged compounds, which could be developed as a separate laboratory exercise.

Other experiments have been published recently that use ruthenium chemistry to cross disciplines in a similar manner. For example, this laboratory exercise complements previous studies of these Ru complexes and their photoactivity by DFT and computational modeling.[203]

Similarly, because ruthenium coordination compounds have been widely applied in the biological sciences, another interdisciplinary experiment includes the use of ruthenium “piano-stool” complexes in DNA binding and cleavage.[204] In our case, we applied the photochemical reaction of $Ru(bpy)_2(CH_3CN)_2$ to advanced laboratory courses in both inorganic synthesis and experimental physical chemistry. Due to course scheduling, many students performed the synthesis laboratory one semester before the physical chemistry laboratory, thus these very complementary experiments were designed to stand alone.

The pedagogical goals for the two experiments described here are as follows: For Advanced Synthesis, students will (1) perform a reaction on a Schlenk line, and purify product by column chromatography, (2) characterize the compound by NMR and cyclic voltammetry, (3) determine a molar absorptivity and describe the electronic transition observed, and (4) demonstrate the application of ligand field theory in an experimental system. For Physical Chemistry, the goals were to (1) provide students with an experimental system with complicated kinetics mechanism, (2) fit data from experiments to formulae derived from basic equations, and (3) discuss the physical meaning of a quantum yield.

A2.2 Inorganic Synthesis Laboratory (8 h total, two 4-h sections)

Synthesis and Characterization of $[Ru(bpy)_2(CH_3CN)_2]Cl_2$ (RuMeCN)

Laboratory sections consisted of 21 students working in lab groups no larger than three. The course was supervised by an instructor and two graduate student TAs. The first 4-hour lab period was used to synthesize and purify RuMeCN, and a second 4-hour lab period was used for characterization.

Synthesis was performed on a 100 mg (0.192 mmol) scale of starting material $Ru(bpy)_2Cl_2$ (SI Section 1B), giving an average yield of 60%, or ~65 mg of product per group. RuMeCN was characterized by ^1H NMR in CD_3CN. This same sample was then used for electrochemical characterization in CH_3CN with $TBAPF_6$ as the electrolyte (SI Section 1C). UV-Vis spectroscopy

was performed in water with concentrations ranging from 0.03 to 0.2 mM. Molar absorptivity was determined by a Beer-Lambert Law plot, and the ligand exchange was observed by UV-Vis spectroscopy upon irradiation with several different light sources, including white LED flashlights and cell phone flashlights.

A2.3 Physical Chemistry Laboratory (4 h section)

Kinetics Studies

Laboratory sections for physical chemistry consisted of 26 students supervised by an instructor and two graduate student TAs. Students worked in pairs to collect UV-Vis absorption spectra showing the spectral shift under visible light irradiation and to determine how long the kinetics trials would take, then collected three kinetics traces observing the absorbance at 450 nm under continuous irradiation.

$[Ru(bpy)_2(CH_3CN)_2]Cl_2$ was synthesized by a lab technician and students were given 7 mg aliquots for their use. Stock (1 mM) solutions of RuMeCN were made, from which students made aliquots to generate photolysis solutions of around 0.03-0.1 mM. Blue presentation laser pointers (max wavelength 405 nm) were used as light sources. The power of the light source was measured before each kinetics trial using a ThorLabs P-100 power meter.

Hazards

Synthesis should be performed in the hood under inert atmosphere. Gloves, lab coats, and goggles should be worn at all times when synthesizing and purifying the compound. Gloves and goggles should be worn when characterizing and performing kinetics studies. Dry silica gel is an inhalation hazard and should be handled in the hood or with face masks. Dichloromethane is an eye and skin irritant and potentially carcinogenic. $Ru(bpy)_2(CH_3CN)_2$ is not considered extremely toxic, but should be handled with care.

A2.5 Results

Advanced Synthesis Lab - Complex Synthesis

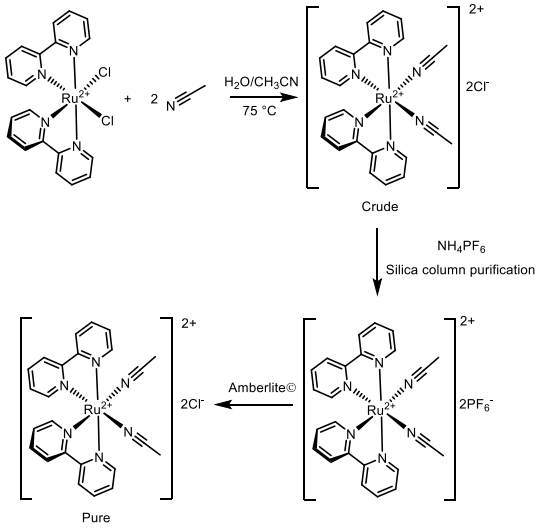

Scheme A2.1. Synthesis and subsequent metathesis reactions to form the final product RuMeCN.

Synthesis on the 100 mg scale provided most groups with sufficient material for all experiments in the Advanced Synthesis Lab. The synthesis was performed in the dark by covering round bottom flasks with foil and turning off the lights. We found it helpful to use desk lamps fitted with red incandescent bulbs to safely illuminate the laboratory during the experiment. The heating step was performed under inert atmosphere (N_2 or Ar) to prevent the formation of reactive oxygen species at the ruthenium, which can lead to side products or degradation during the synthesis.

Once the solution turned orange (as observed by briefly exposing to dim white light), the counterions were exchanged by adding solid NH_4PF_6 and extracting the resultant precipitate with dichloromethane. [RuMeCN]$(PF_6)_2$ is soluble in less polar organic solvents (useful for column chromatography) while [RuMeCN]Cl_2 is soluble in water and more polar solvents such as methanol and acetonitrile. Students checked the suggested solvent ratio and the purity of the reaction by TLC before the column. Once pure, a metathesis was performed again by passing [RuMeCN]$(PF_6)_2$ dissolved in methanol through an anion exchange resin (Amberlite ®). This was then divided into two vials and dried down separately by rotary evaporation.

Advanced Synthesis - Characterization

One vial of [RuMeCN]Cl_2 was used to collect ^{1}H NMR spectrum and cyclic voltammogram (**Figure A2.2, Figure A2.3**), as the sample cannot be reused after the electrochemistry experiment. The NMR spectrum showed the purity of the sample, and students were able to calculate the reduction potential, $E_{1/2}$, for the Ru(III) → Ru(II) redox couple. It has been suggested in the literature that this value trends with the quantum yield of ligand release.[54]

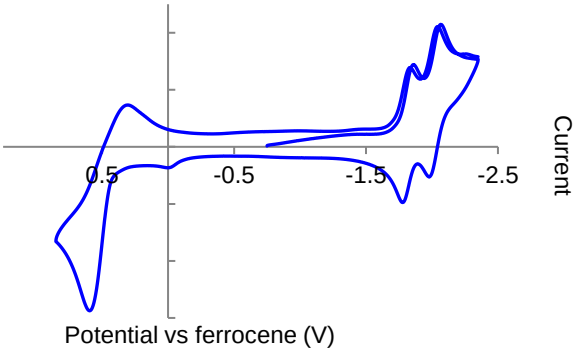

Figure A2.2. Cyclic voltammogram of RuMeCN in acetonitrile. The two peaks at -1.75 V and -2.00 V correspond to sequential bpy/bpy- reduction for each bpy ligand, the major redox event at approx. +0.5 V corresponds to the Ru(III)/Ru(II) couple.

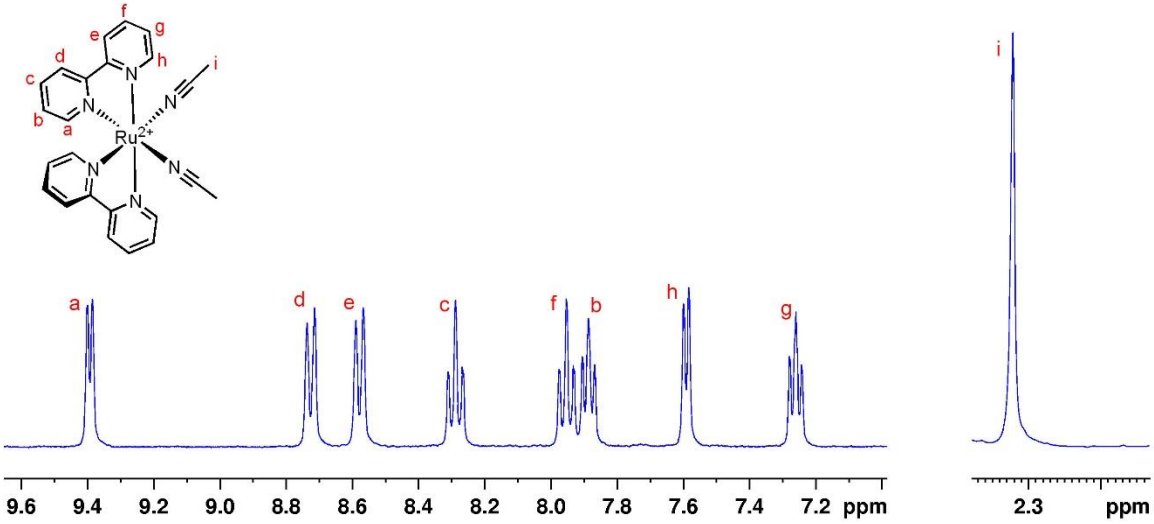

Figure A2.3. Assigned NMR for the product. d^3-acetonitrile was used as NMR solvent.

The contents of the other vial, which must be completely dry, was dissolved in water to make a stock solution of approximately 1 – 5 mM. The molar absorptivity at 420 nm, ε_{420}, was determined by generating a standard curve and fitting to Beer's Law, as well as a series of spectra showing the spectral shift under constant irradiation (**Figure A2.4**). For this lab, many different light sources were used, varying from a simple white LED flashlight to cell phone flashlights. It was found that a less powerful light source gives the clearest shift, though this takes longer for the reaction to go to completion (10 – 20 min). Student results for the molar absorptivity, as well as their average overall synthetic yield, are presented in **Table A2.1**.

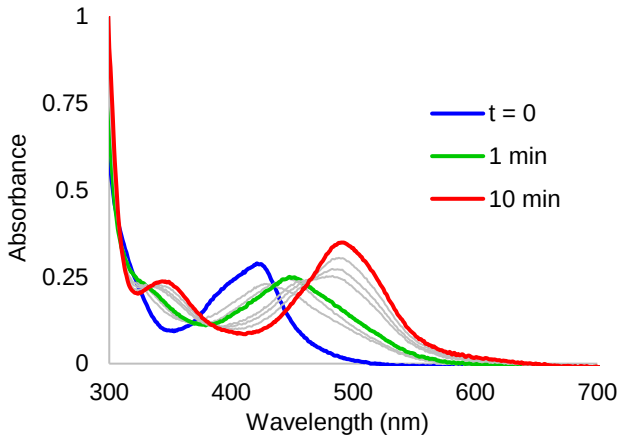

Figure A2.4. UV-Vis spectra of RuMeCN dissolved in water showing the shift in absorbance under continuous irradiation with a bright light source (1-5 mW).

Table A2.1. Percent yield, $E_{1/2}$, and Molar Absorptivity values determined for RuMeCN.

Values	*% Yield*	*$E_{1/2}$[a] (V vs Fc)*	*ε_{420} ($M^{-1}cm^{-1}$)*
Measured	80-96%	1.0[c]	7,300
Students[b]	60 ± 34%	0.8 ± 0.2	5,000 ± 3,000

[a] In acetonitrile, with $TBAPF_6$ as the electrolyte. [b]Average of 12 groups. [c]Pinnick et al.[202]

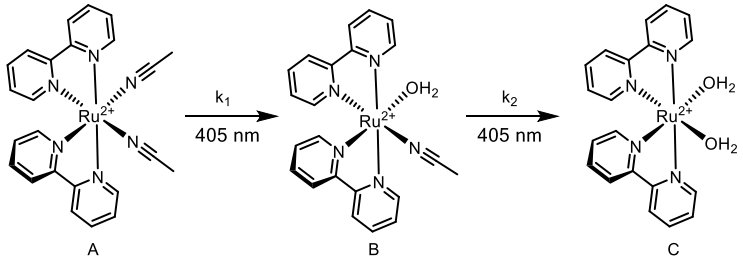

Scheme A2.2. RuMeCN photolysis, investigating observed first (k_1) and second (k_2) ligand exchange rates.

In order to visualize the change in absorbance expected at 450 nm (where the intermediate species B absorbs most strongly), students again collected a series of UV-Vis spectra (similar to **Figure A2.4**, using a 405 nm laser pointer, ~5 mW). Once students had identified a suitable timescale for their kinetics experiments, they set up the spectrometer for constant irradiation while stirring. Blue (405 nm) laser pointers were suspended over the cuvet, which was placed in the spectrometer on a stir plate, and equipped with a stir bar. The students collected at least 3 good kinetics traces to reduce experimental error.

The data were then fit to an equation of the form

$$\mathrm{Abs} = \mathrm{A_1}\, e^{-t/\tau_1} + \mathrm{A_2} e^{-t/\tau_2} + \mathrm{y_o} \tag{1}$$

Which was derived from the integrated rate laws

$$[A] = [A]_i e^{-k_1 t} \tag{2}$$

$$[B] = \frac{k_1}{k_2 - k_1}\left(e^{-k_1 t} - e^{-k_2 t}\right)[A]_i \tag{3}$$

$$[C] = \left(1 + \frac{k_1 e^{-k_1 t} - k_2 e^{-k_2 t}}{k_2 - k_1}\right)[A]_i \tag{4}$$

(full derivation in Appendix 1). Excel Solver was used to fit the data, given a set of sample values for the constants A_1, τ_1, A_2, and τ_2. Most students found an acceptable fit, based on the sum of

the differences squared between experimental and calculated values, and a visual plot of their data (**Figure A2.5**).

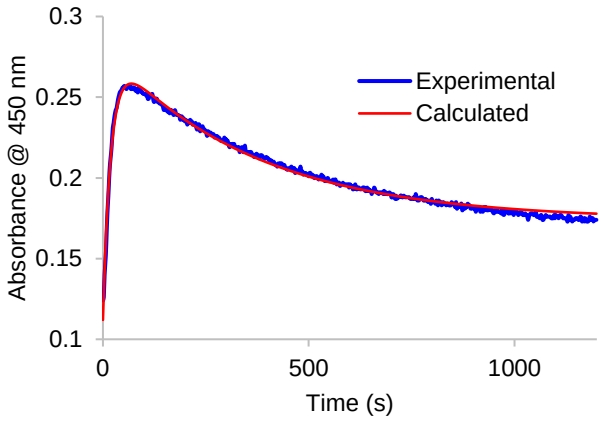

Figure A2.5. Kinetics trace collected by students of the absorbance measured at 450 nm under constant irradiation with a blue laser pointer (~5 mW), plotted against the calculated values determined by Solver.

Quantum Yield – Physical Chemistry Laboratory

The quantum yield calculation required measurement of the power of the light source using a conventional power meter (Thorlabs PM100A). The power of the light source was determined and recorded prior to every kinetics experiment, as the laser pointer power fluctuated somewhat over time.

Using the observed rate constant for the first photolysis step, k_1, as determined by the data fit, the power and wavelength of the light source, the quantum yield for the first ligand photorelease, φ_{pr}, was calculated:

$$\varphi_{pr} = \frac{dA\ (moles)}{dphoton\ (moles)} = \frac{k_1[A]_i V_{sample}}{\frac{P}{E_{ph} N_A}} \quad (5)$$

Where $[A]_I$ is the molar concentration of RuMeCN in the cuvet, V_{sample} is the volume (in L) of solution in the cuvet, P is the measured laser power (J/s), E_{ph} is the energy of the photons (hc/λ, in J), and N_A is Avogadro's number ($mole^{-1}$).

Table A2.2. Observed rate constants and quantum yield values.

Values	k_1 (s^{-1})	k_2 (s^{-1})	Φ_{pr}[a]
Measured	0.33	0.006	0.51
Students[b]	0.1 ± 0.1	0.008 ± 0.004	0.4 ± 0.3

[a]Quantum yield of photorelease. [b]Average of 13 groups

A2.5 Discussion

Upon completion of the Advanced Synthesis laboratory students were required to compile their data and present it in a basic laboratory report with a paragraph discussing their findings and potential applications for this compound. Due to the report requirements in the Physical Chemistry laboratory, students in that class were required to submit a written, full-length laboratory report, including a discussion of their results and the viability of this compound for use in photodynamic therapy, especially regarding photolytic reactivity (related to the magnitude of the quantum yield). Most students found both labs to be a valuable learning experience and engaging on many levels. Students in the Physical Chemistry Laboratory were asked to rate their levels of understanding concerning certain topics before and after the experiment (**Figure A2.6**), and their answers show a positive trend in post-lab comprehension levels, with the greatest improvement in knowledge of data fitting. The quality of student data was generally good (see **Tables A2.1 and A2.2**), with several outliers especially in the calculation of molar absorptivity and the observed rate constants. This was generally due to errors in solution concentration, e.g. if the initial mass was incorrect or students failed to dissolve 100% of their sample. The differences in students' experimental values for both observed rate constants, k_1 and k_2, can be explained by differences in the number of photons delivered to the sample in the different groups (with variability in laser pointer power, illumination path, and stirring efficiency being three important variables).

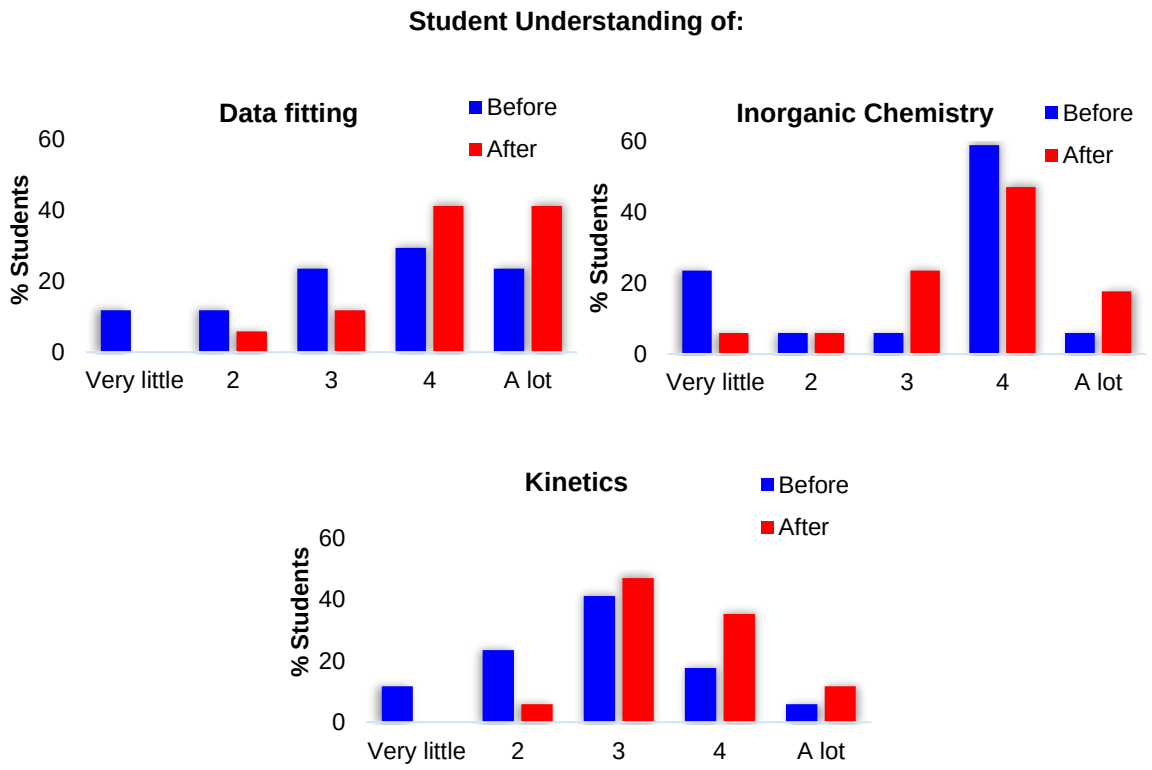

Figure A2.5. Student feedback after the experiment. Students were asked to compare their knowledge about data fitting, ligand field theory and inorganic chemistry, and higher order kinetics before and after the experiment performed in the Physical Chemistry laboratory (26 students).

Further investigations with this system could include performing COSY 2D NMR to assign the peaks in the aromatic region of the proton NMR. Students also suggested exploring other ligand exchange systems, comparing spectroscopic results of the light reaction performed in water or in another coordinating solvent or with different N or S ligands.

APPENDIX 3 – X-Ray Crystal Structures

A3.1 $Ru(bpy)_2(3\text{-ethynylpyridine})_2$ (RuBEP)

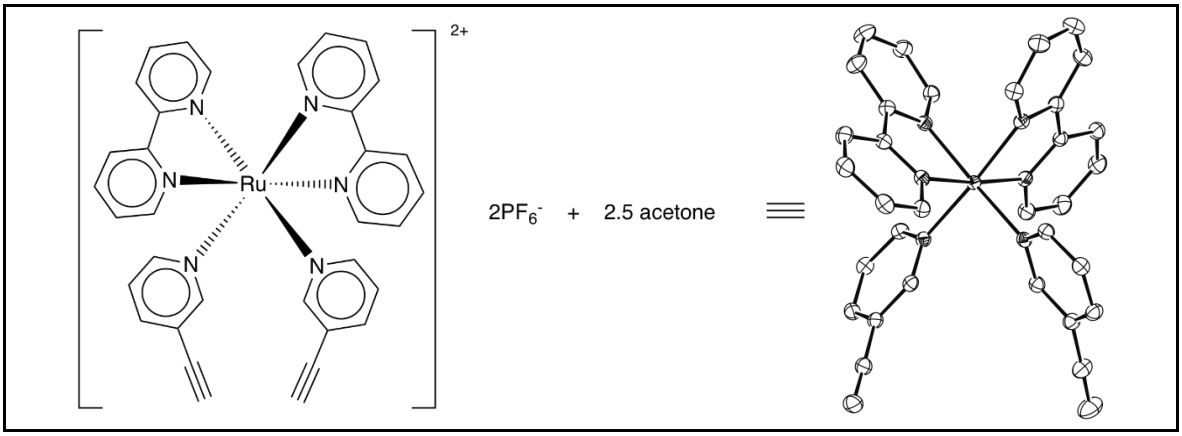

Compound 9718, $C_{34}H_{26}N_6P_2F_{12}Ru \bullet 2½$ acetone, crystallizes in the triclinic space group $P\bar{1}$ with a=11.2159(7)Å, b=12.5550(8)Å, c=18.1382(12)Å, α=70.206(3)°, β=85.323(3)°, γ=67.450(2)°, V=2216.1(2)Å^3, Z=2, and d_{calc}=1.581 g/cm^3 . X-ray intensity data were collected on a Bruker APEXII CCD area detector employing graphite-monochromated Mo-Kα radiation (λ=0.71073 Å) at a temperature of 100(1)K. Preliminary indexing was performed from a series of thirty-six 0.5° rotation frames with exposures of 10 seconds. A total of 3572 frames were collected with a crystal to detector distance of 37.5 mm, rotation widths of 0.5° and exposures of 10 seconds:

scan type	2θ	ω	ϕ	χ	frames
ϕ	19.50	327.79	15.97	36.30	739
ϕ	-20.50	342.55	321.55	-73.06	739
ω	-23.00	333.53	158.99	-70.01	64
ω	-15.50	340.80	341.11	-63.64	99
ω	-25.50	330.51	47.91	-56.95	185
ω	-25.50	239.19	209.98	28.88	204
ω	-18.00	243.20	310.97	36.30	208
ω	27.00	277.79	5.00	57.63	221
ϕ	-10.50	318.39	249.35	52.47	254
ω	17.00	322.24	318.36	83.36	114
ϕ	27.00	352.41	83.39	85.83	157

ϕ	-18.00	124.02	292.98	-95.28	588

Rotation frames were integrated using SAINT[1], producing a listing of unaveraged F^2 and $\sigma(F^2)$ values which were then passed to the SHELXTL[2] program package for further processing and structure solution. A total of 73021 reflections were measured over the ranges $1.86 \leq \theta \leq 27.54°$, $-14 \leq h \leq 14$, $-16 \leq k \leq 16$, $-23 \leq l \leq 23$ yielding 10200 unique reflections (Rint = 0.0189). The intensity data were corrected for Lorentz and polarization effects and for absorption using SADABS[3] (minimum and maximum transmission 0.6876, 0.7456).

The structure was solved by direct methods (SHELXS-97[4]). Refinement was by full-matrix least squares based on F^2 using SHELXL-97.[5] All reflections were used during refinement. The weighting scheme used was $w=1/[\sigma^2(F_o^2)+ (0.0277P)^2 + 3.0501P]$ where $P = (F_o^2 + 2F_c^2)/3$. Non-hydrogen atoms were refined anisotropically and hydrogen atoms were refined using a riding model. Refinement converged to R1=0.0286 and wR2=0.0686 for 9570 observed reflections for which $F > 4\sigma(F)$ and R1=0.0313 and wR2=0.0714 and GOF =1.042 for all 10200 unique, non-zero reflections and 634 variables.[6] The maximum Δ/σ in the final cycle of least squares was 0.002 and the two most prominent peaks in the final difference Fourier were +1.442 and -0.836 e/Å^3.

---

[1]Bruker (2009) SAINT. Bruker AXS Inc., Madison, Wisconsin, USA.

[2]Bruker (2009) SHELXTL. Bruker AXS Inc., Madison, Wisconsin, USA.

[3]Sheldrick, G.M. (2007) SADABS. University of Gottingen, Germany.

[4]Sheldrick, G.M. (2008) Acta Cryst. A64,112-122.

[5]Sheldrick, G.M. (2008) Acta Cryst. A64,112-122.

[6]$R1 = \Sigma||F_o| - |F_c|| / \Sigma |F_o|$
$wR2 = [\Sigma w(F_o^2 - F_c^2)^2/\Sigma w(F_o^2)^2]^{½}$
$GOF = [\Sigma w(F_o^2 - F_c^2)^2/(n - p)]^{½}$
where n = the number of reflections and p = the number of parameters refined.

Table 1. lists cell information, data collection parameters, and refinement data. Final positional and equivalent isotropic thermal parameters are given in Tables 2. and 3. Anisotropic thermal parameters are in Table 4. Tables 5. and 6. list bond distances and bond angles. Figure 1. is an ORTEP[7] representation of the Ru complex with 50% probability thermal ellipsoids displayed.

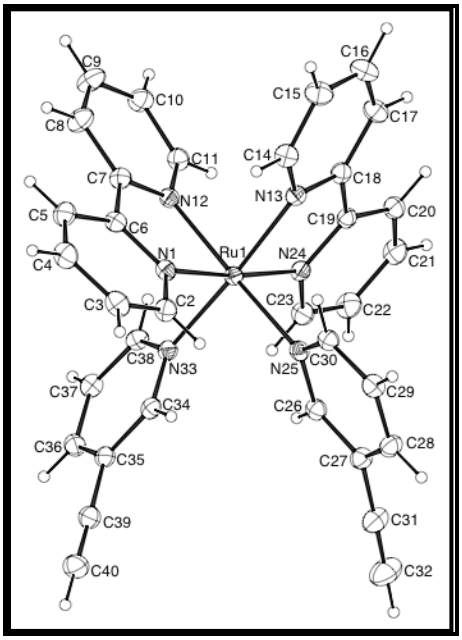

Figure 1. ORTEP drawing of the Ru complex with 50% probability thermal ellipsoids.

Table 1. Summary of Structure Determination of Compound 9718

Empirical formula	$C_{83}H_{82}N_{12}P_4O_5F_{24}Ru_2$
Formula weight	2109.63
Temperature	100(1) K
Wavelength	0.71073 Å
Crystal system	triclinic
Space group	$P\bar{1}$
Cell constants:	

[7]"ORTEP-II: A Fortran Thermal Ellipsoid Plot Program for Crystal Structure Illustrations". C.K. Johnson (1976) ORNL-5138.

a	11.2159(7) Å
b	12.5550(8) Å
c	18.1382(12) Å
α	70.206(3)°
β	85.323(3)°
γ	67.450(2)°
Volume	2216.1(2) $Å^3$
Z	1
Density (calculated)	1.581 Mg/m^3
Absorption coefficient	0.522 mm^{-1}
F(000)	1068
Crystal size	0.42 x 0.26 x 0.10 mm^3
Theta range for data collection	1.86 to 27.54°
Index ranges	$-14 \leq h \leq 14$, $-16 \leq k \leq 16$, $-23 \leq l \leq 23$
Reflections collected	73021
Independent reflections	10200 [R(int) = 0.0189]
Completeness to theta = 27.54°	99.6 %
Absorption correction	Semi-empirical from equivalents
Max. and min. transmission	0.7456 and 0.6876
Refinement method	Full-matrix least-squares on F^2
Data / restraints / parameters	10200 / 113 / 634
Goodness-of-fit on F^2	1.042
Final R indices [I>2sigma(I)]	R1 = 0.0286, wR2 = 0.0686
R indices (all data)	R1 = 0.0313, wR2 = 0.0714
Largest diff. peak and hole	1.442 and -0.836 $e.Å^{-3}$

Table 2. Refined Positional Parameters for Compound 9718

Atom	x	y	z	U_{eq}, $Å^2$
Ru1	0.506257(12)	0.163868(12)	0.264397(8)	0.01292(4)
N1	0.65819(14)	0.13185(13)	0.19097(9)	0.0153(3)
N12	0.45451(14)	0.07305(13)	0.20480(9)	0.0149(3)
N13	0.57465(14)	-0.00630(14)	0.34958(9)	0.0155(3)
N24	0.35556(14)	0.17812(14)	0.33877(9)	0.0154(3)
N25	0.57818(14)	0.24339(14)	0.32653(9)	0.0155(3)
N33	0.41532(14)	0.33224(13)	0.17585(9)	0.0151(3)
C2	0.75830(17)	0.16750(17)	0.18526(11)	0.0188(3)
C3	0.85450(18)	0.14474(18)	0.13324(11)	0.0219(4)

C4	0.84617(19)	0.08519(18)	0.08327(12)	0.0235(4)
C5	0.74281(19)	0.04876(18)	0.08770(11)	0.0218(4)
C6	0.65120(17)	0.07173(16)	0.14270(11)	0.0169(3)
C7	0.54122(17)	0.03183(16)	0.15400(11)	0.0173(3)
C8	0.5281(2)	-0.04635(19)	0.11906(12)	0.0246(4)
C9	0.4250(2)	-0.0838(2)	0.13656(13)	0.0272(4)
C10	0.33655(19)	-0.04140(18)	0.18776(12)	0.0226(4)
C11	0.35400(17)	0.03711(17)	0.22012(11)	0.0180(3)
C14	0.68457(18)	-0.09936(17)	0.34715(11)	0.0196(4)
C15	0.71162(19)	-0.21893(18)	0.39519(12)	0.0247(4)
C16	0.6229(2)	-0.24478(18)	0.44903(13)	0.0262(4)
C17	0.51084(19)	-0.15002(18)	0.45342(12)	0.0223(4)
C18	0.48813(17)	-0.03161(16)	0.40305(10)	0.0166(3)
C19	0.36860(17)	0.07437(16)	0.40005(10)	0.0161(3)
C20	0.27414(19)	0.07006(18)	0.45421(11)	0.0204(4)
C21	0.16280(19)	0.17313(19)	0.44611(12)	0.0235(4)
C22	0.15002(19)	0.27884(19)	0.38423(12)	0.0239(4)
C23	0.24783(18)	0.27819(17)	0.33219(11)	0.0198(4)
C26	0.50883(17)	0.35332(16)	0.33425(10)	0.0173(3)
C27	0.55502(19)	0.40440(17)	0.37743(11)	0.0201(4)
C28	0.67826(19)	0.33912(18)	0.41462(11)	0.0211(4)
C29	0.75015(18)	0.22635(17)	0.40646(11)	0.0198(4)
C30	0.69790(17)	0.18184(16)	0.36276(10)	0.0172(3)
C31	0.4757(2)	0.52329(19)	0.38142(13)	0.0263(4)
C32	0.4114(2)	0.6221(2)	0.38317(15)	0.0367(5)
C34	0.47048(17)	0.41520(16)	0.14776(10)	0.0164(3)
C35	0.41311(18)	0.52534(16)	0.08662(10)	0.0174(3)
C36	0.29400(18)	0.55052(17)	0.05303(11)	0.0191(3)
C37	0.23680(18)	0.46538(17)	0.08155(11)	0.0192(3)
C38	0.29993(17)	0.35805(17)	0.14189(11)	0.0174(3)
C39	0.47888(18)	0.60893(17)	0.05969(11)	0.0202(4)
C40	0.5348(2)	0.67632(19)	0.03667(12)	0.0260(4)
P1	0.91753(5)	0.07849(5)	0.63543(3)	0.01945(10)
F1	0.77189(12)	0.10141(13)	0.61327(9)	0.0342(3)
F2	1.06165(12)	0.05866(14)	0.65718(10)	0.0423(4)
F3	0.92791(16)	-0.04414(14)	0.70347(10)	0.0504(4)
F4	0.97135(14)	0.00550(15)	0.57550(9)	0.0440(4)

F5	0.90456(15)	0.20275(13)	0.56596(9)	0.0429(3)
F6	0.86225(13)	0.15490(14)	0.69371(8)	0.0368(3)
P2	0.86742(5)	0.76441(5)	-0.00468(3)	0.02103(10)
F7	0.8303(2)	0.78272(14)	0.07795(9)	0.0564(5)
F8	0.8974(2)	0.75134(19)	-0.08867(10)	0.0644(6)
F9	0.71658(15)	0.81511(18)	-0.02797(12)	0.0696(6)
F10	0.86399(12)	0.90153(12)	-0.04004(8)	0.0306(3)
F11	1.01548(14)	0.71761(14)	0.01789(12)	0.0552(5)
F12	0.86996(14)	0.62853(12)	0.03176(9)	0.0373(3)
C41	0.8715(2)	0.3326(2)	0.77962(13)	0.0308(5)
C42	1.0085(3)	0.2875(3)	0.7566(2)	0.0539(8)
C43	0.8320(3)	0.2412(2)	0.84170(15)	0.0412(6)
O1	0.7983(2)	0.43757(16)	0.75072(12)	0.0500(5)
C44	0.7922(4)	0.4702(4)	0.2171(3)	0.0288(10)
C45	0.9341(5)	0.4331(5)	0.2064(3)	0.0466(11)
C46	0.7226(6)	0.5913(5)	0.2295(4)	0.0438(14)
O2	0.7351(3)	0.4075(3)	0.2155(2)	0.0438(7)
C47	0.7961(5)	0.5225(5)	0.2708(3)	0.0267(10)
C48	0.6795(8)	0.6368(8)	0.2341(5)	0.0403(18)
C49	0.8508(11)	0.4360(9)	0.2254(6)	0.051(2)
O3	0.8448(3)	0.5036(3)	0.3335(2)	0.0264(7)
C50	0.9425(3)	0.4816(3)	0.4963(2)	0.0661(9)
C51	0.8831(6)	0.4514(5)	0.5654(3)	0.0433(12)
O4	0.8935(3)	0.4859(3)	0.4277(2)	0.0349(7)

$U_{eq}=^{1}/_{3}[U_{11}(aa^*)^2+U_{22}(bb^*)^2+U_{33}(cc^*)^2+2U_{12}aa^*bb^*\cos\gamma+2U_{13}aa^*cc^*\cos\beta+2U_{23}bb^*cc^*\cos\alpha]$

Table 3. Positional Parameters for Hydrogens in Compound 9718

Atom	x	y	z	U_{iso}, Å^2
H2	0.7632	0.2094	0.2178	0.025
H3	0.9235	0.1690	0.1319	0.029
H4	0.9089	0.0698	0.0473	0.031
H5	0.7349	0.0094	0.0543	0.029
H8	0.5881	-0.0732	0.0843	0.033
H9	0.4153	-0.1367	0.1141	0.036
H10	0.2665	-0.0653	0.2003	0.030
H11	0.2935	0.0663	0.2540	0.024
H14	0.7450	-0.0826	0.3116	0.026

H15	0.7882	-0.2811	0.3915	0.033
H16	0.6387	-0.3246	0.4816	0.035
H17	0.4509	-0.1651	0.4898	0.030
H20	0.2856	-0.0018	0.4958	0.027
H21	0.0981	0.1713	0.4815	0.031
H22	0.0766	0.3496	0.3776	0.032
H23	0.2386	0.3499	0.2910	0.026
H26	0.4265	0.3971	0.3097	0.023
H28	0.7113	0.3704	0.4441	0.028
H29	0.8329	0.1810	0.4302	0.026
H30	0.7473	0.1060	0.3580	0.023
H32	0.3608	0.6999	0.3845	0.049
H34	0.5502	0.3985	0.1700	0.022
H36	0.2535	0.6231	0.0122	0.025
H37	0.1569	0.4802	0.0604	0.025
H38	0.2613	0.3009	0.1600	0.023
H40	0.5787	0.7291	0.0186	0.035
H42a	1.0273	0.3552	0.7214	0.081
H42b	1.0201	0.2289	0.7310	0.081
H42c	1.0658	0.2495	0.8027	0.081
H43a	0.8617	0.2329	0.8923	0.062
H43b	0.8693	0.1636	0.8335	0.062
H43c	0.7394	0.2681	0.8394	0.062
H45a	0.9677	0.3548	0.1991	0.070
H45b	0.9767	0.4280	0.2520	0.070
H45c	0.9492	0.4928	0.1611	0.070
H46a	0.6327	0.6050	0.2359	0.066
H46b	0.7313	0.6556	0.1848	0.066
H46c	0.7595	0.5906	0.2757	0.066
H48a	0.6531	0.6841	0.2687	0.060
H48b	0.6102	0.6148	0.2253	0.060
H48c	0.7009	0.6843	0.1850	0.060
H49a	0.9246	0.3674	0.2545	0.077
H49b	0.8766	0.4774	0.1757	0.077
H49c	0.7864	0.4079	0.2170	0.077
H50a	0.9735	0.3980	0.4990	0.031
H50b	0.9017	0.5319	0.4423	0.031

H50c	0.8802	0.4985	0.5325	0.031
H51a	0.8119	0.4321	0.5563	0.065
H51b	0.8518	0.5194	0.5845	0.065
H51c	0.9441	0.3818	0.6036	0.065

Table 4. Refined Thermal Parameters (U's) for Compound 9718

Atom	U_{11}	U_{22}	U_{33}	U_{23}	U_{13}	U_{12}
Ru1	0.01149(7)	0.01408(7)	0.01415(7)	-0.00525(5)	0.00266(5)	-0.00578(5)
N1	0.0133(7)	0.0157(7)	0.0157(7)	-0.0044(6)	0.0024(5)	-0.0052(6)
N12	0.0145(7)	0.0149(7)	0.0149(7)	-0.0042(5)	0.0017(5)	-0.0060(6)
N13	0.0141(7)	0.0169(7)	0.0170(7)	-0.0066(6)	0.0008(5)	-0.0066(6)
N24	0.0153(7)	0.0181(7)	0.0156(7)	-0.0074(6)	0.0027(5)	-0.0082(6)
N25	0.0160(7)	0.0163(7)	0.0146(7)	-0.0047(6)	0.0033(5)	-0.0075(6)
N33	0.0148(7)	0.0161(7)	0.0154(7)	-0.0065(6)	0.0030(5)	-0.0061(6)
C2	0.0171(8)	0.0219(9)	0.0191(8)	-0.0069(7)	0.0028(7)	-0.0095(7)
C3	0.0162(8)	0.0257(9)	0.0230(9)	-0.0054(7)	0.0048(7)	-0.0103(7)
C4	0.0195(9)	0.0263(10)	0.0233(9)	-0.0089(8)	0.0089(7)	-0.0081(8)
C5	0.0221(9)	0.0231(9)	0.0215(9)	-0.0106(7)	0.0062(7)	-0.0081(7)
C6	0.0153(8)	0.0158(8)	0.0183(8)	-0.0049(7)	0.0019(6)	-0.0052(7)
C7	0.0157(8)	0.0174(8)	0.0184(8)	-0.0064(7)	0.0017(6)	-0.0056(7)
C8	0.0230(9)	0.0274(10)	0.0296(10)	-0.0172(8)	0.0072(8)	-0.0103(8)
C9	0.0283(10)	0.0294(10)	0.0349(11)	-0.0196(9)	0.0053(8)	-0.0155(9)
C10	0.0226(9)	0.0247(9)	0.0260(10)	-0.0095(8)	0.0030(7)	-0.0141(8)
C11	0.0166(8)	0.0202(8)	0.0180(8)	-0.0060(7)	0.0026(6)	-0.0084(7)
C14	0.0157(8)	0.0212(9)	0.0219(9)	-0.0072(7)	0.0016(7)	-0.0071(7)
C15	0.0195(9)	0.0190(9)	0.0310(10)	-0.0072(8)	0.0000(8)	-0.0032(7)
C16	0.0276(10)	0.0174(9)	0.0290(10)	-0.0017(8)	-0.0010(8)	-0.0086(8)
C17	0.0220(9)	0.0221(9)	0.0226(9)	-0.0044(7)	0.0028(7)	-0.0112(8)
C18	0.0160(8)	0.0194(8)	0.0167(8)	-0.0067(7)	0.0012(6)	-0.0085(7)
C19	0.0172(8)	0.0185(8)	0.0160(8)	-0.0074(7)	0.0019(6)	-0.0090(7)
C20	0.0237(9)	0.0232(9)	0.0183(8)	-0.0077(7)	0.0055(7)	-0.0133(8)
C21	0.0216(9)	0.0294(10)	0.0246(9)	-0.0140(8)	0.0105(7)	-0.0126(8)
C22	0.0198(9)	0.0251(9)	0.0266(10)	-0.0131(8)	0.0069(7)	-0.0056(8)
C23	0.0188(9)	0.0198(9)	0.0203(9)	-0.0076(7)	0.0035(7)	-0.0064(7)
C26	0.0165(8)	0.0173(8)	0.0170(8)	-0.0052(7)	0.0030(6)	-0.0062(7)
C27	0.0223(9)	0.0190(9)	0.0203(9)	-0.0082(7)	0.0041(7)	-0.0084(7)

C28	0.0236(9)	0.0223(9)	0.0219(9)	-0.0098(7)	0.0009(7)	-0.0111(8)
C29	0.0174(8)	0.0211(9)	0.0202(9)	-0.0050(7)	-0.0007(7)	-0.0076(7)
C30	0.0163(8)	0.0168(8)	0.0178(8)	-0.0052(7)	0.0023(6)	-0.0063(7)
C31	0.0268(10)	0.0265(10)	0.0281(10)	-0.0136(8)	0.0002(8)	-0.0087(8)
C32	0.0350(12)	0.0292(11)	0.0446(14)	-0.0211(10)	-0.0036(10)	-0.0021(9)
C34	0.0152(8)	0.0194(8)	0.0174(8)	-0.0088(7)	0.0039(6)	-0.0075(7)
C35	0.0196(8)	0.0177(8)	0.0167(8)	-0.0082(7)	0.0066(7)	-0.0079(7)
C36	0.0199(9)	0.0170(8)	0.0172(8)	-0.0052(7)	0.0020(7)	-0.0042(7)
C37	0.0161(8)	0.0211(9)	0.0208(9)	-0.0089(7)	0.0009(7)	-0.0061(7)
C38	0.0152(8)	0.0189(8)	0.0211(9)	-0.0089(7)	0.0033(7)	-0.0081(7)
C39	0.0211(9)	0.0196(9)	0.0193(9)	-0.0077(7)	0.0048(7)	-0.0068(7)
C40	0.0298(10)	0.0252(10)	0.0268(10)	-0.0101(8)	0.0096(8)	-0.0149(8)
P1	0.0157(2)	0.0245(2)	0.0209(2)	-0.01087(19)	0.00422(17)	-0.00832(18)
F1	0.0199(6)	0.0420(7)	0.0526(8)	-0.0303(7)	0.0009(5)	-0.0113(5)
F2	0.0166(6)	0.0530(9)	0.0643(10)	-0.0304(8)	-0.0008(6)	-0.0103(6)
F3	0.0471(9)	0.0363(8)	0.0502(9)	0.0053(7)	0.0053(7)	-0.0150(7)
F4	0.0364(8)	0.0535(9)	0.0535(9)	-0.0411(8)	0.0135(7)	-0.0111(7)
F5	0.0426(8)	0.0355(7)	0.0403(8)	-0.0019(6)	0.0113(6)	-0.0151(6)
F6	0.0305(7)	0.0582(9)	0.0378(7)	-0.0358(7)	0.0084(6)	-0.0177(6)
P2	0.0173(2)	0.0287(3)	0.0217(2)	-0.0112(2)	0.00412(18)	-0.0118(2)
F7	0.1077(15)	0.0372(8)	0.0289(7)	-0.0171(6)	0.0305(8)	-0.0324(9)
F8	0.1136(16)	0.0909(14)	0.0410(9)	-0.0448(9)	0.0395(10)	-0.0807(13)
F9	0.0283(8)	0.0711(12)	0.0772(12)	0.0351(10)	-0.0178(8)	-0.0330(8)
F10	0.0298(6)	0.0302(6)	0.0310(7)	-0.0061(5)	0.0064(5)	-0.0149(5)
F11	0.0200(7)	0.0355(8)	0.0979(14)	-0.0065(8)	-0.0153(8)	-0.0079(6)
F12	0.0437(8)	0.0321(7)	0.0453(8)	-0.0163(6)	0.0065(6)	-0.0220(6)
C41	0.0405(12)	0.0272(10)	0.0311(11)	-0.0136(9)	-0.0054(9)	-0.0148(9)
C42	0.0438(15)	0.0596(18)	0.081(2)	-0.0377(17)	0.0062(15)	-0.0311(14)
C43	0.0648(17)	0.0346(12)	0.0320(12)	-0.0191(10)	0.0106(11)	-0.0217(12)
O1	0.0650(13)	0.0274(9)	0.0484(11)	-0.0094(8)	-0.0067(10)	-0.0088(9)
C44	0.030(2)	0.036(2)	0.024(2)	-0.0036(18)	0.0003(19)	-0.021(2)
C45	0.033(2)	0.056(3)	0.047(3)	-0.010(2)	-0.005(2)	-0.017(2)
C46	0.052(4)	0.040(3)	0.051(3)	-0.018(3)	0.016(3)	-0.030(3)
O2	0.0423(17)	0.0428(17)	0.0563(19)	-0.0175(15)	0.0020(14)	-0.0257(14)
C47	0.030(3)	0.024(2)	0.025(2)	0.003(2)	0.000(2)	-0.019(2)
C48	0.038(5)	0.044(5)	0.028(4)	0.003(3)	-0.011(3)	-0.014(3)
C49	0.062(7)	0.055(5)	0.042(4)	-0.022(4)	-0.008(5)	-0.020(5)

O3	0.0253(18)	0.0272(18)	0.0237(17)	-0.0018(14)	-0.0052(14)	-0.0112(15)
C50	0.0554(15)	0.0398(13)	0.1088(19)	-0.0341(13)	0.0174(14)	-0.0185(11)
C51	0.070(4)	0.033(2)	0.030(2)	-0.010(2)	0.008(2)	-0.023(3)
O4	0.0348(17)	0.0317(16)	0.0394(18)	-0.0152(14)	-0.0017(14)	-0.0102(14)

The form of the anisotropic displacement parameter is:
$\exp[-2\pi^2(a^{*2}U_{11}h^2+b^{*2}U_{22}k^2+c^{*2}U_{33}l^2+2b^*c^*U_{23}kl+2a^*c^*U_{13}hl+2a^*b^*U_{12}hk)]$

Table 5. Bond Distances in Compound 9718, Å

Ru1-N13	2.0593(15)	Ru1-N12	2.0616(15)	Ru1-N24	2.0660(15)
Ru1-N1	2.0752(15)	Ru1-N33	2.0981(15)	Ru1-N25	2.1084(15)
N1-C2	1.344(2)	N1-C6	1.359(2)	N12-C11	1.344(2)
N12-C7	1.361(2)	N13-C14	1.345(2)	N13-C18	1.363(2)
N24-C23	1.345(2)	N24-C19	1.361(2)	N25-C26	1.349(2)
N25-C30	1.355(2)	N33-C34	1.346(2)	N33-C38	1.354(2)
C2-C3	1.384(3)	C3-C4	1.384(3)	C4-C5	1.388(3)
C5-C6	1.391(3)	C6-C7	1.476(2)	C7-C8	1.391(3)
C8-C9	1.384(3)	C9-C10	1.381(3)	C10-C11	1.383(3)
C14-C15	1.383(3)	C15-C16	1.387(3)	C16-C17	1.379(3)
C17-C18	1.392(3)	C18-C19	1.471(2)	C19-C20	1.389(2)
C20-C21	1.385(3)	C21-C22	1.383(3)	C22-C23	1.387(3)
C26-C27	1.398(3)	C27-C28	1.395(3)	C27-C31	1.438(3)
C28-C29	1.387(3)	C29-C30	1.382(3)	C31-C32	1.182(3)
C34-C35	1.397(3)	C35-C36	1.391(3)	C35-C39	1.439(3)
C36-C37	1.385(3)	C37-C38	1.382(3)	C39-C40	1.187(3)
P1-F3	1.5831(15)	P1-F4	1.5904(14)	P1-F6	1.5957(13)
P1-F2	1.5998(13)	P1-F5	1.6022(15)	P1-F1	1.6065(13)
P2-F11	1.5716(14)	P2-F8	1.5825(15)	P2-F7	1.5908(15)
P2-F12	1.5969(14)	P2-F9	1.5983(15)	P2-F10	1.6069(13)
C41-O1	1.207(3)	C41-C43	1.488(3)	C41-C42	1.498(4)
C44-O2	1.198(5)	C44-C45	1.493(5)	C44-C46	1.505(6)
C47-O3	1.210(6)	C47-C49	1.499(8)	C47-C48	1.506(7)
C50-C51	1.375(5)	C50-O4	1.378(5)	C50-C50#1	1.557(7)

Symmetry transformations used to generate equivalent atoms:

#1 -x+2,-y+1,-z+1

Table 6. Bond Angles in Compound 9718, °

N13-Ru1-N12	83.16(6)	N13-Ru1-N24	78.72(6)	N12-Ru1-N24	96.51(6)

N13-Ru1-N1	97.01(6)	N12-Ru1-N1	78.85(6)	N24-Ru1-N1	174.11(6)
N13-Ru1-N33	172.47(6)	N12-Ru1-N33	91.25(6)	N24-Ru1-N33	96.98(6)
N1-Ru1-N33	86.80(6)	N13-Ru1-N25	93.45(6)	N12-Ru1-N25	174.24(6)
N24-Ru1-N25	87.35(6)	N1-Ru1-N25	97.01(6)	N33-Ru1-N25	92.52(6)
C2-N1-C6	118.07(15)	C2-N1-Ru1	126.69(12)	C6-N1-Ru1	115.21(12)
C11-N12-C7	118.21(15)	C11-N12-Ru1	125.42(12)	C7-N12-Ru1	115.64(12)
C14-N13-C18	118.03(16)	C14-N13-Ru1	125.12(12)	C18-N13-Ru1	115.43(12)
C23-N24-C19	117.91(15)	C23-N24-Ru1	126.64(12)	C19-N24-Ru1	115.45(12)
C26-N25-C30	117.13(16)	C26-N25-Ru1	123.01(12)	C30-N25-Ru1	119.83(12)
C34-N33-C38	117.45(15)	C34-N33-Ru1	122.42(12)	C38-N33-Ru1	120.04(12)
N1-C2-C3	123.06(17)	C4-C3-C2	118.80(18)	C3-C4-C5	119.01(17)
C4-C5-C6	119.27(18)	N1-C6-C5	121.77(17)	N1-C6-C7	115.09(15)
C5-C6-C7	123.13(17)	N12-C7-C8	121.53(17)	N12-C7-C6	114.78(16)
C8-C7-C6	123.62(17)	C9-C8-C7	119.34(18)	C10-C9-C8	119.14(18)
C9-C10-C11	118.90(18)	N12-C11-C10	122.87(17)	N13-C14-C15	122.82(17)
C14-C15-C16	119.09(18)	C17-C16-C15	118.84(18)	C16-C17-C18	119.57(18)
N13-C18-C17	121.62(17)	N13-C18-C19	114.59(15)	C17-C18-C19	123.73(16)
N24-C19-C20	121.77(17)	N24-C19-C18	114.89(15)	C20-C19-C18	123.33(17)
C21-C20-C19	119.77(18)	C22-C21-C20	118.46(18)	C21-C22-C23	119.33(18)
N24-C23-C22	122.75(18)	N25-C26-C27	123.02(17)	C28-C27-C26	118.88(17)
C28-C27-C31	121.67(18)	C26-C27-C31	119.45(18)	C29-C28-C27	118.27(17)
C30-C29-C28	119.51(17)	N25-C30-C29	123.18(17)	C32-C31-C27	178.6(3)
N33-C34-C35	122.84(16)	C36-C35-C34	118.76(17)	C36-C35-C39	121.86(17)
C34-C35-C39	119.38(17)	C37-C36-C35	118.70(17)	C38-C37-C36	119.19(17)
N33-C38-C37	123.04(17)	C40-C39-C35	178.6(2)	F3-P1-F4	90.54(10)
F3-P1-F6	90.86(9)	F4-P1-F6	178.54(9)	F3-P1-F2	91.14(9)
F4-P1-F2	90.12(8)	F6-P1-F2	90.26(8)	F3-P1-F5	178.94(9)
F4-P1-F5	89.28(9)	F6-P1-F5	89.31(8)	F2-P1-F5	89.91(9)
F3-P1-F1	89.78(9)	F4-P1-F1	90.64(8)	F6-P1-F1	88.96(7)
F2-P1-F1	178.80(8)	F5-P1-F1	89.17(8)	F11-P2-F8	91.46(12)
F11-P2-F7	91.14(11)	F8-P2-F7	177.11(12)	F11-P2-F12	91.15(8)
F8-P2-F12	91.85(9)	F7-P2-F12	89.37(8)	F11-P2-F9	178.69(10)
F8-P2-F9	88.82(12)	F7-P2-F9	88.54(12)	F12-P2-F9	90.12(9)
F11-P2-F10	88.97(8)	F8-P2-F10	89.08(8)	F7-P2-F10	89.70(8)
F12-P2-F10	179.06(8)	F9-P2-F10	89.75(8)	O1-C41-C43	122.0(2)
O1-C41-C42	122.0(3)	C43-C41-C42	116.0(2)	O2-C44-C45	122.1(5)
O2-C44-C46	120.9(5)	C45-C44-C46	117.0(4)	O3-C47-C49	121.9(6)

O3-C47-C48	120.9(6)	C49-C47-C48	117.2(6)	C51-C50-O4	120.3(4)
C51-C50-C50#1	114.0(5)	O4-C50-C50#1	125.6(4)		

Symmetry transformations used to generate equivalent atoms:

#1 -x+2,-y+1,-z+1

A3.2 $Ru(bpy)_2(pyridine)_2$

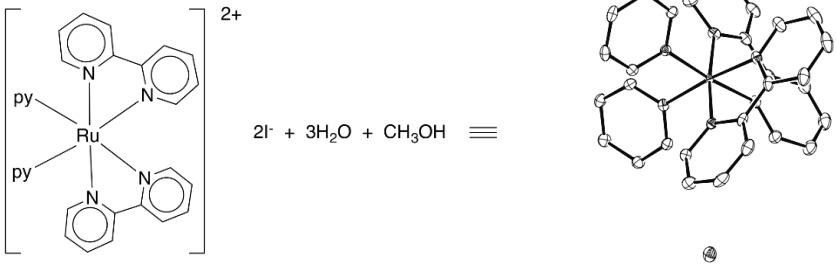

Compound 9719, $C_{31}H_{36}N_3O_2I_2Ru$, crystallizes in the triclinic space group P$\underline{1}$ with a=10.1385(10)Å, b=12.4515(12)Å, c=14.7603(15)Å, a=71.379(5)°, b=74.748(5)°, g=69.932(5)°, V=1633.7(3)Å3, Z=4, and d_{calc}=3.405 g/cm3 . X-ray intensity data were collected on a Bruker APEXII CCD area detector employing graphite-monochromated Mo-Ka radiation (l=0.71073 Å) at a temperature of 100(1)K. Preliminary indexing was performed from a series of thirty-six 0.5° rotation frames with exposures of 10 seconds. A total of 2640 frames were collected with a crystal to detector distance of 37.4 mm, rotation widths of 0.5° and exposures of 5 seconds:

scan type	2q	w	f	c	frames
f	-23.00	315.83	12.48	28.88	739
w	-25.50	330.51	47.91	-56.95	226
w	27.00	290.73	5.00	57.63	197
f	-23.00	328.34	44.17	79.39	739
f	24.50	7.41	12.48	28.88	739

Rotation frames were integrated using SAINT[8], producing a listing of unaveraged F2 and s(F2) values which were then passed to the SHELXTL[9] program package for further processing and structure solution. A total of 41691 reflections were measured over the ranges 1.80 £ q £ 27.60°, -13 £ h £ 13, -16 £ k £ 16, -19 £ l £ 19 yielding 7497 unique reflections (Rint = 0.0251). The intensity data were corrected for Lorentz and polarization effects and for absorption using SADABS[10] (minimum and maximum transmission 0.6699, 0.7456).

The structure was solved by direct methods (SHELXS-97[11]). Refinement was by full-matrix least squares based on F2 using SHELXL-97.[12] All reflections were used during refinement. The weighting scheme used was w=1/[s2(F_o2)+ (0.0141P)2 + 6.1932P] where P = (F_o 2 + 2F_c2)/3. Non-hydrogen atoms were refined anisotropically and hydrogen atoms were refined using a riding model. Refinement converged to R1=0.0306 and wR2=0.0689 for 6969 observed reflections for which F > 4s(F) and R1=0.0340 and wR2=0.0700 and GOF =1.223 for all 7497 unique, non-zero reflections and 398 variables.[13] The maximum D/s in the final cycle of least squares was 0.001 and the two most prominent peaks in the final difference Fourier were +1.800 and -1.037 e/Å3.

---

[8]Bruker (2009) SAINT. Bruker AXS Inc., Madison, Wisconsin, USA.

[9]Bruker (2009) SHELXTL. Bruker AXS Inc., Madison, Wisconsin, USA.

[10]Sheldrick, G.M. (2007) SADABS. University of Gottingen, Germany.

[11]Sheldrick, G.M. (2008) Acta Cryst. A64,112-122.

[12]Sheldrick, G.M. (2008) Acta Cryst. A64,112-122.

[13]$R1 = \Sigma||F_o| - |F_c|| / \Sigma |F_o|$

$wR2 = [\Sigma w(F_o^2 - F_c^2)^2/\Sigma w(F_o^2)^2]^{½}$

$GOF = [\Sigma w(F_o^2 - F_c^2)^2/(n - p)]^{½}$

where n = the number of reflections and p = the number of parameters refined.

Table 1. lists cell information, data collection parameters, and refinement data. Final positional and equivalent isotropic thermal parameters are given in Tables 2. and 3. Anisotropic thermal parameters are in Table 4. Tables 5. and 6. list bond distances and bond angles. Figure 1. is an ORTEP[14] representation of the molecule with 50% probability thermal ellipsoids displayed.

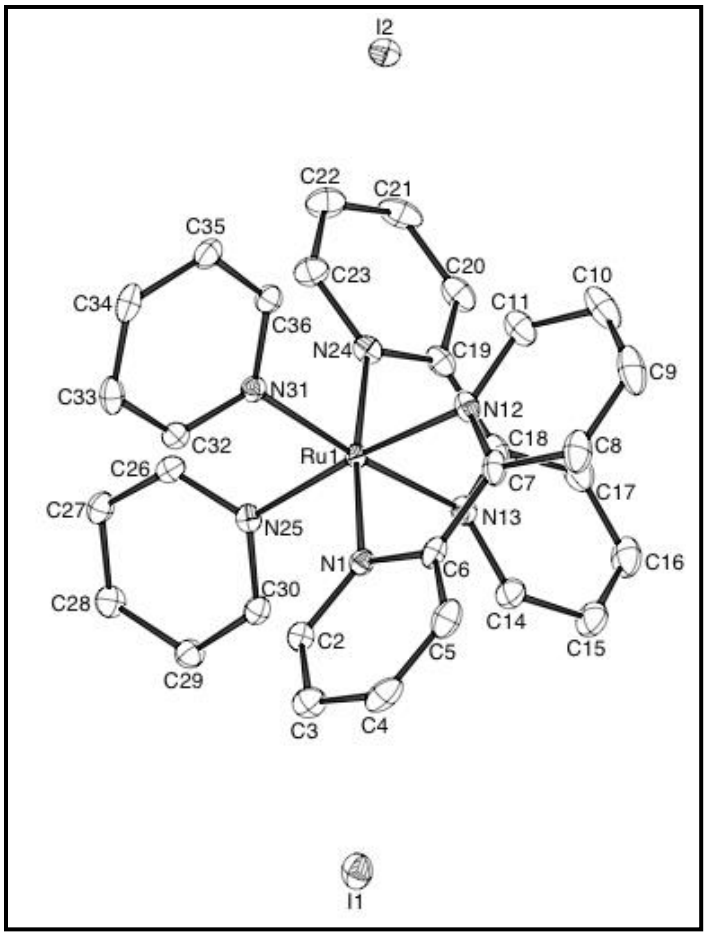

Figure 1. ORTEP drawing of the title compound with 50% probability thermal ellipsoids.

[14]"ORTEP-II: A Fortran Thermal Ellipsoid Plot Program for Crystal Structure Illustrations". C.K. Johnson (1976) ORNL-5138.

Table 1. Summary of Structure Determination of Compound 9719

Empirical formula	$C_{31}H_{36}N_3O_2I_2Ru$
Formula weight	837.50
Temperature	100(1) K
Wavelength	0.71073 Å
Crystal system	triclinic
Space group	P$\underline{1}$
Cell constants:	
a	10.1385(10) Å
b	12.4515(12) Å
c	14.7603(15) Å
a	71.379(5)°
b	74.748(5)°
g	69.932(5)°
Volume	1633.7(3) Å3
Z	4
Density (calculated)	3.405 Mg/m3
Absorption coefficient	4.799 mm-1
F(000)	1636
Crystal size	0.18 x 0.12 x 0.03 mm3
Theta range for data collection	1.80 to 27.60°
Index ranges	-13 £ h £ 13, -16 £ k £ 16, -19 £ l £ 19
Reflections collected	41691
Independent reflections	7497 [R(int) = 0.0251]
Completeness to theta = 27.60°	98.9 %
Absorption correction	Semi-empirical from equivalents
Max. and min. transmission	0.7456 and 0.6699
Refinement method	Full-matrix least-squares on F2
Data / restraints / parameters	7497 / 0 / 398
Goodness-of-fit on F2	1.223
Final R indices [I>2sigma(I)]	R1 = 0.0306, wR2 = 0.0689
R indices (all data)	R1 = 0.0340, wR2 = 0.0700
Largest diff. peak and hole	1.800 and -1.037 e.Å-3

Table 2. Refined Positional Parameters for Compound 9719

Atom	x	y	z	U_{eq}, Å^2
I1	0.96783(3)	0.96809(2)	0.219688(18)	0.02175(6)
I2	0.18530(3)	0.46281(2)	0.201907(18)	0.02001(6)
Ru1	0.58859(3)	0.68965(2)	0.215106(19)	0.01053(6)
N1	0.6796(3)	0.6493(2)	0.3361(2)	0.0127(5)
N12	0.4142(3)	0.6814(2)	0.3243(2)	0.0146(6)
N13	0.5126(3)	0.8696(2)	0.2006(2)	0.0143(6)
N24	0.4772(3)	0.7428(3)	0.1020(2)	0.0147(6)
N25	0.7712(3)	0.7055(2)	0.1117(2)	0.0130(6)
N31	0.6475(3)	0.5068(2)	0.2301(2)	0.0128(6)
C2	0.8193(4)	0.6239(3)	0.3391(3)	0.0155(7)
C3	0.8698(4)	0.5948(3)	0.4245(3)	0.0197(7)
C4	0.7757(5)	0.5934(3)	0.5110(3)	0.0232(8)
C5	0.6331(4)	0.6182(3)	0.5092(3)	0.0221(8)
C6	0.5866(4)	0.6444(3)	0.4219(3)	0.0153(7)
C7	0.4381(4)	0.6672(3)	0.4138(3)	0.0170(7)
C8	0.3264(4)	0.6769(4)	0.4933(3)	0.0260(9)
C9	0.1885(4)	0.7000(4)	0.4797(3)	0.0304(10)
C10	0.1652(4)	0.7132(3)	0.3885(3)	0.0289(10)
C11	0.2795(4)	0.7030(3)	0.3127(3)	0.0207(8)
C14	0.5339(4)	0.9282(3)	0.2550(3)	0.0199(7)
C15	0.4626(4)	1.0457(3)	0.2519(3)	0.0251(8)
C16	0.3651(4)	1.1067(3)	0.1893(3)	0.0266(9)
C17	0.3428(4)	1.0480(3)	0.1321(3)	0.0234(8)
C18	0.4180(4)	0.9296(3)	0.1387(3)	0.0165(7)
C19	0.4023(4)	0.8594(3)	0.0804(3)	0.0161(7)
C20	0.3198(4)	0.9061(3)	0.0081(3)	0.0209(8)
C21	0.3139(4)	0.8351(4)	-0.0459(3)	0.0247(8)
C22	0.3915(4)	0.7175(4)	-0.0244(3)	0.0234(8)
C23	0.4711(4)	0.6746(3)	0.0491(3)	0.0195(7)
C26	0.8174(4)	0.6494(3)	0.0399(3)	0.0154(7)
C27	0.9340(4)	0.6620(3)	-0.0309(3)	0.0172(7)
C28	1.0085(4)	0.7359(3)	-0.0294(3)	0.0180(7)
C29	0.9637(4)	0.7939(3)	0.0438(3)	0.0173(7)
C30	0.8453(4)	0.7773(3)	0.1124(2)	0.0144(7)
C32	0.7812(4)	0.4379(3)	0.2375(2)	0.0140(7)

C33	0.8187(4)	0.3156(3)	0.2570(3)	0.0183(7)
C34	0.7145(4)	0.2606(3)	0.2697(3)	0.0199(8)
C35	0.5769(4)	0.3313(3)	0.2598(3)	0.0183(7)
C36	0.5474(4)	0.4529(3)	0.2409(2)	0.0152(7)
O1	0.7110(5)	0.8941(3)	0.4317(3)	0.0500(10)
O2	0.8416(5)	0.7886(3)	0.5958(3)	0.0523(10)
O3	0.4016(7)	0.9052(6)	0.5048(5)	0.0379(15)
C37	1.1538(7)	-0.0153(5)	0.4068(5)	0.0778(17)
C38	1.0139(8)	0.0750(6)	0.4045(5)	0.089(2)
O37	1.1538(7)	-0.0153(5)	0.4068(5)	0.0778(17)
O38	1.0139(8)	0.0750(6)	0.4045(5)	0.089(2)
$U_{eq}=1/3[U_{11}(aa^*)^2+U_{22}(bb^*)^2+U_{33}(cc^*)^2+2U_{12}aa^*bb^*\cos g+2U_{13}aa^*cc^*\cos b+2U_{23}bb^*cc^*\cos a]$				

Table 3. Positional Parameters for Hydrogens in Compound 9719

Atom	x	y	z	U_{iso}, Å^2
H2	0.8841	0.6261	0.2812	0.021
H3	0.9671	0.5762	0.4236	0.026
H4	0.8076	0.5763	0.5690	0.031
H5	0.5674	0.6173	0.5666	0.029
H8	0.3448	0.6678	0.5542	0.035
H9	0.1128	0.7065	0.5313	0.040
H10	0.0733	0.7290	0.3779	0.038
H11	0.2625	0.7113	0.2516	0.028
H14	0.5996	0.8880	0.2968	0.026
H15	0.4798	1.0832	0.2911	0.033
H16	0.3157	1.1856	0.1860	0.035
H17	0.2781	1.0872	0.0895	0.031
H20	0.2680	0.9855	-0.0045	0.028
H21	0.2594	0.8658	-0.0949	0.033
H22	0.3902	0.6675	-0.0592	0.031
H23	0.5227	0.5952	0.0628	0.026
H26	0.7679	0.5997	0.0383	0.021
H27	0.9624	0.6215	-0.0791	0.023
H28	1.0874	0.7462	-0.0768	0.024
H29	1.0125	0.8434	0.0468	0.023
H30	0.8152	0.8172	0.1611	0.019
H32	0.8518	0.4737	0.2292	0.019
H33	0.9125	0.2710	0.2614	0.024

H34	0.7364	0.1787	0.2844	0.026
H35	0.5052	0.2976	0.2658	0.024
H36	0.4545	0.4994	0.2354	0.020

Table 4. Refined Thermal Parameters (U's) for Compound 9719

Atom	U_{11}	U_{22}	U_{33}	U_{23}	U_{13}	U_{12}
I1	0.02252(13)	0.01788(12)	0.02144(13)	-0.00419(9)	-0.00736(10)	0.00040(9)
I2	0.01750(12)	0.02194(12)	0.02311(13)	-0.00763(9)	-0.00623(9)	-0.00485(9)
Ru1	0.01011(12)	0.01021(12)	0.01038(13)	-0.00203(9)	-0.00210(10)	-0.00208(9)
N1	0.0145(14)	0.0120(13)	0.0115(13)	-0.0032(10)	-0.0029(11)	-0.0030(11)
N12	0.0125(14)	0.0104(13)	0.0168(15)	-0.0003(11)	-0.0011(11)	-0.0021(11)
N13	0.0140(14)	0.0134(13)	0.0133(14)	-0.0021(11)	0.0005(11)	-0.0045(11)
N24	0.0145(14)	0.0152(14)	0.0128(14)	-0.0001(11)	-0.0036(11)	-0.0046(11)
N25	0.0138(14)	0.0121(13)	0.0108(13)	-0.0006(10)	-0.0026(11)	-0.0023(11)
N31	0.0141(14)	0.0139(13)	0.0104(13)	-0.0035(11)	-0.0023(11)	-0.0036(11)
C2	0.0160(17)	0.0145(16)	0.0154(17)	-0.0044(13)	-0.0021(13)	-0.0035(13)
C3	0.0230(19)	0.0194(17)	0.0172(18)	-0.0029(14)	-0.0083(15)	-0.0046(15)
C4	0.039(2)	0.0177(18)	0.0157(18)	-0.0041(14)	-0.0145(16)	-0.0040(16)
C5	0.031(2)	0.0181(18)	0.0142(17)	-0.0049(14)	-0.0010(15)	-0.0046(15)
C6	0.0203(18)	0.0109(15)	0.0135(16)	-0.0042(12)	0.0001(13)	-0.0041(13)
C7	0.0170(17)	0.0123(16)	0.0165(17)	-0.0032(13)	0.0042(14)	-0.0034(13)
C8	0.026(2)	0.025(2)	0.021(2)	-0.0081(16)	0.0066(16)	-0.0055(16)
C9	0.021(2)	0.025(2)	0.030(2)	-0.0023(17)	0.0112(17)	-0.0034(16)
C10	0.0144(18)	0.0187(18)	0.040(2)	0.0060(17)	-0.0011(17)	-0.0038(15)
C11	0.0161(17)	0.0137(16)	0.026(2)	0.0022(14)	-0.0055(15)	-0.0020(14)
C14	0.0202(18)	0.0170(17)	0.0240(19)	-0.0077(14)	-0.0014(15)	-0.0067(14)
C15	0.027(2)	0.0169(18)	0.033(2)	-0.0107(16)	0.0000(17)	-0.0078(16)
C16	0.025(2)	0.0138(17)	0.036(2)	-0.0068(16)	0.0025(17)	-0.0040(15)
C17	0.0183(18)	0.0157(17)	0.029(2)	-0.0004(15)	-0.0011(16)	-0.0025(14)
C18	0.0108(16)	0.0161(16)	0.0174(17)	-0.0006(13)	0.0020(13)	-0.0043(13)
C19	0.0123(16)	0.0172(17)	0.0148(17)	0.0010(13)	-0.0011(13)	-0.0048(13)
C20	0.0155(17)	0.0197(18)	0.0212(19)	0.0032(14)	-0.0065(15)	-0.0027(14)
C21	0.0217(19)	0.033(2)	0.0197(19)	0.0049(16)	-0.0122(15)	-0.0121(17)
C22	0.029(2)	0.028(2)	0.0170(18)	-0.0032(15)	-0.0088(16)	-0.0118(17)
C23	0.0236(19)	0.0196(17)	0.0169(18)	-0.0028(14)	-0.0077(15)	-0.0067(15)
C26	0.0187(17)	0.0138(16)	0.0152(17)	-0.0037(13)	-0.0048(14)	-0.0049(13)
C27	0.0209(18)	0.0175(17)	0.0125(16)	-0.0054(13)	-0.0023(14)	-0.0034(14)

C28	0.0190(18)	0.0217(18)	0.0122(16)	-0.0033(14)	0.0005(14)	-0.0078(14)
C29	0.0179(17)	0.0187(17)	0.0165(17)	-0.0048(14)	-0.0011(14)	-0.0074(14)
C30	0.0170(17)	0.0134(15)	0.0121(16)	-0.0033(12)	-0.0035(13)	-0.0027(13)
C32	0.0151(16)	0.0203(17)	0.0071(15)	-0.0040(13)	-0.0024(12)	-0.0048(13)
C33	0.0180(17)	0.0185(17)	0.0116(16)	-0.0034(13)	-0.0009(13)	0.0017(14)
C34	0.027(2)	0.0129(16)	0.0152(17)	-0.0052(13)	0.0011(15)	-0.0015(14)
C35	0.0220(18)	0.0187(17)	0.0163(17)	-0.0085(14)	0.0004(14)	-0.0074(14)
C36	0.0169(17)	0.0157(16)	0.0133(16)	-0.0042(13)	-0.0025(13)	-0.0043(13)
O1	0.073(3)	0.046(2)	0.034(2)	-0.0115(16)	0.0030(18)	-0.028(2)
O2	0.074(3)	0.0309(18)	0.040(2)	-0.0072(16)	0.0088(19)	-0.0158(18)
O3	0.031(3)	0.034(3)	0.041(4)	-0.009(3)	0.010(3)	-0.013(3)
C37	0.081(4)	0.067(4)	0.085(4)	-0.010(3)	-0.019(4)	-0.025(3)
C38	0.109(6)	0.089(5)	0.080(5)	-0.019(4)	-0.022(4)	-0.041(4)
O37	0.081(4)	0.067(4)	0.085(4)	-0.010(3)	-0.019(4)	-0.025(3)
O38	0.109(6)	0.089(5)	0.080(5)	-0.019(4)	-0.022(4)	-0.041(4)

The form of the anisotropic displacement parameter is:
$\exp[-2p^2(a^{*2}U_{11}h^2+b^{*2}U_{22}k^2+c^{*2}U_{33}l^2+2b^*c^*U_{23}kl+2a^*c^*U_{13}hl+2a^*b^*U_{12}hk)]$

Table 5. Bond Distances in Compound 9719, Å

Ru1-N12	2.062(3)	Ru1-N13	2.063(3)	Ru1-N1	2.066(3)
Ru1-N24	2.067(3)	Ru1-N25	2.090(3)	Ru1-N31	2.099(3)
N1-C2	1.350(4)	N1-C6	1.364(4)	N12-C11	1.344(5)
N12-C7	1.351(5)	N13-C14	1.342(5)	N13-C18	1.359(5)
N24-C23	1.349(5)	N24-C19	1.364(4)	N25-C26	1.347(4)
N25-C30	1.355(4)	N31-C32	1.344(4)	N31-C36	1.348(4)
C2-C3	1.379(5)	C3-C4	1.377(6)	C4-C5	1.377(6)
C5-C6	1.390(5)	C6-C7	1.463(5)	C7-C8	1.404(5)
C8-C9	1.383(6)	C9-C10	1.376(7)	C10-C11	1.386(6)
C14-C15	1.383(5)	C15-C16	1.387(6)	C16-C17	1.380(6)
C17-C18	1.393(5)	C18-C19	1.476(5)	C19-C20	1.385(5)
C20-C21	1.389(6)	C21-C22	1.381(6)	C22-C23	1.382(5)
C26-C27	1.374(5)	C27-C28	1.384(5)	C28-C29	1.383(5)
C29-C30	1.380(5)	C32-C33	1.388(5)	C33-C34	1.389(5)
C34-C35	1.388(5)	C35-C36	1.387(5)	C37-C38	1.478(9)

Table 6. Bond Angles in Compound 9719, °

N12-Ru1-N13	84.78(11)	N12-Ru1-N1	78.99(12)	N13-Ru1-N1	96.47(11)

N12-Ru1-N24	95.80(12)	N13-Ru1-N24	78.76(12)	N1-Ru1-N24	173.31(11)
N12-Ru1-N25	174.71(12)	N13-Ru1-N25	92.49(11)	N1-Ru1-N25	96.86(11)
N24-Ru1-N25	88.09(11)	N12-Ru1-N31	91.75(11)	N13-Ru1-N31	174.93(11)
N1-Ru1-N31	86.47(11)	N24-Ru1-N31	97.96(11)	N25-Ru1-N31	91.26(11)
C2-N1-C6	117.6(3)	C2-N1-Ru1	127.3(2)	C6-N1-Ru1	115.0(2)
C11-N12-C7	118.3(3)	C11-N12-Ru1	126.3(3)	C7-N12-Ru1	114.9(2)
C14-N13-C18	118.0(3)	C14-N13-Ru1	125.8(2)	C18-N13-Ru1	115.6(2)
C23-N24-C19	117.9(3)	C23-N24-Ru1	126.8(2)	C19-N24-Ru1	115.3(2)
C26-N25-C30	117.1(3)	C26-N25-Ru1	122.3(2)	C30-N25-Ru1	120.6(2)
C32-N31-C36	117.5(3)	C32-N31-Ru1	122.3(2)	C36-N31-Ru1	120.0(2)
N1-C2-C3	122.8(3)	C2-C3-C4	119.8(4)	C3-C4-C5	118.1(3)
C4-C5-C6	120.4(4)	N1-C6-C5	121.2(3)	N1-C6-C7	114.8(3)
C5-C6-C7	124.0(3)	N12-C7-C8	121.8(4)	N12-C7-C6	115.9(3)
C8-C7-C6	122.3(4)	C9-C8-C7	119.0(4)	C10-C9-C8	118.9(4)
C9-C10-C11	119.7(4)	N12-C11-C10	122.4(4)	N13-C14-C15	123.0(4)
C14-C15-C16	118.9(4)	C17-C16-C15	118.8(4)	C16-C17-C18	119.4(4)
N13-C18-C17	121.7(4)	N13-C18-C19	114.7(3)	C17-C18-C19	123.6(3)
N24-C19-C20	121.3(3)	N24-C19-C18	115.0(3)	C20-C19-C18	123.7(3)
C19-C20-C21	120.4(4)	C22-C21-C20	118.0(3)	C21-C22-C23	119.6(4)
N24-C23-C22	122.9(4)	N25-C26-C27	123.3(3)	C26-C27-C28	119.0(3)
C29-C28-C27	118.9(3)	C30-C29-C28	119.0(3)	N25-C30-C29	122.8(3)
N31-C32-C33	122.9(3)	C32-C33-C34	119.3(3)	C33-C34-C35	118.1(3)
C36-C35-C34	119.3(3)	N31-C36-C35	122.9(3)		

A3.3 $Ru(bpy)_2(3\text{-pyridinaldehyde})_2$ (RuAldehyde)

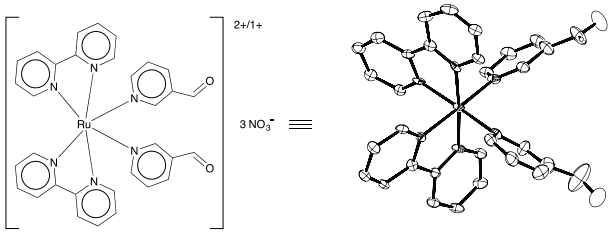

Compound 9723, $C_{64}H_{52}N_{15}O_{13}Ru_2$, crystallizes in the triclinic space group $P\bar{1}$ with a=9.9943(8)Å, b=13.2770(11)Å, c=14.9233(12)Å, α=69.352(2)°, β=89.598(2)°, γ=88.444(2)°, V=1852.3(3)$Å^3$, Z=1, and d_{calc}=1.292 g/cm_3 . X-ray intensity data were collected on a Bruker D8QUEST [1] CMOS area detector employing graphite-monochromated Mo-Kα radiation (λ=0.71073Å) at a temperature of 100K. Preliminary indexing was performed from a series of twenty-four 0.5° rotation frames with exposures of 10 seconds. A total of 2180 frames were collected with a crystal to detector distance of 50.0 mm, rotation widths of 0.5° and exposures of 30 seconds:

scan type	2θ	ω	φ	χ	Frames
ω	11.01	189.76	288.00	54.72	365
ω	11.01	189.76	144.00	54.72	365
ω	11.01	189.76	0.00	54.72	365
ω	11.01	189.76	72.00	54.72	365
ϕ	11.01	14.01	0.00	54.72	720

The crystal grew as a non-merohedral twin; the program CELL_NOW [2] was used to index the diffraction images and to determine the twinning mechanism. The crystal was twinned by a rotation of 180° about the 001 reciprocal direction. Rotation frames were

integrated using SAINT [3], producing a listing of unaveraged F^2 and $\sigma(F^2)$ values. A total of 57336 reflections were measured over the ranges $5.834 \leq 2\theta \leq 55.13°$, $-12 \leq h \leq 12$, $-15 \leq k \leq 17$, $0 \leq l \leq 19$ yielding 8497 unique reflections ($R_{int} = 0.0785$). The intensity data were corrected for Lorentz and polarization effects and for absorption using TWINABS [4] (minimum and maximum transmission 0.5692, 0.7456). The structure was solved by direct methods - SHELXT [5]. The aldehyde group (H38-C38-O2) was disordered by a rotation of approximately 180° about the C34-C38 bond. The relative occupancies of the two conformations were 0.55/0.45. There was a region of disordered solvent for which a reliable disorder model could not be devised; the X-ray data were corrected for the presence of disordered solvent using SQUEEZE [6]. Refinement was by full-matrix least squares based on F^2 using SHELXL-2014 [7]. All reflections were used during refinement. The weighting scheme used was $w=1/[\sigma^2(F_o^2)+ (0.0612P)^2 + 1.0285P]$ where $P = (F_o^2 + 2F_c^2)/3$. Non-hydrogen atoms were refined anisotropically and hydrogen atoms were refined using a riding model. Refinement converged to R1=0.0777 and wR2=0.1798 for 6462 observed reflections for which $F > 4\sigma(F)$ and R1=0.1097 and wR2=0.1978 and GOF =1.072 for all 8497 unique, non-zero reflections and 443 variables. The maximum Δ/σ in the final cycle of least squares was 0.008 and the two most prominent peaks in the final difference Fourier were +1.56 and -1.39 e/Å^3. The twinning parameter refined to a value of 0.347(3).

Table 1. lists cell information, data collection parameters, and refinement data. Final positional and equivalent isotropic thermal parameters are given in Tables 2. and 3. Anisotropic thermal parameters are in Table 4. Tables 5. and 6. list bond distances and

bond angles. Figure 1. is an ORTEP representation of the molecule with 30% probability thermal ellipsoids displayed.

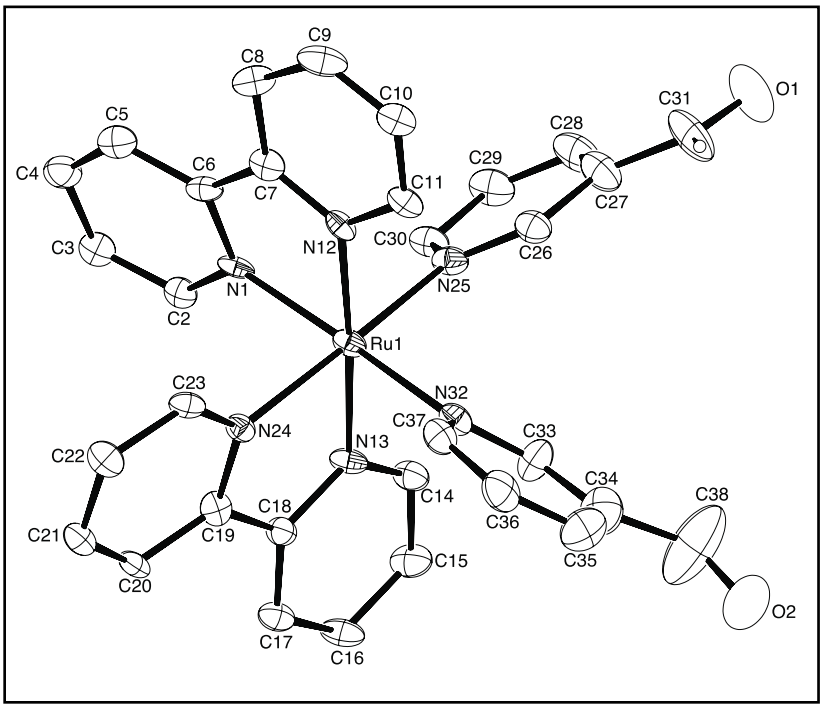

Figure 1. ORTEP drawing of the title compound with 30% thermal ellipsoids.

Table 1. Summary of Structure Determination of Compound 9723

Empirical formula	$C_{64}H_{52}N_{15}O_{13}Ru_2$
Formula weight	1441.34
Temperature/K	100
Crystal system	triclinic
Space group	$P\bar{1}$
a	9.9943(8)Å
b	13.2770(11)Å
c	14.9233(12)Å
α	69.352(2)°
β	89.598(2)°
γ	88.444(2)°
Volume	1852.3(3)Å^3
Z	1
d_{calc}	1.292 g/cm^3
μ	0.473 mm^{-1}
F(000)	733.0
Crystal size, mm	0.28 × 0.23 × 0.05
2θ range for data collection	5.834 - 55.13°
Index ranges	-12 ≤ h ≤ 12, -15 ≤ k ≤ 17, 0 ≤ l ≤ 19
Reflections collected	57336
Independent reflections	8497[R(int) = 0.0785]
Data/restraints/parameters	8497/32/443
Goodness-of-fit on F^2	1.072
Final R indexes [I>=2σ (I)]	R_1 = 0.0777, wR_2 = 0.1798
Final R indexes [all data]	R_1 = 0.1097, wR_2 = 0.1978
Largest diff. peak/hole	1.56/-1.39 eÅ^{-3}

Table 2 . Refined Positional Parameters for Compound 9723

Atom	*x*	*y*	*z*	U(eq)
Ru1	0.25119(8)	0.81564(6)	0.33177(4)	0.02857(16)
N1	0.1569(6)	0.8526(5)	0.4387(5)	0.0267(16)
C2	0.0553(8)	0.7997(7)	0.4950(6)	0.031(2)
C3	0.0140(9)	0.8157(7)	0.5744(7)	0.037(2)
C4	0.0783(10)	0.8912(7)	0.6034(8)	0.043(2)
C5	0.1821(9)	0.9488(7)	0.5477(8)	0.039(2)
C6	0.2206(9)	0.9299(6)	0.4649(7)	0.032(2)
C7	0.3274(8)	0.9843(7)	0.4017(7)	0.032(2)
C8	0.3891(10)	1.0736(8)	0.4093(8)	0.043(2)
C9	0.4868(9)	1.1242(7)	0.3408(9)	0.047(3)
C10	0.5146(9)	1.0880(7)	0.2717(7)	0.038(2)
C11	0.4522(8)	0.9986(6)	0.2682(7)	0.0311(19)
N12	0.3604(6)	0.9459(5)	0.3330(5)	0.0277(15)
N13	0.1432(6)	0.6820(5)	0.3399(6)	0.0297(16)
C14	0.0468(9)	0.6791(7)	0.2800(7)	0.038(2)
C15	-0.0167(10)	0.5842(8)	0.2851(8)	0.044(2)
C16	0.0247(10)	0.4886(7)	0.3570(8)	0.042(2)
C17	0.1213(9)	0.4913(7)	0.4206(7)	0.034(2)
C18	0.1814(9)	0.5881(6)	0.4104(6)	0.0302(19)
C19	0.2892(8)	0.5992(7)	0.4729(6)	0.0306(19)
C20	0.3308(9)	0.5165(6)	0.5565(6)	0.0302(19)
C21	0.4331(9)	0.5331(7)	0.6083(7)	0.034(2)
C22	0.4948(9)	0.6313(7)	0.5778(7)	0.038(2)
C23	0.4476(8)	0.7117(6)	0.4946(7)	0.0291(19)
N24	0.3472(7)	0.6971(5)	0.4439(5)	0.0264(15)
N25	0.1273(7)	0.9265(5)	0.2282(6)	0.0332(17)
C26	0.1713(9)	0.9929(7)	0.1444(6)	0.038(2)
C27	0.0862(11)	1.0675(8)	0.0745(8)	0.054(3)
C28	-0.0471(11)	1.0695(8)	0.0974(8)	0.060(3)
C29	-0.0944(10)	1.0015(8)	0.1831(8)	0.049(3)

C30	-0.0045(9)	0.9303(7)	0.2479(7)	0.037(2)
C31	0.1523(13)	1.1399(9)	-0.0163(9)	0.076(4)
O1	0.0812(10)	1.1990(7)	-0.0779(6)	0.090(3)
N32	0.3738(7)	0.7783(6)	0.2321(5)	0.0342(17)
C33	0.3279(10)	0.7573(8)	0.1562(7)	0.048(2)
C34	0.4126(12)	0.7311(10)	0.0942(9)	0.065(3)
C35	0.5491(11)	0.7158(9)	0.1131(9)	0.059(3)
C36	0.5978(11)	0.7335(8)	0.1914(7)	0.051(3)
C37	0.5077(9)	0.7648(7)	0.2481(7)	0.040(2)
C38	0.3596(18)	0.721(2)	0.0055(15)	0.140(8)
O2	0.428(2)	0.6823(17)	-0.0424(14)	0.086(5)
O2'	0.2427(17)	0.7113(15)	-0.0035(12)	0.091(5)
N39	0.7501(8)	0.7849(7)	0.4181(4)	0.0344(12)
O3	0.7544(8)	0.7543(6)	0.5075(4)	0.0418(12)
O4	0.6933(6)	0.8734(5)	0.3711(5)	0.0456(18)
O5	0.8026(6)	0.7280(5)	0.3751(5)	0.0389(16)
O6	0.6551(15)	1.0312(16)	0.0455(14)	0.088(6)
O7	0.5416(12)	0.9698(10)	-0.0510(7)	0.113(4)
N40	0.5532(19)	1.0141(16)	0.0104(13)	0.070(5)

Table 3 . Positional Parameters for Hydrogens in Compound 9723

Atom	*x*	*y*	*z*	U(eq)
H2	0.0106	0.7477	0.4768	0.041
H3	-0.0581	0.7762	0.6107	0.049
H4	0.0516	0.9031	0.6602	0.057
H5	0.2266	1.0009	0.566	0.052
H8	0.366	1.0997	0.4592	0.057
H9	0.5323	1.1843	0.3449	0.063
H10	0.5778	1.1235	0.224	0.05
H11	0.4746	0.9729	0.2179	0.041

H14	0.0195	0.7446	0.2313	0.05
H15	-0.0855	0.585	0.2412	0.059
H16	-0.0137	0.4223	0.3616	0.056
H17	0.1473	0.4273	0.4715	0.045
H20	0.2878	0.4493	0.5768	0.04
H21	0.4622	0.4775	0.6653	0.046
H22	0.5677	0.6439	0.6127	0.05
H23	0.4894	0.7795	0.4737	0.039
H26	0.264	0.9904	0.1305	0.051
H28	-0.1071	1.1186	0.0531	0.079
H29	-0.1868	1.0027	0.1984	0.065
H30	-0.0371	0.8831	0.3074	0.049
H31	0.2467	1.1383	-0.0241	0.101
H33	0.2342	0.7606	0.1451	0.064
H35	0.6071	0.6936	0.0725	0.078
H36	0.6905	0.7245	0.2065	0.068
H37	0.5422	0.7779	0.302	0.053
H38	0.2707	0.7459	-0.0144	0.186
H38'	0.4191	0.7231	-0.0449	0.186

Table 4 . Refined Thermal Parameters (U's) for Compound 9723

Atom	U_{11}	U_{22}	U_{33}	U_{23}	U_{13}	U_{12}
Ru1	0.0224(2)	0.0235(3)	0.0362(3)	-0.0061(3)	-0.0061(4)	0.00096(18)
N1	0.017(3)	0.014(3)	0.044(4)	-0.004(3)	-0.005(3)	0.003(2)
C2	0.025(4)	0.030(4)	0.036(5)	-0.009(4)	-0.007(4)	0.003(3)
C3	0.027(5)	0.037(5)	0.044(6)	-0.012(4)	-0.002(4)	0.002(4)
C4	0.044(6)	0.036(5)	0.048(6)	-0.014(4)	-0.001(5)	0.007(4)
C5	0.029(4)	0.038(5)	0.052(6)	-0.018(4)	-0.011(4)	0.005(4)
C6	0.028(4)	0.022(4)	0.046(5)	-0.013(4)	-0.009(4)	0.004(3)
C7	0.020(3)	0.033(3)	0.042(4)	-0.010(3)	-0.011(3)	0.003(3)
C8	0.036(5)	0.037(5)	0.063(7)	-0.027(5)	0.002(5)	-0.001(4)
C9	0.028(4)	0.028(4)	0.082(8)	-0.014(5)	0.003(5)	-0.003(3)
C10	0.028(4)	0.032(4)	0.049(5)	-0.009(4)	0.001(4)	-0.001(3)
C11	0.018(4)	0.027(4)	0.041(5)	-0.003(3)	-0.001(3)	0.005(3)
N12	0.022(3)	0.024(3)	0.029(3)	0.001(3)	-0.003(3)	0.001(3)
N13	0.018(3)	0.021(3)	0.048(4)	-0.010(3)	-0.004(3)	0.004(2)
C14	0.039(5)	0.029(4)	0.043(5)	-0.010(4)	-0.006(4)	0.003(4)
C15	0.039(5)	0.040(5)	0.059(6)	-0.024(5)	-0.016(5)	0.000(4)
C16	0.037(5)	0.023(4)	0.064(6)	-0.012(4)	-0.002(4)	-0.007(3)
C17	0.029(4)	0.026(4)	0.044(5)	-0.009(4)	0.004(4)	0.001(3)
C18	0.032(4)	0.026(4)	0.031(4)	-0.008(3)	0.003(3)	0.001(3)
C19	0.018(4)	0.039(5)	0.033(5)	-0.010(4)	0.004(3)	0.000(3)
C20	0.034(4)	0.018(4)	0.031(4)	0.000(3)	0.003(3)	0.000(3)
C21	0.032(5)	0.029(4)	0.034(5)	-0.002(4)	0.000(4)	0.003(3)
C22	0.024(4)	0.040(5)	0.043(6)	-0.008(4)	-0.008(4)	0.006(4)
C23	0.019(4)	0.023(4)	0.044(5)	-0.011(4)	0.004(4)	0.003(3)
N24	0.024(3)	0.024(3)	0.028(4)	-0.005(3)	0.002(3)	0.001(3)
N25	0.028(4)	0.028(3)	0.045(4)	-0.014(3)	-0.009(3)	0.003(3)
C26	0.036(4)	0.033(4)	0.044(5)	-0.012(4)	-0.002(4)	-0.004(3)
C27	0.054(6)	0.042(5)	0.052(6)	-0.001(4)	-0.012(5)	0.004(4)
C28	0.051(6)	0.043(5)	0.071(7)	-0.004(5)	-0.023(5)	0.011(4)
C29	0.033(5)	0.044(5)	0.068(7)	-0.017(5)	-0.012(5)	0.005(4)

C30	0.030(5)	0.030(4)	0.051(6)	-0.013(4)	-0.012(4)	0.002(4)
C31	0.072(8)	0.061(7)	0.064(7)	0.017(6)	-0.031(6)	0.006(6)
O1	0.096(7)	0.084(6)	0.061(5)	0.011(4)	-0.025(5)	0.007(5)
N32	0.033(4)	0.029(3)	0.035(4)	-0.003(3)	0.003(3)	-0.003(3)
C33	0.042(5)	0.067(6)	0.044(5)	-0.032(5)	-0.002(4)	0.006(4)
C34	0.062(7)	0.074(7)	0.061(7)	-0.024(6)	-0.004(5)	-0.013(6)
C35	0.043(6)	0.070(7)	0.072(7)	-0.037(6)	0.014(5)	-0.001(5)
C36	0.047(6)	0.050(6)	0.047(6)	-0.006(5)	0.016(5)	-0.003(4)
C37	0.040(5)	0.038(5)	0.036(5)	-0.006(4)	-0.005(4)	0.001(4)
C38	0.076(8)	0.26(2)	0.145(15)	-0.151(17)	-0.013(8)	0.009(9)
O2	0.091(9)	0.107(9)	0.075(8)	-0.049(7)	0.012(7)	-0.011(7)
O2'	0.079(8)	0.130(13)	0.094(11)	-0.077(10)	-0.020(8)	0.018(9)
N39	0.017(2)	0.028(3)	0.054(3)	-0.009(4)	-0.007(4)	-0.002(2)
O3	0.031(2)	0.046(3)	0.047(3)	-0.015(4)	-0.004(4)	0.004(2)
O4	0.036(4)	0.032(3)	0.063(5)	-0.009(3)	-0.012(3)	0.004(3)
O5	0.033(3)	0.032(3)	0.052(4)	-0.015(3)	0.003(3)	-0.001(3)
O6	0.037(8)	0.112(14)	0.092(13)	-0.009(11)	-0.022(9)	0.019(8)
O7	0.103(7)	0.149(8)	0.074(6)	-0.022(5)	-0.002(5)	-0.017(6)
N40	0.068(13)	0.088(14)	0.052(11)	-0.023(10)	0.009(11)	0.007(12)

Table 5 . Bond Distances in Compound 9723, Å

Ru1-N1	2.046(8)	Ru1-N12	2.075(7)	Ru1-N13	2.068(7)
Ru1-N24	2.069(7)	Ru1-N25	2.101(7)	Ru1-N32	2.103(8)
N1-C2	1.357(11)	N1-C6	1.390(11)	C2-C3	1.336(13)
C3-C4	1.397(14)	C4-C5	1.390(14)	C5-C6	1.396(14)
C6-C7	1.448(13)	C7-C8	1.390(13)	C7-N12	1.332(12)
C8-C9	1.410(14)	C9-C10	1.307(15)	C10-C11	1.373(12)
C11-N12	1.347(10)	N13-C14	1.330(11)	N13-C18	1.365(10)
C14-C15	1.405(13)	C15-C16	1.396(13)	C16-C17	1.369(13)
C17-C18	1.392(12)	C18-C19	1.473(12)	C19-C20	1.397(11)

C19-N24	1.361(11)	C20-C21	1.355(12)	C21-C22	1.382(13)
C22-C23	1.396(11)	C23-N24	1.319(11)	N25-C26	1.330(11)
N25-C30	1.351(11)	C26-C27	1.425(12)	C27-C28	1.374(15)
C27-C31	1.517(16)	C28-C29	1.370(15)	C29-C30	1.399(12)
C31-O1	1.198(12)	N32-C33	1.343(12)	N32-C37	1.358(11)
C33-C34	1.376(15)	C34-C35	1.390(16)	C34-C38	1.48(2)
C35-C36	1.366(16)	C36-C37	1.384(14)	C38-O2	1.22(2)
C38-O2'	1.19(2)	N39-O3	1.250(7)	N39-O4	1.259(9)
N39-O5	1.253(10)	O6-N40	1.21(2)	O7-N40	1.176(15)
O7-N40	1.260(15)				

[1]1-X,2-Y,-Z

Table 6 . Bond Angles in Compound 9723, °

N1-Ru1-N12	79.0(3)	N1-Ru1-N13	98.4(3)	N1-Ru1-N24	83.89(18)
N1-Ru1-N25	91.0(3)	N1-Ru1-N32	171.8(3)	N12-Ru1-N25	87.3(3)
N12-Ru1-N32	95.6(3)	N13-Ru1-N12	176.3(2)	N13-Ru1-N24	78.8(3)
N13-Ru1-N25	95.4(3)	N13-Ru1-N32	86.7(3)	N24-Ru1-N12	98.3(3)
N24-Ru1-N25	171.5(3)	N24-Ru1-N32	90.8(3)	N25-Ru1-N32	95.0(2)
C2-N1-Ru1	127.5(6)	C2-N1-C6	117.6(8)	C6-N1-Ru1	114.0(6)
C3-C2-N1	124.5(9)	C2-C3-C4	119.1(9)	C5-C4-C3	118.9(10)
C4-C5-C6	119.8(9)	N1-C6-C7	115.1(8)	C5-C6-N1	120.2(9)
C5-C6-C7	124.7(8)	C8-C7-C6	122.6(9)	N12-C7-C6	115.8(8)
N12-C7-C8	121.6(9)	C7-C8-C9	118.0(10)	C10-C9-C8	119.8(9)
C9-C10-C11	119.9(9)	N12-C11-C10	122.6(9)	C7-N12-Ru1	115.2(6)
C7-N12-C11	118.0(7)	C11-N12-Ru1	126.6(6)	C14-N13-Ru1	125.9(6)
C14-N13-C18	118.3(7)	C18-N13-Ru1	115.8(6)	N13-C14-C15	123.3(8)
C16-C15-C14	117.7(9)	C17-C16-C15	119.4(8)	C16-C17-C18	119.8(8)
N13-C18-C17	121.5(8)	N13-C18-C19	114.3(7)	C17-C18-C19	124.2(8)
C20-C19-C18	123.4(8)	N24-C19-C18	115.4(7)	N24-C19-C20	121.2(8)
C21-C20-C19	119.4(8)	C20-C21-C22	119.6(8)	C21-C22-C23	118.5(9)
N24-C23-C22	122.5(8)	C19-N24-Ru1	115.0(6)	C23-N24-Ru1	125.8(5)

C23-N24-C19	118.7(7)	C26-N25-Ru1	123.7(6)	C26-N25-C30	118.3(8)
C30-N25-Ru1	118.0(6)	N25-C26-C27	123.2(9)	C26-C27-C31	116.8(9)
C28-C27-C26	116.8(9)	C28-C27-C31	126.3(9)	C29-C28-C27	120.9(9)
C28-C29-C30	118.9(9)	N25-C30-C29	121.9(9)	O1-C31-C27	117.6(12)
C33-N32-Ru1	124.4(6)	C33-N32-C37	116.2(9)	C37-N32-Ru1	119.1(7)
N32-C33-C34	122.0(9)	C33-C34-C35	120.5(11)	C33-C34-C38	120.2(12)
C35-C34-C38	119.2(13)	C36-C35-C34	118.4(11)	C35-C36-C37	117.9(10)
N32-C37-C36	124.7(10)	O2-C38-C34	121.1(18)	O2'-C38-C34	120.7(18)
O3-N39-O4	119.8(9)	O3-N39-O5	120.4(8)	O4-N39-O5	119.9(6)
O6-N40-O7	128(2)	O7-N40-O6[1]	111.0(19)	O7-N40-O7[1]	120(2)

[1]1-X,2-Y,-Z

This report has been created with Olex2 [6], compiled on 2017.07.20 svn.r3457 for OlexSys.

References

[1] APEX3 2016.1-0

[2] CELL_NOW v2008/4
[3] SAINT v8.37A
[4] TWINABS v2012/1
[5] SHELXT v2014/5
[6] PLATON (V-150216)
[7] SHELXL-2014/7
[8] Olex2 (Dolomanov et al., 2009)

A3.4 Ru(biq)$_2$(4-pentynenitrile)$_2$ (Ru530)

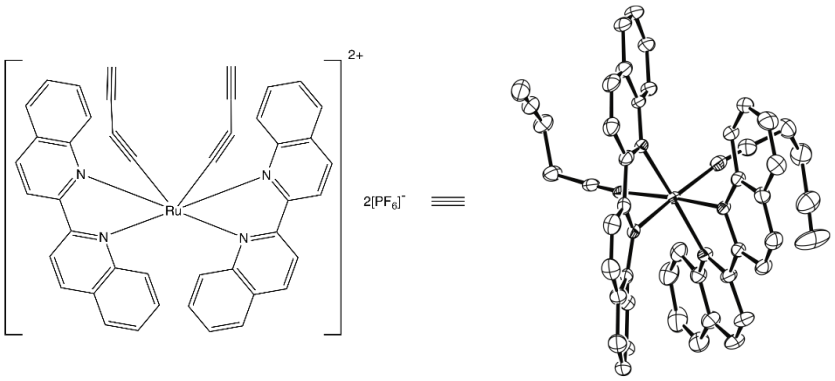

Compound 9721, $C_{46}H_{34}N_6P_2F_{12}Ru$, crystallizes in the monoclinic space group $P2_1/c$ (systematic absences 0k0: k=odd and h0l: l=odd) with a=11.1852(6)Å, b=16.4112(10)Å, c=23.1159(13)Å, b=96.108(3)°, V=4219.1(4)Å3, Z=4, and d_{calc}=1.672 g/cm3 . X-ray intensity data were collected on a Bruker APEXII CCD area detector employing graphite-monochromated Mo-Ka radiation (l=0.71073 Å) at a temperature of 100(1)K. Preliminary indexing was performed from a series of thirty-six 0.5° rotation frames with exposures of 10 seconds. A total of 2400 frames were collected with a crystal to detector distance of 37.5 mm, rotation widths of 0.5° and exposures of 30 seconds:

scan type	2q	w	f	c	frames
f	-23.00	315.83	13.08	28.88	732
f	24.50	7.41	155.80	28.88	311
f	22.00	321.06	56.24	41.79	132
f	-23.00	328.34	49.47	79.39	725
f	-23.00	334.21	38.95	73.66	500

Rotation frames were integrated using SAINT[15], producing a listing of unaveraged F2 and s(F2) values which were then passed to the SHELXTL[16] program package for further processing and

[15]Bruker (2009) SAINT. Bruker AXS Inc., Madison, Wisconsin, USA.

[16]Bruker (2009) SHELXTL. Bruker AXS Inc., Madison, Wisconsin, USA.

structure solution. A total of 88028 reflections were measured over the ranges 1.52 £ q £ 27.52°, -14 £ h £ 14, -18 £ k £ 21, -29 £ l £ 30 yielding 9685 unique reflections (Rint = 0.0814). The intensity data were corrected for Lorentz and polarization effects and for absorption using SADABS[17] (minimum and maximum transmission 0.6934, 0.7456).

The structure was solved by direct methods (SHELXS-97[18]). Refinement was by full-matrix least squares based on F2 using SHELXL-97.[19] All reflections were used during refinement. The weighting scheme used was w=1/[s2(F_o2)+ (0.0744P)2 + 16.0979P] where P = (F_o 2 + 2F_c2)/3. Non-hydrogen atoms were refined anisotropically and hydrogen atoms were refined using a riding model. Refinement converged to R1=0.0611 and wR2=0.1435 for 6260 observed reflections for which F > 4s(F) and R1=0.1070 and wR2=0.1676 and GOF =1.016 for all 9685 unique, non-zero reflections and 623 variables.[20] The maximum D/s in the final cycle of least squares was 0.000 and the two most prominent peaks in the final difference Fourier were +1.577 and -1.362 e/Å3.

Table 1. lists cell information, data collection parameters, and refinement data. Final positional and equivalent isotropic thermal parameters are given in Tables 2. and 3. Anisotropic thermal parameters are in Table 4. Tables 5. and 6. list bond distances and bond angles. Figure 1. is an ORTEP[21] representation of the molecule with 50% probability thermal ellipsoids displayed.

---

[17]Sheldrick, G.M. (2007) SADABS. University of Gottingen, Germany.

[18]Sheldrick, G.M. (2008) Acta Cryst. A64,112-122.

[19]Sheldrick, G.M. (2008) Acta Cryst. A64,112-122.

[20]$R1 = \Sigma||F_o| - |F_c|| / \Sigma |F_o|$

$wR2 = [\Sigma w(F_o^2 - F_c^2)^2/\Sigma w(F_o^2)^2]^{½}$

$GOF = [\Sigma w(F_o^2 - F_c^2)^2/(n - p)]^{½}$

where n = the number of reflections and p = the number of parameters refined.

[21]"ORTEP-II: A Fortran Thermal Ellipsoid Plot Program for Crystal Structure Illustrations". C.K. Johnson

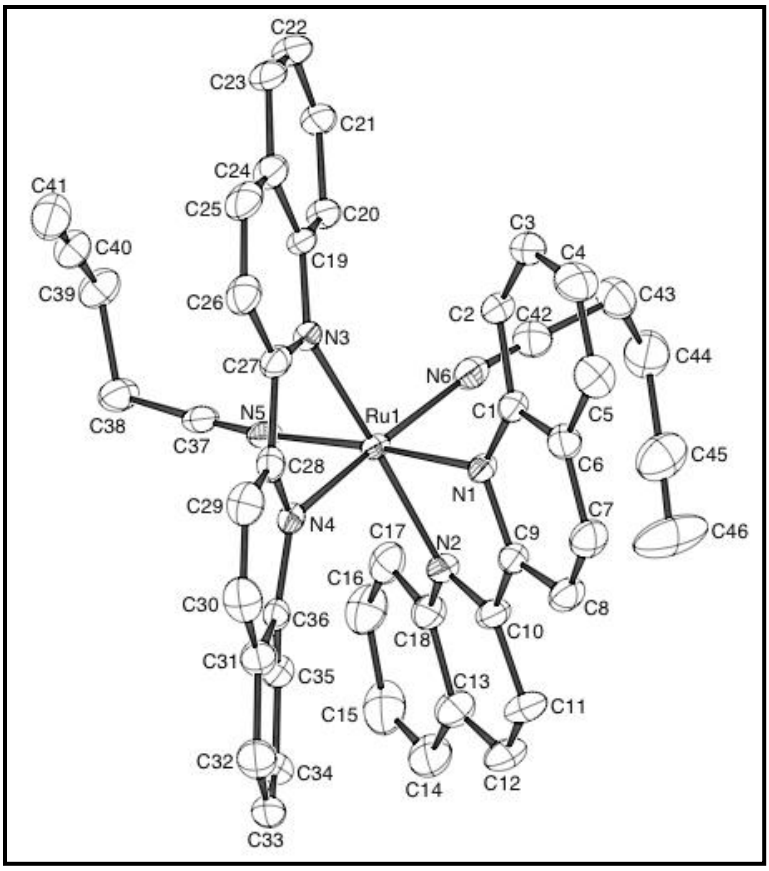

Figure 1. ORTEP drawing of the title compound with 50% probability thermal ellipsoids.

Table 1. Summary of Structure Determination of Compound 9721

Empirical formula	$C_{46}H_{34}N_6P_2F_{12}Ru$
Formula weight	1061.80
Temperature	100(1) K
Wavelength	0.71073 Å
Crystal system	monoclinic
Space group	$P2_1/c$
Cell constants:	

(1976) ORNL-5138.

a	11.1852(6) Å
b	16.4112(10) Å
c	23.1159(13) Å
b	96.108(3)°
Volume	4219.1(4) Å3
Z	4
Density (calculated)	1.672 Mg/m3
Absorption coefficient	0.545 mm-1
F(000)	2136
Crystal size	0.10 x 0.06 x 0.04 mm3
Theta range for data collection	1.52 to 27.52°
Index ranges	-14 £ h £ 14, -18 £ k £ 21, -29 £ l £ 30
Reflections collected	88028
Independent reflections	9685 [R(int) = 0.0814]
Completeness to theta = 27.52°	99.8 %
Absorption correction	Semi-empirical from equivalents
Max. and min. transmission	0.7456 and 0.6934
Refinement method	Full-matrix least-squares on F2
Data / restraints / parameters	9685 / 473 / 623
Goodness-of-fit on F2	1.016
Final R indices [I>2sigma(I)]	R1 = 0.0611, wR2 = 0.1435
R indices (all data)	R1 = 0.1070, wR2 = 0.1676
Largest diff. peak and hole	1.577 and -1.362 e.Å-3

Table 2. Refined Positional Parameters for Compound 9721

Atom	x	y	z	U_{eq}, Å^2
Ru1	0.43347(3)	0.24845(2)	0.386782(14)	0.01759(11)
N1	0.5386(3)	0.3165(2)	0.33467(15)	0.0202(8)
N2	0.3101(4)	0.2772(2)	0.31507(16)	0.0228(8)
N3	0.5735(4)	0.2142(2)	0.44927(16)	0.0221(8)
N4	0.5071(3)	0.1486(2)	0.34806(15)	0.0203(8)
N5	0.3318(3)	0.1740(2)	0.43330(16)	0.0213(8)
N6	0.3824(4)	0.3561(3)	0.42079(17)	0.0261(9)
C1	0.6514(4)	0.3488(3)	0.34970(19)	0.0225(10)
C2	0.6937(4)	0.3641(3)	0.4083(2)	0.0248(10)
C3	0.8053(5)	0.3956(3)	0.4223(2)	0.0295(11)
C4	0.8811(5)	0.4147(4)	0.3796(2)	0.0357(13)
C5	0.8417(5)	0.4033(3)	0.3224(2)	0.0327(12)
C6	0.7248(5)	0.3707(3)	0.3055(2)	0.0266(11)
C7	0.6772(5)	0.3639(3)	0.2467(2)	0.0309(12)
C8	0.5618(5)	0.3409(3)	0.2338(2)	0.0285(11)
C9	0.4920(4)	0.3173(3)	0.27847(19)	0.0228(10)
C10	0.3645(4)	0.2971(3)	0.26754(19)	0.0245(10)
C11	0.3007(5)	0.2999(3)	0.2115(2)	0.0321(12)
C12	0.1829(5)	0.2812(4)	0.2042(2)	0.0361(13)
C13	0.1222(5)	0.2622(3)	0.2529(2)	0.0348(13)
C14	-0.0011(5)	0.2405(4)	0.2473(3)	0.0412(14)
C15	-0.0565(6)	0.2255(4)	0.2957(3)	0.0489(17)
C16	0.0058(5)	0.2361(4)	0.3518(3)	0.0398(14)
C17	0.1260(5)	0.2547(3)	0.3583(2)	0.0306(11)
C18	0.1874(5)	0.2653(3)	0.3092(2)	0.0269(11)
C19	0.5921(5)	0.2386(3)	0.50720(19)	0.0251(11)
C20	0.4991(5)	0.2756(3)	0.5341(2)	0.0281(11)
C21	0.5189(6)	0.3002(3)	0.5916(2)	0.0354(13)
C22	0.6316(6)	0.2889(4)	0.6231(2)	0.0405(14)
C23	0.7210(5)	0.2512(4)	0.5989(2)	0.0378(13)
C24	0.7050(5)	0.2234(3)	0.5401(2)	0.0301(12)
C25	0.7952(5)	0.1822(3)	0.5136(2)	0.0342(13)
C26	0.7705(5)	0.1539(3)	0.4585(2)	0.0300(11)
C27	0.6576(4)	0.1707(3)	0.4270(2)	0.0237(10)
C28	0.6235(4)	0.1368(3)	0.3686(2)	0.0228(10)

C29	0.7030(5)	0.0944(3)	0.3368(2)	0.0307(12)
C30	0.6647(5)	0.0650(3)	0.2830(2)	0.0336(12)
C31	0.5435(5)	0.0720(3)	0.2616(2)	0.0275(11)
C32	0.4958(5)	0.0430(3)	0.2058(2)	0.0330(12)
C33	0.3772(5)	0.0488(3)	0.1882(2)	0.0334(13)
C34	0.2970(5)	0.0778(3)	0.2266(2)	0.0294(11)
C35	0.3391(4)	0.1066(3)	0.2804(2)	0.0246(10)
C36	0.4634(4)	0.1102(3)	0.29740(19)	0.0201(9)
C37	0.2863(4)	0.1324(3)	0.46329(19)	0.0237(10)
C38	0.2305(5)	0.0803(3)	0.5044(2)	0.0313(12)
C39	0.2850(5)	0.0935(4)	0.5673(2)	0.0337(12)
C40	0.4137(5)	0.0701(3)	0.5779(2)	0.0330(12)
C41	0.5167(6)	0.0519(4)	0.5868(3)	0.0404(14)
C42	0.3573(5)	0.4198(3)	0.4331(2)	0.0318(12)
C43	0.3270(5)	0.5043(3)	0.4459(3)	0.0382(13)
C44	0.1966(6)	0.5252(4)	0.4242(3)	0.0451(15)
C45	0.1652(6)	0.5072(4)	0.3612(3)	0.0488(16)
C46	0.1360(6)	0.4918(6)	0.3139(3)	0.071(3)
P1	0.04497(9)	-0.02662(7)	0.36058(4)	0.0273(3)
F1	-0.08338(11)	-0.03106(13)	0.33035(9)	0.0459(8)
F2	0.00683(19)	-0.07675(16)	0.41132(8)	0.0902(17)
F3	0.17331(11)	-0.02217(14)	0.39082(9)	0.0518(9)
F4	0.0831(2)	0.02352(16)	0.30985(8)	0.0783(14)
F5	0.07660(19)	-0.10509(11)	0.32988(11)	0.0767(14)
F6	0.01333(19)	0.05186(11)	0.39128(11)	0.0738(13)
P2	0.1192(3)	0.3523(2)	0.54759(15)	0.0385(10)
F7	0.0511(5)	0.4311(2)	0.5306(3)	0.066(2)
F8	0.1198(7)	0.3743(4)	0.61194(16)	0.080(2)
F9	0.1873(5)	0.2736(3)	0.5645(3)	0.082(2)
F10	0.1186(6)	0.3303(4)	0.48324(16)	0.088(2)
F11	-0.0003(4)	0.3076(3)	0.5494(3)	0.088(2)
F12	0.2387(4)	0.3971(4)	0.5458(4)	0.076(2)
P2'	0.1360(4)	0.3399(3)	0.55373(19)	0.0432(12)
F7'	0.0374(6)	0.3805(4)	0.5126(3)	0.076(2)
F8'	0.0964(8)	0.3891(6)	0.6046(3)	0.083(3)
F9'	0.2346(5)	0.2993(4)	0.5949(3)	0.059(2)
F10'	0.1755(8)	0.2907(5)	0.5029(2)	0.091(3)
F11'	0.0486(6)	0.2719(5)	0.5660(4)	0.094(3)

F12'	0.2234(7)	0.4079(4)	0.5415(4)	0.084(2)

$U_{eq}=1/3[U_{11}(aa^*)^2+U_{22}(bb^*)^2+U_{33}(cc^*)^2+2U_{12}aa^*bb^*\cos g+2U_{13}aa^*cc^*\cos b+2U_{23}bb^*cc^*\cos a]$

Table 3. Positional Parameters for Hydrogens in Compound 9721

Atom	x	y	z	U_{iso}, Å^2
H2	0.6451	0.3527	0.4375	0.033
H3	0.8322	0.4047	0.4612	0.039
H4	0.9579	0.4351	0.3903	0.047
H5	0.8914	0.4169	0.2940	0.043
H7	0.7250	0.3753	0.2171	0.041
H8	0.5280	0.3405	0.1953	0.038
H11	0.3401	0.3146	0.1796	0.043
H12	0.1415	0.2808	0.1671	0.048
H14	-0.0439	0.2364	0.2107	0.055
H15	-0.1361	0.2082	0.2920	0.065
H16	-0.0352	0.2304	0.3845	0.053
H17	0.1666	0.2602	0.3953	0.041
H20	0.4242	0.2836	0.5133	0.037
H21	0.4570	0.3242	0.6094	0.047
H22	0.6450	0.3078	0.6611	0.054
H23	0.7946	0.2431	0.6209	0.050
H25	0.8709	0.1744	0.5336	0.045
H26	0.8275	0.1235	0.4414	0.040
H29	0.7822	0.0863	0.3525	0.041
H30	0.7189	0.0404	0.2605	0.045
H32	0.5471	0.0198	0.1812	0.044
H33	0.3481	0.0335	0.1506	0.044
H34	0.2147	0.0773	0.2152	0.039
H35	0.2852	0.1240	0.3059	0.033
H38a	0.2407	0.0236	0.4939	0.042
H38b	0.1450	0.0916	0.5015	0.042
H39a	0.2771	0.1506	0.5771	0.045
H39b	0.2396	0.0620	0.5929	0.045
H41	0.5974	0.0377	0.5939	0.054
H43a	0.3803	0.5406	0.4277	0.051
H43b	0.3398	0.5130	0.4876	0.051
H44a	0.1435	0.4946	0.4466	0.060
H44b	0.1832	0.5827	0.4309	0.060
H46	0.1121	0.4792	0.2751	0.095

Table 4. Refined Thermal Parameters (U's) for Compound 9721

Atom	U_{11}	U_{22}	U_{33}	U_{23}	U_{13}	U_{12}
Ru1	0.01999(18)	0.01973(18)	0.01259(16)	0.00107(15)	-0.00037(11)	0.00058(17)
N1	0.025(2)	0.019(2)	0.0158(18)	0.0021(15)	-0.0002(15)	0.0025(16)
N2	0.026(2)	0.022(2)	0.0186(18)	0.0004(15)	-0.0029(16)	0.0017(17)
N3	0.029(2)	0.020(2)	0.0169(18)	0.0037(15)	-0.0021(16)	-0.0041(17)
N4	0.026(2)	0.018(2)	0.0169(18)	0.0034(15)	0.0026(15)	-0.0003(16)
N5	0.020(2)	0.027(2)	0.0163(18)	-0.0008(16)	-0.0016(15)	-0.0045(17)
N6	0.028(2)	0.030(2)	0.0197(19)	0.0034(17)	0.0005(16)	-0.0006(19)
C1	0.027(3)	0.020(2)	0.019(2)	0.0015(18)	-0.0001(19)	0.003(2)
C2	0.030(3)	0.025(3)	0.019(2)	0.0014(19)	-0.0001(19)	0.001(2)
C3	0.036(3)	0.028(3)	0.024(2)	0.000(2)	-0.002(2)	-0.006(2)
C4	0.026(3)	0.041(3)	0.039(3)	-0.002(2)	0.000(2)	-0.011(2)
C5	0.026(3)	0.036(3)	0.038(3)	0.000(2)	0.011(2)	-0.004(2)
C6	0.031(3)	0.024(3)	0.025(2)	0.000(2)	0.005(2)	-0.002(2)
C7	0.038(3)	0.033(3)	0.022(2)	0.002(2)	0.010(2)	0.001(2)
C8	0.037(3)	0.030(3)	0.018(2)	0.002(2)	0.004(2)	0.004(2)
C9	0.031(3)	0.019(2)	0.018(2)	0.0002(18)	0.0006(19)	0.003(2)
C10	0.028(3)	0.027(3)	0.018(2)	0.0004(19)	-0.0025(19)	0.004(2)
C11	0.034(3)	0.042(3)	0.018(2)	0.001(2)	-0.004(2)	0.003(2)
C12	0.037(3)	0.042(3)	0.026(3)	0.003(2)	-0.012(2)	0.003(3)
C13	0.032(3)	0.035(3)	0.034(3)	0.003(2)	-0.011(2)	0.006(2)
C14	0.031(3)	0.041(4)	0.047(3)	0.007(3)	-0.014(2)	0.001(3)
C15	0.029(3)	0.042(4)	0.072(5)	0.015(3)	-0.011(3)	-0.003(3)
C16	0.028(3)	0.043(4)	0.048(3)	0.011(3)	0.003(2)	0.006(2)
C17	0.029(3)	0.029(3)	0.033(3)	0.005(2)	0.002(2)	0.010(2)
C18	0.028(3)	0.025(3)	0.027(2)	0.0012(19)	-0.002(2)	0.004(2)
C19	0.034(3)	0.023(3)	0.016(2)	0.0049(18)	-0.0065(18)	-0.010(2)
C20	0.038(3)	0.028(3)	0.018(2)	0.0014(19)	-0.001(2)	-0.007(2)
C21	0.057(4)	0.031(3)	0.017(2)	0.002(2)	0.000(2)	-0.013(3)
C22	0.062(4)	0.039(3)	0.018(2)	0.002(2)	-0.006(3)	-0.011(3)
C23	0.047(3)	0.037(3)	0.025(2)	0.008(3)	-0.017(2)	-0.015(3)
C24	0.032(3)	0.031(3)	0.026(2)	0.006(2)	-0.005(2)	-0.004(2)
C25	0.026(3)	0.038(3)	0.035(3)	0.012(2)	-0.013(2)	-0.003(2)
C26	0.025(3)	0.029(3)	0.035(3)	0.007(2)	-0.003(2)	0.002(2)
C27	0.024(3)	0.026(3)	0.020(2)	0.0058(19)	0.0006(19)	-0.004(2)
C28	0.023(3)	0.018(2)	0.027(2)	0.0045(19)	0.0021(19)	-0.002(2)

C29	0.024(3)	0.031(3)	0.037(3)	0.004(2)	0.006(2)	0.007(2)
C30	0.036(3)	0.030(3)	0.037(3)	-0.002(2)	0.016(2)	0.004(2)
C31	0.035(3)	0.026(3)	0.022(2)	-0.001(2)	0.009(2)	0.000(2)
C32	0.045(3)	0.031(3)	0.026(3)	-0.004(2)	0.013(2)	0.001(2)
C33	0.056(4)	0.025(3)	0.019(2)	-0.001(2)	0.002(2)	-0.008(3)
C34	0.037(3)	0.024(3)	0.027(3)	-0.004(2)	-0.002(2)	-0.001(2)
C35	0.029(3)	0.022(2)	0.022(2)	0.0008(19)	0.0001(19)	0.002(2)
C36	0.027(3)	0.016(2)	0.018(2)	0.0022(17)	0.0051(18)	-0.0008(19)
C37	0.026(3)	0.028(3)	0.016(2)	-0.0033(19)	-0.0025(18)	0.000(2)
C38	0.032(3)	0.040(3)	0.022(2)	0.002(2)	0.001(2)	-0.012(2)
C39	0.037(3)	0.041(3)	0.024(2)	0.004(2)	0.009(2)	0.001(3)
C40	0.041(3)	0.032(3)	0.025(3)	0.004(2)	0.005(2)	-0.003(3)
C41	0.040(4)	0.038(3)	0.043(3)	0.009(3)	0.001(3)	-0.001(3)
C42	0.037(3)	0.031(3)	0.027(3)	-0.002(2)	0.004(2)	-0.001(2)
C43	0.049(4)	0.028(3)	0.038(3)	-0.005(2)	0.007(3)	0.000(3)
C44	0.055(4)	0.042(4)	0.040(3)	-0.001(3)	0.013(3)	0.005(3)
C45	0.041(4)	0.065(5)	0.041(4)	0.010(3)	0.005(3)	-0.005(3)
C46	0.050(4)	0.141(8)	0.023(3)	0.009(4)	0.009(3)	-0.036(5)
P1	0.0267(7)	0.0305(7)	0.0248(6)	-0.0028(5)	0.0037(5)	0.0042(5)
F1	0.0386(19)	0.056(2)	0.0424(19)	-0.0058(16)	0.0006(15)	0.0056(16)
F2	0.056(3)	0.132(4)	0.088(3)	0.076(3)	0.031(2)	0.039(3)
F3	0.0381(19)	0.069(3)	0.047(2)	-0.0177(18)	-0.0042(15)	0.0011(17)
F4	0.056(3)	0.119(4)	0.062(3)	0.041(3)	0.012(2)	-0.011(3)
F5	0.040(2)	0.071(3)	0.118(4)	-0.056(3)	-0.001(2)	0.014(2)
F6	0.068(3)	0.066(3)	0.081(3)	-0.042(2)	-0.023(2)	0.025(2)
P2	0.0371(18)	0.053(2)	0.0251(17)	-0.0029(16)	0.0000(14)	0.0079(15)
F7	0.066(4)	0.055(4)	0.078(5)	0.012(3)	0.004(4)	0.013(3)
F8	0.102(6)	0.099(6)	0.035(3)	-0.011(3)	-0.004(3)	0.021(4)
F9	0.109(5)	0.061(3)	0.074(5)	0.002(3)	0.004(4)	0.036(4)
F10	0.130(7)	0.098(7)	0.036(3)	-0.014(3)	0.006(3)	0.014(4)
F11	0.071(4)	0.067(5)	0.126(7)	-0.004(4)	0.013(4)	-0.016(3)
F12	0.049(3)	0.094(5)	0.086(6)	0.006(4)	0.008(3)	0.002(3)
P2'	0.069(3)	0.031(2)	0.029(2)	0.0019(17)	0.003(2)	0.0073(18)
F7'	0.075(4)	0.082(5)	0.066(5)	0.009(4)	-0.018(4)	0.022(4)
F8'	0.095(7)	0.091(6)	0.065(4)	-0.023(4)	0.015(4)	0.038(4)
F9'	0.047(4)	0.076(6)	0.053(4)	0.020(4)	0.006(3)	0.011(4)
F10'	0.108(7)	0.110(7)	0.053(4)	-0.036(4)	0.003(4)	0.038(4)
F11'	0.094(5)	0.100(5)	0.078(6)	0.032(4)	-0.033(5)	-0.048(5)

F12'	0.087(4)	0.073(5)	0.089(7)	0.036(4)	0.000(5)	-0.017(4)

The form of the anisotropic displacement parameter is:
$\exp[-2p^2(a^{*2}U_{11}h^2+b^{*2}U_{22}k^2+c^{*2}U_{33}l^2+2b^*c^*U_{23}kl+2a^*c^*U_{13}hl+2a^*b^*U_{12}hk)]$

Table 5. Bond Distances in Compound 9721, Å

Ru1-N6	2.039(4)	Ru1-N5	2.050(4)	Ru1-N4	2.079(4)
Ru1-N3	2.091(4)	Ru1-N1	2.093(4)	Ru1-N2	2.095(4)
N1-C9	1.347(6)	N1-C1	1.378(6)	N2-C10	1.351(6)
N2-C18	1.379(6)	N3-C27	1.328(6)	N3-C19	1.392(6)
N4-C28	1.351(6)	N4-C36	1.374(6)	N5-C37	1.132(6)
N6-C42	1.127(7)	C1-C2	1.410(6)	C1-C6	1.424(6)
C2-C3	1.357(7)	C3-C4	1.404(7)	C4-C5	1.362(8)
C5-C6	1.429(7)	C6-C7	1.409(7)	C7-C8	1.347(7)
C8-C9	1.413(6)	C9-C10	1.459(7)	C10-C11	1.412(6)
C11-C12	1.346(8)	C12-C13	1.408(8)	C13-C14	1.417(8)
C13-C18	1.425(7)	C14-C15	1.357(9)	C15-C16	1.415(9)
C16-C17	1.371(8)	C17-C18	1.398(7)	C19-C20	1.407(7)
C19-C24	1.425(7)	C20-C21	1.383(7)	C21-C22	1.399(8)
C22-C23	1.348(9)	C23-C24	1.426(7)	C24-C25	1.409(8)
C25-C26	1.356(7)	C26-C27	1.415(7)	C27-C28	1.472(7)
C28-C29	1.398(7)	C29-C30	1.361(8)	C30-C31	1.397(8)
C31-C32	1.426(7)	C31-C36	1.427(6)	C32-C33	1.349(8)
C33-C34	1.410(7)	C34-C35	1.368(7)	C35-C36	1.405(7)
C37-C38	1.466(7)	C38-C39	1.531(7)	C39-C40	1.485(8)
C40-C41	1.186(8)	C42-C43	1.465(8)	C43-C44	1.530(9)
C44-C45	1.489(9)	C45-C46	1.137(9)	P1-F6	1.5299
P1-F4	1.5300	P1-F5	1.5300	P1-F3	1.5300
P1-F1	1.5300	P1-F2	1.5300	P2-F7'	1.244(7)
P2-F8'	1.496(8)	P2-F12'	1.499(9)	P2-F11	1.5299
P2-F12	1.5300	P2-F9	1.5300	P2-F7	1.5301
P2-F8	1.5301	P2-F10	1.5301	P2-F11'	1.618(8)
P2-F10'	1.621(8)	P2-F9'	1.821(7)	F7-F7'	0.935(9)
F7-P2'	1.822(7)	F8-P2'	1.488(7)	F9-F9'	0.934(9)
F9-P2'	1.244(7)	F9-F10'	1.446(9)	F9-F11'	1.556(10)
F10-F10'	0.986(8)	F10-F7'	1.447(9)	F10-P2'	1.628(7)
F11-F11'	0.863(9)	F11-F7'	1.552(10)	F11-P2'	1.608(8)
F12-P2'	1.510(9)	P2'-F12'	1.5299	P2'-F8'	1.5300
P2'-F7'	1.5300	P2'-F10'	1.5300	P2'-F9'	1.5301
P2'-F11'	1.5301				

Table 6. Bond Angles in Compound 9721, °

N6-Ru1-N5	96.89(16)	N6-Ru1-N4	171.36(16)	N5-Ru1-N4	91.35(15)
N6-Ru1-N3	100.73(16)	N5-Ru1-N3	83.92(15)	N4-Ru1-N3	77.51(15)
N6-Ru1-N1	87.57(15)	N5-Ru1-N1	175.32(15)	N4-Ru1-N1	84.25(15)
N3-Ru1-N1	96.64(15)	N6-Ru1-N2	85.51(16)	N5-Ru1-N2	101.18(15)
N4-Ru1-N2	95.44(15)	N3-Ru1-N2	171.49(15)	N1-Ru1-N2	77.72(15)
C9-N1-C1	119.3(4)	C9-N1-Ru1	112.1(3)	C1-N1-Ru1	128.0(3)
C10-N2-C18	119.0(4)	C10-N2-Ru1	112.5(3)	C18-N2-Ru1	127.6(3)
C27-N3-C19	119.1(4)	C27-N3-Ru1	112.7(3)	C19-N3-Ru1	127.8(3)
C28-N4-C36	118.4(4)	C28-N4-Ru1	111.9(3)	C36-N4-Ru1	127.4(3)
C37-N5-Ru1	172.6(4)	C42-N6-Ru1	171.2(4)	N1-C1-C2	121.1(4)
N1-C1-C6	119.9(4)	C2-C1-C6	119.0(5)	C3-C2-C1	120.2(5)
C2-C3-C4	121.8(5)	C5-C4-C3	119.7(5)	C4-C5-C6	120.6(5)
C7-C6-C1	119.0(5)	C7-C6-C5	122.2(5)	C1-C6-C5	118.6(4)
C8-C7-C6	119.3(5)	C7-C8-C9	120.4(5)	N1-C9-C8	121.3(5)
N1-C9-C10	115.8(4)	C8-C9-C10	122.8(4)	N2-C10-C11	121.8(5)
N2-C10-C9	115.5(4)	C11-C10-C9	122.7(4)	C12-C11-C10	120.0(5)
C11-C12-C13	120.0(5)	C12-C13-C14	122.1(5)	C12-C13-C18	118.6(5)
C14-C13-C18	119.3(5)	C15-C14-C13	119.8(6)	C14-C15-C16	120.6(6)
C17-C16-C15	120.6(6)	C16-C17-C18	120.0(5)	N2-C18-C17	120.6(4)
N2-C18-C13	120.1(5)	C17-C18-C13	119.3(5)	N3-C19-C20	120.5(4)
N3-C19-C24	119.8(5)	C20-C19-C24	119.6(4)	C21-C20-C19	120.0(5)
C20-C21-C22	120.3(6)	C23-C22-C21	120.8(5)	C22-C23-C24	121.2(5)
C25-C24-C19	119.1(5)	C25-C24-C23	123.0(5)	C19-C24-C23	117.9(5)
C26-C25-C24	119.3(5)	C25-C26-C27	119.8(5)	N3-C27-C26	122.4(4)
N3-C27-C28	115.6(4)	C26-C27-C28	121.9(5)	N4-C28-C29	121.9(4)
N4-C28-C27	114.5(4)	C29-C28-C27	123.5(5)	C30-C29-C28	120.1(5)
C29-C30-C31	119.5(5)	C30-C31-C32	123.2(5)	C30-C31-C36	118.5(4)
C32-C31-C36	118.3(5)	C33-C32-C31	120.7(5)	C32-C33-C34	120.4(5)
C35-C34-C33	120.6(5)	C34-C35-C36	120.2(5)	N4-C36-C35	120.6(4)
N4-C36-C31	120.4(4)	C35-C36-C31	119.0(4)	N5-C37-C38	177.4(5)
C37-C38-C39	112.2(4)	C40-C39-C38	113.7(4)	C41-C40-C39	179.3(7)
N6-C42-C43	176.7(6)	C42-C43-C44	112.3(5)	C45-C44-C43	113.2(5)
C46-C45-C44	176.6(7)	F6-P1-F4	90.0	F6-P1-F5	180.0
F4-P1-F5	90.0	F6-P1-F3	90.0	F4-P1-F3	90.0
F5-P1-F3	90.0	F6-P1-F1	90.0	F4-P1-F1	90.0
F5-P1-F1	90.0	F3-P1-F1	180.0	F6-P1-F2	90.0
F4-P1-F2	180.0	F5-P1-F2	90.0	F3-P1-F2	90.0

F1-P1-F2	90.0	F7'-P2-F8'	103.9(5)	F7'-P2-F12'	103.8(5)
F8'-P2-F12'	92.5(4)	F7'-P2-F11	67.1(5)	F8'-P2-F11	86.5(7)
F12'-P2-F11	170.2(5)	F7'-P2-F12	112.9(5)	F8'-P2-F12	93.5(7)
F12'-P2-F12	9.8(5)	F11-P2-F12	180.0	F7'-P2-F9	142.4(4)
F8'-P2-F9	104.0(5)	F12'-P2-F9	99.6(5)	F11-P2-F9	90.0
F12-P2-F9	90.0	F7'-P2-F7	37.6(4)	F8'-P2-F7	76.0(5)
F12'-P2-F7	80.3(5)	F11-P2-F7	90.0	F12-P2-F7	90.0
F9-P2-F7	180.0	F7'-P2-F8	118.1(5)	F8'-P2-F8	14.5(4)
F12'-P2-F8	91.4(7)	F11-P2-F8	90.0	F12-P2-F8	90.0
F9-P2-F8	90.0	F7-P2-F8	90.0	F7'-P2-F10	61.9(5)
F8'-P2-F10	165.5(4)	F12'-P2-F10	88.5(7)	F11-P2-F10	90.0
F12-P2-F10	90.0	F9-P2-F10	90.0	F7-P2-F10	90.0
F8-P2-F10	180.0	F7'-P2-F11'	97.4(5)	F8'-P2-F11'	87.9(5)
F12'-P2-F11'	158.1(5)	F11-P2-F11'	31.7(3)	F12-P2-F11'	148.3(3)
F9-P2-F11'	59.1(4)	F7-P2-F11'	120.9(4)	F8-P2-F11'	83.6(5)
F10-P2-F11'	96.4(5)	F7'-P2-F10'	97.2(4)	F8'-P2-F10'	158.1(5)
F12'-P2-F10'	87.7(5)	F11-P2-F10'	96.8(5)	F12-P2-F10'	83.2(5)
F9-P2-F10'	54.5(3)	F7-P2-F10'	125.5(3)	F8-P2-F10'	143.7(3)
F10-P2-F10'	36.3(3)	F11'-P2-F10'	83.8(3)	F7'-P2-F9'	173.2(5)
F8'-P2-F9'	80.8(3)	F12'-P2-F9'	80.7(3)	F11-P2-F9'	108.7(4)
F12-P2-F9'	71.3(4)	F9-P2-F9'	30.8(4)	F7-P2-F9'	149.2(4)
F8-P2-F9'	66.4(4)	F10-P2-F9'	113.6(4)	F11'-P2-F9'	77.7(3)
F10'-P2-F9'	77.7(3)	F7'-F7-P2	54.4(4)	F7'-F7-P2'	57.1(4)
P2-F7-P2'	2.7(2)	P2'-F8-P2	11.4(3)	F9'-F9-P2'	88.1(7)
F9'-F9-F10'	129.6(10)	P2'-F9-F10'	68.9(4)	F9'-F9-P2	92.1(6)
P2'-F9-P2	4.0(3)	F10'-F9-P2	65.9(3)	F9'-F9-F11'	118.6(9)
P2'-F9-F11'	65.2(4)	F10'-F9-F11'	92.2(4)	P2-F9-F11'	63.3(3)
F10'-F10-F7'	124.5(7)	F10'-F10-P2	76.9(4)	F7'-F10-P2	49.3(3)
F10'-F10-P2'	66.5(4)	F7'-F10-P2'	59.3(3)	P2-F10-P2'	10.4(2)
F11'-F11-P2	79.8(6)	F11'-F11-F7'	124.8(8)	P2-F11-F7'	47.6(3)
F11'-F11-P2'	69.1(5)	P2-F11-P2'	10.7(3)	F7'-F11-P2'	57.9(3)
P2'-F12-P2	11.4(3)	F9-P2'-F8	104.4(5)	F9-P2'-F12	103.2(5)
F8-P2'-F12	92.4(4)	F9-P2'-F12'	112.7(5)	F8-P2'-F12'	91.9(7)
F12-P2'-F12'	9.8(5)	F9-P2'-F8'	118.2(4)	F8-P2'-F8'	14.5(4)
F12-P2'-F8'	93.0(7)	F12'-P2'-F8'	90.0	F9-P2'-F7'	142.4(4)
F8-P2'-F7'	104.3(4)	F12-P2'-F7'	99.3(5)	F12'-P2'-F7'	90.0
F8'-P2'-F7'	90.0	F9-P2'-F10'	61.8(4)	F8-P2'-F10'	165.5(4)
F12-P2'-F10'	87.1(7)	F12'-P2'-F10'	90.0	F8'-P2'-F10'	180.0

F7'-P2'-F10'	90.0	F9-P2'-F9'	37.6(4)	F8-P2'-F9'	75.7(4)
F12-P2'-F9'	80.7(5)	F12'-P2'-F9'	90.0	F8'-P2'-F9'	90.0
F7'-P2'-F9'	180.0	F10'-P2'-F9'	90.0	F9-P2'-F11'	67.3(5)
F8-P2'-F11'	88.1(7)	F12-P2'-F11'	170.2(5)	F12'-P2'-F11'	180.0
F8'-P2'-F11'	90.0	F7'-P2'-F11'	90.0	F10'-P2'-F11'	90.0
F9'-P2'-F11'	90.0	F9-P2'-F11	97.9(5)	F8-P2'-F11	88.6(5)
F12-P2'-F11	157.9(5)	F12'-P2'-F11	148.2(3)	F8'-P2'-F11	82.7(5)
F7'-P2'-F11	59.2(3)	F10'-P2'-F11	97.3(5)	F9'-P2'-F11	120.7(3)
F11'-P2'-F11	31.8(3)	F9-P2'-F10	96.9(4)	F8-P2'-F10	158.2(5)
F12-P2'-F10	87.1(5)	F12'-P2'-F10	84.0(5)	F8'-P2'-F10	143.8(3)
F7'-P2'-F10	54.4(3)	F10'-P2'-F10	36.2(3)	F9'-P2'-F10	125.6(3)
F11'-P2'-F10	96.0(5)	F11-P2'-F10	83.9(3)	F9-P2'-F7	173.3(5)
F8-P2'-F7	81.0(3)	F12-P2'-F7	80.4(3)	F12'-P2'-F7	70.7(4)
F8'-P2'-F7	66.9(4)	F7'-P2'-F7	30.9(4)	F10'-P2'-F7	113.1(4)
F9'-P2'-F7	149.1(4)	F11'-P2'-F7	109.3(4)	F11-P2'-F7	78.0(3)
F10-P2'-F7	77.5(3)	F7-F7'-P2	88.0(7)	F7-F7'-F10	129.3(10)
P2-F7'-F10	68.8(4)	F7-F7'-P2'	92.1(6)	P2-F7'-P2'	4.1(3)
F10-F7'-P2'	66.2(3)	F7-F7'-F11	118.8(9)	P2-F7'-F11	65.3(4)
F10-F7'-F11	92.3(4)	P2'-F7'-F11	62.9(3)	P2-F8'-P2'	11.4(3)
F9-F9'-P2'	54.3(4)	F9-F9'-P2	57.1(4)	P2'-F9'-P2	2.8(2)
F10-F10'-F9	124.7(7)	F10-F10'-P2'	77.3(5)	F9-F10'-P2'	49.3(3)
F10-F10'-P2	66.8(4)	F9-F10'-P2	59.5(3)	P2'-F10'-P2	10.5(2)
F11-F11'-P2'	79.1(6)	F11-F11'-F9	124.4(8)	P2'-F11'-F9	47.5(3)
F11-F11'-P2	68.5(5)	P2'-F11'-P2	10.5(3)	F9-F11'-P2	57.6(3)
P2-F12'-P2'	11.4(3)				

A3.5 $Ru(biq)_2(5\text{-hexynenitrile})_2$ (Ru530B)

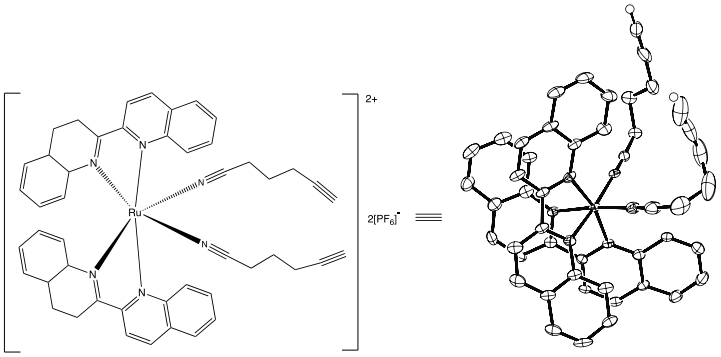

Compound 9724, $C_{48}H_{38}F_{12}N_6P_2Ru$, crystallizes in the monoclinic space group $P2_1$ (systematic absences 0k0: k=odd) with a=11.3357(9)Å, b=31.071(3)Å, c=12.8113(11)Å, β=99.628(5)°, °V=4448.7(7)$Å^3$, Z=4, and d_{calc}=1.627 g/cm_3 . X-ray intensity data were collected on a Bruker APEXII [1] CCD area detector employing graphite-monochromated Mo-Kα radiation (λ=0.71073Å) at a temperature of 100K. Preliminary indexing was performed from a series of thirty-six 0.5° rotation frames with exposures of 10 seconds. A total of 2249 frames were collected with a crystal to detector distance of 54.7 mm, rotation widths of 0.5° and exposures of 30 seconds:

scan type	2θ	ω	φ	χ	Frames
ϕ	-33.00	301.86	19.62	43.59	739
ϕ	29.50	108.32	6.43	-46.47	611
ϕ	34.50	311.98	167.97	65.91	196
ω	-23.00	321.68	226.55	-73.06	89
ω	29.50	119.68	26.51	-76.00	99
ϕ	-33.00	308.05	27.50	57.63	510

Rotation frames were integrated using SAINT [2], producing a listing of unaveraged F^2 and $\sigma(F^2)$ values. A total of 59533 reflections were measured over the ranges 3.224 ≤ 2θ ≤ 55.074°, -14 ≤ h ≤ 14, -40 ≤ k ≤ 40, -16 ≤ l ≤ 16 yielding 19666 unique reflections (R_{int} = 0.0541). The intensity data were corrected for Lorentz and polarization effects and for absorption using SADABS [3]

(minimum and maximum transmission 0.6698, 0.7456). The structure was solved by direct methods - ShelXS-97 [4]. Refinement was by full-matrix least squares based on F^2 using SHELXL-2017 [5]. All reflections were used during refinement. The weighting scheme used was $w=1/[\sigma^2(F_o^2)+ (0.0764P)^2 + 1.3878P]$ where $P = (F_o^2 + 2F_c^2)/3$. Non-hydrogen atoms were refined anisotropically and hydrogen atoms were refined using a riding model. Refinement converged to R1=0.0525 and wR2=0.1221 for 17036 observed reflections for which $F > 4\sigma(F)$ and R1=0.0660 and wR2=0.1322 and GOF =1.067 for all 19666 unique, non-zero reflections and 1243 variables. The maximum Δ/σ in the final cycle of least squares was 0.001 and the two most prominent peaks in the final difference Fourier were +1.63 and -0.79 e/Å^3.

Table 1. lists cell information, data collection parameters, and refinement data. Final positional and equivalent isotropic thermal parameters are given in Tables 2. and 3. Anisotropic thermal parameters are in Table 4. Tables 5. and 6. list bond distances and bond angles. Figures 1. and 2. are ORTEP representations of the molecule with 50% probability thermal ellipsoids displayed.

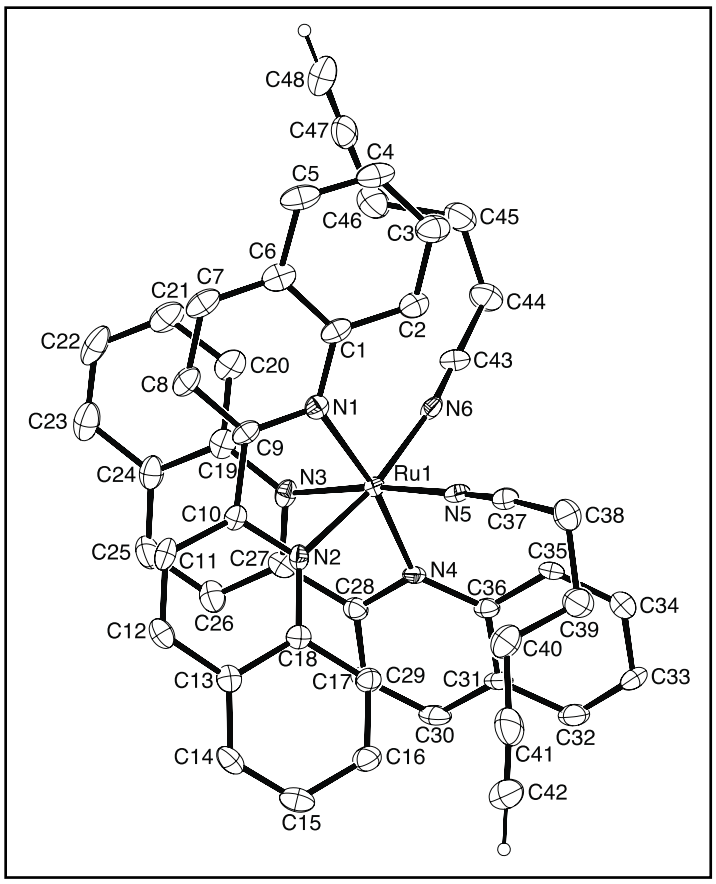

Figure 1. ORTEP drawing of molecule no.1 of the asymmetric unit with 50% thermal ellipsoids.

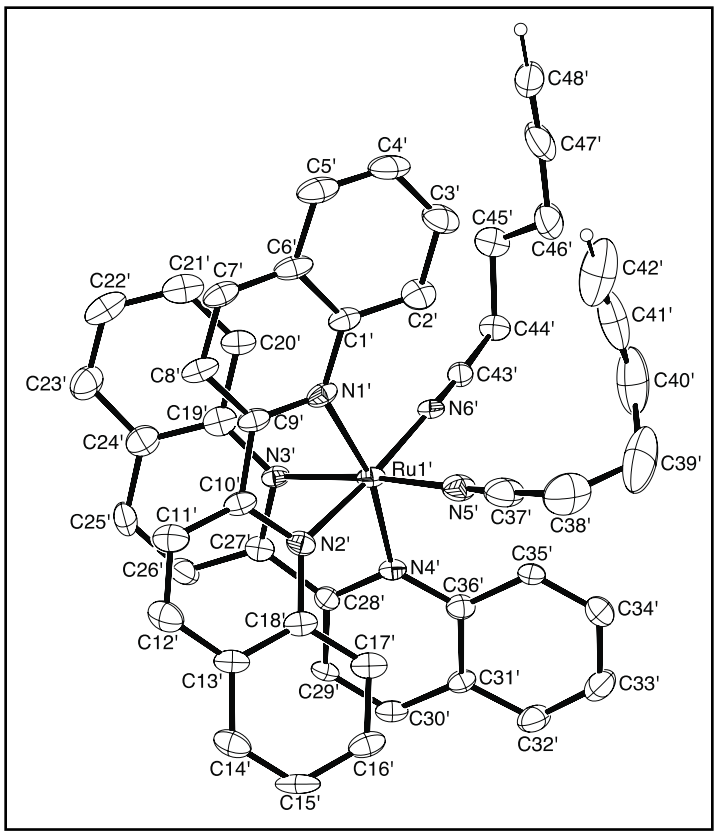

Figure 2. ORTEP drawing of molecule no.2 of the asymmetric unit with 50% thermal ellipsoids.

Table 1. Summary of Structure Determination of Compound 9724

Empirical formula	$C_{48}H_{38}F_{12}N_6P_2Ru$
Formula weight	1089.85
Temperature/K	100
Crystal system	monoclinic
Space group	$P2_1$
a	11.3357(9)Å
b	31.071(3)Å
c	12.8113(11)Å
β	99.628(5)°
Volume	4448.7(7)$Å^3$
Z	4

d_{calc}	1.627 g/cm^3
μ	0.519 mm^{-1}
F(000)	2200.0
Crystal size, mm	0.17 × 0.11 × 0.05
2θ range for data collection	3.224 - 55.074°
Index ranges	-14 ≤ h ≤ 14, -40 ≤ k ≤ 40, -16 ≤ l ≤ 16
Reflections collected	59533
Independent reflections	19666[R(int) = 0.0541]
Data/restraints/parameters	19666/73/1243
Goodness-of-fit on F^2	1.067
Final R indexes [I>=2σ (I)]	R_1 = 0.0525, wR_2 = 0.1221
Final R indexes [all data]	R_1 = 0.0660, wR_2 = 0.1322
Largest diff. peak/hole	1.63/-0.79 eÅ^{-3}
Flack parameter	0.066(10)

Table 2 . Refined Positional Parameters for Compound 9724

Atom	*x*	*y*	*z*	U(eq)
Ru1	0.31093(4)	0.11876(2)	0.38528(4)	0.01455(12)
N1	0.2676(5)	0.16227(19)	0.4954(4)	0.0168(12)
N2	0.4462(5)	0.1645(2)	0.3909(4)	0.0158(12)
N3	0.4401(5)	0.08681(19)	0.4925(4)	0.0181(12)
N4	0.3828(5)	0.07563(19)	0.2872(4)	0.0150(11)
N5	0.2012(5)	0.1521(2)	0.2726(4)	0.0175(12)
N6	0.1873(5)	0.0739(2)	0.4057(4)	0.0179(12)
C1	0.1620(6)	0.1658(2)	0.5347(5)	0.0206(15)
C2	0.0537(6)	0.1498(3)	0.4762(6)	0.0222(15)
C3	-0.0503(7)	0.1527(3)	0.5166(6)	0.0302(18)
C4	-0.0509(7)	0.1703(3)	0.6170(6)	0.0311(18)
C5	0.0508(8)	0.1865(3)	0.6753(7)	0.034(2)
C6	0.1609(7)	0.1854(2)	0.6343(6)	0.0233(16)
C7	0.2667(7)	0.2030(3)	0.6896(6)	0.0296(17)

C8	0.3680(7)	0.2040(3)	0.6437(6)	0.0257(16)
C9	0.3650(6)	0.1831(2)	0.5442(5)	0.0189(14)
C10	0.4668(6)	0.1840(2)	0.4860(5)	0.0157(13)
C11	0.5748(7)	0.2049(3)	0.5247(6)	0.0230(15)
C12	0.6616(6)	0.2071(2)	0.4625(6)	0.0219(15)
C13	0.6414(6)	0.1900(2)	0.3581(5)	0.0185(14)
C14	0.7243(6)	0.1930(3)	0.2884(6)	0.0247(16)
C15	0.6975(7)	0.1774(3)	0.1881(6)	0.0265(17)
C16	0.5829(6)	0.1594(3)	0.1520(6)	0.0246(16)
C17	0.5006(6)	0.1554(2)	0.2166(5)	0.0192(15)
C18	0.5279(6)	0.1696(2)	0.3237(5)	0.0167(14)
C19	0.4596(6)	0.0892(2)	0.6029(5)	0.0211(14)
C20	0.3639(7)	0.0956(2)	0.6562(6)	0.0247(15)
C21	0.3845(8)	0.1003(3)	0.7643(6)	0.0306(17)
C22	0.4991(8)	0.0979(3)	0.8217(6)	0.035(2)
C23	0.5941(8)	0.0903(3)	0.7726(6)	0.0325(18)
C24	0.5764(7)	0.0840(3)	0.6610(6)	0.0252(16)
C25	0.6713(6)	0.0736(3)	0.6040(6)	0.0307(18)
C26	0.6472(6)	0.0659(3)	0.4991(6)	0.0258(16)
C27	0.5288(6)	0.0724(2)	0.4444(6)	0.0213(15)
C28	0.4942(6)	0.0638(2)	0.3298(5)	0.0180(14)
C29	0.5715(6)	0.0415(2)	0.2714(6)	0.0224(15)
C30	0.5323(6)	0.0327(3)	0.1676(6)	0.0240(16)
C31	0.4153(6)	0.0435(2)	0.1203(5)	0.0200(14)
C32	0.3689(6)	0.0346(3)	0.0120(6)	0.0264(16)
C33	0.2545(6)	0.0449(3)	-0.0295(5)	0.0278(17)
C34	0.1784(6)	0.0635(3)	0.0347(6)	0.0255(16)
C35	0.2200(5)	0.0724(2)	0.1386(5)	0.0195(14)
C36	0.3399(6)	0.0638(2)	0.1840(5)	0.0171(13)
C37	0.1397(6)	0.1701(3)	0.2061(5)	0.0207(15)
C38	0.0716(6)	0.1925(3)	0.1140(6)	0.0261(16)
C39	0.1485(7)	0.1978(3)	0.0271(6)	0.0320(19)

C40	0.2573(7)	0.2257(3)	0.0634(6)	0.0320(18)
C41	0.3421(8)	0.2284(4)	-0.0114(7)	0.044(2)
C42	0.4155(8)	0.2307(5)	-0.0645(7)	0.057(3)
C43	0.1239(6)	0.0488(3)	0.4301(6)	0.0228(15)
C44	0.0396(7)	0.0168(3)	0.4611(6)	0.0302(17)
C45	-0.0244(7)	0.0336(3)	0.5485(6)	0.0318(18)
C46	0.0580(7)	0.0390(4)	0.6551(7)	0.046(3)
C47	0.0041(7)	0.0613(4)	0.7351(6)	0.040(2)
C48	-0.0407(9)	0.0802(4)	0.7976(7)	0.051(3)
P1	0.86894(17)	0.05574(7)	0.15623(19)	0.0300(5)
F1	0.8935(4)	0.0436(2)	0.0405(4)	0.0455(13)
F2	0.9426(5)	0.09927(19)	0.1536(6)	0.0591(17)
F3	0.8447(4)	0.0671(2)	0.2729(5)	0.0546(16)
F4	0.7966(4)	0.01165(15)	0.1589(4)	0.0385(12)
F5	0.7487(4)	0.07959(18)	0.1050(5)	0.0504(15)
F6	0.9892(4)	0.03091(17)	0.2076(4)	0.0349(11)
P2	0.75523(18)	0.20797(8)	0.86053(16)	0.0300(5)
F7	0.7256(5)	0.1767(2)	0.7626(4)	0.0482(14)
F8	0.8409(5)	0.2346(2)	0.7989(5)	0.0523(15)
F9	0.7877(8)	0.2384(3)	0.9602(6)	0.095(3)
F10	0.6709(5)	0.1810(2)	0.9233(4)	0.0486(14)
F11	0.6433(6)	0.2373(2)	0.8102(6)	0.0700(19)
F12	0.8637(6)	0.1770(3)	0.9032(6)	0.084(2)
Ru1'	0.44114(4)	0.38239(2)	0.87854(4)	0.01936(13)
N1'	0.2945(5)	0.3407(2)	0.8678(5)	0.0229(14)
N2'	0.4701(5)	0.3405(2)	0.7609(5)	0.0216(13)
N3'	0.3585(5)	0.41924(19)	0.7520(5)	0.0178(12)
N4'	0.5779(5)	0.4230(2)	0.8494(5)	0.0188(12)
N5'	0.5308(6)	0.3429(2)	0.9904(5)	0.0287(15)
N6'	0.4013(5)	0.4270(2)	0.9843(5)	0.0219(14)
C1'	0.2160(6)	0.3343(2)	0.9382(6)	0.0229(16)
C2'	0.2451(7)	0.3486(3)	1.0431(6)	0.0294(18)

C3'	0.1658(7)	0.3425(3)	1.1128(7)	0.036(2)
C4'	0.0562(7)	0.3226(3)	1.0787(8)	0.039(2)
C5'	0.0265(7)	0.3075(3)	0.9785(7)	0.036(2)
C6'	0.1063(6)	0.3128(3)	0.9046(7)	0.0285(18)
C7'	0.0810(6)	0.2965(3)	0.8011(7)	0.0273(17)
C8'	0.1613(6)	0.3009(3)	0.7333(7)	0.0275(17)
C9'	0.2708(6)	0.3233(2)	0.7706(6)	0.0221(15)
C10'	0.3676(6)	0.3250(2)	0.7082(6)	0.0223(15)
C11'	0.3553(7)	0.3107(3)	0.6039(7)	0.0294(17)
C12'	0.4522(8)	0.3106(3)	0.5552(7)	0.0337(19)
C13'	0.5661(6)	0.3213(3)	0.6125(6)	0.0274(17)
C14'	0.6735(7)	0.3173(3)	0.5696(7)	0.0314(18)
C15'	0.7808(7)	0.3259(3)	0.6294(8)	0.037(2)
C16'	0.7872(6)	0.3382(3)	0.7360(7)	0.0290(17)
C17'	0.6861(6)	0.3430(2)	0.7806(7)	0.0255(16)
C18'	0.5743(6)	0.3356(2)	0.7178(6)	0.0236(16)
C19'	0.2395(6)	0.4193(2)	0.7113(6)	0.0244(15)
C20'	0.1527(6)	0.4150(2)	0.7781(6)	0.0239(15)
C21'	0.0363(7)	0.4110(3)	0.7375(7)	0.0332(19)
C22'	-0.0035(7)	0.4117(3)	0.6287(8)	0.039(2)
C23'	0.0770(7)	0.4192(3)	0.5632(7)	0.036(2)
C24'	0.1996(7)	0.4239(3)	0.6023(7)	0.0307(18)
C25'	0.2862(7)	0.4342(3)	0.5366(6)	0.0322(19)
C26'	0.4034(7)	0.4400(3)	0.5811(6)	0.0285(17)
C27'	0.4381(6)	0.4316(2)	0.6909(6)	0.0199(14)
C28'	0.5595(6)	0.4370(2)	0.7485(5)	0.0183(14)
C29'	0.6513(6)	0.4576(2)	0.7034(5)	0.0187(14)
C30'	0.7593(6)	0.4644(2)	0.7650(6)	0.0228(15)
C31'	0.7798(6)	0.4525(2)	0.8718(6)	0.0208(14)
C32'	0.8890(6)	0.4606(3)	0.9419(6)	0.0319(18)
C33'	0.9018(7)	0.4502(3)	1.0451(7)	0.042(2)
C34'	0.8065(7)	0.4313(3)	1.0878(6)	0.036(2)

C35'	0.7008(6)	0.4227(3)	1.0231(6)	0.0270(17)
C36'	0.6835(6)	0.4326(2)	0.9139(6)	0.0217(15)
C37'	0.5760(8)	0.3182(3)	1.0493(8)	0.042(2)
C38'	0.6325(10)	0.2885(4)	1.1330(9)	0.059(3)
C39'	0.6488(14)	0.3120(5)	1.2404(11)	0.088(5)
C40'	0.5392(14)	0.3303(4)	1.2709(9)	0.078(4)
C41'	0.4442(14)	0.2980(5)	1.2845(8)	0.069(4)
C42'	0.3712(14)	0.2706(5)	1.2956(11)	0.084(5)
C43'	0.3797(6)	0.4549(3)	1.0355(5)	0.0218(15)
C44'	0.3466(7)	0.4903(3)	1.0987(6)	0.0300(17)
C45'	0.2335(8)	0.4809(4)	1.1431(7)	0.044(2)
C46'	0.2550(9)	0.4480(4)	1.2318(7)	0.053(3)
C47'	0.1452(10)	0.4341(4)	1.2660(7)	0.058(3)
C48'	0.0560(9)	0.4199(5)	1.2881(8)	0.070(4)
P1'	0.63953(19)	0.45801(8)	0.35168(17)	0.0337(5)
F1'	0.7659(6)	0.4376(3)	0.3486(5)	0.070(2)
F2'	0.6687(6)	0.4946(2)	0.2735(5)	0.0606(16)
F3'	0.5134(5)	0.4798(2)	0.3574(5)	0.0644(18)
F4'	0.6108(6)	0.4215(2)	0.4301(5)	0.0611(17)
F5'	0.6940(5)	0.4872(2)	0.4506(5)	0.0612(17)
F6'	0.5803(7)	0.4305(2)	0.2507(5)	0.070(2)
P2'	0.0134(2)	0.28833(8)	0.39060(17)	0.0364(5)
F7'	0.1199(7)	0.3090(3)	0.3474(6)	0.091(2)
F8'	-0.0022(9)	0.2517(4)	0.3067(7)	0.112(3)
F9'	-0.0962(6)	0.2690(3)	0.4355(5)	0.072(2)
F10'	0.0329(8)	0.3229(3)	0.4826(8)	0.104(3)
F11'	0.1024(8)	0.2593(3)	0.4689(7)	0.090(2)
F12'	-0.0685(8)	0.3183(4)	0.3131(8)	0.120(3)

Table 3 . Positional Parameters for Hydrogens in Compound 9724

Atom	***x***	***y***	***z***	**U(eq)**

H2	0.053372	0.137043	0.408735	0.03
H3	-0.12298	0.142593	0.47608	0.04
H4	-0.123375	0.170874	0.645052	0.041
H5	0.048853	0.198585	0.743064	0.046
H7	0.268683	0.2142	0.758843	0.039
H8	0.438219	0.218222	0.677429	0.034
H11	0.587454	0.2175	0.593268	0.031
H12	0.73636	0.220072	0.489455	0.029
H14	0.800001	0.205964	0.311631	0.033
H15	0.755271	0.178677	0.142329	0.035
H16	0.563646	0.149823	0.080691	0.033
H17	0.424578	0.143076	0.190665	0.026
H20	0.28453	0.096809	0.617964	0.033
H21	0.318912	0.10518	0.80031	0.041
H22	0.511367	0.101697	0.896373	0.046
H23	0.672529	0.089257	0.812603	0.043
H25	0.751482	0.072272	0.640339	0.041
H26	0.708342	0.056152	0.46237	0.034
H29	0.649306	0.032997	0.304459	0.03
H30	0.584367	0.019176	0.126717	0.032
H32	0.418673	0.021358	-0.031478	0.035
H33	0.225297	0.039503	-0.102284	0.037
H34	0.097671	0.069828	0.005359	0.034
H35	0.167414	0.084591	0.181123	0.026
H38a	0.046396	0.221161	0.135822	0.035
H38b	-0.001195	0.175776	0.086124	0.035
H39a	0.174932	0.16906	0.006674	0.043
H39b	0.09963	0.210915	-0.036114	0.043
H40a	0.229791	0.255109	0.076703	0.043
H40b	0.300004	0.214252	0.13149	0.043
H42	0.475518	0.232507	-0.107906	0.076
H44a	0.083963	-0.009704	0.485811	0.04

H44b	-0.020517	0.009334	0.398423	0.04
H45a	-0.089591	0.013472	0.55737	0.042
H45b	-0.061276	0.061797	0.526489	0.042
H46a	0.084403	0.010195	0.682367	0.062
H46b	0.130109	0.055155	0.643638	0.062
H48	-0.076895	0.095434	0.848201	0.068
H2'	0.319526	0.362518	1.066357	0.039
H3'	0.186216	0.351851	1.184075	0.048
H4'	0.001082	0.319542	1.126571	0.052
H5'	-0.047854	0.293283	0.957413	0.048
H7'	0.007062	0.282275	0.77792	0.036
H8'	0.145201	0.289365	0.663649	0.037
H11'	0.279962	0.301126	0.567479	0.039
H12'	0.4438	0.303453	0.482247	0.045
H14'	0.669753	0.308356	0.498221	0.042
H15'	0.851816	0.32377	0.599483	0.049
H16'	0.863235	0.343329	0.778003	0.039
H17'	0.691801	0.351117	0.852793	0.034
H20'	0.177237	0.414862	0.85276	0.032
H21'	-0.020143	0.407724	0.783927	0.044
H22'	-0.08552	0.407007	0.600697	0.052
H23'	0.049558	0.42139	0.489157	0.048
H25'	0.262207	0.437099	0.462202	0.043
H26'	0.460332	0.449505	0.539549	0.038
H29'	0.637121	0.46651	0.631472	0.025
H30'	0.821723	0.477484	0.735114	0.03
H32'	0.95381	0.473535	0.915259	0.042
H33'	0.975859	0.45554	1.090058	0.056
H34'	0.816177	0.424598	1.161085	0.048
H35'	0.637521	0.409709	1.05206	0.036
H38a'	0.711157	0.278911	1.117753	0.079
H38b'	0.581383	0.262758	1.135182	0.079

H39a'	0.684184	0.29151	1.296172	0.118
H39b'	0.707162	0.335579	1.238834	0.118
H40a'	0.504711	0.351381	1.216217	0.103
H40b'	0.561698	0.346221	1.338271	0.103
H42'	0.314089	0.249077	1.30428	0.112
H44a'	0.334446	0.516503	1.054423	0.04
H44b'	0.412928	0.495929	1.157869	0.04
H45a'	0.203564	0.507877	1.170236	0.058
H45b'	0.171296	0.469911	1.085777	0.058
H46a'	0.295777	0.422636	1.207487	0.071
H46b'	0.308871	0.460646	1.292873	0.071
H48'	-0.015815	0.408491	1.305818	0.093

Table 4 . Refined Thermal Parameters (U's) for Compound 9724

Atom	U_{11}	U_{22}	U_{33}	U_{23}	U_{13}	U_{12}
Ru1	0.0138(2)	0.0178(3)	0.0124(2)	-0.0008(2)	0.00322(17)	-0.0004(2)
N1	0.019(3)	0.016(3)	0.016(3)	0.003(2)	0.002(2)	0.002(2)
N2	0.016(3)	0.016(3)	0.014(3)	0.001(2)	-0.002(2)	-0.002(2)
N3	0.024(3)	0.015(3)	0.015(3)	0.000(2)	-0.001(2)	-0.002(2)
N4	0.014(2)	0.018(3)	0.015(3)	-0.001(2)	0.007(2)	-0.002(2)
N5	0.019(3)	0.021(3)	0.015(3)	-0.001(2)	0.009(2)	0.001(2)
N6	0.022(3)	0.022(3)	0.010(3)	-0.003(2)	0.003(2)	0.000(2)
C1	0.032(4)	0.015(4)	0.016(3)	0.006(3)	0.008(3)	0.004(3)
C2	0.025(3)	0.022(4)	0.020(3)	0.003(3)	0.006(3)	0.008(3)
C3	0.029(4)	0.035(5)	0.028(4)	0.007(3)	0.009(3)	0.009(3)
C4	0.036(4)	0.033(5)	0.029(4)	0.005(4)	0.018(3)	0.011(4)
C5	0.042(5)	0.033(5)	0.033(4)	-0.002(4)	0.022(4)	0.008(4)
C6	0.033(4)	0.013(4)	0.026(4)	0.004(3)	0.010(3)	0.008(3)
C7	0.045(5)	0.025(4)	0.022(4)	-0.005(3)	0.012(3)	0.004(4)
C8	0.035(4)	0.023(4)	0.019(3)	-0.008(3)	0.005(3)	-0.001(3)
C9	0.028(3)	0.016(4)	0.014(3)	0.004(3)	0.006(3)	0.001(3)

C10	0.021(3)	0.011(3)	0.014(3)	0.003(2)	0.001(2)	-0.002(3)
C11	0.029(4)	0.022(4)	0.016(3)	-0.003(3)	-0.004(3)	0.002(3)
C12	0.017(3)	0.017(4)	0.030(4)	0.000(3)	0.000(3)	0.000(3)
C13	0.019(3)	0.014(4)	0.022(3)	0.000(3)	0.001(3)	0.004(3)
C14	0.016(3)	0.026(4)	0.032(4)	0.003(3)	0.003(3)	-0.005(3)
C15	0.025(4)	0.022(4)	0.036(4)	0.005(3)	0.014(3)	0.000(3)
C16	0.027(4)	0.026(4)	0.022(4)	-0.005(3)	0.009(3)	-0.002(3)
C17	0.021(3)	0.019(4)	0.017(3)	0.003(3)	0.004(3)	-0.001(3)
C18	0.018(3)	0.014(4)	0.018(3)	0.003(3)	0.003(3)	0.002(3)
C19	0.029(4)	0.012(4)	0.022(3)	0.003(3)	0.002(3)	-0.005(3)
C20	0.038(4)	0.014(4)	0.022(3)	0.008(3)	0.006(3)	-0.004(3)
C21	0.048(5)	0.024(4)	0.022(4)	0.005(3)	0.011(3)	-0.005(4)
C22	0.063(6)	0.024(4)	0.015(3)	0.002(3)	0.000(4)	-0.013(4)
C23	0.043(4)	0.027(5)	0.023(4)	0.003(3)	-0.006(3)	-0.007(4)
C24	0.030(4)	0.022(4)	0.021(4)	0.003(3)	-0.004(3)	-0.001(3)
C25	0.020(3)	0.041(5)	0.029(4)	0.003(4)	-0.005(3)	-0.002(3)
C26	0.022(3)	0.024(4)	0.029(4)	-0.003(3)	-0.001(3)	0.002(3)
C27	0.018(3)	0.020(4)	0.027(4)	0.000(3)	0.005(3)	-0.001(3)
C28	0.017(3)	0.018(4)	0.020(3)	0.000(3)	0.005(3)	-0.002(3)
C29	0.015(3)	0.022(4)	0.031(4)	0.000(3)	0.006(3)	-0.002(3)
C30	0.022(3)	0.025(4)	0.029(4)	-0.004(3)	0.015(3)	0.001(3)
C31	0.020(3)	0.022(4)	0.020(3)	-0.002(3)	0.012(3)	-0.002(3)
C32	0.027(4)	0.030(5)	0.026(4)	-0.007(3)	0.015(3)	-0.005(3)
C33	0.030(4)	0.041(5)	0.014(3)	-0.004(3)	0.009(3)	-0.007(3)
C34	0.018(3)	0.033(5)	0.026(4)	-0.001(3)	0.003(3)	-0.002(3)
C35	0.013(3)	0.028(4)	0.019(3)	-0.001(3)	0.008(2)	-0.001(3)
C36	0.019(3)	0.016(4)	0.019(3)	-0.004(3)	0.009(3)	-0.002(3)
C37	0.019(3)	0.025(4)	0.019(3)	-0.003(3)	0.007(3)	0.002(3)
C38	0.024(3)	0.024(4)	0.030(4)	0.002(3)	0.001(3)	0.001(3)
C39	0.026(4)	0.044(5)	0.026(4)	0.012(4)	0.003(3)	0.001(4)
C40	0.038(4)	0.035(5)	0.022(4)	0.006(3)	0.001(3)	0.002(4)
C41	0.028(4)	0.064(7)	0.034(5)	0.010(5)	-0.008(4)	0.000(4)

C42	0.035(5)	0.110(11)	0.028(5)	-0.008(5)	0.009(4)	0.003(5)
C43	0.023(3)	0.027(4)	0.022(3)	0.000(3)	0.011(3)	0.001(3)
C44	0.028(4)	0.030(5)	0.034(4)	0.004(3)	0.010(3)	-0.006(3)
C45	0.024(4)	0.037(5)	0.035(4)	0.005(4)	0.007(3)	-0.004(3)
C46	0.024(4)	0.079(8)	0.035(5)	0.007(5)	0.003(3)	-0.002(4)
C47	0.027(4)	0.067(7)	0.023(4)	0.014(4)	-0.005(3)	-0.010(4)
C48	0.046(5)	0.078(8)	0.025(4)	-0.005(5)	-0.005(4)	-0.003(5)
P1	0.0169(8)	0.0265(12)	0.0485(13)	-0.0034(9)	0.0108(8)	-0.0011(8)
F1	0.026(2)	0.064(4)	0.047(3)	-0.001(3)	0.006(2)	0.004(2)
F2	0.035(3)	0.034(3)	0.112(5)	-0.004(3)	0.024(3)	-0.011(2)
F3	0.037(3)	0.063(4)	0.069(4)	-0.026(3)	0.024(3)	-0.001(3)
F4	0.021(2)	0.023(3)	0.072(4)	0.001(2)	0.007(2)	-0.0019(18)
F5	0.028(2)	0.035(3)	0.092(4)	0.019(3)	0.019(3)	0.009(2)
F6	0.017(2)	0.044(3)	0.043(3)	-0.006(2)	0.0046(18)	0.0027(19)
P2	0.0266(10)	0.0377(13)	0.0274(10)	-0.0045(9)	0.0096(8)	-0.0108(9)
F7	0.054(3)	0.057(4)	0.036(3)	-0.011(2)	0.016(2)	-0.025(3)
F8	0.053(3)	0.048(3)	0.065(3)	-0.007(3)	0.039(3)	-0.018(3)
F9	0.114(5)	0.109(5)	0.074(4)	-0.051(4)	0.046(4)	-0.066(4)
F10	0.062(3)	0.053(3)	0.036(3)	0.006(2)	0.023(2)	-0.014(3)
F11	0.058(3)	0.060(4)	0.100(4)	0.024(3)	0.036(3)	0.014(3)
F12	0.063(4)	0.099(5)	0.085(4)	0.018(4)	-0.004(3)	0.015(4)
Ru1'	0.0159(2)	0.0186(3)	0.0253(3)	0.0025(2)	0.0084(2)	-0.0007(2)
N1'	0.015(3)	0.020(4)	0.033(3)	0.010(3)	0.004(2)	0.001(2)
N2'	0.024(3)	0.019(3)	0.023(3)	0.003(2)	0.008(2)	0.000(2)
N3'	0.015(3)	0.014(3)	0.025(3)	-0.002(2)	0.006(2)	-0.003(2)
N4'	0.016(3)	0.019(3)	0.023(3)	-0.001(2)	0.007(2)	0.001(2)
N5'	0.027(3)	0.030(4)	0.032(4)	0.010(3)	0.011(3)	0.001(3)
N6'	0.013(3)	0.032(4)	0.022(3)	0.001(3)	0.007(2)	-0.002(2)
C1'	0.017(3)	0.019(4)	0.034(4)	0.009(3)	0.007(3)	0.002(3)
C2'	0.032(4)	0.022(4)	0.035(4)	0.008(3)	0.010(3)	-0.007(3)
C3'	0.040(5)	0.039(6)	0.034(4)	0.011(4)	0.018(4)	0.001(4)
C4'	0.028(4)	0.045(6)	0.050(6)	0.015(5)	0.021(4)	0.003(4)

C5'	0.024(4)	0.031(5)	0.056(6)	0.018(4)	0.016(4)	0.002(3)
C6'	0.019(3)	0.018(4)	0.050(5)	0.009(4)	0.013(3)	0.001(3)
C7'	0.017(3)	0.020(4)	0.045(5)	0.008(3)	0.007(3)	0.003(3)
C8'	0.018(3)	0.019(4)	0.047(5)	-0.002(3)	0.009(3)	-0.001(3)
C9'	0.017(3)	0.016(4)	0.034(4)	0.003(3)	0.008(3)	0.003(3)
C10'	0.018(3)	0.014(4)	0.036(4)	-0.001(3)	0.008(3)	0.003(3)
C11'	0.030(4)	0.021(4)	0.040(5)	-0.004(3)	0.014(3)	-0.004(3)
C12'	0.042(5)	0.027(5)	0.035(4)	-0.013(4)	0.016(4)	-0.007(4)
C13'	0.025(4)	0.025(4)	0.036(4)	0.002(3)	0.016(3)	0.001(3)
C14'	0.040(4)	0.024(5)	0.035(4)	-0.008(3)	0.020(4)	0.000(3)
C15'	0.027(4)	0.032(5)	0.058(6)	-0.004(4)	0.029(4)	-0.002(3)
C16'	0.020(3)	0.023(4)	0.046(5)	0.005(4)	0.009(3)	0.005(3)
C17'	0.026(4)	0.014(4)	0.039(4)	0.002(3)	0.014(3)	0.001(3)
C18'	0.022(3)	0.016(4)	0.035(4)	0.002(3)	0.011(3)	0.002(3)
C19'	0.027(4)	0.010(4)	0.037(4)	0.000(3)	0.008(3)	0.001(3)
C20'	0.024(3)	0.014(4)	0.037(4)	0.001(3)	0.012(3)	0.003(3)
C21'	0.030(4)	0.019(4)	0.053(5)	0.009(4)	0.015(4)	0.003(3)
C22'	0.021(4)	0.030(5)	0.066(6)	0.004(4)	0.004(4)	-0.002(3)
C23'	0.029(4)	0.039(5)	0.039(5)	0.011(4)	0.000(3)	0.003(4)
C24'	0.028(4)	0.026(5)	0.038(5)	0.001(4)	0.005(3)	0.006(3)
C25'	0.036(4)	0.043(5)	0.016(3)	0.000(3)	0.000(3)	-0.003(4)
C26'	0.030(4)	0.035(5)	0.023(4)	0.004(3)	0.011(3)	0.003(3)
C27'	0.023(3)	0.013(4)	0.025(4)	0.000(3)	0.008(3)	-0.001(3)
C28'	0.020(3)	0.017(4)	0.019(3)	-0.002(3)	0.005(3)	0.002(3)
C29'	0.020(3)	0.019(4)	0.019(3)	0.003(3)	0.011(3)	0.001(3)
C30'	0.020(3)	0.020(4)	0.031(4)	0.002(3)	0.012(3)	-0.001(3)
C31'	0.016(3)	0.020(4)	0.027(4)	0.001(3)	0.005(3)	-0.005(3)
C32'	0.021(3)	0.039(5)	0.037(4)	0.011(4)	0.006(3)	-0.002(3)
C33'	0.021(4)	0.065(7)	0.038(5)	0.009(5)	-0.001(3)	-0.005(4)
C34'	0.033(4)	0.055(6)	0.022(4)	0.008(4)	0.007(3)	-0.004(4)
C35'	0.018(3)	0.043(5)	0.021(4)	0.004(3)	0.008(3)	-0.004(3)
C36'	0.022(3)	0.019(4)	0.025(4)	0.004(3)	0.007(3)	0.000(3)

C37'	0.036(5)	0.049(6)	0.045(5)	0.017(5)	0.018(4)	0.004(4)
C38'	0.052(6)	0.053(7)	0.073(8)	0.031(6)	0.011(5)	0.021(5)
C39'	0.091(11)	0.089(12)	0.067(9)	0.027(8)	-0.039(8)	-0.015(9)
C40'	0.119(12)	0.055(8)	0.045(7)	0.001(6)	-0.029(7)	0.020(8)
C41'	0.118(11)	0.056(8)	0.025(5)	-0.009(5)	-0.006(6)	0.007(8)
C42'	0.094(11)	0.058(9)	0.082(10)	-0.013(8)	-0.039(8)	0.007(8)
C43'	0.019(3)	0.026(4)	0.020(3)	0.002(3)	0.004(3)	-0.006(3)
C44'	0.025(4)	0.039(5)	0.028(4)	-0.001(3)	0.009(3)	0.003(3)
C45'	0.034(4)	0.066(7)	0.035(5)	-0.004(5)	0.012(4)	-0.003(4)
C46'	0.043(5)	0.092(9)	0.024(4)	0.010(5)	0.003(4)	-0.019(5)
C47'	0.060(6)	0.097(10)	0.020(4)	0.002(5)	0.010(4)	-0.027(6)
C48'	0.035(5)	0.144(13)	0.029(5)	0.013(6)	0.000(4)	-0.027(6)
P1'	0.0339(11)	0.0397(14)	0.0296(11)	-0.0008(9)	0.0112(9)	-0.0008(9)
F1'	0.065(4)	0.093(6)	0.059(4)	0.024(4)	0.034(3)	0.039(4)
F2'	0.086(4)	0.051(4)	0.050(3)	0.004(3)	0.024(3)	-0.015(3)
F3'	0.044(3)	0.087(5)	0.063(4)	-0.008(4)	0.011(3)	0.007(3)
F4'	0.093(5)	0.047(4)	0.054(4)	0.006(3)	0.043(3)	-0.002(3)
F5'	0.060(4)	0.077(5)	0.045(3)	-0.014(3)	0.006(3)	-0.016(3)
F6'	0.100(5)	0.069(5)	0.044(3)	-0.019(3)	0.021(3)	-0.035(4)
P2'	0.0381(12)	0.0436(15)	0.0277(11)	0.0065(10)	0.0065(9)	-0.0084(10)
F7'	0.077(4)	0.111(5)	0.091(4)	0.035(4)	0.036(4)	-0.018(4)
F8'	0.118(5)	0.131(6)	0.091(5)	-0.054(4)	0.035(4)	-0.021(5)
F9'	0.073(4)	0.086(5)	0.064(4)	-0.005(3)	0.031(3)	-0.030(3)
F10'	0.110(5)	0.093(5)	0.113(5)	-0.033(4)	0.027(4)	-0.030(4)
F11'	0.094(5)	0.073(5)	0.098(5)	0.019(4)	-0.005(4)	-0.001(4)
F12'	0.086(5)	0.137(6)	0.130(6)	0.050(5)	-0.005(4)	0.014(5)

Table 5 . Bond Distances in Compound 9724, Å

Ru1-N1	2.072(6)	Ru1-N2	2.084(6)	Ru1-N3	2.084(6)
Ru1-N4	2.093(6)	Ru1-N5	2.025(6)	Ru1-N6	2.024(6)
N1-C1	1.378(9)	N1-C9	1.341(9)	N2-C10	1.346(9)

N2-C18	1.375(8)	N3-C19	1.397(9)	N3-C27	1.340(9)
N4-C28	1.341(8)	N4-C36	1.380(8)	N5-C37	1.153(9)
N6-C43	1.140(9)	C1-C2	1.418(10)	C1-C6	1.415(10)
C2-C3	1.368(10)	C3-C4	1.399(11)	C4-C5	1.362(13)
C5-C6	1.432(10)	C6-C7	1.398(12)	C7-C8	1.375(11)
C8-C9	1.425(10)	C9-C10	1.474(9)	C10-C11	1.402(10)
C11-C12	1.368(10)	C12-C13	1.422(10)	C13-C14	1.404(10)
C13-C18	1.435(9)	C14-C15	1.358(11)	C15-C16	1.420(10)
C16-C17	1.354(9)	C17-C18	1.425(10)	C19-C20	1.390(10)
C19-C24	1.416(10)	C20-C21	1.374(10)	C21-C22	1.384(12)
C22-C23	1.356(12)	C23-C24	1.423(10)	C24-C25	1.434(11)
C25-C26	1.347(11)	C26-C27	1.422(10)	C27-C28	1.480(10)
C28-C29	1.423(10)	C29-C30	1.358(10)	C30-C31	1.404(10)
C31-C32	1.427(10)	C31-C36	1.424(9)	C32-C33	1.355(11)
C33-C34	1.412(10)	C34-C35	1.365(10)	C35-C36	1.412(9)
C37-C38	1.472(10)	C38-C39	1.533(10)	C39-C40	1.516(12)
C40-C41	1.469(12)	C41-C42	1.161(13)	C43-C44	1.477(10)
C44-C45	1.525(11)	C45-C46	1.529(12)	C46-C47	1.452(14)
C47-C48	1.175(14)	P1-F1	1.599(6)	P1-F2	1.593(6)
P1-F3	1.604(6)	P1-F4	1.600(5)	P1-F5	1.593(5)
P1-F6	1.608(5)	P2-F7	1.579(6)	P2-F8	1.584(5)
P2-F9	1.581(7)	P2-F10	1.587(5)	P2-F11	1.607(7)
P2-F12	1.584(8)	Ru1'-N1'	2.094(6)	Ru1'-N2'	2.060(6)
Ru1'-N3'	2.076(6)	Ru1'-N4'	2.080(6)	Ru1'-N5'	2.027(7)
Ru1'-N6'	2.040(6)	N1'-C1'	1.383(9)	N1'-C9'	1.343(10)
N2'-C10'	1.332(9)	N2'-C18'	1.393(9)	N3'-C19'	1.362(9)
N3'-C27'	1.346(8)	N4'-C28'	1.348(9)	N4'-C36'	1.369(9)
N5'-C37'	1.137(11)	N6'-C43'	1.139(10)	C1'-C2'	1.402(11)
C1'-C6'	1.414(10)	C2'-C3'	1.382(10)	C3'-C4'	1.391(13)
C4'-C5'	1.356(14)	C5'-C6'	1.424(11)	C6'-C7'	1.404(12)
C7'-C8'	1.367(10)	C8'-C9'	1.434(10)	C9'-C10'	1.463(10)
C10'-C11'	1.393(11)	C11'-C12'	1.350(11)	C12'-C13'	1.413(11)

C13'-C14'	1.422(10)	C13'-C18'	1.410(11)	C14'-C15'	1.352(12)
C15'-C16'	1.409(12)	C16'-C17'	1.371(10)	C17'-C18'	1.402(11)
C19'-C20'	1.414(10)	C19'-C24'	1.402(11)	C20'-C21'	1.341(11)
C21'-C22'	1.391(13)	C22'-C23'	1.359(12)	C23'-C24'	1.404(11)
C24'-C25'	1.432(11)	C25'-C26'	1.367(11)	C26'-C27'	1.420(10)
C27'-C28'	1.458(10)	C28'-C29'	1.423(9)	C29'-C30'	1.357(10)
C30'-C31'	1.399(10)	C31'-C32'	1.424(10)	C31'-C36'	1.436(9)
C32'-C33'	1.346(12)	C33'-C34'	1.417(11)	C34'-C35'	1.364(11)
C35'-C36'	1.415(10)	C37'-C38'	1.476(13)	C38'-C39'	1.542(19)
C39'-C40'	1.48(2)	C40'-C41'	1.50(2)	C41'-C42'	1.21(2)
C43'-C44'	1.450(11)	C44'-C45'	1.515(11)	C45'-C46'	1.516(14)
C46'-C47'	1.453(13)	C47'-C48'	1.180(14)	P1'-F1'	1.574(6)
P1'-F2'	1.587(6)	P1'-F3'	1.595(6)	P1'-F4'	1.585(6)
P1'-F5'	1.597(6)	P1'-F6'	1.601(7)	P2'-F7'	1.549(7)
P2'-F8'	1.555(9)	P2'-F9'	1.574(6)	P2'-F10'	1.583(9)
P2'-F11'	1.582(8)	P2'-F12'	1.552(9)		

Table 6 . Bond Angles in Compound 9724, °

N1-Ru1-N2	77.8(2)	N1-Ru1-N3	94.7(2)	N1-Ru1-N4	170.8(2)
N2-Ru1-N4	95.7(2)	N3-Ru1-N2	82.6(2)	N3-Ru1-N4	77.9(2)
N5-Ru1-N1	88.0(2)	N5-Ru1-N2	92.1(2)	N5-Ru1-N3	173.3(2)
N5-Ru1-N4	98.8(2)	N6-Ru1-N1	96.5(2)	N6-Ru1-N2	170.7(2)
N6-Ru1-N3	90.7(2)	N6-Ru1-N4	89.1(2)	N6-Ru1-N5	95.0(2)
C1-N1-Ru1	128.4(5)	C9-N1-Ru1	111.2(4)	C9-N1-C1	119.3(6)
C10-N2-Ru1	110.7(4)	C10-N2-C18	118.8(6)	C18-N2-Ru1	128.8(5)
C19-N3-Ru1	128.1(5)	C27-N3-Ru1	110.8(4)	C27-N3-C19	118.6(6)
C28-N4-Ru1	111.4(4)	C28-N4-C36	118.3(6)	C36-N4-Ru1	129.4(4)
C37-N5-Ru1	177.9(6)	C43-N6-Ru1	171.5(6)	N1-C1-C2	120.4(6)
N1-C1-C6	120.2(7)	C6-C1-C2	119.3(6)	C3-C2-C1	120.1(7)
C2-C3-C4	120.7(8)	C5-C4-C3	121.0(7)	C4-C5-C6	120.0(7)

C1-C6-C5	118.7(7)	C7-C6-C1	119.2(7)	C7-C6-C5	122.1(7)
C8-C7-C6	119.9(7)	C7-C8-C9	118.4(7)	N1-C9-C8	122.0(6)
N1-C9-C10	115.3(6)	C8-C9-C10	122.7(7)	N2-C10-C9	114.7(6)
N2-C10-C11	122.5(6)	C11-C10-C9	122.7(6)	C12-C11-C10	119.2(6)
C11-C12-C13	120.8(6)	C12-C13-C18	116.7(6)	C14-C13-C12	123.7(7)
C14-C13-C18	119.7(6)	C15-C14-C13	120.7(7)	C14-C15-C16	119.8(7)
C17-C16-C15	121.6(7)	C16-C17-C18	119.9(7)	N2-C18-C13	121.4(6)
N2-C18-C17	120.4(6)	C17-C18-C13	118.2(6)	N3-C19-C24	120.2(6)
C20-C19-N3	120.1(6)	C20-C19-C24	119.8(7)	C21-C20-C19	119.7(7)
C20-C21-C22	121.1(8)	C23-C22-C21	120.7(7)	C22-C23-C24	120.1(8)
C19-C24-C23	118.3(7)	C19-C24-C25	118.2(7)	C23-C24-C25	123.4(7)
C26-C25-C24	120.2(7)	C25-C26-C27	118.9(7)	N3-C27-C26	122.7(7)
N3-C27-C28	115.0(6)	C26-C27-C28	122.3(6)	N4-C28-C27	115.4(6)
N4-C28-C29	122.7(6)	C29-C28-C27	121.7(6)	C30-C29-C28	118.9(6)
C29-C30-C31	120.4(6)	C30-C31-C32	122.8(6)	C30-C31-C36	118.2(6)
C36-C31-C32	119.0(6)	C33-C32-C31	120.6(6)	C32-C33-C34	120.4(7)
C35-C34-C33	120.5(7)	C34-C35-C36	121.0(6)	N4-C36-C31	121.2(6)
N4-C36-C35	120.3(6)	C35-C36-C31	118.5(6)	N5-C37-C38	173.6(7)
C37-C38-C39	110.3(6)	C40-C39-C38	111.8(7)	C41-C40-C39	114.9(7)
C42-C41-C40	175.2(9)	N6-C43-C44	178.8(8)	C43-C44-C45	112.1(7)
C44-C45-C46	113.5(7)	C47-C46-C45	114.6(7)	C48-C47-C46	178.0(11)
F1-P1-F3	179.1(4)	F1-P1-F4	89.3(3)	F1-P1-F6	89.9(3)
F2-P1-F1	90.4(3)	F2-P1-F3	90.3(3)	F2-P1-F4	179.2(3)
F2-P1-F6	90.2(3)	F3-P1-F6	89.4(3)	F4-P1-F3	90.0(3)
F4-P1-F6	89.0(3)	F5-P1-F1	89.9(3)	F5-P1-F2	90.7(3)
F5-P1-F3	90.8(3)	F5-P1-F4	90.1(3)	F5-P1-F6	179.1(3)
F7-P2-F8	89.5(3)	F7-P2-F9	178.4(5)	F7-P2-F10	90.6(3)
F7-P2-F11	89.0(4)	F7-P2-F12	87.1(4)	F8-P2-F10	179.2(4)
F8-P2-F11	90.7(3)	F8-P2-F12	89.1(4)	F9-P2-F8	90.6(4)
F9-P2-F10	89.2(4)	F9-P2-F11	92.7(5)	F9-P2-F12	91.2(5)
F10-P2-F11	90.1(3)	F12-P2-F10	90.2(4)	F12-P2-F11	176.1(5)
N2'-Ru1'-N1'	77.4(2)	N2'-Ru1'-N3'	83.3(2)	N2'-Ru1'-N4'	92.2(2)

N3'-Ru1'-N1'	92.3(2)	N3'-Ru1'-N4'	77.2(2)	N4'-Ru1'-N1'	166.1(2)
N5'-Ru1'-N1'	88.3(3)	N5'-Ru1'-N2'	90.7(3)	N5'-Ru1'-N3'	173.7(3)
N5'-Ru1'-N4'	101.2(2)	N5'-Ru1'-N6'	94.7(3)	N6'-Ru1'-N1'	101.7(2)
N6'-Ru1'-N2'	174.5(3)	N6'-Ru1'-N3'	91.3(2)	N6'-Ru1'-N4'	87.8(2)
C1'-N1'-Ru1'	129.5(6)	C9'-N1'-Ru1'	110.1(4)	C9'-N1'-C1'	119.8(6)
C10'-N2'-Ru1'	111.5(5)	C10'-N2'-C18'	119.1(6)	C18'-N2'-Ru1'	127.4(5)
C19'-N3'-Ru1'	126.0(5)	C27'-N3'-Ru1'	110.6(4)	C27'-N3'-C19'	119.7(6)
C28'-N4'-Ru1'	111.6(4)	C28'-N4'-C36'	119.2(6)	C36'-N4'-Ru1'	128.9(5)
C37'-N5'-Ru1'	174.6(8)	C43'-N6'-Ru1'	173.0(6)	N1'-C1'-C2'	120.4(7)
N1'-C1'-C6'	119.9(7)	C2'-C1'-C6'	119.7(7)	C3'-C2'-C1'	120.1(8)
C2'-C3'-C4'	120.2(8)	C5'-C4'-C3'	121.2(8)	C4'-C5'-C6'	120.3(8)
C1'-C6'-C5'	118.5(8)	C7'-C6'-C1'	119.2(7)	C7'-C6'-C5'	122.2(7)
C8'-C7'-C6'	120.8(7)	C7'-C8'-C9'	117.9(8)	N1'-C9'-C8'	122.2(6)
N1'-C9'-C10'	116.2(6)	C8'-C9'-C10'	121.4(7)	N2'-C10'-C9'	113.9(7)
N2'-C10'-C11'	122.7(6)	C11'-C10'-C9'	123.4(7)	C12'-C11'-C10'	119.0(8)
C11'-C12'-C13'	120.2(8)	C12'-C13'-C14'	123.1(7)	C18'-C13'-C12'	118.6(6)
C18'-C13'-C14'	118.3(7)	C15'-C14'-C13'	120.8(8)	C14'-C15'-C16'	119.9(7)
C17'-C16'-C15'	121.5(7)	C16'-C17'-C18'	118.8(8)	N2'-C18'-C13'	119.3(7)
N2'-C18'-C17'	120.0(7)	C17'-C18'-C13'	120.6(7)	N3'-C19'-C20'	120.9(7)
N3'-C19'-C24'	121.0(7)	C24'-C19'-C20'	118.1(7)	C21'-C20'-C19'	120.8(8)
C20'-C21'-C22'	121.4(7)	C23'-C22'-C21'	118.8(8)	C22'-C23'-C24'	121.6(8)
C19'-C24'-C23'	118.7(7)	C19'-C24'-C25'	118.0(7)	C23'-C24'-C25'	123.3(8)
C26'-C25'-C24'	119.8(7)	C25'-C26'-C27'	118.6(7)	N3'-C27'-C26'	121.8(6)
N3'-C27'-C28'	114.0(6)	C26'-C27'-C28'	124.1(6)	N4'-C28'-C27'	115.4(6)
N4'-C28'-C29'	121.9(6)	C29'-C28'-C27'	122.6(6)	C30'-C29'-C28'	118.9(6)
C29'-C30'-C31'	120.9(6)	C30'-C31'-C32'	123.7(6)	C30'-C31'-C36'	117.9(6)
C32'-C31'-C36'	118.3(6)	C33'-C32'-C31'	121.1(7)	C32'-C33'-C34'	121.0(8)
C35'-C34'-C33'	119.7(7)	C34'-C35'-C36'	121.3(7)	N4'-C36'-C31'	120.7(6)
N4'-C36'-C35'	120.8(6)	C35'-C36'-C31'	118.5(6)	N5'-C37'-C38'	175.1(11)
C37'-C38'-C39'	109.0(10)	C40'-C39'-C38'	116.0(10)	C39'-C40'-C41'	115.0(12)
C42'-C41'-C40'	177.2(15)	N6'-C43'-C44'	177.5(7)	C43'-C44'-C45'	112.2(8)
C46'-C45'-C44'	111.8(8)	C47'-C46'-C45'	112.9(9)	C48'-C47'-C46'	174.4(14)

F1'-P1'-F2'	89.2(4)	F1'-P1'-F3'	178.2(4)	F1'-P1'-F4'	90.7(4)
F1'-P1'-F5'	90.9(4)	F1'-P1'-F6'	91.4(4)	F2'-P1'-F3'	90.4(4)
F2'-P1'-F5'	90.0(4)	F2'-P1'-F6'	88.6(3)	F3'-P1'-F5'	87.3(4)
F3'-P1'-F6'	90.3(4)	F4'-P1'-F2'	179.8(5)	F4'-P1'-F3'	89.7(4)
F4'-P1'-F5'	89.8(4)	F4'-P1'-F6'	91.6(4)	F5'-P1'-F6'	177.2(4)
F7'-P2'-F8'	93.5(5)	F7'-P2'-F9'	178.0(5)	F7'-P2'-F10'	88.0(5)
F7'-P2'-F11'	90.6(5)	F7'-P2'-F12'	86.6(5)	F8'-P2'-F9'	88.1(5)
F8'-P2'-F10'	175.6(6)	F8'-P2'-F11'	90.4(6)	F9'-P2'-F10'	90.5(4)
F9'-P2'-F11'	90.5(4)	F11'-P2'-F10'	85.4(5)	F12'-P2'-F8'	90.6(6)
F12'-P2'-F9'	92.2(5)	F12'-P2'-F10'	93.6(6)	F12'-P2'-F11'	177.1(5)

This report has been created with Olex2 [6], compiled on 2018.04.18 svn.r3501 for OlexSys.

References

[1] APEX2 2014.11-0: Bruker-AXS, Madison, Wisconsin, USA (2014).

[2] SAINT v8.34A: Bruker-AXS, Madison, Wisconsin, USA (2014).

[3] SADABS v2014/5: Krause, L., Herbst-Irmer, R., Sheldrick, G.M. & Stalke, D., J. Appl. Cryst., 48, 3-10 (2015).

[4] SHELXS-97: Sheldrick, G.M., Acta Cryst., A64, 112-122 (2008).

[5] SHELXL-2017/1: Sheldrick, G.M., Acta Cryst., A71, 3-8 (2015).

[6] Olex2: Dolomanov,O.V., Bourhis, L.J., Gildea, R.J., Howard, J.A.K., Puschmann, H., J. Appl. Cryst., 42, 339-341 (2009)

APPENDIX 4 – Assigned ^{1}H NMRs

A4.1 Ru(bpy)$_2$(3-ethynylpyridine)$_2$ (RuBEP) ^{1}H NMR

In CD_3CN

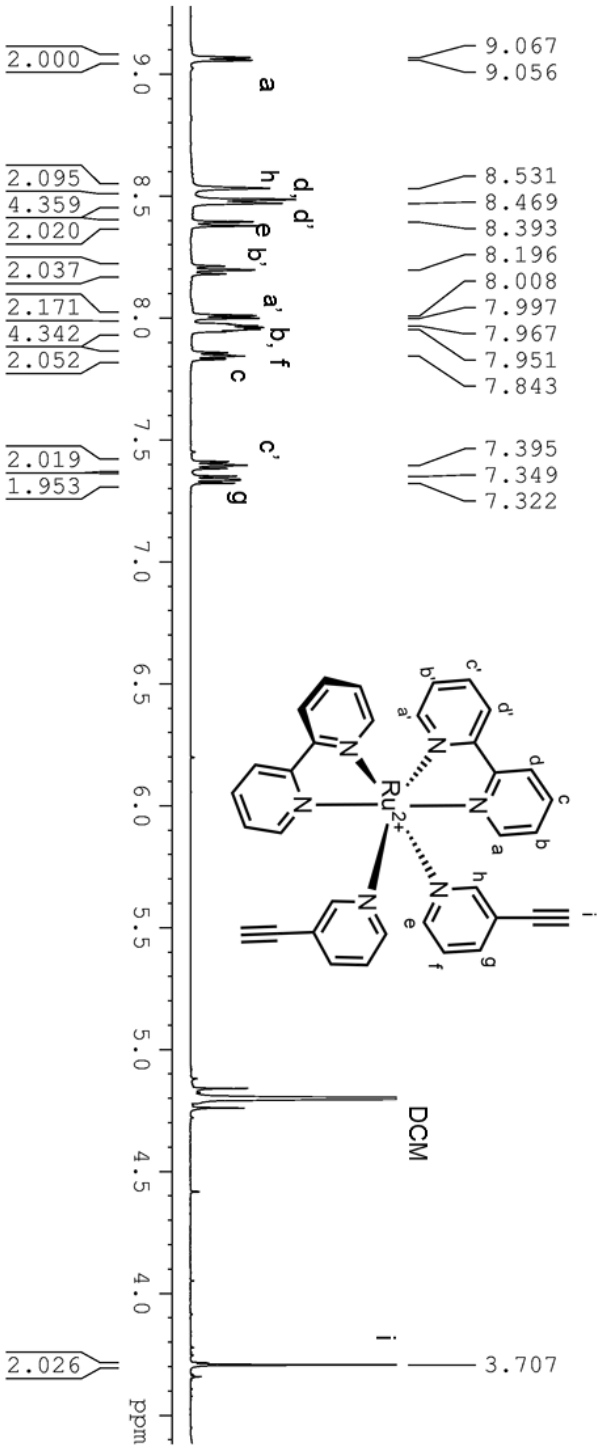

A4.2 $Ru(bpy)_2(3\text{-pyridinaldehyde})_2$ (RuAldehyde) ^1H NMR

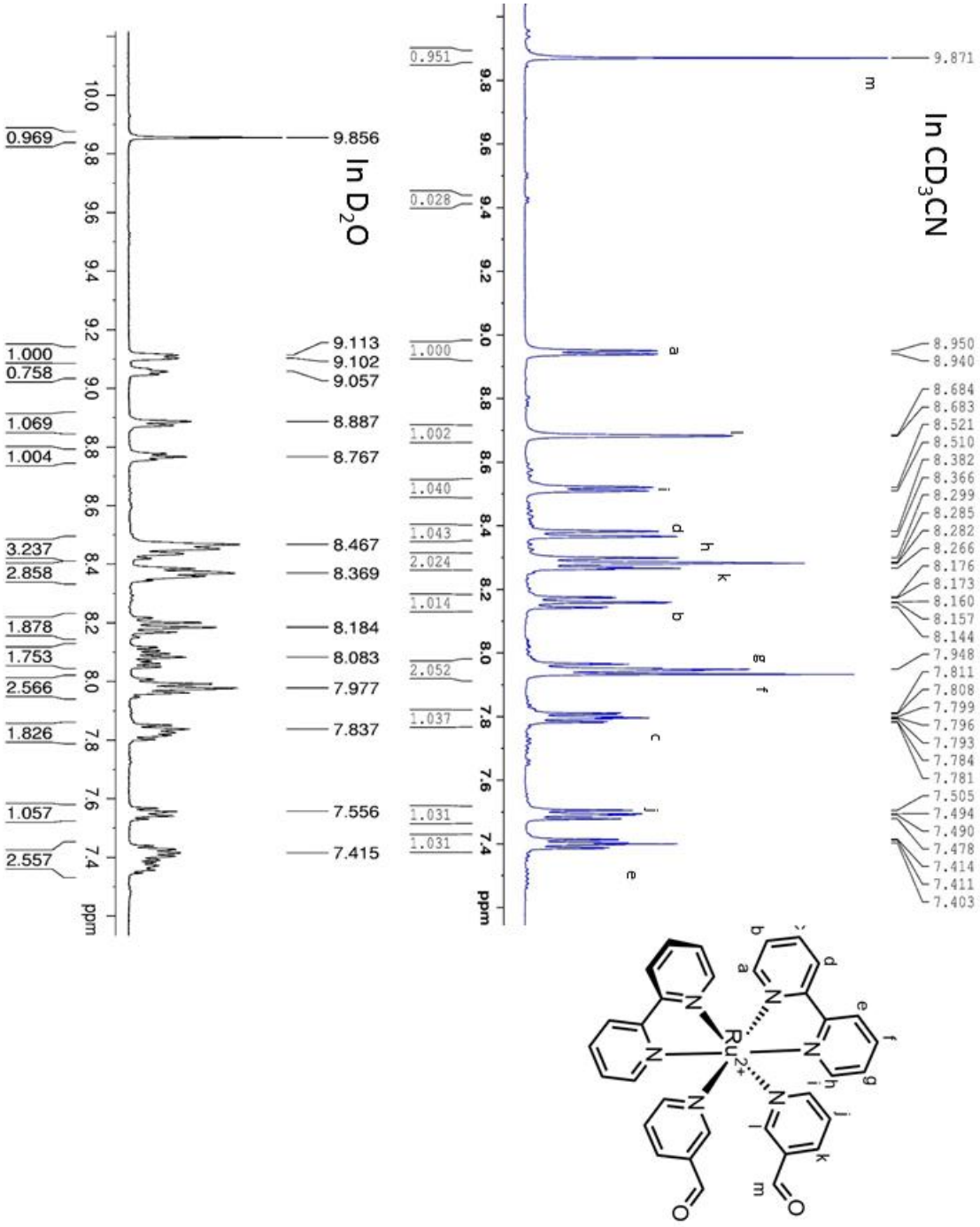

A4.3 RuAldehyde COSY

In CD_3CN

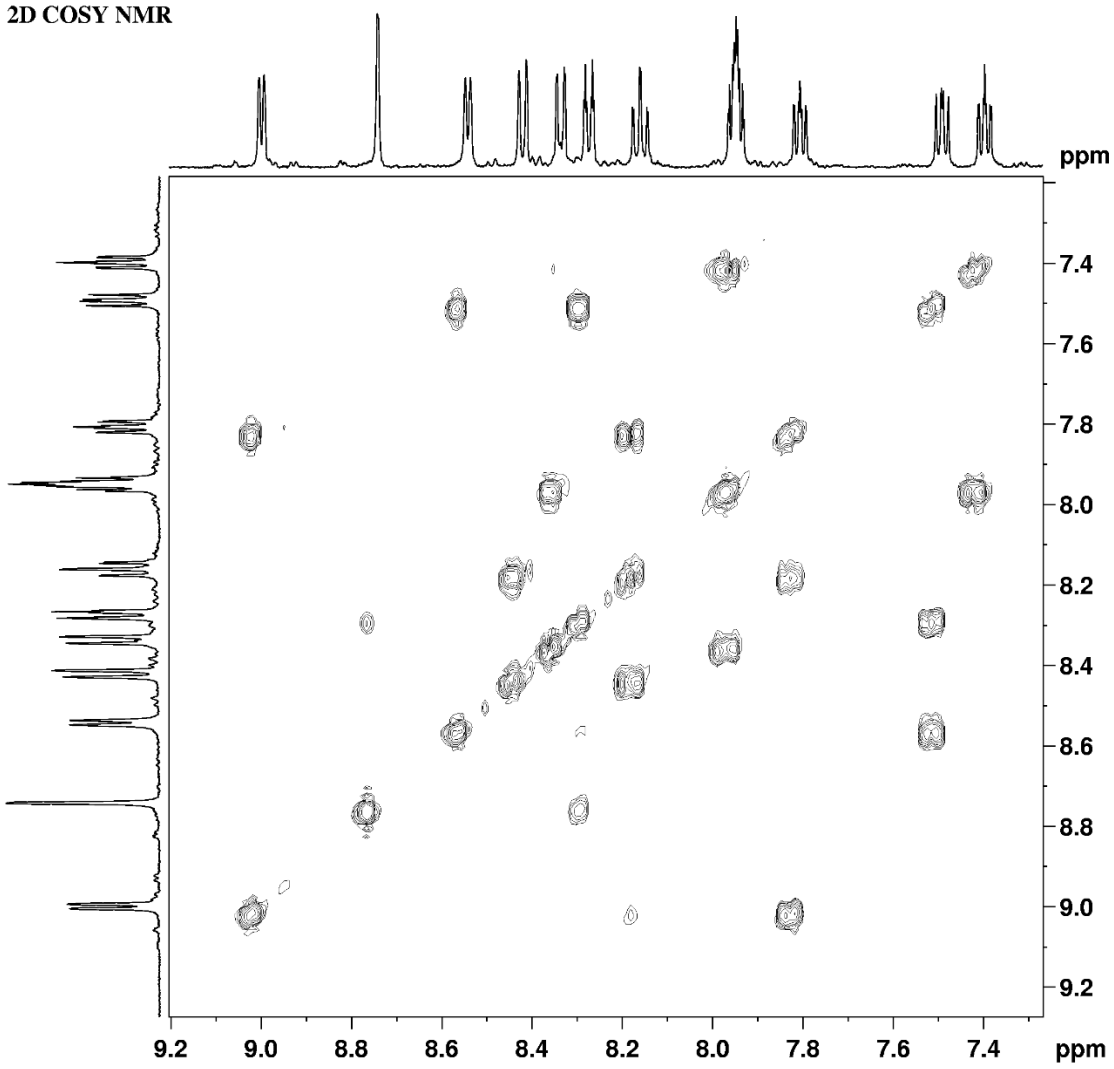

A4.4 $Ru(bpy)_2(4\text{-pentynenitrile})_2$ (Ru420)

In D_2O

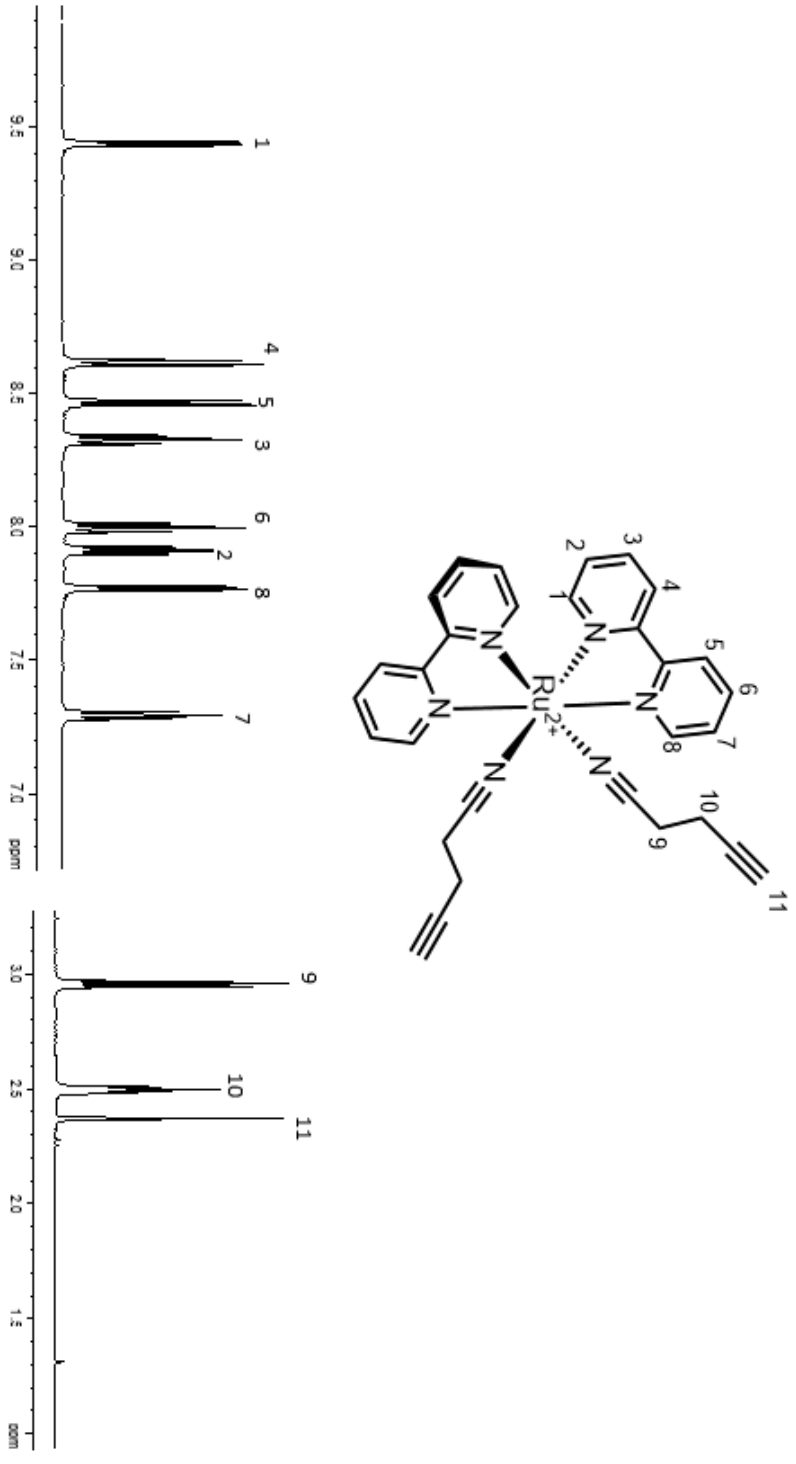

A4.4 Ru420 COSY

In CD_3CN

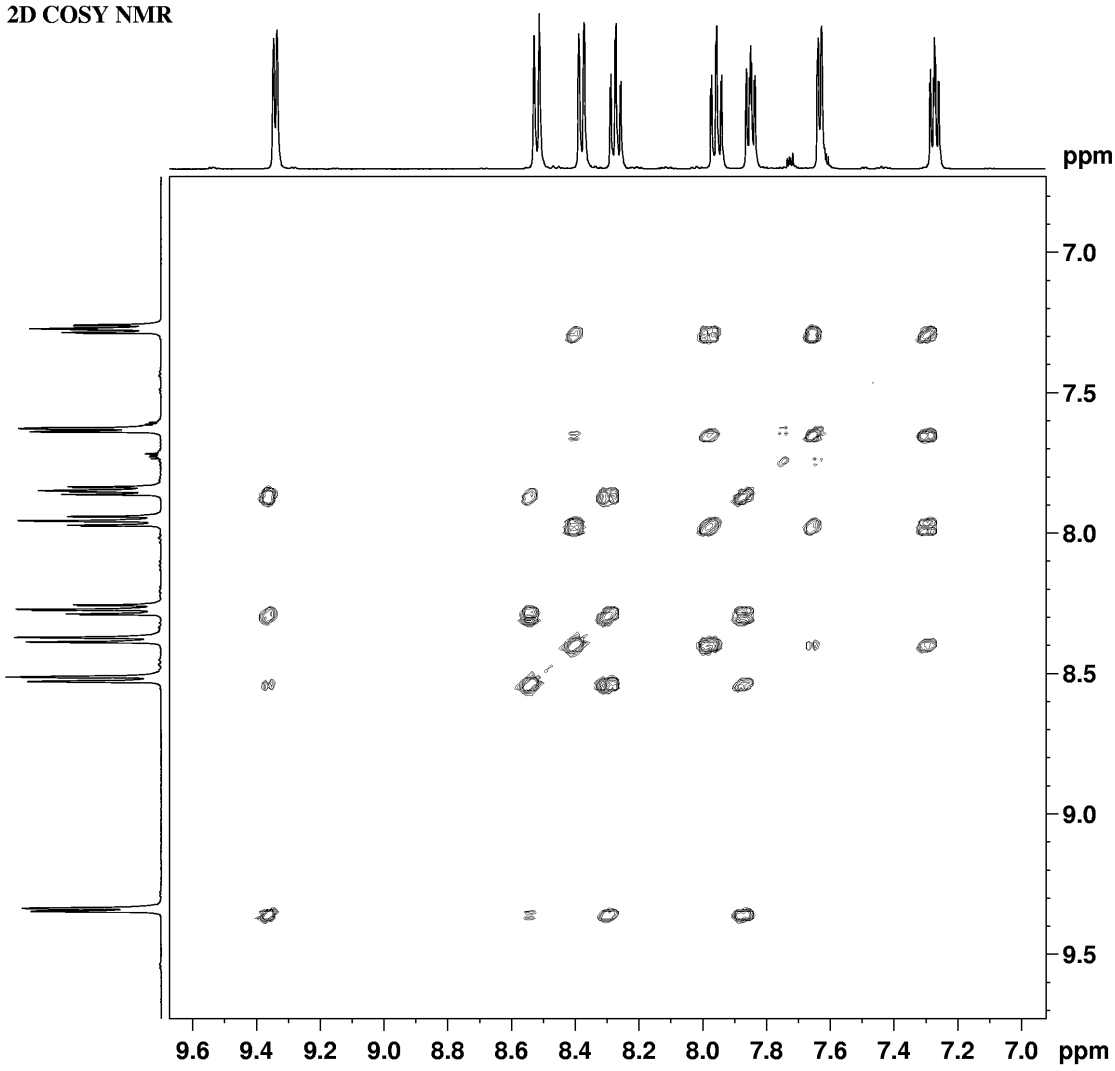

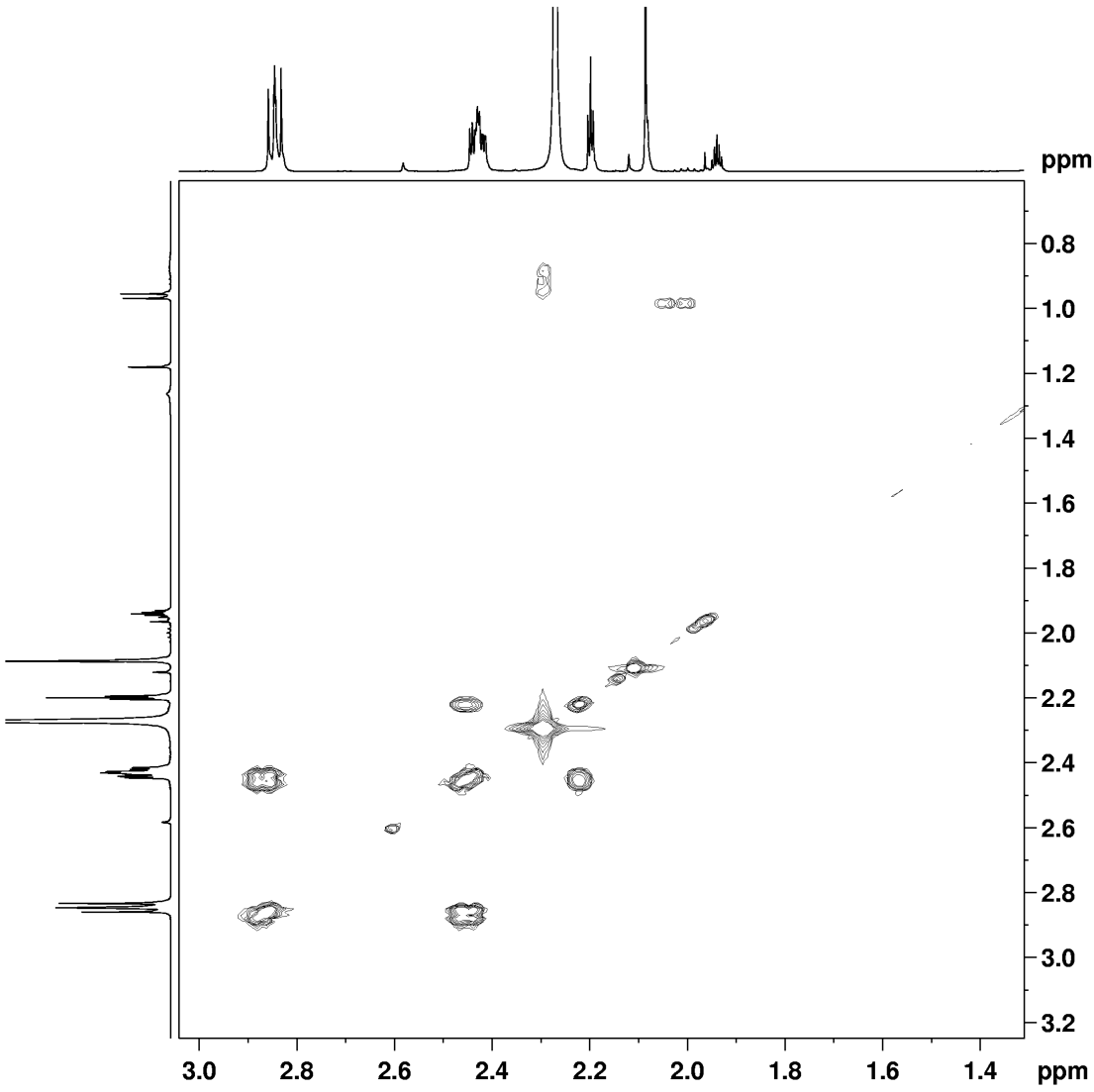
ppm
0.8
1.0
1.2
1.4
1.6
1.8
2.0
2.2
2.4
2.6
2.8
3.0
3.2
3.0
2.8
2.6
2.4
2.2
2.0
1.8
1.6
1.4
ppm

A4.5 $Ru(biq)_2(4\text{-pentynenitrile})_2$ (Ru530)

In D_2O

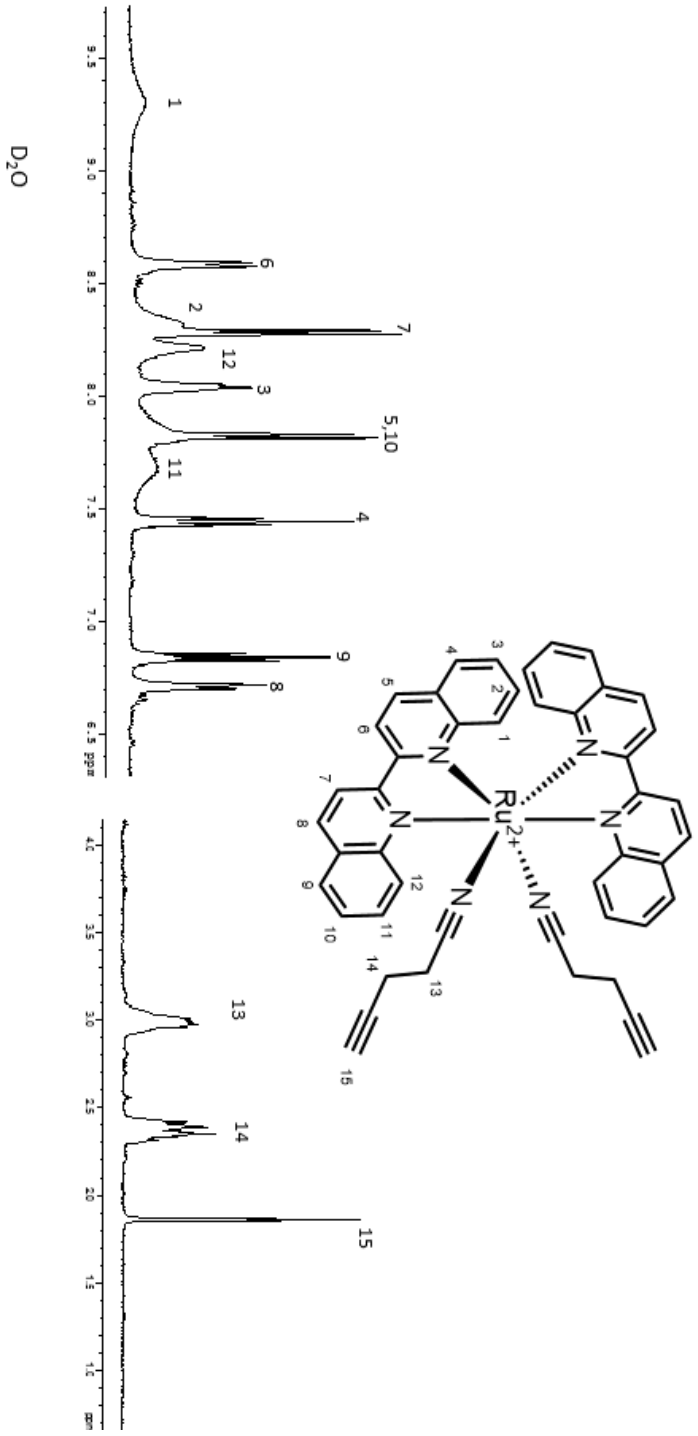

A4.6 Ru(bpy)(biq)(4-pyridinepropanal)$_2$ (RuAldehyde-Red) COSY

In CD_3CN

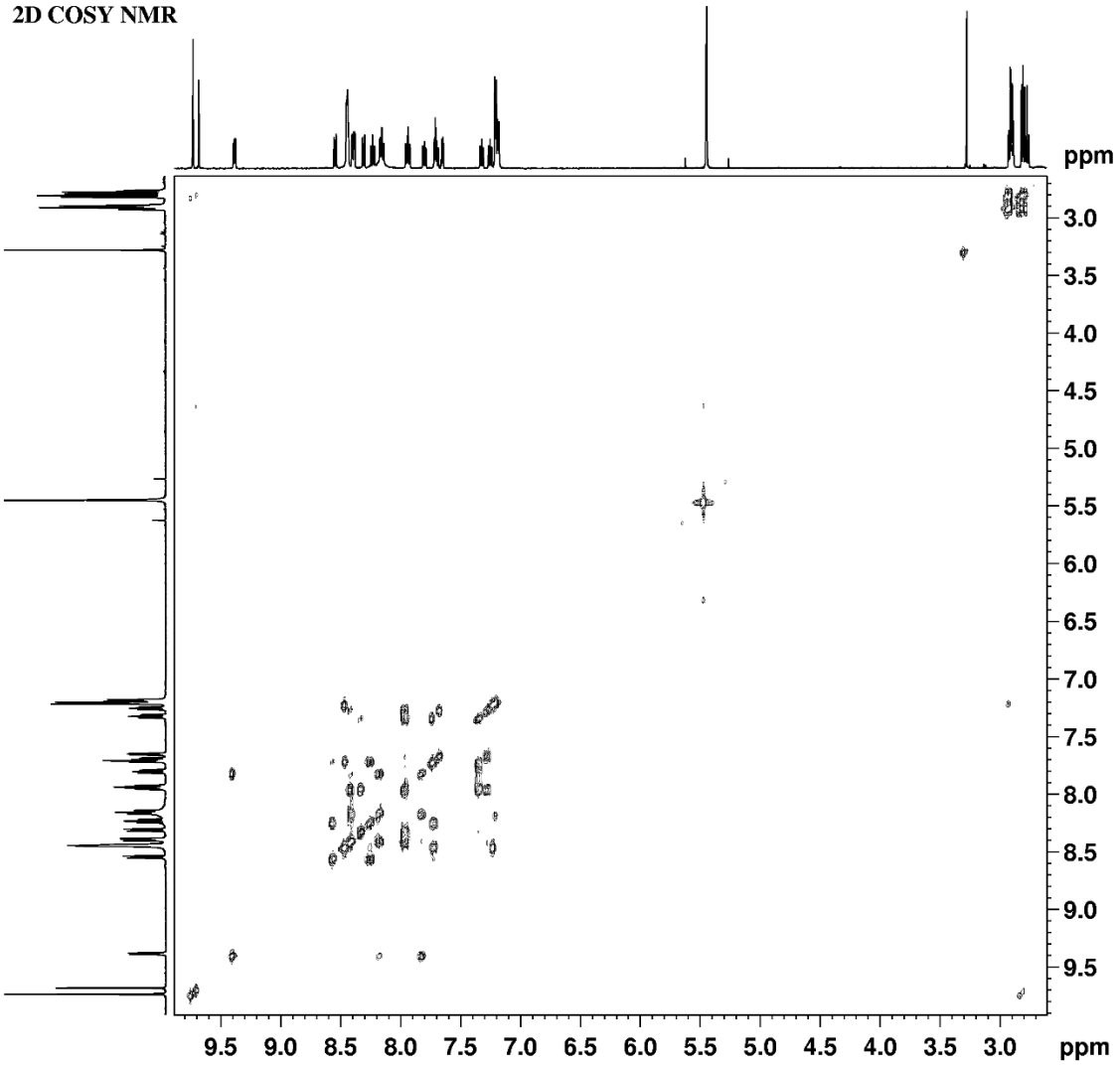

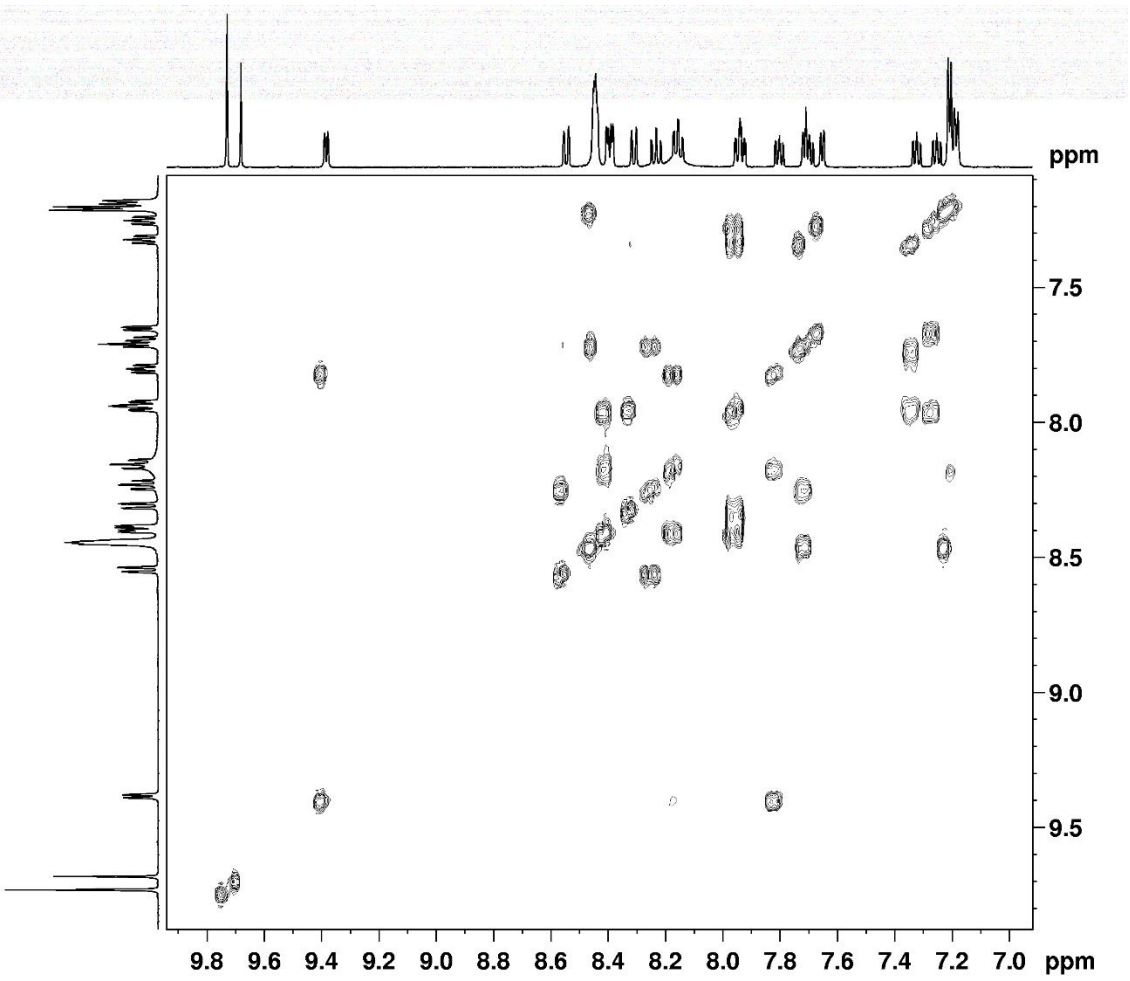
ppm
7.5
8.0
8.5
9.0
9.5
9.8 9.6 9.4 9.2 9.0 8.8 8.6 8.4 8.2 8.0 7.8 7.6 7.4 7.2 7.0 ppm

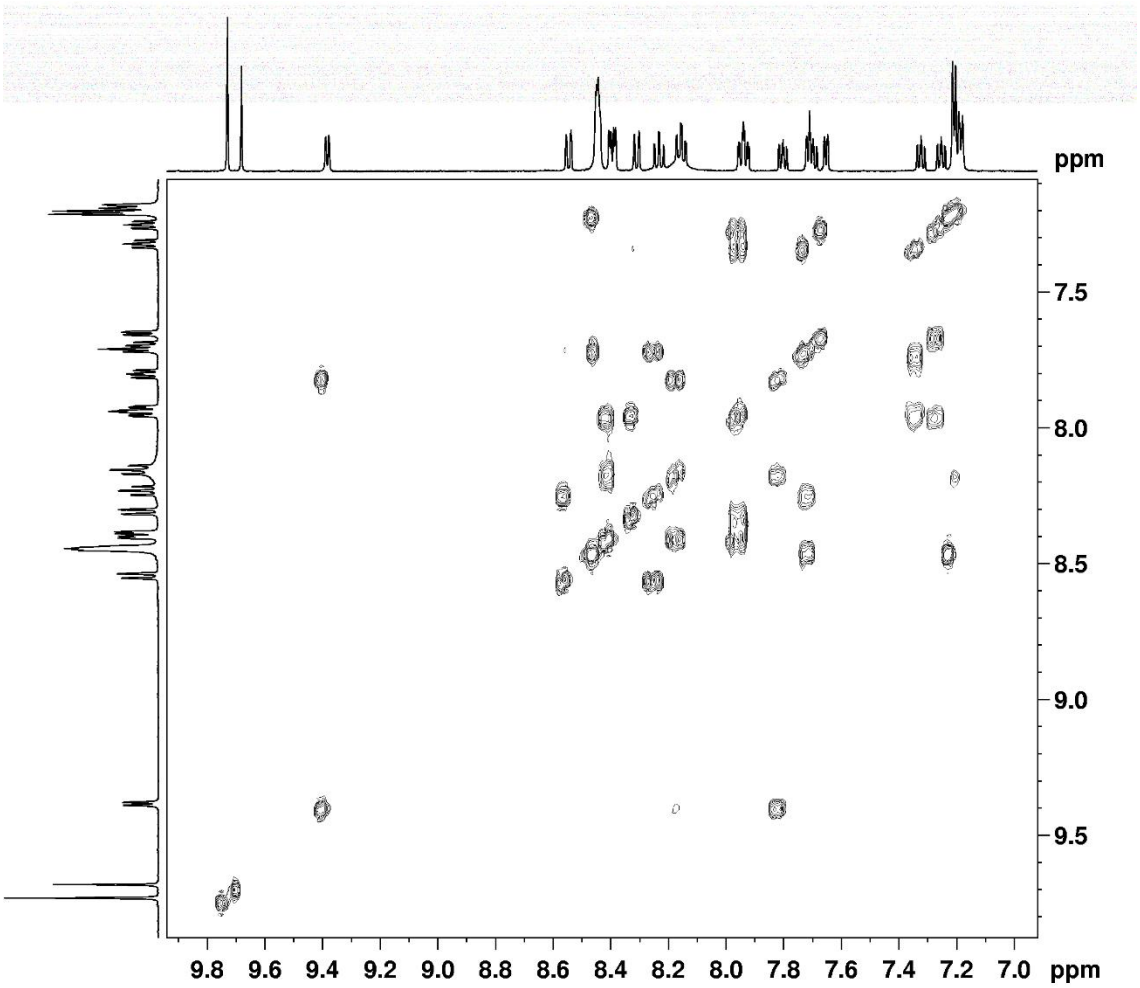
ppm
7.5
8.0
8.5
9.0
9.5
9.8 9.6 9.4 9.2 9.0 8.8 8.6 8.4 8.2 8.0 7.8 7.6 7.4 7.2 7.0 ppm

BIBLIOGRAPHY

1. Burnstall, F. H. Optical Activity dependent on Co-ordinated Bivalent Ruthenium. *J. Chem. Soc.* 173–175 (1936).

2. Paris, J. P. & Brandt, W. W. CHARGE TRANSFER LUMINESCENCE OF A RUTHENIUM(II) CHELATE. *J. Am. Chem. Soc.* **81,** 5001–5002 (1959).

3. Dwyer, F., Reid, I., Shulman, A., Laycock, G. M. & Dixson, S. The Biological Actions of 1,10-phenanthroline and 2,2′-bipyridine Hydrochlorides, Quaternary Salts and Metal Chelates and Related Compounds. *Aust. J. Exp. Biol. Med. Sci.* **47,** 203–218 (1969).

4. Dwyer, F. P. J. & Mellor, D. P. *Chelating agents and metal chelates*. (Academic Press, 1964).

5. Bosnich, B. & Dwyer, F. Bis-1,10-phenanthroline complexes of divalent ruthenium. *Aust. J. Chem.* **19,** 2229 (1966).

6. Gleria, M., Minto, F., Beggiato, G. & Bortolus, P. Photochemistry of tris(2,2′-bipyridine)ruthenium(II) in chlorinated solvents. *J. Chem. Soc., Chem. Commun.* **0,** 285 (1978).

7. Durham, B., Walsh, J. L., Carter, C. L. & Meyer, T. J. Synthetic Applications of Photosubstitution Reactions of Poly(pyridyl) Complexes of Ruthenium(II). *Inorg. Chem* **19,** 860–865 (1980).

8. Durham, B., Caspar, J., Nagle, J. & Meyer, T. Photochemistry of Ru(bpy)32+. *J. Am. Chem. Soc.* **104,** 4803–4810 (1982).

9. Salassa, L., Garino, C., Salassa, G., Gobetto, R. & Nervi, C. Mechanism of Ligand Photodissociation in Photoactivable [Ru(bpy)2L2]2+ Complexes: A Density Functional Theory Study. *J. Am. Chem. Soc.* **130,** 9590–9597 (2008).

10. Loftus, L. M. *et al.* Unusual Role of Excited State Mixing in the Enhancement of Photoinduced Ligand Exchange in Ru(II) Complexes. *J. Am. Chem. Soc.* **139,** 18295–18306 (2017).

11. Winkler, J. R., Nocera, D. G., Yocom, K. M., Bordignon, E. & Gray, H. B. Electron-transfer kinetics of pentaammineruthenium(III)(histidine-33)-ferricytochrome c. Measurement of the rate of intramolecular electron transfer between redox centers separated by 15.ANG. in a protein. *J. Am. Chem. Soc.* **104,** 5798–5800 (1982).

12. Meyer, T. J. Chemical Approaches to Artificial Photosynthesis. *Acc. Chem. Res.* **22,** 163–170 (1989).

13. Suen, H.-F., Wilson, S. W., Pomerantz, M. & Walsh, J. L. Photosubstitution Reactions of Terpyridine Complexes of Ru(II). *Inorg. Chem.* **28,** 786–791 (1989).

14. Weber, W. & Ford, P. Photosubstitution Reactions of the Ruthenium(II) Aren Complexes Ru(n6-arene)L3 2+ (L = NH3 or H2O) in Aqueous Solution. *Inorg. Chem.* **25,** 1088–1092 (1986).

15. Arakawa, R. *et al.* On-Line Mass Analysis of Reaction Products by Electrospray Ionization. Photosubstitution of Ruthenium(II) Diimine Complexes. *Inorg. Chem* **34,** 3874–3878 (1995).

16. Hecker, C. R., Fanwick, P. E. & McMillin, D. R. Evidence for dissociative photosubstitution

reactions of (acetonitrile)(bipyridine)(terpyridine)ruthenium(2+). Crystal and molecular structure of [Ru(trpy)(bpy)(py)](PF6)2(CH3)2CO. *Inorg. Chem.* **30,** 659–666 (1991).

17. Zayat, L., Calero, C., Alborés, P., Baraldo, L. & Etchenique, R. A new strategy for neurochemical photodelivery: metal-ligand heterolytic cleavage. *J. Am. Chem. Soc.* **125,** 882–3 (2003).

18. Vélez, P., Györke, S., Escobar, A. L., Vergara, J. & Fill, M. Adaptation of Single Cardiac Ryanodine Receptor Channels. *Biophys. J.* **72,** 691–697 (1997).

19. De Leo, M. & Ford, P. C. Reversible Photolabilization of NO from Chromium(III)-Coordinated Nitrite. A New Strategy for Nitric Oxide Delivery. *J. Am. Chem. Soc.* **121,** 1980–1981 (1999).

20. Nikolenko, V., Yuste, R., Zayat, L., Baraldo, L. M. & Etchenique, R. Two-photon uncaging of neurochemicals using inorganic metal complexes. *Chem. Commun.* **0,** 1752 (2005).

21. Zayat, L. *et al.* Ruthenium(II) bipyridyl complexes as photolabile caging groups for amines. *Inorg. Chem.* **45,** 1728–1731 (2006).

22. Zayat, L. *et al.* A New Inorganic Photolabile Protecting Group for Highly Efficient Visible Light GABA Uncaging. *ChemBioChem* **8,** 2035–2038 (2007).

23. Salierno, M., Marceca, E., Peterka, D. S., Yuste, R. & Etchenique, R. A fast ruthenium polypyridine cage complex photoreleases glutamate with visible or IR light in one and two photon regimes. *J. Inorg. Biochem.* **104,** 418–422 (2010).

24. Filevich, Oscar; Salierno, Marcello; Etchenique, R. A caged nicotine with nanosecond range kinetics and visible light sensitivity. *J. Inorg. Biochem.* **104,** 1248–1251 (2010).

25. Singh, T. N. & Turro, C. Photoinitiated DNA Binding by cis-[Ru(bpy)2(NH3)2]2+. *Inorg. Chem.* **43,** 7260–7262 (2004).

26. Garner, R. N., Gallucci, J. C., Dunbar, K. R. & Turro, C. [Ru(bpy)2(5-cyanouracil)2]2+ as a Potential Light-Activated Dual-Action Therapeutic Agent. *Inorg. Chem.* **50,** 9213–9215 (2011).

27. Sgambellone, M. A., David, A., Garner, R. N., Dunbar, K. R. & Turro, C. Cellular Toxicity Induced by the Photorelease of a Caged Bioactive Molecule : Design of A Potential Dual-Action Ru (II) Complex Cellular Toxicity Induced by the Photorelease of a Caged Bioactive Molecule : Design of A Potential Dual-Action Ru (II) Com. (2013). doi:10.1021/ja4045604

28. Li, A., Turro, C. & Kodanko, J. J. Ru(ii) polypyridyl complexes as photocages for bioactive compounds containing nitriles and aromatic heterocycles. *Chem. Commun.* **54,** 1280–1290 (2018).

29. Turk, B. Targeting proteases: successes, failures and future prospects. *Nat. Rev. Drug Discov.* **5,** 785–799 (2006).

30. Frizler, M., Stirnberg, M., Sisay, M. & Gutschow, M. Development of Nitrile-Based Peptidic Inhibitors of Cysteine Cathepsins. *Curr. Top. Med. Chem.* **10,** 294–322 (2010).

31. Respondek, T. *et al.* Inhibition of Cathepsin Activity in a Cell-Based Assay by a Light-Activated Ruthenium Compound. *ChemMedChem* **9,** 1306–1315 (2014).

32. Respondek, T. *et al.* Light Activation of a Cysteine Protease Inhibitor: Caging of a

Peptidomimetic Nitrile with Ru ^{II} (bpy) $_2$. *J. Am. Chem. Soc.* **133,** 17164–17167 (2011).

33. Liu, Y. *et al.* Ultrafast ligand exchange: Detection of a pentacoordinate Ru(ll) intermediate and product formation. *J. Am. Chem. Soc.* **131,** 26–27 (2009).

34. Greenough, S. E. *et al.* Excited-State Dynamics of a Two-Photon-Activatable Ruthenium Prodrug. *ChemPhysChem* **17,** 221–224 (2016).

35. Knoll, J. D., Albani, B. A., Durr, C. B. & Turro, C. Unusually Efficient Pyridine Photodissociation from Ru(II) Complexes with Sterically Bulky Bidentate Ancillary Ligands. *J. Phys. Chem. A* **118,** 10603–10610 (2014).

36. Knoll, J. D., Albani, B. A. & Turro, C. New Ru(II) Complexes for Dual Photoreactivity: Ligand Exchange and ^{1} O $_2$ Generation. *Acc. Chem. Res.* **48,** 2280–2287 (2015).

37. Lawrence, M. A. W., Bullock, J. L. & Holder, A. A. *Ruthenium Complexes - Photochemical and Biomedical Applications - Basic Coordination Chemistry of Ruthenium*. (Wiley-VCH, 2018).

38. Sears, R. B. *et al.* Photoinduced ligand exchange and DNA binding of cis-[Ru(phpy)(phen)(CH3CN)2]+ with long wavelength visible light. *J. Inorg. Biochem.* **121,** 77–87 (2013).

39. Albani, B. A., Durr, C. B. & Turro, C. Selective Photoinduced Ligand Exchange in a New Tris-Heteroleptic Ru (II) Complex Selective Photoinduced Ligand Exchange in a New Tris-Heteroleptic Ru (II) Complex. *J. Phys. Chem. A* **117,** 13885–13892 (2013).

40. Albani, B. A. *et al.* A dinuclear Ru(ii) complex capable of photoinduced ligand exchange at both metal centers. *Chem. Commun.* **51,** 16522–16525 (2015).

41. Zeng, X., Zhou, X. & Wu, S. Red and Near-Infrared Light-Cleavable Polymers. *Macromol. Rapid Commun.* 1800034 (2018). doi:10.1002/marc.201800034

42. Theis, S. *et al.* Metallo-Supramolecular Gels that are Photocleavable with Visible and Near-Infrared Irradiation. *Angew. Chemie Int. Ed.* **56,** 15857–15860 (2017).

43. Leonardo, Z., Cecilia, C., Pablo, A., Baraldo, L. & Etchenique, R. A New Strategy for Neurochemical Photodelivery: Metal−Ligand Heterolytic Cleavage. *J. Am. Chem. Soc.* **125,** 882–883 (2003).

44. Smith, N. A. *et al.* Combatting AMR: photoactivatable ruthenium(ii)-isoniazid complex exhibits rapid selective antimycobacterial activity. *Chem. Sci.* **8,** 395–404 (2017).

45. Mosquera, J., Sánchez, M. I., Mascareñas, J. L. & Eugenio Vázquez, M. Synthetic peptides caged on histidine residues with a bisbipyridyl ruthenium(ii) complex that can be photolyzed by visible light. *Chem. Commun.* **51,** 5501–5504 (2015).

46. Zamora, A. *et al.* Ruthenium-containing P450 inhibitors for dual enzyme inhibition and DNA damage. *Dalt. Trans.* **46,** 2165–2173 (2017).

47. Lameijer, L. N. *et al.* A Red-Light-Activated Ruthenium-Caged NAMPT Inhibitor Remains Phototoxic in Hypoxic Cancer Cells. *Angew. Chemie Int. Ed.* **56,** 11549–11553 (2017).

48. Loftus, L. M. *et al.* New Ru (II) Complex for Dual Activity: Photoinduced Ligand Release and 1O2 Production. *Chem. - A Eur. J.* **22,** 3704–3708 (2016).

49. Garner, R. N., Gallucci, J. C., Dunbar, K. R. & Turro, C. [Ru(bpy) 2 (5-cyanouracil) 2] 2+

as a Potential Light-Activated Dual-Action Therapeutic Agent. *Inorg. Chem.* **50,** 9213–9215 (2011).

50. Filevich, O., Zayat, L., Baraldo, L. M. & Etchenique, R. in 47–68 (Springer, Berlin, Heidelberg, 2014). doi:10.1007/430_2014_169

51. Bryant, J. R. & Mayer, J. M. Oxidation of C-H bonds by [(bpy)2(py)RuIVO]2+ occurs by hydrogen atom abstraction. *J. Am. Chem. Soc.* **125,** 10351–61 (2003).

52. Gatterdam, V. *et al.* Three-Dimensional Protein Networks Assembled by Two-Photon Activation. *Angew. Chemie Int. Ed.* **53,** 5680–5684 (2014).

53. Furuta, T. *et al.* Brominated 7-hydroxycoumarin-4-ylmethyls: photolabile protecting groups with biologically useful cross-sections for two photon photolysis. *Proc. Natl. Acad. Sci. U. S. A.* **96,** 1193–200 (1999).

54. Lever, A. B. P. Electrochemical parametrization of metal complex redox potentials, using the ruthenium(III)/ruthenium(II) couple to generate a ligand electrochemical series. *Inorg. Chem.* **29,** 1271–1285 (1990).

55. McCusker, J. K. Femtosecond Absorption Spectroscopy of Transition Metal Charge-Transfer Complexes. *Acc. Chem. Res.* **36,** 876–887 (2003).

56. Greenough, S. E. *et al.* Ultrafast photo-induced ligand solvolysis of cis-[Ru(bipyridine) $_2$ (nicotinamide) $_2$] $^{2+}$: experimental and theoretical insight into its photoactivation mechanism. *Phys. Chem. Chem. Phys.* **16,** 19141–19155 (2014).

57. Deiters, A. Principles and Applications of the Photochemical Control of Cellular Processes. *ChemBioChem* **11,** 47–53 (2009).

58. Kaplan, J. H., Forbush III, B. & Hoffman, J. F. Rapid Photolytic Release of Adenosine S'-Triphosphate from a Protected Analogue: Utilization by the Na:K Pump of Human Red Blood Cell Ghosts'^. *Biochemistry* **17,** 1929–1935 (1978).

59. Lovatt, D. *et al.* Transcriptome in vivo analysis (TIVA) of spatially defined single cells in live tissue. *Nat. Methods* **11,** 190–196 (2014).

60. Griepenburg, J. C., Ruble, B. K. & Dmochowski, I. J. Caged oligonucleotides for bidirectional photomodulation of let-7 miRNA in zebrafish embryos. *Bioorg. Med. Chem.* **21,** 6198–6204 (2013).

61. Wang, Y., Shim, M. S., Levinson, N. S., Sung, H. W. & Xia, Y. Stimuli-responsive materials for controlled release of theranostic agents. *Adv. Funct. Mater.* **24,** 4206–4220 (2014).

62. Kamat, N. P. *et al.* A generalized system for photoresponsive membrane rupture in polymersomes. *Adv. Funct. Mater.* **20,** 2588–2596 (2010).

63. Robbins, G. P. *et al.* Photoinitiated destruction of composite Porphyrin-Protein polymersomes. *J. Am. Chem. Soc.* **131,** 3872–3874 (2009).

64. Griepenburg, J. C. *et al.* Caging metal ions with visible light-responsive nanopolymersomes. *Langmuir* **31,** 799–807 (2015).

65. Rosales, A. M. & Anseth, K. S. The design of reversible hydrogels to capture extracellular matrix dynamics. *Nat. Rev. Mater.* **1,** 15012 (2016).

66. Burdick, J. a & Murphy, W. L. Moving from static to dynamic complexity in hydrogel design. *Nat. Commun.* **3,** 1269 (2012).

67. Vermonden, T., Censi, R. & Hennink, W. E. Hydrogels for protein delivery. *Chemical Reviews* **112,** 2853–2888 (2012).

68. Wang, Y. & Kohane, D. S. External triggering and triggered targeting strategies for drug delivery. *Nat. Rev. Mater.* **2,** 17020 (2017).

69. Steinhilber, D. *et al.* A microgel construction kit for bioorthogonal encapsulation and pH-controlled release of living cells. *Angew. Chemie - Int. Ed.* **52,** 13538–13543 (2013).

70. Purcell, B. P. *et al.* Injectable and bioresponsive hydrogels for on-demand matrix metalloproteinase inhibition. *Nat. Mater.* **13,** 653–661 (2014).

71. Epstein-Barash, H. *et al.* A microcomposite hydrogel for repeated on-demand ultrasound-triggered drug delivery. *Biomaterials* **31,** 5208–5217 (2010).

72. Satarkar, N. S. & Hilt, J. Z. Magnetic hydrogel nanocomposites for remote controlled pulsatile drug release. *J. Control. Release* **130,** 246–251 (2008).

73. Ma, C., Shi, Y., Pena, D. A., Peng, L. & Yu, G. Thermally Responsive Hydrogel Blends: A General Drug Carrier Model for Controlled Drug Release. *Angew. Chemie - Int. Ed.* **54,** 7376–7380 (2015).

74. Rwei, A. Y. *et al.* Repeatable and adjustable on-demand sciatic nerve block with phototriggerable liposomes. *Proc. Natl. Acad. Sci. U. S. A.* **112,** 15719–24 (2015).

75. Magnusson, J. P., Saeed, A. O., Fernández-Trillo, F. & Alexander, C. Synthetic polymers for biopharmaceutical delivery. *Polym. Chem.* **2,** 48 (2011).

76. Bjerregaard, S. *et al.* Sustained elevated plasma aprotinin concentration in mice following intraperitoneal injections of w/o emulsions incorporating aprotinin. *J. Control. Release* **71,** 87–98 (2001).

77. Azagarsamy, M. A. & Anseth, K. S. Wavelength-controlled photocleavage for the orthogonal and sequential release of multiple proteins. *Angew. Chemie - Int. Ed.* **52,** 13803–13807 (2013).

78. Elisseeff, J. *et al.* Transdermal photopolymerization for minimally invasive implantation. *Proc. Natl. Acad. Sci. U. S. A.* **96,** 3104–3107 (1999).

79. Kloxin, A. M., Kasko, A. M., Salinas, C. N. & Anseth, K. S. Photodegradable hydrogels for dynamic tuning of physical and chemical properties. *Science (80-.).* **324,** 59–63 (2009).

80. Lee, T. T. *et al.* Light-triggered in vivo activation of adhesive peptides regulates cell adhesion, inflammation and vascularization of biomaterials. *Nat. Mater.* **14,** 352–60 (2015).

81. Pawley, J. B. *Handbook of Biological Confocal Microscopy*. *Springer* (2006).

82. Wang, D., Wagner, M., Butt, H.-J. & Wu, S. Supramolecular hydrogels constructed by red-light-responsive host-guest interactions for photo-controlled protein release in deep tissue. *Soft Matter* **11,** 7656–62 (2015).

83. Yan, B., Boyer, J.-C., Habault, D., Branda, N. R. & Zhao, Y. Near Infrared Light Triggered Release of Biomacromolecules from Hydrogels Loaded with Upconversion Nanoparticles.

J. Am. Chem. Soc. **134,** 16558–16561 (2012).

84. Brown, T. E., Marozas, I. A. & Anseth, K. S. Amplified Photodegradation of Cell-Laden Hydrogels via an Addition–Fragmentation Chain Transfer Reaction. *Adv. Mater.* **29,** (2017).

85. Breivogel, A., Kreitner, C. & Heinze, K. Redox and Photochemistry of Bis(terpyridine)ruthenium(II) Amino Acids and Their Amide Conjugates - from Understanding to Applications. *Eur. J. Inorg. Chem.* **2014,** 5468–5490 (2014).

86. Griepenburg, J. C., Rapp, T. L., Carroll, P. J., Eberwine, J. & Dmochowski, I. J. Ruthenium-caged antisense morpholinos for regulating gene expression in zebrafish embryos. *Chem. Sci.* **6,** 2342–2346 (2015).

87. Zayat, L., Filevich, O., Baraldo, L. M. & Etchenique, R. Ruthenium polypyridyl phototriggers: from beginnings to perspectives. *Philos. Trans. A. Math. Phys. Eng. Sci.* **371:201203,** http://dx.doi.org/10.1098/rsta.2012.0330 (2013).

88. Lancaster, K. M., Gerken, J. B., Durrell, A. C., Palmer, J. H. & Gray, H. B. Electronic structures, photophysical properties, and electrochemistry of ruthenium(II)(bpy)2 pyridylimidazole complexes. *Coord. Chem. Rev.* **254,** 1803–1811 (2010).

89. Highley, C. B., Prestwich, G. D. & Burdick, J. A. Recent advances in hyaluronic acid hydrogels for biomedical applications. *Curr Opin Biotechnol* **40,** 35–40 (2016).

90. Burdick, J. A. & Prestwich, G. D. Hyaluronic Acid Hydrogels for Biomedical Applications. *Adv. Mater.* **23,** H41–H56 (2011).

91. Ruggiero, E., Habtemariam, A., Yate, L., Mareque-Rivas, J. C. & Salassa, L. Near infrared photolysis of a Ru polypyridyl complex by upconverting nanoparticles. *Chem. Commun.* **50,** 1715 (2014).

92. Chen, Z., He, S., Butt, H.-J. & Wu, S. Photon Upconversion Lithography: Patterning of Biomaterials Using Near-Infrared Light. *Adv. Mater.* **27,** 2203–2206 (2015).

93. Azagarsamy, M. A., McKinnon, D. D., Alge, D. L. & Anseth, K. S. Coumarin-Based Photodegradable Hydrogel: Design, Synthesis, Gelation, and Degradation Kinetics. *ACS Macro Lett.* **3,** 515–519 (2014).

94. Sun, W. *et al.* Ruthenium-Containing Block Copolymer Assemblies: Red-Light-Responsive Metallopolymers with Tunable Nanostructures for Enhanced Cellular Uptake and Anticancer Phototherapy. *Adv. Healthc. Mater.* **5,** 467–473 (2016).

95. Wang, Y., Roose, B. W., Palovcak, E. J., Carnevale, V. & Dmochowski, I. J. A Genetically Encoded β-Lactamase Reporter for Ultrasensitive 129Xe NMR in Mammalian Cells. *Angew. Chemie - Int. Ed.* **55,** 8984–8987 (2016).

96. Lutolf, M. P. *et al.* Repair of bone defects using synthetic mimetics of collagenous extracellular matrices. *Nat. Biotechnol.* **21,** 513–518 (2003).

97. Lu, C., Liu, D., Liu, H. & Motchnik, P. Characterization of monoclonal antibody size variants containing extra light chains. *MAbs* **5,** 102–13 (2013).

98. Grim, J. C., Marozas, I. A. & Anseth, K. S. Thiol-ene and photo-cleavage chemistry for controlled presentation of biomolecules in hydrogels. *J. Control. Release* **219,** 95–106 (2015).

99. Sarode, B. R., Kover, K., Tong, P. Y., Zhang, C. & Friedman, S. H. Light Control of Insulin Release and Blood Glucose Using an Injectable Photoactivated Depot. *Mol. Pharm.* **13,** 3835–3841 (2016).

100. Shah, R. K. *et al.* Designer emulsions using microfluidics. *Materials Today* **11,** 18–27 (2008).

101. McKinnon, D. D., Domaille, D. W., Cha, J. N. & Anseth, K. S. Biophysically defined and cytocompatible covalently adaptable networks as viscoelastic 3d cell culture systems. *Adv. Mater.* **26,** 865–872 (2014).

102. Highley, C. B., Kim, M., Lee, D. & Burdick, J. A. Near-infrared light triggered release of molecules from supramolecular hydrogel-nanorod composites. *Nanomedicine (Lond).* **11,** 1579–90 (2016).

103. Liau, A., Karnik, R., Majumdar, A. & Doudna Cate, J. H. Mixing Crowded Biological Solutions in Milliseconds. *Anal. Chem.* **77,** 7618–7625 (2005).

104. Reeßing, F. & Szymanski, W. Beyond Photodynamic Therapy: Light-Activated Cancer Chemotherapy. *Curr. Med. Chem.* **24,** (2018).

105. Döbber, A. *et al.* Development and Biological Evaluation of a Photoactivatable Small Molecule Microtubule-Targeting Agent. *ACS Med. Chem. Lett.* **8,** 395–400 (2017).

106. Dcona, M. M. *et al.* Photocaged permeability: a new strategy for controlled drug release. *Chem. Commun.* **48,** 4755 (2012).

107. Ki Choi, S. *et al.* Light-controlled release of caged doxorubicin from folate receptor-targeting PAMAM dendrimer nanoconjugate. *Chem. Commun.* **46,** 2632 (2010).

108. Ovsianikov, A. *et al.* Laser Fabrication of Three-Dimensional CAD Scaffolds from Photosensitive Gelatin for Applications in Tissue Engineering. *Biomacromolecules* **12,** 851–858 (2011).

109. Shin, D.-S. *et al.* Photodegradable Hydrogels for Capture, Detection, and Release of Live Cells. *Angew. Chemie Int. Ed.* **53,** 8221–8224 (2014).

110. Peng, K. *et al.* Dextran based photodegradable hydrogels formed via a Michael addition. *Soft Matter* **7,** 4881 (2011).

111. Kirschner, C. M., Alge, D. L., Gould, S. T. & Anseth, K. S. Clickable, Photodegradable Hydrogels to Dynamically Modulate Valvular Interstitial Cell Phenotype. *Adv. Healthc. Mater.* **3,** 649–657 (2014).

112. Arakawa, C. K., Badeau, B. A., Zheng, Y. & DeForest, C. A. Multicellular Vascularized Engineered Tissues through User-Programmable Biomaterial Photodegradation. *Adv. Mater.* **29,** 1703156 (2017).

113. Griffin, D. R. & Kasko, A. M. Photodegradable Macromers and Hydrogels for Live Cell Encapsulation and Release. *J. Am. Chem. Soc.* **134,** 13103–13107 (2012).

114. Rosales, A. M., Mabry, K. M., Nehls, E. M. & Anseth, K. S. Photoresponsive Elastic Properties of Azobenzene-Containing Poly(ethylene-glycol)-Based Hydrogels. *Biomacromolecules* **16,** 798–806 (2015).

115. Brown, T. E., Marozas, I. A. & Anseth, K. S. Amplified Photodegradation of Cell-Laden Hydrogels via an Addition-Fragmentation Chain Transfer Reaction. *Adv. Mater.* **29,**

1605001 (2017).

116. Hemphill, J., Borchardt, E. K., Brown, K., Asokan, A. & Deiters, A. Optical Control of CRISPR/Cas9 Gene Editing. *J. Am. Chem. Soc.* **137,** 5642–5645 (2015).

117. Wu, L. *et al.* Caged circular antisense oligonucleotides for photomodulation of RNA digestion and gene expression in cells. *Nucleic Acids Res.* **41,** 677–686 (2013).

118. Kröck, L. & Heckel, A. Photoinduced Transcription by Using Temporarily Mismatched Caged Oligonucleotides. *Angew. Chemie Int. Ed.* **44,** 471–473 (2005).

119. Young, D. D., Lively, M. O. & Deiters, A. Activation and Deactivation of DNAzyme and Antisense Function with Light for the Photochemical Regulation of Gene Expression in Mammalian Cells. *J. Am. Chem. Soc.* **132,** 6183–6193 (2010).

120. Yamazoe, S., Liu, Q., McQuade, L. E., Deiters, A. & Chen, J. K. Sequential Gene Silencing Using Wavelength-Selective Caged Morpholino Oligonucleotides. *Angew. Chemie Int. Ed.* **53,** 10114–10118 (2014).

121. Yamazoe, S., Shestopalov, I. A., Provost, E., Leach, S. D. & Chen, J. K. Cyclic Caged Morpholinos: Conformationally Gated Probes of Embryonic Gene Function. *Angew. Chemie Int. Ed.* **51,** 6908–6911 (2012).

122. Goguen, B. N., Hoffman, B. D., Sellers, J. R., Schwartz, M. A. & Imperiali, B. Light-Triggered Myosin Activation for Probing Dynamic Cellular Processes. *Angew. Chemie* **123,** 5785–5788 (2011).

123. Riggsbee, C. W. & Deiters, A. Recent advances in the photochemical control of protein function. *Trends Biotechnol.* **28,** 468–475 (2010).

124. Ankenbruck, N., Courtney, T., Naro, Y. & Deiters, A. Optochemical Control of Biological Processes in Cells and Animals. *Angew. Chemie Int. Ed.* **57,** 2768–2798 (2018).

125. Mura, S., Nicolas, J. & Couvreur, P. Stimuli-responsive nanocarriers for drug delivery. *Nat. Mater.* **12,** 991–1003 (2013).

126. Huisman, M. *et al.* Caging the uncageable: using metal complex release for photochemical control over irreversible inhibition. *Chem. Commun.* **52,** 12590–12593 (2016).

127. Walker, J. W., Mccray, J. A. & Hess, G. P. Photolabile Protecting Groups for an Acetylcholine Receptor Ligand. Synthesis and Photochemistry of a New Class of o-Nitrobenzyl Derivatives and Their Effects on Receptor Function1" *Biochemistry* **25,** 1799–1805 (1986).

128. Aujard, I. *et al.* o-Nitrobenzyl Photolabile Protecting Groups with Red-Shifted Absorption: Syntheses and Uncaging Cross-Sections for One- and Two-Photon Excitation. *Chem. - A Eur. J.* **12,** 6865–6879 (2006).

129. Wylie, R. G. & Shoichet, M. S. Two-photon micropatterning of amines within an agarose hydrogel. *J. Mater. Chem.* **18,** 2716 (2008).

130. Yan, B., Boyer, J.-C., Branda, N. R. & Zhao, Y. Near-Infrared Light-Triggered Dissociation of Block Copolymer Micelles Using Upconverting Nanoparticles. *J. Am. Chem. Soc.* **133,** 19714–19717 (2011).

131. Rapp, T. L., Highley, C. B., Manor, B. C., Burdick, J. A. & Dmochowski, I. J. Ruthenium-

Crosslinked Hydrogels with Rapid, Visible-Light Degradation. *Chem. - A Eur. J.* **24,** 2328–2333 (2018).

132. Huisman, M. *et al.* Caging the uncageable: using metal complex release for photochemical control over irreversible inhibition. *Chem. Commun.* **52,** 12590–12593 (2016).

133. Lameijer, L. N. *et al.* A Red-Light-Activated Ruthenium-Caged NAMPT Inhibitor Remains Phototoxic in Hypoxic Cancer Cells. *Angew. Chemie Int. Ed.* **56,** 11549–11553 (2017).

134. Sharma, R. *et al.* Ruthenium Tris(2-pyridylmethyl)amine as an Effective Photocaging Group for Nitriles. *Inorg. Chem.* **53,** 3272–3274 (2014).

135. Garner, R. N., Joyce, L. E. & Turro, C. Effect of Electronic Structure on the Photoinduced Ligand Exchange of Ru(II) Polypyridine Complexes. *Inorg. Chem.* **50,** 4384–4391 (2011).

136. Elliott, M. G., Zhang, S. & Shepherd, R. E. Pentaammineruthenium(II), Pentaammineosmium(II), and (N-(Hydroxylethyl)ethylenediaminetriacetato)ruthenate(II) Complexes of Styrenes. *Inorg. Chem.* **28,** 3036–3043 (1989).

137. Wieder, N. L., Carroll, P. J. & Berry, D. H. Structure and Reactivity of Acetylene Complexes of Bis(imino)pyridine Ruthenium(0). *Organometallics* **30,** 2125–2136 (2011).

138. Crescenzi, V., Cornelio, L., Meo, C. Di, Nardecchia, S. & Lamanna, R. Novel Hydrogels via Click Chemistry: Synthesis and Potential Biomedical Applications. *Biomacromolecules* **8,** 1844–1850 (2007).

139. Hu, X., Li, D., Zhou, F. & Gao, C. Biological hydrogel synthesized from hyaluronic acid, gelatin and chondroitin sulfate by click chemistry. *Acta Biomater.* **7,** 1618–1626 (2011).

140. Liu, S. Q., Rachel Ee, P. L., Ke, C. Y., Hedrick, J. L. & Yang, Y. Y. Biodegradable poly(ethylene glycol)–peptide hydrogels with well-defined structure and properties for cell delivery. *Biomaterials* **30,** 1453–1461 (2009).

141. Heller, D. A. *et al.* Modular 'Click-in-Emulsion' Bone-Targeted Nanogels. *Adv. Mater.* **25,** 1449–1454 (2013).

142. Ossipov, D. A. & Hilborn, J. Poly(vinyl alcohol)-Based Hydrogels Formed by "Click Chemistry". *Macromolecules* **39,** 1709–1718 (2006).

143. Jiang, Y., Chen, J., Deng, C., Suuronen, E. J. & Zhong, Z. Click hydrogels, microgels and nanogels: Emerging platforms for drug delivery and tissue engineering. *Biomaterials* **35,** 4969–4985 (2014).

144. Adzima, B. J. *et al.* Spatial and temporal control of the alkyne–azide cycloaddition by photoinitiated Cu(II) reduction. *Nat. Chem.* **3,** 256–259 (2011).

145. Cutler, J. I., Auyeung, E. & Mirkin, C. A. Spherical Nucleic Acids. *J. Am. Chem. Soc.* **134,** 1376–1391 (2012).

146. Geary, R. S., Norris, D., Yu, R. & Bennett, C. F. Pharmacokinetics, biodistribution and cell uptake of antisense oligonucleotides. *Adv. Drug Deliv. Rev.* **87,** 46–51 (2015).

147. Stephenson, M. L. & Zamecnik, P. C. Inhibition of Rous sarcoma viral RNA translation by a specific oligodeoxyribonucleotide. *Proc. Natl. Acad. Sci. U. S. A.* **75,** 285–8 (1978).

148. Zamecnik, P. C. & Stephenson, M. L. Inhibition of Rous sarcoma virus replication and cell

transformation by a specific oligodeoxynucleotide. *Proc. Natl. Acad. Sci. U. S. A.* **75,** 280–4 (1978).

149. Yang, L. *et al.* Efficient synthesis of light-triggered circular antisense oligonucleotides targeting cellular protein expression. *ChemBioChem* (2018). doi:10.1002/cbic.201800012

150. Yeldell, S. B., Ruble, B. K. & Dmochowski, I. J. Oligonucleotide modifications enhance probe stability for single cell transcriptome in vivo analysis (TIVA). *Org. Biomol. Chem.* **15,** 10001–10009 (2017).

151. Stein, C. A. & Castanotto, D. FDA-Approved Oligonucleotide Therapies in 2017. *Mol. Ther.* **25,** 1069–1075 (2017).

152. Egholm, M., Buchardt, O., Nielsen, P. E. & Berg, R. H. Peptide nucleic acids (PNA). Oligonucleotide analogs with an achiral peptide backbone. *J. Am. Chem. Soc.* **114,** 1895–1897 (1992).

153. Shestopalov, I. A. & Chen, J. K. Spatiotemporal Control of Embryonic Gene Expression Using Caged Morpholinos. *Methods Cell Biol.* **104,** 151–172 (2011).

154. Badeau, B. A., Comerford, M. P., Arakawa, C. K., Shadish, J. A. & DeForest, C. A. Engineered modular biomaterial logic gates for environmentally triggered therapeutic delivery. *Nat. Chem.* **10,** 251–258 (2018).

155. Ohtsuka, E., Tanaka, S. & Ikehara, M. Studies on transfer ribonucleic acids and related compounds. IX [(1)] Ribo-oligonucleotide synthesis using a photosensitive o-nitrobenzyl protection at the 2′-hydroxyl group. *Nucleic Acids Res.* **1,** 1351–1358 (1974).

156. Bai, X., Li, Z., Jockusch, S., Turro, N. J. & Ju, J. Photocleavage of a 2-nitrobenzyl linker bridging a fluorophore to the 5’ end of DNA. *Proc. Natl. Acad. Sci. U. S. A.* **100,** 409–13 (2003).

157. Heckel, A. & Mayer, G. Light Regulation of Aptamer Activity: An Anti-Thrombin Aptamer with Caged Thymidine Nucleobases. *J. Am. Chem. Soc.* **127,** 822–823 (2005).

158. Lusic, H., Young, D., Lively, M. & Deiters, A. Photochemical DNA Activation. *Org. Lett.* **9,** 1903–1906 (2007).

159. Tang, X. & Dmochowski, I. J. Regulating gene expression with light-activated oligonucleotides. *Mol. BioSyst.* **3,** 100–110 (2007).

160. Shestopalov, I. A., Sinha, S. & Chen, J. K. Light-controlled gene silencing in zebrafish embryos. *Nat. Chem. Biol.* **3,** 650–651 (2007).

161. Givens, R. S. & Matuszewski, B. Photochemistry of phosphate esters: an efficient method for the generation of electrophiles. *J. Am. Chem. Soc.* **106,** 6860–6861 (1984).

162. Givens, R. S., Rubina, M. & Wirz, J. Applications of p-hydroxyphenacyl (pHP) and coumarin-4-ylmethyl photoremovable protecting groups. *Photochem. Photobiol. Sci.* **11,** 472 (2012).

163. Shembekar, V. R., Chen, Y., Carpenter, B. K. & Hess, G. P. A Protecting Group for Carboxylic Acids That Can Be Photolyzed by Visible Light†. *Biochemistry* **44,** 7107–7114 (2005).

164. Shembekar, V. R., Chen, Y., Carpenter, B. K. & Hess, G. P. Coumarin-Caged Glycine that Can Be Photolyzed within 3 μs by Visible Light†. *Biochemistry* **46,** 5479–5484 (2007).

165. Fan, L., Lewis, R. W., Hess, G. P. & Ganem, B. A new synthesis of caged GABA compounds for studying GABAA receptors. *Bioorg. Med. Chem. Lett.* **19,** 3932–3933 (2009).

166. Subramaniam, R. *et al.* Light-mediated and H-bond facilitated liposomal release: the role of lipid head groups in release efficiency. *Tetrahedron Lett.* **51,** 529–532 (2010).

167. Yamazoe, S., Liu, Q., McQuade, L. E., Deiters, A. & Chen, J. K. Sequential Gene Silencing Using Wavelength-Selective Caged Morpholino Oligonucleotides. *Angew. Chemie Int. Ed.* **53,** 10114–10118 (2014).

168. Wang, Y. *et al.* Manipulation of gene expression in zebrafish using caged circular morpholino oligomers. *Nucleic Acids Res.* **40,** 11155–62 (2012).

169. Kim, S. H., Mok, H., Jeong, J. H., Kim, S. W. & Park, T. G. Comparative Evaluation of Target-Specific GFP Gene Silencing Efficiencies for Antisense ODN, Synthetic siRNA, and siRNA Plasmid Complexed with PEI−PEG−FOL Conjugate. *Bioconjug. Chem.* **17,** 241–244 (2006).

170. Wuttke, D. s., Bjerrum, M. J., Winkler, J. R. & Gray, H. B. Electron-Tunneling Pathways in Cytochrome c. *Science (80-.).* **256,** 1007–1009 (1992).

171. Bjerrum, M. J. *et al.* Electron transfer in ruthenium-modified proteins. *J. Bioenerg. Biomembr.* **27,** 295–302 (1995).

172. Goldbach, R. E., Rodriguez-Garcia, I., van Lenthe, J. H., Siegler, M. A. & Bonnet, S. N-Acetylmethionine and Biotin as Photocleavable Protective Groups for Ruthenium Polypyridyl Complexes. *Chem. - A Eur. J.* **17,** 9924–9929 (2011).

173. Palmer, A. M. *et al.* Cytotoxicity of cyclometallated ruthenium complexes: the role of ligand exchange on the activity. *Philos. Trans. A. Math. Phys. Eng. Sci.* **371,** 20120135 (2013).

174. Getahun, Z. *et al.* Using Nitrile-Derivatized Amino Acids as Infrared Probes of Local Environment. *J. Am. Chem. Soc.* **125,** 405–411 (2002).

175. Tucker, M. J., Oyola, R. & Gai, F. A novel fluorescent probe for protein binding and folding studies:p-cyano-phenylalanine. *Biopolymers* **83,** 571–576 (2006).

176. Blumenthal, S. G., Hendrickson, H. R., Abrol, Y. P. & Conn, E. E. Cyanide Metabolism in Higher Plants The Biosynthesis of b-cyanoalanine. *J. Biol. Chem.* **243,** 5302–5307 (1963).

177. FLOSS, H. G., HADWIGER, L. & CONN, E. E. Enzymatic Formation of β-Cyanoalanine from Cyanide. *Nature* **208,** 1207–1208 (1965).

178. Cociancich, S. *et al.* The gyrase inhibitor albicidin consists of p-aminobenzoic acids and cyanoalanine. *Nat. Chem. Biol.* **11,** 195–197 (2015).

179. Severin, K., Bergs, R. & Beck, W. Bioorganometallic Chemistry - Transition Metal Complexes withα-Amino Acids and Peptides. *Angew. Chemie Int. Ed.* **37,** 1634–1654 (1998).

180. Sheldrick, W. S. & Gleichmann, A. η5-Pentamethylcyclopentadienylruthenium(II) complexes containing η6-coordinated α-amino acids. *J. Organomet. Chem.* **470,** 183–187 (1994).

181. Sheldrick, W. S. & Exner, R. Synthesis and structural characterization of ruthenium(II) complexes of histidine and methionine derivatives. *Inorganica Chim. Acta* **195,** 1–9

(1992).

182. Krämer, R., Polborn, K., Wanjek, H., Zahn, I. & Beck, W. Chiral Half-Sandwich Complexes of Rhodium(III), Iridium(III), Iridium(I) and Ruthenium(II) with a-Amino Acid Anions. *Chem. Ber.* **123,** 767–778 (1990).

183. Sheldrick, W. S. & Exner, R. Synthesis and stereochemistry of diene-ruthenium(II) complexes of α-amino acids. Crystal structures of [(cod)Ru(d,l-phe)Cl]4 and Δ-[(nbd)Ru(l-phe)2]. *Inorganica Chim. Acta* **166,** 213–219 (1989).

184. Sheldrick, W. S. & Exner, R. Synthesis and stereochemistry of diene-ruthenium(II) complexes of sulphur-containing α-amino acids. *J. Organomet. Chem.* **386,** 375–387 (1990).

185. Margalit, R. *et al.* Preparation and characterization of pentaammineruthenium-(histidine-83)azurin: thermodynamics of intramolecular electron transfer from ruthenium to copper. *Proc. Natl. Acad. Sci. U. S. A.* **81,** 6554–8 (1984).

186. Kalbag, S. M. & Roeske, R. W. Photolabile protecting group for histidine. *J. Am. Chem. Soc.* **97,** 440–441 (1975).

187. Nakayama, K., Heise, I., Görner, H. & Gärtner, W. Peptide Release upon Photoconversion of 2-Nitrobenzyl Compounds into Nitroso Derivatives. *Photochem. Photobiol.* **87,** 1031–1035 (2011).

188. Chang, I. J., Gray, H. B. & Winkler, J. R. High-driving-force electron transfer in metalloproteins: intramolecular oxidation of ferrocytochrome c by Ru(2,2'-bpy)2(im)(his-33)3+. *J. Am. Chem. Soc.* **113,** 7056–7057 (1991).

189. Albani, B. A., Peña, B., Dunbar, K. R. & Turro, C. New cyclometallated Ru(II) complex for potential application in photochemotherapy? *Photochem. Photobiol. Sci.* **13,** 272–80 (2014).

190. Sears, R. B. *et al.* Photoinduced ligand exchange and DNA binding of cis-[Ru(phpy)(phen)(CH3CN)2]+ with long wavelength visible light. *J. Inorg. Biochem.* **121,** 77–87 (2013).

191. Zeng, X., Zhou, X. & Wu, S. Red and Near-Infrared Light-Cleavable Polymers. *Macromol. Rapid Commun.* 1800034 (2018). doi:10.1002/marc.201800034

192. Vitaku, E., Smith, D. T. & Njardarson, J. T. Analysis of the Structural Diversity, Substitution Patterns, and Frequency of Nitrogen Heterocycles among U.S. FDA Approved Pharmaceuticals. *J. Med. Chem.* **57,** 10257–10274 (2014).

193. Ruengwit Kitbunnadaj *et al.* Identification of 4-(1H-Imidazol-4(5)-ylmethyl)pyridine (Immethridine) as a Novel, Potent, and Highly Selective Histamine H3 Receptor Agonist. *J. Med. Chem.* **47,** 2414–2417 (2004).

194. Monga, V., Bussière, G., Crichton, P. & Daswani, S. Synthesis and Decomposition Kinetic Studies of Bis(lutidine)silver(I) Nitrate Complexes as an Interdisciplinary Undergraduate Chemistry Experiment. *J. Chem. Educ.* **93,** 958–962 (2016).

195. Van Hecke, G. R., Karukstis, K. K., Haskell, R. C., McFadden, C. S. & Wettack, F. S. An Integration of Chemistry, Biology, and Physics: The Interdisciplinary Laboratory. *J. Chem. Educ.* **79,** 837 (2002).

196. Hansen, S. J. R. *et al.* Bridging the Gap between Instructional and Research Laboratories: Teaching Data Analysis Software Skills through the Manipulation of Original Research Data. *J. Chem. Educ.* **93,** 663–668 (2016).

197. Kasting, B. J., Bowser, A. K., Anderson-Wile, A. M. & Wile, B. M. Synthesis and Metalation of a Ligand: An Interdisciplinary Laboratory Experiment for Second-Year Organic and Introductory Inorganic Chemistry Students. *J. Chem. Educ.* **92,** 1103–1109 (2015).

198. Smellie, I. A. *et al.* Solvent Extraction of Copper: An Extractive Metallurgy Exercise for Undergraduate Teaching Laboratories. *J. Chem. Educ.* **93,** 362–367 (2016).

199. Locock, K., Bakas, T., Sanai, F., Allan, R. & Hinton, T. What Is the “Areca” in “Areca Nuts”? Extraction and Neuroactive Bioassay of Arecoline. *J. Chem. Educ.* **93,** 197–201 (2016).

200. Salassa, L., Garino, C., Salassa, G., Gobetto, R. & Nervi, C. Mechanism of ligand photodissociation in photoactivable Ru(bpy)(2)L(2) (2+) complexes: A density functional theory study. *J. Am. Chem. Soc.* **130,** 9590–9597 (2008).

201. Palmer, A. M. *et al.* Cytotoxicity of cyclometallated ruthenium complexes : the role of ligand exchange on the activity Cytotoxicity of cyclometallated ruthenium complexes : the role of ligand exchange on the activity. (2013).

202. Pinnick, D. V. & Durham, B. Photosubstitution reactions of Ru(bpy)2XYn+ complexes. *Inorg. Chem.* **23,** 1440–1445 (1984).

203. Garino, C., Terenzi, A., Barone, G. & Salassa, L. Teaching Inorganic Photophysics and Photochemistry with Three Ruthenium(II) Polypyridyl Complexes: A Computer-Based Exercise. *J. Chem. Educ.* **93,** 292–298 (2016).

204. Rabago Smith, M., McAllister, R., Newkirk, K., Basing, A. & Wang, L. Development of an Interdisciplinary Experimental Series for the Laboratory Courses of Cell and Molecular Biology and Advance Inorganic Chemistry. *J. Chem. Educ.* **89,** 150–155 (2012).